A close range baseband radar transceiver for application in borehole radar systems

P.J. van der Merwe

Dissertation presented for the degree of Doctor of Philosophy in Engineering at the Stellenbosch University

Promoters

Prof. J.H. Cloete

Prof. P.W. van der Walt

December 2007

Declaration

By submitting this dissertation electronically, I declare that the entirety of the work contained therein is my own, original work, that I am the owner of the copyright thereof (unless to the extent explicitly otherwise stated) and that I have not previously in its entirety or in part submitted it for obtaining any qualification.

December 2007

Abstract

A monostatic baseband radar is required with the capability of detecting close range targets that appear at distances comparable to the system's resolution, without compromising the radar's maximum range. The application in borehole radar imposes further constraints associated with the physical limitations and variable electromagnetic environment of different borehole diameters and conditions. This dissertation discusses the complete design process of the analog section of a monostatic radar that successfully addresses these issues.

The proposed transceiver employs a series duplexing arrangement consisting of an antenna, transmitter, receiver and an isolation switch. An exponentially decaying tail is observed in the current flowing on a borehole radar antenna when excited by pulse waveforms. The characteristics of this tail depend strongly on the borehole environment. A measurement technique is developed that accurately quantifies this exponential decay by digitizing a logarithmic representation of the antenna current while it is operating in various boreholes. Transmitters are then designed to drive these antennas with waveforms that prevent the formation of current tails. This is achieved through the use of pole-zero networks or alternatively by generating certain asymmetric, bipolar waveforms. The transmitters are simultaneously designed to have an output impedance approximating a short circuit after the transient is generated. In the series configuration proposed here, the duplexing of the antenna between transmitter and receiver is then reduced to simply isolating the receiver during transmit-mode. The switch responsible for this isolation disconnects the receiver and presents a short circuit between antenna and transmitter during transmit-mode, while connecting the receiver terminals between the antenna and the short circuited transmitter terminals in receive-mode. The required close-in performance of the transceiver dictates that the transition between these two states of the isolation switch occur in a time similar to the duration of the transmitter waveform. The switching artefacts generated by the switch are consequently similar to the radar data signal. The isolation switch employs an innovative configuration (using both transistors and diodes) which accepts a single control signal and causes the switching artefacts to be generated as a common mode signal, while a differential path is created for the radar data signal which is being switched. This leads to effective suppression of the switching signal in the signal passed to the receiver. Dissipative filtering is advocated as a fundamental design principle for high fidelity receivers and it is shown how it can be applied by using constant impedance equalizers and diplexers as basic building blocks. This principle is used as the basis for the design of this transceiver's receivers, which incorporate both standard gain blocks and operational amplifiers.

A complete borehole radar system, based on the transceiver developed here, was built and tested; resulting in the first known practical monostatic borehole radar system. Data obtained in field trials are presented and suggest that the monostatic system compares well with current state of the art bi-static systems.

Opsomming

Die behoefte is geïdentifiseer vir 'n monostatiese basisbandradar wat oor die vermoë beskik om nabygeleë teikens op 'n afstand soortgelyk aan die resolusie van die stelsel waar te neem, sonder om die maksimum bereik van die stelsel in te kort. Die toepassing daarvan in 'n boorgatradarstelsel lei tot verdere vereistes vanweë die fisiese beperkings en veranderende elektromagnetiese omgewing van boorgate met verskillende deursnitte en toestande. Hierdie proefskrif is gemoeid met die volledige ontwerpsprosedure van die analoog gedeelte van 'n monostatiese radar wat al hierdie kwessies aanspreek.

'n Serie verbinding van antenne, sender, ontvanger en isolasieskakelaar word ingespan vir hierdie ontwerp. Eksponensieel wegsterwende stertjies word waargeneem in die antennestroom van 'n boorgatradarantenne wanneer dit aangedryf word deur puls golfvorms. 'n Meettegniek word ontwikkel wat hierdie eksponensiële verslapping noukeurig kan monitor deur 'n logaritmiese voorstelling van die antennastroom te versyfer terwyl dit ontplooi word in verskillende boorgate. Senders word dan ontwikkel om hierdie antennes aan te dryf met golfvorms wat juis die vorming van hierdie stertjies voorkom. Dit word bewerkstellig deur die gebruik van pool-zero netwerke of andersins deur die opwek van sekere asimmetriese, bipolêre golfvorms. Die senders se uittree-impedansies moet egter terselfdertyd ontwerp word om 'n kortsluiting te benader sodra die oorgang klaar opgewek is. Met die serie verbinding wat hier gebruik word, raak die vereiste tyddeling van die antenna tussen die sender en ontvanger dan bloot 'n geval van ontvanger-isolasie gedurende uitsaai-modus. Die skakelaar wat verantwoordelik is vir hierdie isolasie ontkoppel die ontvanger en vertoon soos 'n kortsluiting tussen sender en antenne tydens uitsaai-modus, maar verbind weer die terminale van die ontvanger tussen die antenne en kortgeslote senderterminale tydens ontvang-modus. Die vereiste kortafstand vermoë van die stelsel veroorsaak dat die tysduur van die oorgang tussen hierdie twee modusse soortgelyk is aan dié van die sender golfvorm en enige skakelverskynsels wat opgewek word deur die skakelaar is gevolglik soortgelyk aan die radardatasein self. Die isolasieskakelaar gebruik egter 'n innoverende konfigurasie (met transistors sowel as diodes) wat funksioneer met 'n enkele beheersein en die skakelverskynsels as gemene modus seine opwek, terwyl 'n differensiële seinpad geskep word vir die radardatasein wat geskakel word. Die skakelseine word gevolglik effektief onderdruk in die sein wat oorgedra word aan die ontvanger. Die gebruik van verkwistende filters word voorgestel as 'n fundamentele ontwerpsbeginsel vir hoëtrou ontvangers en daar word getoon hoe dit toegepas kan word met konstante impedansie vereffeningsbane en dipleksers. Hierdie beginsel is dan ook gebruik as basis vir die ontwerp van hierdie stelsel se ontvangers, wat gebruik maak van beide standard aanwinsblokke sowel as operasionel versterkers.

'n Volledige boorgatradarstelsel, gebaseer op die stelsel wat hier ontwikkel is, is gebou en getoets. Die gevolg is die eerste bekende, praktiese monostatiese boorgatradarstelsel. Data wat hiermee verwerf is word aangebied en dui daarop dat die monostatiese stelsel baie goed opweeg teen huidige bi-statiese stelsels.

To Liezel-

my wife

Acknowledgements

I am indebted to a number of people who assisted in some special way during this project.

My Almighty Father - who not only gives us the feet of a klipspringer, but who also wants us to play safely on the high hills (Hab. 3:19.)

Prof. Cloete, my promoter – the value of your mentorship during this project is only surpassed by the defining role you have played in my development as an engineer and as a person. Thank you.

Prof. van der Walt, my promoter – I admire your vast knowledge ranging from complex theory right through to commercial component choices. It has been a privilege to work under your guidance.

Prof. Mason, from the University of Sydney – your insistence that the system can be improved led to the final results of this project. Thank you for all the invaluable inputs along the way.

Everyone at GeoMole – this has been an incredible journey to quite literally the ends of the world (and under it), with moments of euphoria back to back with absolute disappointment and frustration. Thank you for the opportunity to share this with you. Special thanks to Brian Woods and Tim Sindle, who probably wouldn't need to read this dissertation, as they already know everything in it (and not in it) – thanks for the camaraderie.

Jan Steenkamp from Digital Surveying - who performed a large number of the borehole radar surveys found in this dissertation. You have the ability to perform the most meticulous borehole radar surveys under circumstances which are, for all intents and purposes, impossible to work in. Pushing a scotch car together for a couple of kilometres, 3 km underground, somehow forges a bond which is not easily broken.

Mike Smart and Henk van der Kleef from the Department of Water Affairs and Forestry, Chris Hartnady from Umvuto, Freek van Zyl from the farm Rooivlei, Ricky Murray from Groundwater Africa and Calvinia municipality – my progress would have been infinitely slower had it not been for your generosity in making boreholes available for my experiments.

My family and friends – sometimes a simple word of support or show of belief is all one needs.

Liezel, my lovely wife – because nothing inspires a man more than the girl of his dreams telling him he *can*.

This project was generously funded by GeoMole and ARCOlab.

Table of Contents

List of figures

List of tables

List of abbreviations used

AGC	Automatic gain control
ADC	Analog to digital converter
FD-TD	Finite difference time domain
FET	Field effect transistor
FPGA	Field programmable gate array
GaAs	Gallium arsenide
HV	High voltage
MMIC	Monolithic microwave integrated circuits
MoM	Method of moments
MOS	Metal oxide semiconductor
PRF	Pulse repetition frequency
RC	Resistor capacitor
RF	Radio frequency
Rx	Receiver
STC	Sensitivity time control
T/R	Transmit/receive
TLIR	Time limited impulse response
Tx	Transmitter
UWB	Ultra wideband
VGA	Variable gain amplifier

CHAPTER 1

Introduction

1.1. Background

This dissertation addresses the development of a monostatic, baseband radar system capable of detecting targets over a large range of distances, starting from virtually against the radar. It is further required that the system must be able to function as part of a borehole radar system, deployed in boreholes with a wide range of diameters and conditions.

A bi-static radar system is defined [1] as a system where the transmitter and receiver modules, each with their own antenna, are physically removed from one another. A monostatic radar system is conversely defined as a system where the transmitter and receiver are collocated and use the same antenna. The term *transceiver* [2] will be used throughout this dissertation to refer to the analog section of a monostatic radar system, comprising antenna, transmitter, isolation switch and receiver. The focus will be on the development of these analog modules.

Baseband radar [3] refers to systems that use short duration, carrierless pulses to perform the radar function. These systems are characterized by a large instantaneous bandwidth effectively starting at zero frequency and are often referred to as ultra wideband (UWB) systems [4]. No modulation or demodulation is performed on the signal and the resolution is directly dependent on the pulse duration.

Close range radar is clearly a relative concept and will be considered in terms of the system's resolution [2]. The close range systems in which this design will find application can in general be defined as systems of which the closest discernable target is at a distance comparable to the range resolution of the system. The implication for a monostatic baseband radar system is that reflected signals arriving at the antenna must be detected as soon as the transmitter has completed driving the antenna with the transmit pulse.

It is often assumed during the design of these systems that the antenna characteristics are known and predictable. This is generally not the case in surface penetrating radar systems [5] where the antenna is closely coupled to a complex, variable medium. The effect is especially pronounced in borehole radar systems (discussed in section 1.3) where the borehole in which the system is deployed varies from dry to filled with liquid of variable characteristics as well as varying in diameters

and host rock. The resultant variation in electromagnetic environment introduces various design challenges.

A number of additional constraints are further introduced by a borehole radar system, including the physical constraints of building a deployable probe, power considerations of being battery operated and robust packaging for operation in the harsh mining environment.

1.2. Fundamental differences between monostatic and bi-static radar operation

1.2.1. Isolation

The primary reason for using a bi-static setup is the isolation afforded by the physical spacing between the transmitter and receiver. By ensuring that each unit resides in the null of the other unit's antenna, the direct electrodynamic coupling can be minimized.

The electroquasistatic and magnetoquasistatic responses of the transmitter in a bi-static system do not usually warrant much attention as they do not have a significant influence on the radar data. The coupling thereof to the receiver can furthermore be assumed to be negligible due to its rapid decay over distance [6].

This is not the case for a monostatic system where the transmitter and receiver electronics are typically in close proximity to each other and the two subsystems share an antenna. Any signal introduced on the antenna by the transmitter will necessarily be seen by the receiver and particular attention must consequently be paid to the receiver's isolation while the transmitter drives the antenna, as well as to the antenna's response to the transmitter drive, both dynamic and quasistatic. Any electromagnetic coupling between the high powered transmitter and sensitive receiver, apart from that through the designed interface of the two modules, must also be avoided.

The finite duration of the transition between transmit and receive mode associated with a monostatic system does typically result in "dead time." This represents the time immediately after the transmitter fired and before the receiver gains access to the antenna. Data loss then occurs in the area immediately surrounding the antenna. It is therefore an important objective of a monostatic system to make this transition as rapid as possible to minimize the data loss.

1.2.2. Propagation path

The path of electromagnetic propagation differs between monostatic and bi-static radar systems and results in a fundamental difference in the relationship between propagation time and distance to reflector for the two systems. This can simplistically be explained with the use of the diagram in Figure 1-1, using omnidirectional point elements for a bi-static transmitter and receiver as well as for a monostatic transceiver.

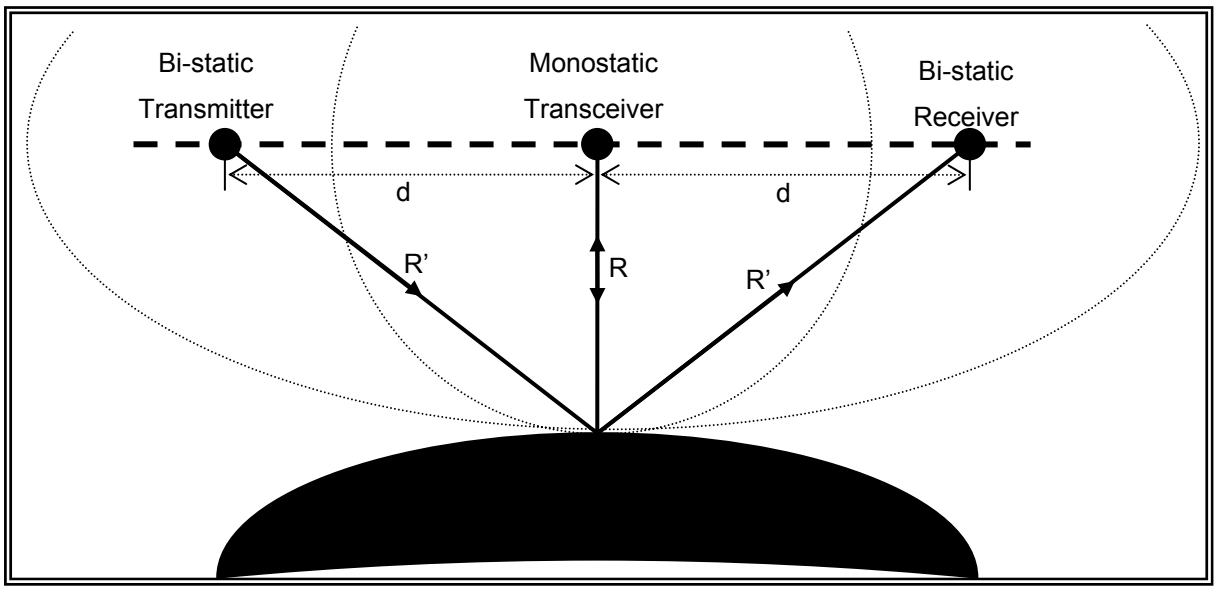

FIGURE 1-1: DIFFERENCE IN PROPAGATION PATHS BETWEEN MONOSTATIC AND BI-STATIC SYSTEM

The distance an electromagnetic signal has to travel from the monostatic transceiver to the reflector and back is simply 2R. For a given propagation velocity ν, the propagation time is therefore directly proportional to the distance from the reflector:

$$t = \frac{2R}{\nu} \qquad \rightarrow \quad (1\text{-}1)$$

The distance travelled in the bi-static case is conversely:

$$2R' = 2\sqrt{R^2 + d^2}\ . \qquad \rightarrow \quad (1\text{-}2)$$

The propagation time is then given by:

$$t = \frac{2\sqrt{R^2 + d^2}}{\nu} \qquad \rightarrow \quad (1\text{-}3)$$

This difference is illustrated by the graph in Figure 1-2, which shows the propagation time of the electromagnetic signal for a reflector at various distances with a propagation velocity of ν=1 and a spacing between transmitter and receiver of d=1. The distance from the reflector is expressed as multiples of this distance between the transmitter and receiver. It is clear that the close-in targets will be distorted in the radar image of the bi-static system, especially if the signal is sampled in time with a relatively low sample frequency.

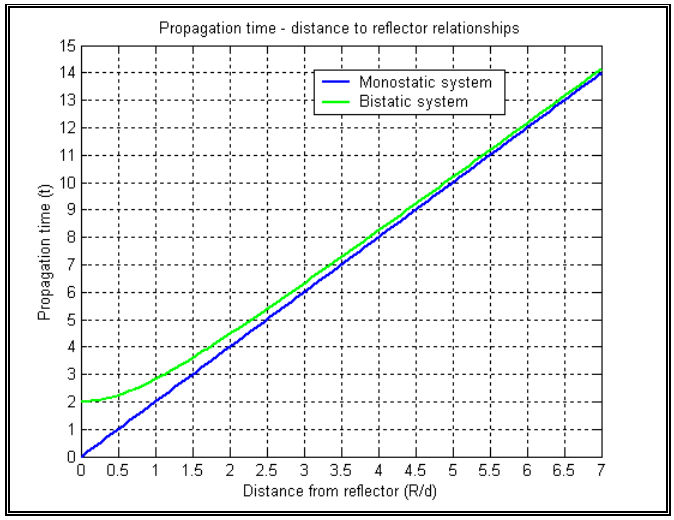

FIGURE 1-2: RELATIONSHIP BETWEEN PROPAGATION TIME AND DISTANCE TO REFLECTOR

It should further be noted that, in the plane of Figure 1-1, reflections from correctly angled reflectors located on the circumference of a circle surrounding the monostatic will coincide. The reflectors which will coincide with the bi-static system are located on the circumference of an ellipse with the 2 foci located on the transmitter and receiver respectively. Antennas with higher directivity towards broadside in this plane will naturally make this less significant, but will in turn result in degradation of the bi-static system's close in performance, where reflectors occur at an increasingly oblique angle to the two antennas.

1.2.3. Synchronization

A basic principle for the operation of a baseband radar system is the careful synchronization between the transmitter and receiver modules; it is essential for the receiver to know the exact time the pulse was transmitted to ensure the distance to the reflector can be calculated correctly in a repeatable fashion. This is particularly critical for systems where averaging is employed. It is a simple matter in a monostatic system where the transmitter and receiver are collocated. It can be slightly more complicated in a bi-static system were a trigger signal must be passed over the distance between the transmitter and receiver in a jitter free fashion and immune to false triggering which may occur due to coupling or interference.

1.3. Borehole radar system

Borehole radar is proposed as an application for the transceiver developed in this dissertation. It has established itself as a potentially valuable geophysical imaging tool in the mining industry during recent years [7], [8], [9], [10] and could benefit significantly from this development.

A borehole radar system [11] generally consists of separate transmitter and receiver probes (bi-static setup) which are deployed downhole. Typical systems vary in the extent to which the electronic subsystems are incorporated into the probes themselves, from just the antenna (with the electronics at the borehole collar), through to systems having all the electronics as well as data storage on board the downhole probe. Commercial borehole radar systems include systems such as the BR40 Aardwolf system (www.aardwolf.co.za) from the Council for Scientific and Industrial research (CSIR), the Ramac/GPR borehole radar system from Malä Geoscience (www.malags.com) and the PulseEKKO PRO system from Sensors & Software (www.sensoft.ca). The GeoMole (www.geomole.com) borehole radar is an example of a system incorporating all the electronics and data storage onboard the probe and an overview of this system (compiled from internal documentation) is included here for background. This bi-static system will be used as the basis for the transceiver of the monostatic system developed here.

Transmitter:

The transmitter generates a step waveform (400 V amplitude, 5ns fall time) through the switching action of a power MOSFET. This is radiated by an antenna consisting of a resistively loaded dipole arm driven against a conductive arm, which houses the electronics and batteries. The probe is packaged as a watertight, 1.6 m long probe with a diameter of 32 mm. The resultant spectrum occupied by the transmitted waveform was found to be the best compromise between resolution and range.

Receiver:

The receiver probe comprises batteries, electronics and the same antenna configuration as the transmitter. The signal detected by the antenna is amplified by an analog amplifier section (60 dB gain, 10 – 100 MHz bandwidth) and fed to an 8 bit analog to digital converter (ADC) running at a sample frequency of 250 MHz. The maximum swing of the digitised signal is $1V_{pp}$. The central control of the system is done by a field programmable gate array (FPGA). It controls the synchronization, digitization, data storage on flash memory and communication to personal computer via a Bluetooth® module. The probe housing is similar to that of the transmitter.

Transmitter-receiver link:

Synchronization between receiver and transmitter is achieved by a reinforced optical fibre link between the two probes. It plugs into the two probes through water tight connectors and has a typical length of 3 m. A trigger signal is sent from the FPGA to the transmitter via this optical fibre link, which is immune to coupling from the transmitted pulse and does not influence the radiation pattern of the antennas.

Despite the success of bi-static borehole radars in geophysical imaging of ore bodies, they are not routinely deployed in the mining industry - primarily due to the logistical problems associated with their deployment, which typically entail:

- Making a sensitive optical connection and careful handling of optical fibres in harsh and dusty environments

- Managing a system with total length in excess of 6 m.

The requirement is thus apparent for a monostatic borehole radar: a single, manageable radar probe, no longer than approximately 2 metre, consisting of a synchronized transmitter and receiver sharing a single antenna.

It should be noted that these radars are typically deployed in diamond drilled boreholes of which the core has been extracted and logged. This provides additional information about the area immediately surrounding the borehole and mitigates some of the possible data loss associated with monostatic systems, as discussed in 1.2.1.

No known practical solution has been published in the open literature for the monostatic borehole radar problem. Previous attempts [12], [13] could not achieve the required isolation, spurious free operation and sufficient immunity to varying electromagnetic environments.

The application of borehole radar will be used throughout to verify and evaluate operation of the systems developed in this dissertation. It is assumed that the performance of the GeoMole bi-static system is satisfactory and its specifications are consequently used as the design specifications for the designed monostatic system. The digital control circuitry incorporated into the receiver of this system will further be used, and the transceiver will be designed to interface with the ADC, trigger signal from the central control unit and the power supply.

1.4. Overview of dissertation

A fundamental principle on which this transceiver will be based is the unusual interconnection of the various modules (see Figure 1-3.) It will be discussed extensively in subsequent chapters, but is presented at this stage to put the basic structure of the dissertation into perspective. The general approach adopted in this dissertation is to discuss each of these modules individually. Each module is introduced by a brief discussion of some relevant theory leading to the development of design equations and design principles. These equations and principles will then be applied as general guidelines during the subsequent design of practical electronic circuits that meet the requirements of the eventual transceiver.

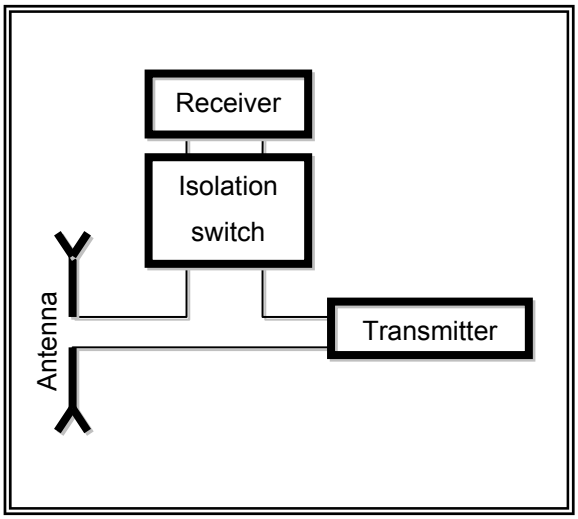

FIGURE 1-3: SYSTEMS LEVEL DIAGRAM OF PROPOSED TRANSCEIVER

The designs will be evaluated through the building and testing of a prototype for each module, specifically developed for application in a monostatic borehole radar system. The developed monostatic borehole radar modules will eventually be integrated and tested through laboratory and field measurements to validate performance of a complete system.

The antennas currently used in borehole radar systems have been extensively researched, including their suitability for a monostatic radar and these antennas will be reviewed in chapter 2 as alternatives for the transceiver developed here. A fundamental requirement for the antenna of this transceiver will be highlighted and a novel measurement technique will be devised to quantify this characteristic.

Chapter 3 will formalize the fundamental principles and requirements for the transmitter module. These will then be applied to develop generic transmitter configurations suitable for the transceiver. Monostatic borehole radar transmitters will be built to evaluate the designs.

In chapter 4, a completely new isolation switch will be developed to fulfil the requirements of this transceiver. The complete design process of such an isolation switch will be discussed, from the required specifications to the electronic implementation. Prototypes specifically designed for application in borehole radar will again be built and tested as proof of concept.

Chapter 5 will introduce a fresh approach to the design of baseband radar receivers and illustrate its application with the design and testing of two borehole radar receiver configurations.

This research culminates with chapter 6, where the different modules developed in the preceding sections are integrated into a complete monostatic borehole radar system. Its operation is verified through laboratory measurements as well as extensive field measurements of various combinations of the developed modules. The chapter will conclude with a recommendation as to the preferred configuration for a monostatic borehole radar, on the basis of the results obtained with the field measurements.

1.5. Original contributions

The following concepts developed in this dissertation are considered original contributions:

- A new technique is developed to characterize the slow response of the current on a borehole radar antenna while deployed down a borehole by means of an *in-situ* measurement system and parameter extraction.

- An electronic circuit to generate a bipolar waveform with the ability to zero out the residual current by adjustment of the waveform symmetry is presented. It has not been published in open literature before.

- This is the first known instance where a pole-zero network is employed to remove the exponentially decaying tail observed in the current flowing on a broadband antenna, even though the basic concept of a pole zero network is well established.

- The isolation switch of chapter 4's principle of operation is a novel concept, as set out in the patent protecting it [14]. The switching signal is separated from the RF signal by using a differential signal path for the RF signal while the switching signals are generated as common mode signals. The resourceful use of both FETs and diodes as switching elements also enables the use of a single control signal.

- An unorthodox interconnection of the various modules employs a transmitter which isolates itself during receive mode, so that a single throw isolation switch can be used to isolate the receiver from the transmitter current, instead of the standard double throw transmit-receive switch.

- Dissipative filtering is argued as a basic principle in the design of high fidelity systems. Equalizers and diplexers are shown to be superior to the commonly used reflective filter networks and it is recommended that they replace the reflective filters as basic filtering elements in these systems.

- The development of what is believed to be the first ever monostatic borehole radar is presented in this dissertation and chapter 6 contains the only known radar images obtained with a monostatic borehole radar system to date.

CHAPTER 2

Antenna evaluation

2.1. Background

2.1.1. Ultra wideband antennas

The approach for designing ultra wideband (UWB) or baseband antennas differ substantially from the classic approach employed for narrowband antennas [15], [16]. The emphasis here is generally on the transient response, since an important parameter in the design of these antennas is the change occurring in the shape of the signal waveform at various stages of radar operation. In the frequency domain, these antennas are designed for large instantaneous bandwidth and aspects that receive particular attention include linear phase characteristics, a constant phase centre and constant gain.

Ground penetrating radar, as an application of baseband radar, introduces further aspects where the design philosophy used for narrowband systems cannot be followed. Propagation of the electromagnetic signal occurs in media which are typically inhomogeneous, even anisotropic, and are generally dispersive [5], [9]. Reflectors can be located in the near field of the antenna and the layered structure of the medium influence the radiation pattern. The proximity of varying media influences the current distribution and the eventual impulse response of the antenna.

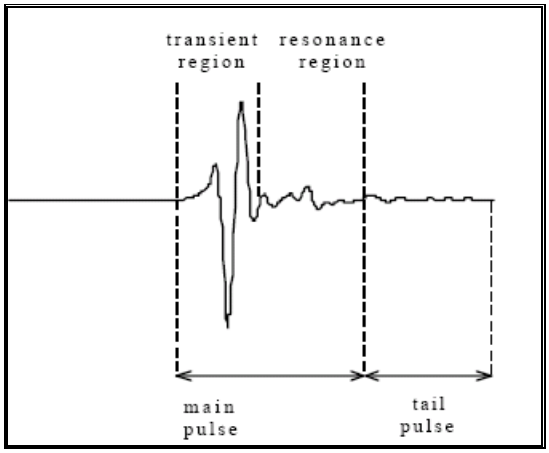

FIGURE 2-1: TIME DOMAIN ANTENNA RESPONSE, FROM [17]

It has been noted [17] that the time domain response of such an antenna can be divided into 2 parts (see Figure 2-1): the main pulse (consisting of the transient region and the resonance region) and the tail pulse. The transient region is related to the radiation of the UWB signal and the resonance region is associated with reflections of the signal on the antenna. The tail is usually an exponential decay and ground penetrating radar antennas are typically designed to minimize the resonance and tail. This partitioning of the response will be adopted for the purpose of the discussion.

Borehole radar is a special form of ground penetrating radar and a brief overview of research on this type of antenna is presented below.

2.1.2. Application: Borehole radar antennas

Claassen [18] proposed an asymmetrical dipole as a practical antenna for a borehole radar system. The proposed antenna consisted of a hollow, conducting arm to house the electronics (either the receiver or the transmitter) and the batteries, while the other arm was loaded with discrete resistors at fixed spacing. Pure resistive loading with values chosen according to the magnitude of a Wu-King [19] loading profile was shown to be preferable to constant impedance loading. It was found that the pulse response of this antenna was satisfactory, with increased efficiency at higher frequencies (although with slight squinting in the radiation pattern.)

Keller [20] investigated the effect of various loading profiles for the loaded arm of the Claassen antenna through simulation. Variations of the Wu-King profile, both resistive and reactive, the Formato profile and other were evaluated and the trade-offs associated with each profile were indicated. It was further recommended that the resistive Wu-King profile be used, but scaled according to the effective permittivity of the surrounding medium.

Van Wyk [21] performed extensive numerical modelling of resistively loaded antennas with both a M*ethod of Moments* (MoM) and a F*inite Difference Time Domain* (FD-TD) formulation. The time domain approach provided insight into the fundamental operation of the antenna. The use of a more sparsely populated loaded antenna was also recommended.

Woods [12] presented a practical solution for the use of a symmetrical antenna in a borehole radar system. Each arm of the dipole consisted of a hollow conducting section followed by a resistively loaded section. The conducting section of one dipole arm housed the electronics, while the other housed the batteries. The feed point was designed to allow for the DC power to be fed through from the battery section to the electronic section, while the two dipole arms could still be accessed by the RF-electronics.

Gouws [22], working in close collaboration with the project described here, focused on optimising the antenna specifically for use in a monostatic borehole radar. The antenna response in various environments (i.e. various borehole diameters, dry, water filled etc.) was simulated with MoM and *Finite Integration Technique* formulations and lumped element equivalent models were extracted for the antenna under these conditions. A resistive-capacitive loading was further recommended for a monostatic borehole radar antenna, instead of the traditional resistive loading.

2.1.3. Interfaces with other modules

The systems level design of the transceiver (Figure 2-2) was already presented in Figure 1-3. It is important to note at this point that due to the series connection of the modules, current flowing on the antenna (be it the transmitter current driving the antenna or the current induced by reflected electromagnetic signals arriving at the antenna) flows through both the isolation switch and the transmitter.

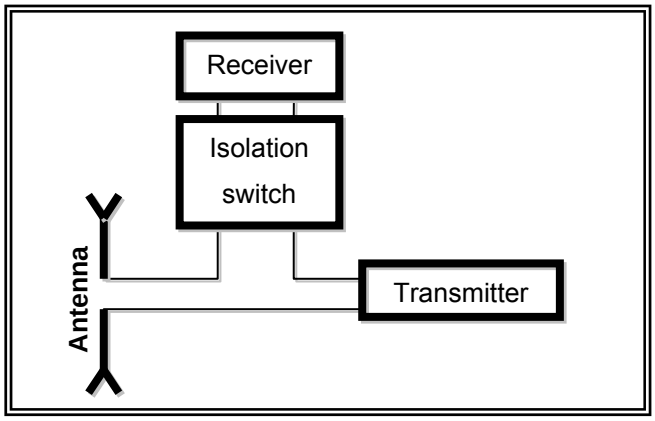

FIGURE 2-2:SYSTEMS LEVEL DIAGRAM OF TRANSCEIVER

The only distinction between transmit-current and receive-current is the time at which they flow and their routing relies on the fact that the isolation switch is a short circuit when transmit-current flows, while the transmitter is a short circuit when receive-current flows. The transmit-current is typically orders of magnitude larger than the receive current for which the receiver is designed and the isolation switch can only switch from its short circuit state when the transmit current has decayed to a sufficiently low amplitude.

The presence of a tail in the typical time domain response of an antenna was highlighted in section 2.1.1 and it is therefore clear that the duration of transmit-current flow is a crucial parameter for the performance of this transceiver. This is heavily dependent on both the transmitter waveform and the antenna's response to the particular waveform.

The approach adopted in this dissertation is to use established antennas and quantify their relevant characteristics to enable the accurate prediction of the antenna response to any transmitter waveform in various environments. This is then assumed as a constant and the transmitter waveform is designed to yield the desired response when driving the antenna.

These established antennas have been researched extensively and have been proven in the field. It can therefore be assumed that their radiation characteristics are adequate. Stated another way, the main pulse of their time domain response (see section 2.1.2), comprising the transient and resonance regions, are satisfactory. The tail in the impulse response has not received much attention and will be investigated here. The approach will be to characterize the antenna's input impedances, which will enable the prediction of their response to various transmitter waveforms.

The antenna is indicated as a balanced device in Figure 2-2, but can be unbalanced as long as either the transmitter or isolation switch is also unbalanced.

2.1.4. Overview of chapter

In line with the approach set out above, this chapter will aim to characterize the impedance of two existing and well documented borehole radar antenna configurations.

The first outcome of this chapter will be equivalent circuits for these antennas in various environments, which can then be used during the design of the transmitter waveforms in the next chapter. The equivalent circuits will facilitate accurate reproduction of the antenna's borehole response while in a controlled laboratory environment. This will also result in the more effective use of the limited opportunities to perform field experiments. The second outcome of this chapter is a practical method to determine the impedance of antennas while deployed in the field. The last outcome is a recommendation as to an antenna to be used for a monostatic borehole radar receiver.

Borehole radar antennas deployed in boreholes are used as basis for this discussion, but the principles should be universally applicable.

A brief overview of the antennas chosen for this study is provided in section 2.2 and represents the implementation of the research mentioned in section 2.1.2. A complete probe is designed in section 2.3 to practically monitor the impedance of these antennas while in a borehole. It discusses the basic concept of operation, the design and calibration of the system. Section 2.4 illustrates the operation of this measurement probe with an example and presents the results obtained in the field.

2.2. Details of antennas used

Both antennas used for this investigation will adopt the asymmetric configuration proposed by Claassen. This is also a practical configuration for use in a monostatic borehole radar system due to the ease with which the electronics can be housed in the hollow conducting arm. The length of the conducting arm will in both cases be 1m, which should be sufficient to house the electronics and batteries of a monostatic borehole radar. Both antennas will be housed in a watertight PVC housing and the only difference between the two is the loading of the one dipole arm.

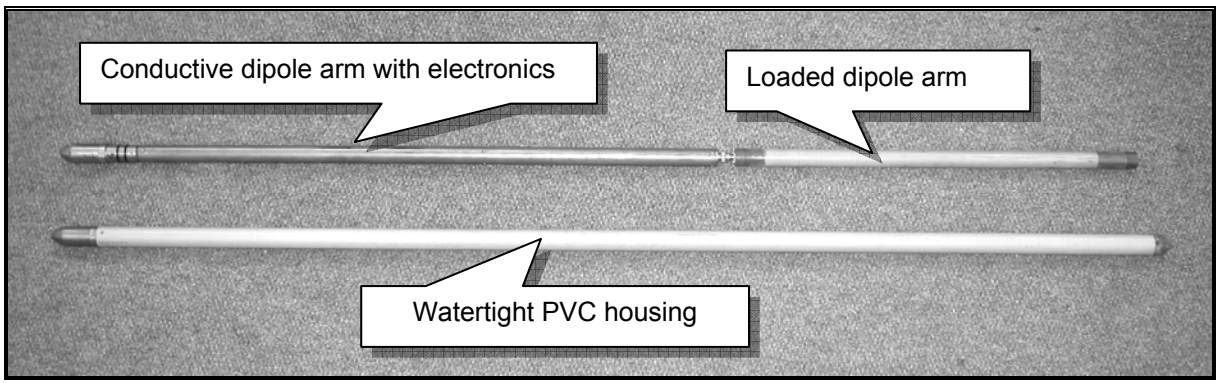

FIGURE 2-3: THE ANTENNA STRUCTURE

2.2.1. The resistively loaded antenna

The first antenna evaluated here uses a 600 mm copper strip with surface mount resistors dispersed along its length to implement the loaded arm of the dipole. The details of the resistive loading are given in Table 2-1. It is housed in a dielectric tube for mechanical support.

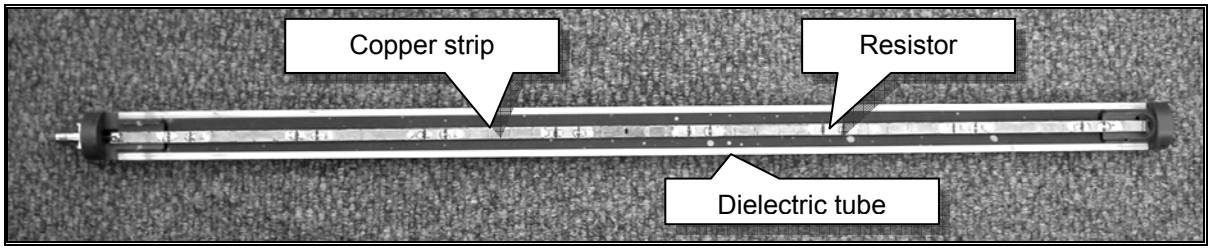

FIGURE 2-4: DETAILS OF LOADED DIPOLE ARM

Position [mm]	25	75	125	175	225	275	325	375	425	475	525	575
Resistor value [Ω]	78	83	94	103	118	136	161	196	248	349	563	1919

TABLE 2-1: LOADING PROFILE FOR RESISTIVELY LOADED ANTENNA

Gouws [22] employed a Foster type 2 method to synthesize the circuit in Figure 2-5 as a lumped element equivalent of antennas typically used in borehole radar systems, such as this one. Note that this equivalent circuit is only valid for the frequency band below the first resonance region, consistent with the range of operation in borehole radar systems.

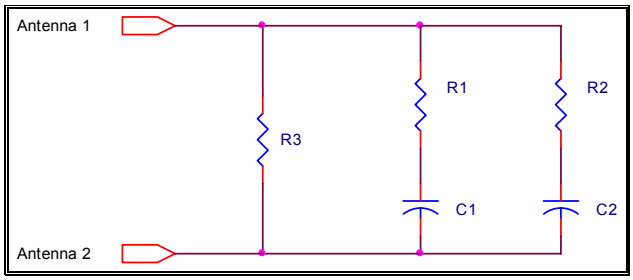

FIGURE 2-5: PROPOSED EQUIVALENT CIRCUIT FOR RESISTIVELY LOADED ANTENNA

The component values for this antenna in various boreholes were further extracted through simulation and his results are summarized in Table 2-2 for air-filled boreholes and in Table 2-3 for water filled boreholes.

Borehole diameter [mm]	R_1 [Ω]	R_2 [Ω]	R_3 [kΩ]	C_1 [pF]	C_2 [pF]
50	181	536	641	3.10	16.0
60	180	520	570	2.57	14.1
75	167	522	523	2.30	12.4
100	151	520	474	2.05	10.7
140	152	528	503	1.83	9.23
200	147	533	539	1.70	8.18

TABLE 2-2: EQUIVALENT CIRCUITS OF RESISTIVELY LOADED ANTENNA IN AIRFILLED BOREHOLES

Borehole diameter [mm]	R_1 [Ω]	R_2 [Ω]	R_3 [kΩ]	C_1 [pF]	C_2 [pF]
50	135	668	45.3	7.90	31.9
60	136	706	51.5	7.70	31.0
75	133	735	69.8	8.53	34.0
100	132	750	107	9.33	37.1
140	127	724	182	10.6	44.1
200	137	711	268	10.4	42.3

TABLE 2-3: EQUIVALENT CIRCUITS OF RESISTIVELY LOADED ANTENNA IN WATERFILLED BOREHOLES

R_3 is an artefact of the synthesis method when performed on band limited data. Its value is in all cases several orders of magnitude larger than the other resistor values and is in disagreement with physical arguments. It will consequently be ignored (assumed to be an open circuit) – as proposed by Gouws [22].

It has been pointed out that the parameters contained in these tables are extremely important in the design of the transmitter. These simulated values will consequently be verified through measurements. This antenna has been used extensively by the bi-static borehole radar system and yielded satisfactory results. It can easily be incorporated into a monostatic borehole radar system.

2.2.2. The resistive-capacitively loaded antenna

Gouws [22] adopted the opposite approach of this dissertation: The transmitter waveform was taken as fixed and the antenna was optimised to minimize the duration of the transmit current. The result was the proposal of a resistive-capacitively loaded antenna, which will be the second antenna evaluated here. A 600 mm copper strip is again used, but a series combination of a surface mount resistor and capacitor are used loading elements. The details of the loading profile are supplied in Table 2-4.

Position [mm]	37.5	112.5	187.5	262.5	337.5	412.5	487.5	562.5
Resistor Value [Ω]	120	142	168	206	265	371	620	1860
Capacitor Value [pF]	39	33	27	22	18	12	8.2	2.2

TABLE 2-4: LOADING PROFILE OF RESISTIVE-CAPACATIVELY LOADED ANTENNA

This antenna lends itself to easy incorporation with a monostatic borehole radar and accurate characterization of its equivalent input impedance is also essential.

2.3. Design of an *in-situ* measurement system

The effect of the environment on the duration of transmit current flow was first proposed and verified qualitatively during field trials performed in a borehole on the farm Rooivlei near Calvinia in the Great Karoo. This drew attention to the need for a quantitative study, in the light of the deleterious effect it will have on the operation of a transceiver like the one designed here.

A probe will now be designed to measure the antenna impedance while it is deployed in a borehole. These results will also serve to verify the simulated values shown in Table 2-2 and Table 2-3. The probe must be similar to a radar probe and deployed down a borehole in a similar fashion, while just recording information regarding the antenna impedance instead of radar data. The data will also be digitised and stored down hole – the only difference between a monostatic borehole radar and this probe will in fact be the replacement of the analog radar transceiver with a module that converts the antenna current to a format suitable for the digital recorder.

2.3.1. Concept of operation

The underlying principle of this measurement system is to drive the antenna with a known step waveform while monitoring the current flowing between the step waveform generator and the antenna. The logarithm of the current is then calculated so that a straight line approximation can be used to extract the component values of a lumped element equivalent RC-circuit of the antenna. This equivalent circuit will then allow for the antenna response to any practical transmitted waveform (provided the frequency content is below the first resonance region) to be predicted and reconstructed.

The emphasis will be on the characteristics of the antenna specifically responsible for prolonged effects, as this is the crucial parameter for the design of the transceiver.

2.3.1.a. Current associated with step waveform

Consider a step waveform with a linear rise time of T_{rise} and amplitude A:

$$V_{step} = \begin{cases} 0 & t<0 \\ \dfrac{A}{T_{rise}}\, t & 0 \le t<T_{rise} \\ A & t \ge T_{rise} \end{cases} \quad \rightarrow \quad (2\text{-}1)$$

Assuming the lumped element equivalent circuit of Figure 2-5, the current flowing after the step transient can be expected to be of the form:

$$i_{TX}(t) = I_1 e^{-\frac{t-T_{rise}}{R_1 C_1}} + I_2 e^{-\frac{t-T_{rise}}{R_2 C_2}}$$

with

$$I_1 = \frac{AC_1}{T_{rise}}\left(1 - e^{\frac{T_{rise}}{R_1 C_1}}\right) \quad \rightarrow \quad (2\text{-}2)$$

$$I_2 = \frac{AC_2}{T_{rise}}\left(1 - e^{\frac{T_{rise}}{R_2 C_2}}\right)$$

This is the sum of two typical exponential decays with time constants governed by the product of the resistor and capacitor value of each of the equivalent circuit's sections. A cursory glance at the simulated resistor and capacitor values in section 2.2.1 reveals that RC time constants between a few hundred picoseconds and about 30 ns can be expected. It is further noted that R_1C_1 is generally an order of magnitude smaller than R_2C_2, so that the tail of the antenna's time domain response is dominated by the R_2C_2 time constant.

$$i_{TX}(t) \approx I_2 e^{-\frac{t - T_{rise}}{R_2 C_2}} \quad \rightarrow \quad (2\text{-}3)$$

R_2 and C_2 are therefore the two unknowns that need to be determined to accurately model the late time section of the current response.

2.3.1.b. *Logarithmic representation*

Accurate measurement of an exponential decay like that of equation (2-3) is quite demanding on the sample rate and dynamic range of a digital measurement system. It is however noted that these constraints can be significantly eased if the logarithm of this function is rather digitised. This is a particularly useful result, since commercial devices exist which approximate this operation. Taking the natural logarithm of the current, equation (2-3) becomes:

$$\ln\left(i_{TX}(t)\right) = \ln\left(I_2\right) - \frac{t - T_{rise}}{R_2 C_2} \quad \rightarrow \quad (2\text{-}4)$$

This can be represented by a straight line, from which the two equations required to determine the two unknowns can be extracted:

$$\ln\left[i_{TX}\left(T_{rise}\right)\right] = \ln\left(I_2\right) = \ln\left(\frac{AC_2}{T_{rise}}\left(1 - e^{\frac{T_{rise}}{R_2 C_2}}\right)\right) \quad \rightarrow \quad (2\text{-}5)$$

and

$$\frac{d}{dt}\left(\ln\left(i_{TX}\right)\right) = -\frac{1}{R_2 C_2} \quad \rightarrow \quad (2\text{-}6)$$

Note that these are only valid after the contribution of the section with the small time constant to I_{TX} (see equation (2-2)) has decayed sufficiently.

2.3.1.c. *Extraction of parameters*

The method for extracting the parameters R_2 and C_2, given the logarithm of the antenna current as data, can be summarized as follows:

1. Fit a straight line to the latter section of the data.
2. Find the slope of the line and determine the product R_2C_2 through equation (2-6).
3. Find the extrapolated value of the data at the time when the step waveform reaches its peak. Substitute this and the calculated value for R_2C_2 into equation (2-5) and determine C_2.
4. Find R_2 by substituting the calculated value of C_2 back into equation (2-6).

2.3.2. Measurement probe

The concept set out above was implemented electronically by a circuit which, at a systems level, appears as in Figure 2-6. The detail circuit diagram can be found in addendum A.

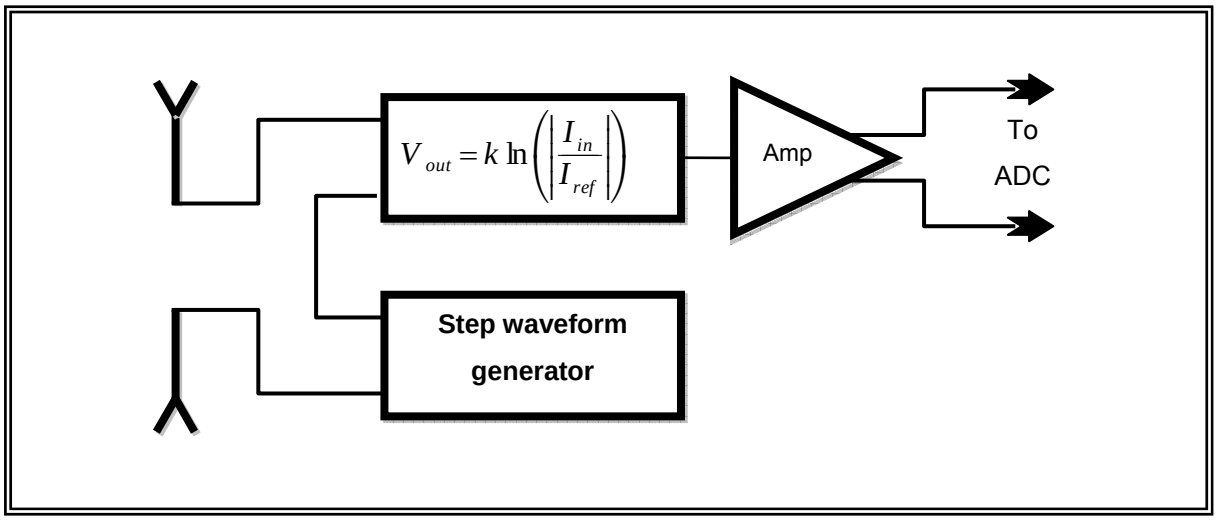

FIGURE 2-6: BLOCK DIAGRAM OF ANTENNA MEASUREMENT PROBE

The step waveform is generated by a MOSFET driver. The operation of determining the logarithm is performed by a commercial device that outputs a current proportional to the logarithm of its input voltage relative to some reference voltage. The input terminals of the device are placed in series with the antenna and step waveform generator with the help of a transformer. A small shunt resistor was placed across the input terminals to convert the current flowing between the step waveform generator and antenna to an input voltage for the device without adding significantly to the impedance of the antenna. An amplifier was added to convert the output current to a voltage and condition it (signal level, bias point etc.) for sensible digitisation by the analog to digital converter.

This system was then incorporated with the antennas described in section 2.2, with the electronics housed in the conducting arm. This probe is in essence a monostatic borehole radar of which the analog transceiver is replaced by the current measurement circuit depicted in addendum A. The batteries and digital control circuitry to be used for the monostatic borehole radar remains unchanged and this measurement circuit interfaces with it at the antenna terminals, power supply, trigger signal and the data output to the ADC. The data stored on the probe will be a digitised representation of the antenna current, in the form:

$$k_1 \ln\left(\left|\frac{I_{TX}}{I_{ref}}\right|\right) \quad \rightarrow \quad (2\text{-}7)$$

The function $\ln\left(I_{TX}\right)$, as used for the extraction of the equivalent circuit in section 2.3.1, can readily be found from this. The characteristics of the step waveform (amplitude and rise time) can be measured with an oscilloscope and synchronized with the eventual data to find the instant when it

reached its maximum (T_{rise} in equation (2-3).) The parameters k_1 (a combination of the logarithmic device's transfer function, the input transformer and resistors as well as the output amplifier) and I_{ref} can be calculated theoretically with the help of datasheet specifications, but should be calibrated.

The process of extracting the values of R_2 and C_2 described in 2.3.1.c was automated by software.

2.3.3. Calibration

2.3.3.a. Step waveform generator

The output of the step waveform generator had to be characterized first – the functioning of this measurement probe relies on the fact that this step output can be accurately approximated by equation (2-1). Although the small output impedance of the MOSFET driver makes the output voltage relatively immune to moderate changes in the load, the waveform while driving various lumped element loads instead of the antenna (within the limits of what can be expected according to Table 2-2 and Table 2-3) were monitored nonetheless. It was found that a step function of the form (2-1), with A = 7.7 and $T_{rise}=6x10^{-9}$ is a fair approximation of the step waveform generator's output .

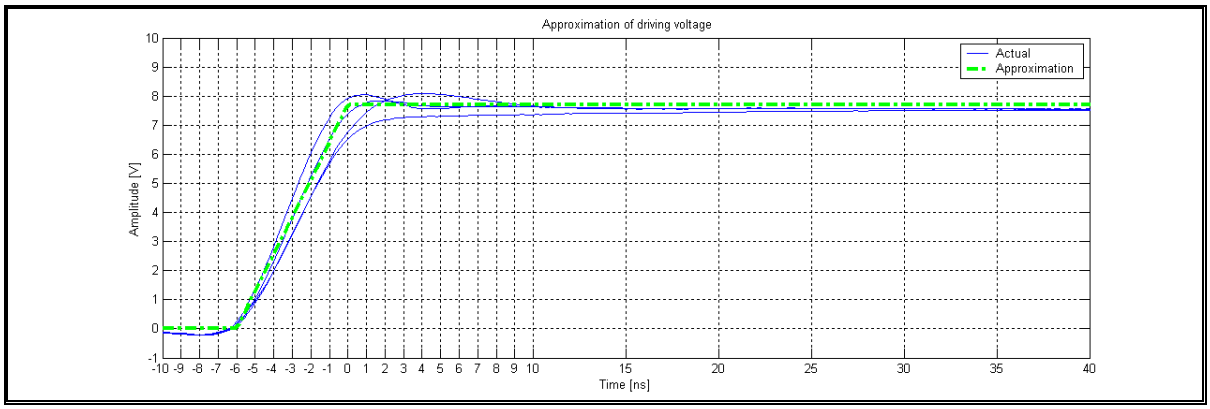

FIGURE 2-7: OUTPUT OF STEP WAVEFORM GENERATOR

2.3.3.b. Logarithmic approximation

The parameters k_1 and I_{ref} associated with the probe's calculation of the logarithm (see equation (2-7)) had to be determined next. Lumped element loads were again used instead of the antenna and an oscilloscope was set up to monitor the actual current flowing into the lumped element loads while the data was acquired. The current measured by the oscilloscope was then substituted into equation (2-7) as I_{TX} and the parameters k_1 and I_{ref} were determined and optimised through comparison with the logged signal. The calibration parameters for the circuit in addendum A were found to be $k_1=120x10^{-3}$ and I_{ref} = 1/6500. Figure 2-8 shows the logged signal together with $120\times10^{-3}\ln\left(\left|6500\,I_{TX}\right|\right)$, where I_{TX} represents the current measured by the oscilloscope, under various load conditions.

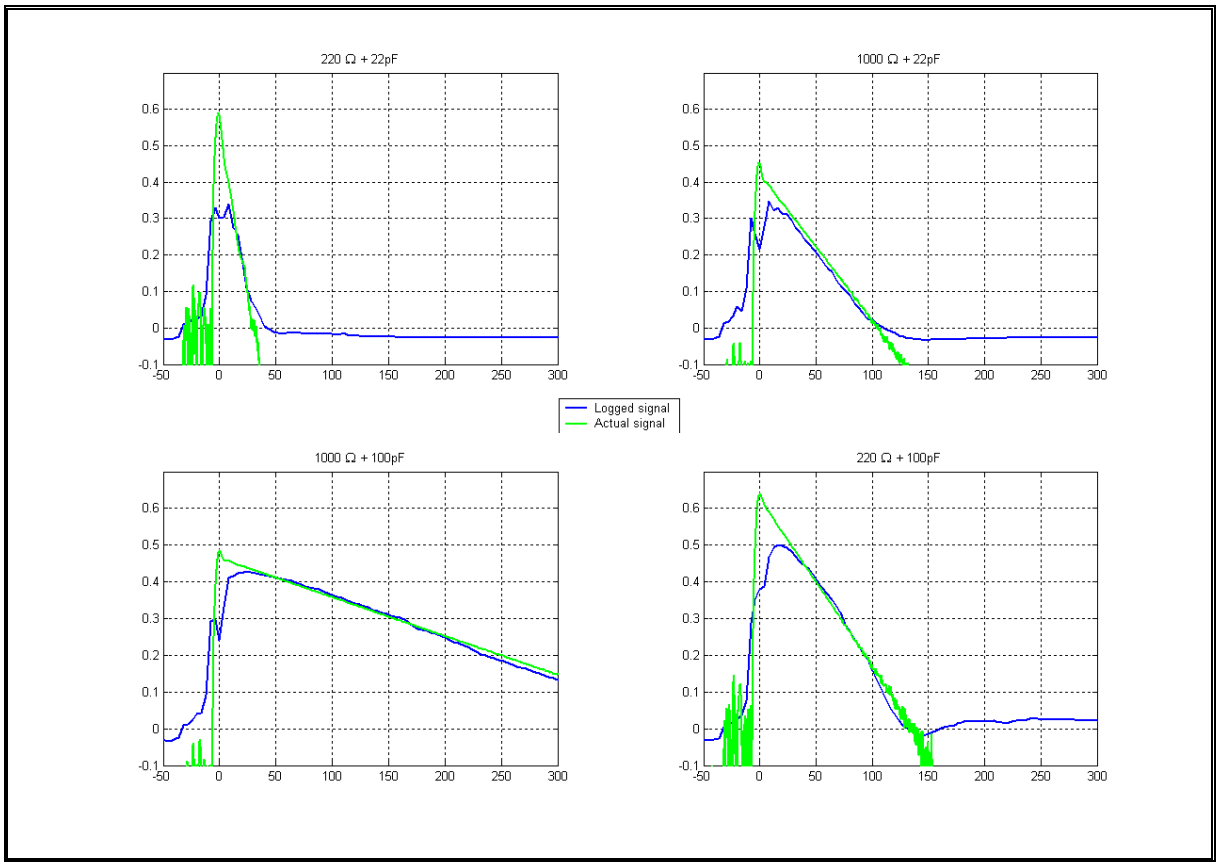

FIGURE 2-8: COMPARISON BETWEEN ACTUAL CURRENT AND LOGGED SIGNAL

2.3.3.c. Verification of extracted parameters

An additional form of calibration can be performed by verifying the extracted lumped element equivalent circuit after the measurement. This is done by replacing the antenna with a physical circuit comprising the calculated R_2 and C_2 and repeating the measurement. The data recorded by the probe should be the same for the field measurement and the measurement performed on the equivalent circuit if the equivalent circuit is accurate. This allows for fine tuning of the equivalent circuit to accurately reproduce the data obtained in the field.

2.4. Equivalent circuits for borehole radar antennas

The process of determining equivalent circuits for antennas in boreholes with this measurement probe will be briefly illustrated through an example, followed by results from experiments in boreholes.

2.4.1. Example

The probe with the resistive antenna was deployed in a 48 mm diameter, water filled borehole and the data was downloaded to a computer. A screen capture of the computer program determining the

lumped element values (as discussed in section 2.3.1.c) is shown during operation. The imported data consists of a number of traces obtained in the borehole – the response did not vary too much. The intercept and slope of the straight line can be adjusted to fit the data. The values for R_2 and C_2 are calculated (using the calibration coefficients of the probe determined earlier) and updated as the parameters of the line are varied.

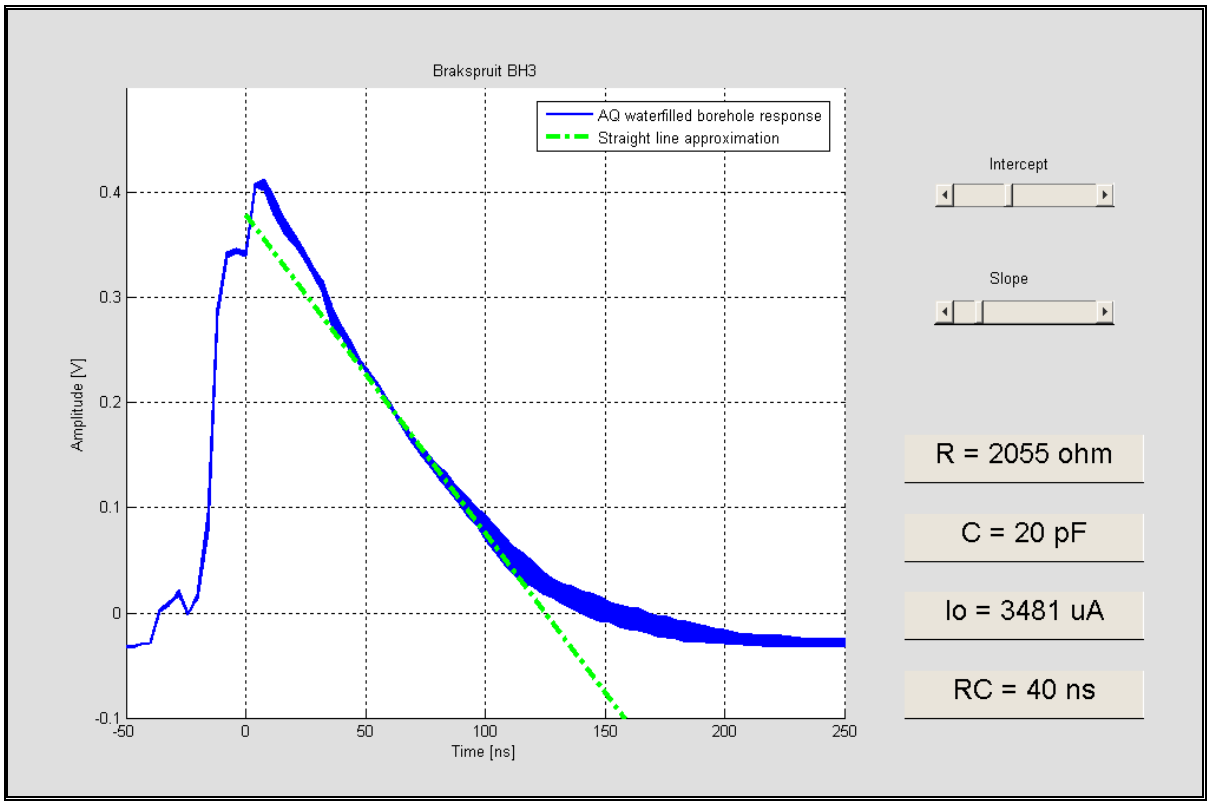

FIGURE 2-9: SCREEN CAPTURE OF COMPUTER PROGRAM CALCULATING R_2 AND C_2 FOR A 48 MM DIAMETER, WATER FILLED BOREHOLE.

The straight line approximation shown above indicates an equivalent circuit with R_2 = 2055 Ω and C_2 = 20pF. Note that the initial response is ignored (as discussed before), as well as the section representing extremely small currents, which are not as accurate. The antenna was then replaced by a lumped element circuit with these values, the measurement repeated in the laboratory and the two datasets compared (as proposed in section 2.3.1.c). The system is remarkably sensitive to component values and fine-tuning of the lumped element circuit revealed that the best approximation was found with R_2 = 2038 Ω and C_2 = 20 pF. The data obtained with this lumped element load and the original data obtained with the antenna in the borehole are compared in Figure 2-10.

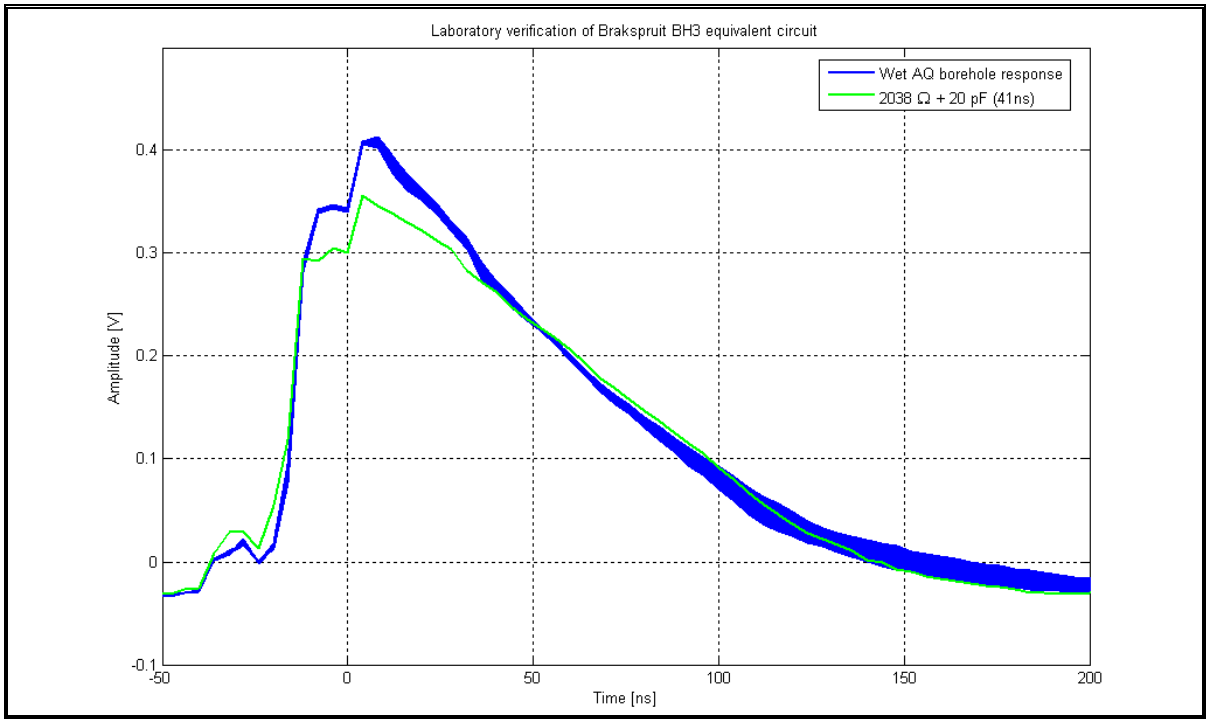

FIGURE 2-10: VERFICATION OF LUMPED ELEMENT EQUIVALENT CIRCUIT

The slow response with the lumped element load is extremely close to that obtained with the antenna in the borehole. It is clear that this model is not accurate in the interval immediately after the step transient, but the technique does not attempt to approximate this early time response.

2.4.2. Results

The component values extracted from the measurements taken in the field are shown below.

Resistive antenna				
Diameter [mm]	**Condition**	**R_2 [Ω]**	**C_2 [pF]**	**R_2C_2 [ns]**
48	Air filled	1897	10	19
48	Water filled	2038	20	41
152	Water filled	1111	25	28
∞	(free air)	3900	3.3	12

TABLE 2-5: LUMPED ELEMENT EQUIVALENT CIRCUITS FOR RESISTIVE ANTENNA, AS OBTAINED WITH MEASUREMENT PROBE

Resistive-capacitive antenna				
Diameter [mm]	**Condition**	**R_2 [Ω]**	**C_2 [pF]**	**R_2C_2 [ns]**
152	Water filled	3300	3.3	7.3
∞	(free air)	3400	2.2	7.5

TABLE 2-6: LUMPED ELEMENT EQUIVALENT CIRCUITS FOR RESISTIVE-CAPACITIVE ANTENNA, AS OBTAINED WITH MEASUREMENT PROBE

The measurements performed here represent the extremes of conditions that can be expected. AQ diamond drilled boreholes [23] are generally the smallest diameter borehole (with a diameter of 48 mm) in which the eventual monostatic borehole radar will be deployed, while the 6" (152 mm) percussion drilled holes are generally the largest diameter holes.

A comparison of the antenna parameters inside and outside a borehole reveals the pronounced effect of the borehole on the resistive antenna. The environment was found to have a minimal effect on the resistive-capacitive antenna however – even between free air and a 152 mm diameter water filled borehole.

These values, although of the same order, do not correspond well with those found by Gouws through simulation (see section 2.2.1.) The water conductivity of the water filled boreholes could unfortunately not be determined and might be a contributing factor. This difference between the measured and simulated results warrants further attention and provides scope for future work.

Although further measurements are required, these values provide a reasonable indication of what can be expected for the component values of the equivalent circuit.

2.5. Synopsis

A novel measurement probe was presented which can perform *in-situ* measurements of the antenna characteristics associated with the tail in their impulse response.

Lumped element equivalent circuits for the frequency range below the first resonance region of the antenna were determined for two borehole radar antennas in various environments. These circuits can be used during the development of the transmitter to predict the antenna response to the designed waveforms, which will typically occupy only the frequency range for which the equivalent circuits are valid.

The two antennas tested here, the resistively loaded and the resistive-capacitively loaded antenna, are both well suited for a monostatic borehole radar probe and transmit waveforms should be designed to drive these antennas in a way suitable for this application. The resistive-capacitively loaded antenna exhibits a response with a faster natural decay of its tail; the resistively loaded antenna has been tested and proven extensively in the field with bistatic systems. Both antennas will be considered for the purpose of this design.

CHAPTER 3

Transmitter design

3.1. Background

3.1.1. Ultra wideband transmitters

The design of ultra wideband transmitters is closely linked to the ability to generate fast switching transients with high instantaneous power [4]. The output of such a switching element is typically used directly for transmitters where pulse shape is not that important. The added complexity of pulse shaping topologies in the transmitter and associated deconvolution in the receiver is however justified in certain applications; the reason might be linked to the characteristics of the transducer (antenna) being driven or requirements on the received signal. Switching can be done with a large variety of devices such as spark gaps, semiconductors (normal switching or in avalanche mode [24]) and photoconductive switches, while pulse shaping can be performed with devices such as transmission lines, magnetic switches and step recovery diodes, [25], [26], [27].

3.1.2. Application: Borehole radar system

The transmitter of a typical bi-static borehole radar system [11] employs a basic MOSFET configuration to generate a switching transient and applies it to an antenna. The transient created is a single falling edge with a typical duration of 5 nanoseconds. The transmitter antenna is not used for the rest of the pulse repetition interval, so the only requirement during this interval is for the voltage and current of the transmitter to return to the steady state condition in time for the next transmitter transient. Pulse shaping is minimal and centres on generating a waveform with fall time rapid enough to achieve the desired bandwidth.

3.1.3. Interfaces with other modules

Figure 3-1 (repeat of Figure 1-3) is a systems level diagram of the complete transceiver to be developed here, indicating the interconnection of the various modules. This already reveals important fundamental issues to be considered in the design of a monostatic radar.

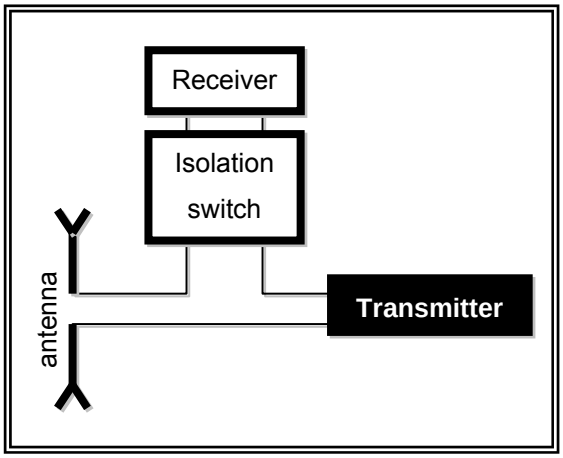

FIGURE 3-1:SYSTEMS LEVEL DIAGRAM OF TRANSCEIVER

The transmitter supplies pulse power to the system during the transmit mode. It must ideally also present a short circuit at its output port during the acquisition time of the receiver (receive mode), when it effectively appears in series between the antenna terminals and the receiver terminals (isolation switch is in through-mode.)

According to this argument, the required transmitter configuration is defined as a voltage source. Current flowing between the antenna and the transmitter will necessarily flow through the input port of the isolation switch as well and eventually into the receiver when the isolation switch changes over to through-mode. This current might push the receiver into its non-linear mode of operation and blind the system. No current associated with the transmitter should ideally flow when the isolation switch is in through-mode (i.e. the current should return to zero as soon as possible after the transient.) This control over current is not a characteristic of a voltage source.

Devices meeting all these requirements have been described as having a time limited impulse response (TLIR) [3] and can be achieved by matching the waveform to the load (antenna in this case). This system is therefore in the class of UWB transmitters that require pulse shaping.

The output should only be differential if the transducer is a differential device, such as a dipole antenna.

3.1.4. Overview of chapter

A number of general principles will be presented in the next section to serve as guidelines for the design of such a transmitter module. Two generic modules will then be designed in the following sections, using these principles. Prototypes of these modules will be purpose-built to meet the requirements of the borehole radar system and will be evaluated as such.

3.2. Basic concepts

3.2.1. Time domain waveform

Waveforms typically employed for UWB systems include unipolar pulses, monocycles, polycycles or coded versions of the aforementioned [4]. It has been shown in the previous section that the transmitter must function as a voltage source with low output impedance. The resultant current when driving a typical load must ideally have a time limited impulse response as well.

3.2.1.a. Voltage-current relationship

It was shown in the previous chapter that a typical borehole radar antenna can be represented in the low frequency regime by two parallel sections, each comprising a series combination of a resistor and capacitor.

The current flowing in such a section (see Figure 3-2) in response to an applied voltage can be expressed by

$$i_{in}(t) = h(t) * v_{in}(t) \quad \rightarrow \quad (3\text{-}1)$$

where the transfer function is given by

$$h(t) = \frac{1}{R}\left(\delta(t) - \frac{1}{RC}\, e^{-\frac{t}{RC}}\right) \ldots \text{for } t>0 \quad \rightarrow \quad (3\text{-}2)$$

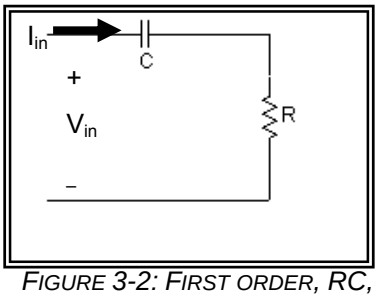

FIGURE 3-2: FIRST ORDER, RC, HIGH PASS STRUCTURE

The current flowing in response to various input signals can thus be calculated as

$$i_{in}(t) = \int_{-\infty}^{\infty} h(\lambda)\, v_{in}(t-\lambda)\, d\lambda$$

$$i_{in}(t) = \frac{v_{in}(t)}{R} - \frac{1}{R^2 C} \int_{0}^{\infty} e^{-\frac{\lambda}{RC}}\, v_{in}(t-\lambda)\, d\lambda \quad \rightarrow \quad (3\text{-}3)$$

v_{in} is causal and will return to zero after a finite duration T for pulse systems, so that

$$i_{in}(t) = \begin{cases} 0 & \ldots t<0 \\ i_{in}(t) = \dfrac{v_{in}(t)}{R} - \dfrac{1}{R^2 C} \displaystyle\int_{0}^{t} e^{-\frac{\lambda}{RC}}\, v_{in}(t-\lambda)\, d\lambda & \ldots 0 \le t \le T \\ i_{in}(t) = 0 - \dfrac{1}{R^2 C} \displaystyle\int_{t-T}^{t} e^{-\frac{\lambda}{RC}}\, v_{in}(t-\lambda)\, d\lambda & \ldots t>T \end{cases} \quad \rightarrow \quad (3\text{-}4)$$

The current must equate to zero at t > T in systems with a time limited response. $e^{-\frac{\lambda}{RC}}$ is positive throughout the interval, implying that v_{in} must at least have a positive and negative swing in the interval 0 ≤ t ≤ T for the integral defining the response at t > T to be zero.

The following progression of ideal waveforms will be used to illustrate this derivation.

3.2.1.b. Step

A step waveform with infinitely short rise time and amplitude A (positive value) can be expressed piecewise as:

$$v_{in}(t) = \begin{cases} 0 & t<0 \\ A & t \geq 0 \end{cases} \quad \rightarrow \quad (3\text{-}5)$$

Note that this waveform is positive throughout and the duration (T) is not defined. The resulting current into the RC-load is calculated as:

$$i_{in}(t) = \begin{cases} 0 & t<0 \\ \frac{A}{R} e^{-\frac{t}{RC}} & t \geq 0 \end{cases} \quad \rightarrow \quad (3\text{-}6)$$

An example is depicted in Figure 3-3 with A=1, R=1 and C=1.

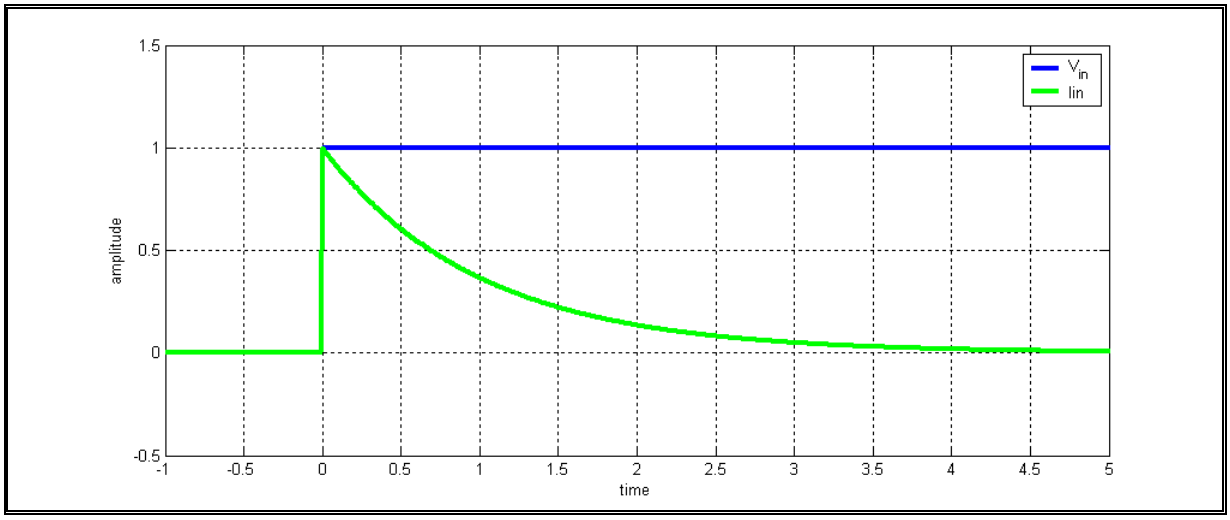

FIGURE 3-3: STEP VOLTAGE DRIVING RC-LOAD

The decay of the current after the transient is exponential from its maximum value to zero, governed by the load. This response is clearly not time limited.

3.2.1.c. Unipolar pulse

A natural evolution is to consider a perfectly square pulse with positive amplitude A and width T_1 given by:

$$v_{in}(t) = \begin{cases} 0 & t<0 \\ A & 0 \leq t \leq T_1 \\ 0 & t>T_1 \end{cases} \quad \rightarrow \quad (3\text{-}7)$$

This will cause the following current to flow into the RC load:

$$i_{in}(t)=\begin{cases} 0 & t<0 \\ \frac{A}{R}e^{-\frac{t}{RC}} & 0\le t\le T_1 \\ \frac{A}{R}e^{-\frac{t}{RC}}\left[1-e^{\frac{T_1}{RC}}\right] & T_1<t \end{cases} \quad \rightarrow \quad (3\text{-}8)$$

An example with A=1, R=1, C=1 and T_1 varied between 0.25 and 2, is included as illustration in Figure 3-4.

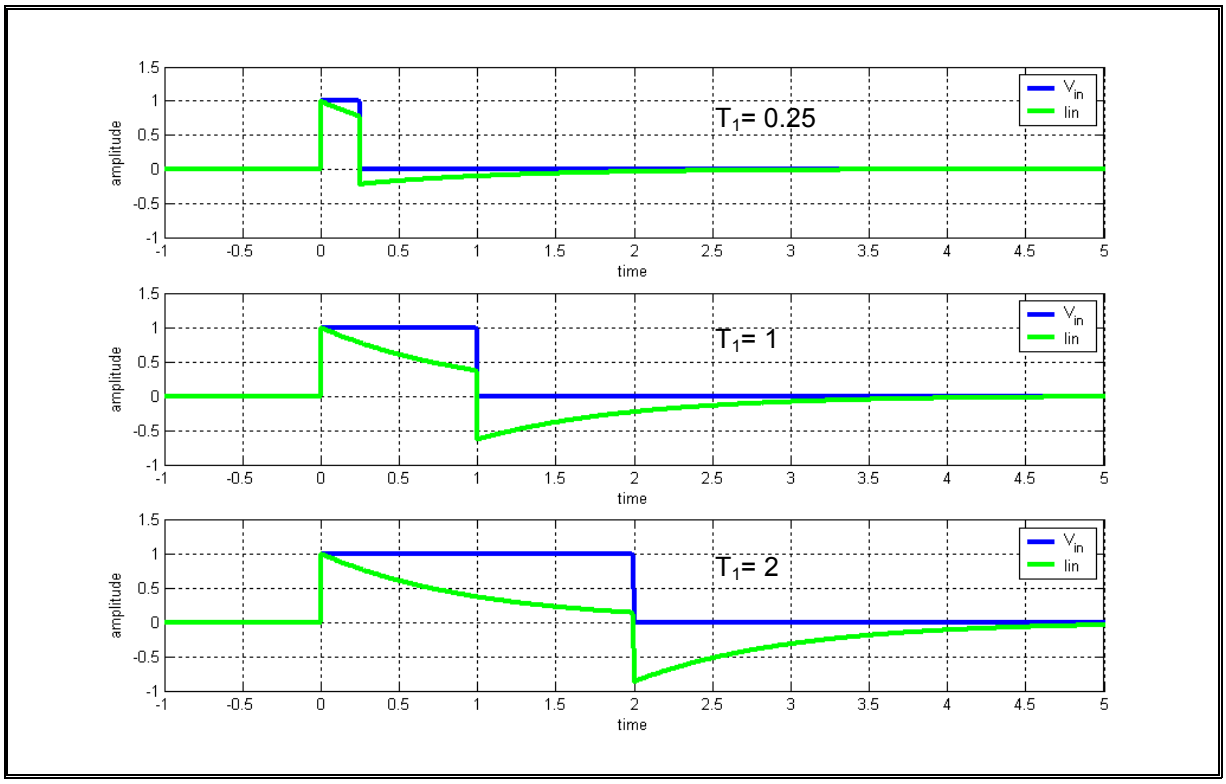

FIGURE 3-4: UNIPOLAR VOLTAGE DRIVING RC-LOAD

The current recovery is again exponential, although the amplitude can be varied through adjusting the pulse width. The current will only be time limited in the ideal case where the pulse is infinitely short ($T_1 \rightarrow 0$).

3.2.1.d. Bipolar pulse

The next step is to consider a bipolar pulse defined as (A, B are positive):

$$v_{in}(t)=\begin{cases} 0 & t<0 \\ A & 0\le t\le T_1 \\ -B & T_1<t\le T_2 \\ 0 & t>T_2 \end{cases} \quad \rightarrow \quad (3\text{-}9)$$

This is a waveform with both a positive and negative swing, as required for a time limited response. The current can be calculated as

$$i_{in}(t)=\begin{cases} 0 & t<0 \\ \frac{A}{R}e^{-\frac{t}{RC}} & 0\le t\le T_1 \\ \left[\frac{A}{R}-\frac{B}{R}e^{\frac{T_1}{RC}}-\frac{A}{R}e^{\frac{T_1}{RC}}\right]e^{-\frac{t}{RC}} & T_1<t\le T_2 \\ \left[\frac{A}{R}-\frac{A}{R}e^{\frac{T_1}{RC}}-\frac{B}{R}e^{\frac{T_1}{RC}}+\frac{B}{R}e^{\frac{T_2}{RC}}\right]e^{-\frac{t}{RC}} & T_2<t \end{cases} \quad \rightarrow \quad (3\text{-}10)$$

and an example is shown in Figure 3-5 for A=1,B=1, R=1, C=1, T_2=1 and T_1 varied.

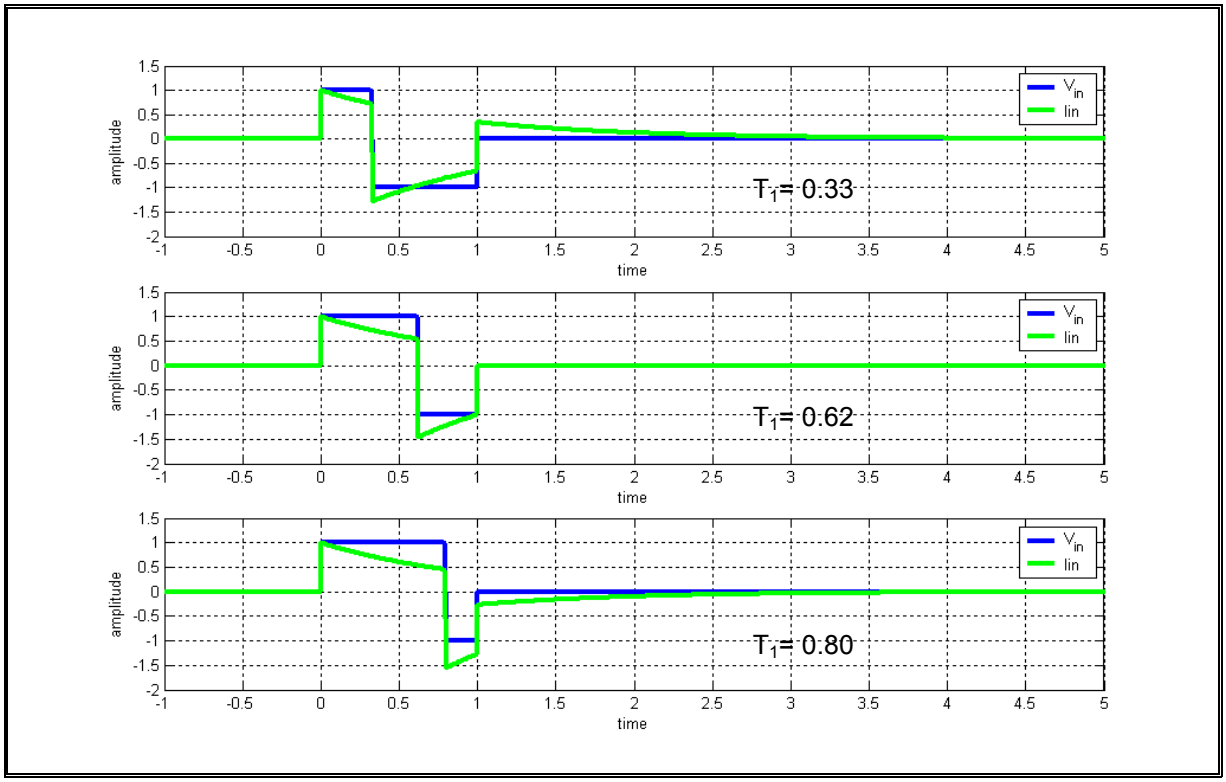

FIGURE 3-5: BIPOLAR VOLTAGE DRIVING RC-LOAD

It is clear that a careful choice of T_1 and T_2, together with A and B, can result in the current to be zero at t > T_2 when driving an RC load– as shown in the middle response of Figure 3-5.

3.2.1.e. Conclusion

Given a transmitter voltage waveform of finite duration T, it should in general be bipolar for the current response (when driving an RC-load) to be time limited. The waveform (v_{in}) should, more specifically, satisfy the equation

$$\int_{t-T}^{t} e^{-\frac{\lambda}{RC}} v_{in}(t-\lambda)\,d\lambda = 0 \quad \ldots \text{for } t>T \quad \rightarrow \quad (3\text{-}11)$$

It should be noted that the ideal waveform described by this equation is still dependent on the slow time constant of the load, with the RC term still appearing in the equation. The faster time constants can typically be ignored, since their contribution to the total antenna current would have reached a

sufficiently low value when the isolation switch changes over to transmission mode. Sensitivity to variations in the load should be considered when the waveform is designed.

3.2.2. Frequency domain waveforms

The choice of frequency spectrum occupied by an UWB transmitter waveform is a trade-off between range and resolution [28]. It can be expected that low frequencies will achieve longer range, while higher frequencies provide more resolution. Using an ultra wideband signal attempts to tap into the advantages of both. The lower end of the frequency spectrum is further limited by the physical constraints (a larger antenna is required.)

The ideal waveform, when considered in the frequency domain, should therefore have maximum occupation of the desired frequency spectrum. This spectrum ranges from the lower limit of the antenna to the maximum frequency that provides the required resolution with sufficient range.

3.2.2.a. Spectra

Waveforms similar to those considered in the previous section will now be evaluated on their spectra. The idealized, infinitely short transitions will however be replaced by more realistic sine and cosine based edges. This is to simplify the frequency domain expressions calculated analytically with the Fourier transform and to make the interpretation clearer.

	Time domain expression	Frequency domain expression
Step	$v_{step}(t)=\begin{cases} 0 & t<0 \\ 1-\cos\left(2\pi f_0 t\right) & 0<t<\frac{1}{2f_0} \\ 1 & t>\frac{1}{2f_0} \end{cases}$	$V_{step}(f)=\frac{f_0^2 e^{\frac{-j\pi f}{2f_0}}}{j\pi f\left(f_0^2-f^2\right)}\cos\left(\frac{\pi f}{2f_0}\right)$
Unipolar pulse	$v_{unip}(t)=\begin{cases} 0 & t<0 \\ 1-\cos\left(2\pi f_0 t\right) & 0<t<\frac{1}{f_0} \\ 0 & t>\frac{1}{f_0} \end{cases}$	$V_{unip}(f)=\frac{f_0^2 e^{\frac{-j\pi f}{f_0}}}{\pi f\left(f_0^2-f^2\right)}\sin\left(\frac{\pi f}{f_0}\right)$
Bipolar pulse	$v_{bip}(t)=\begin{cases} 0 & t<0 \\ \sin\left(2\pi f_0 t\right) & 0<t<\frac{1}{f_0} \\ 0 & t>\frac{1}{f_0} \end{cases}$	$V_{bip}(f)=\frac{je^{\frac{-j\pi f}{f_0}}}{\pi\left(f_0^2-f^2\right)}\sin\left(\frac{\pi f}{f_0}\right)$

TABLE 3-1: FOURIER TRANSFORMS OF THEORETICAL TRANSMITTER WAVEFORMS

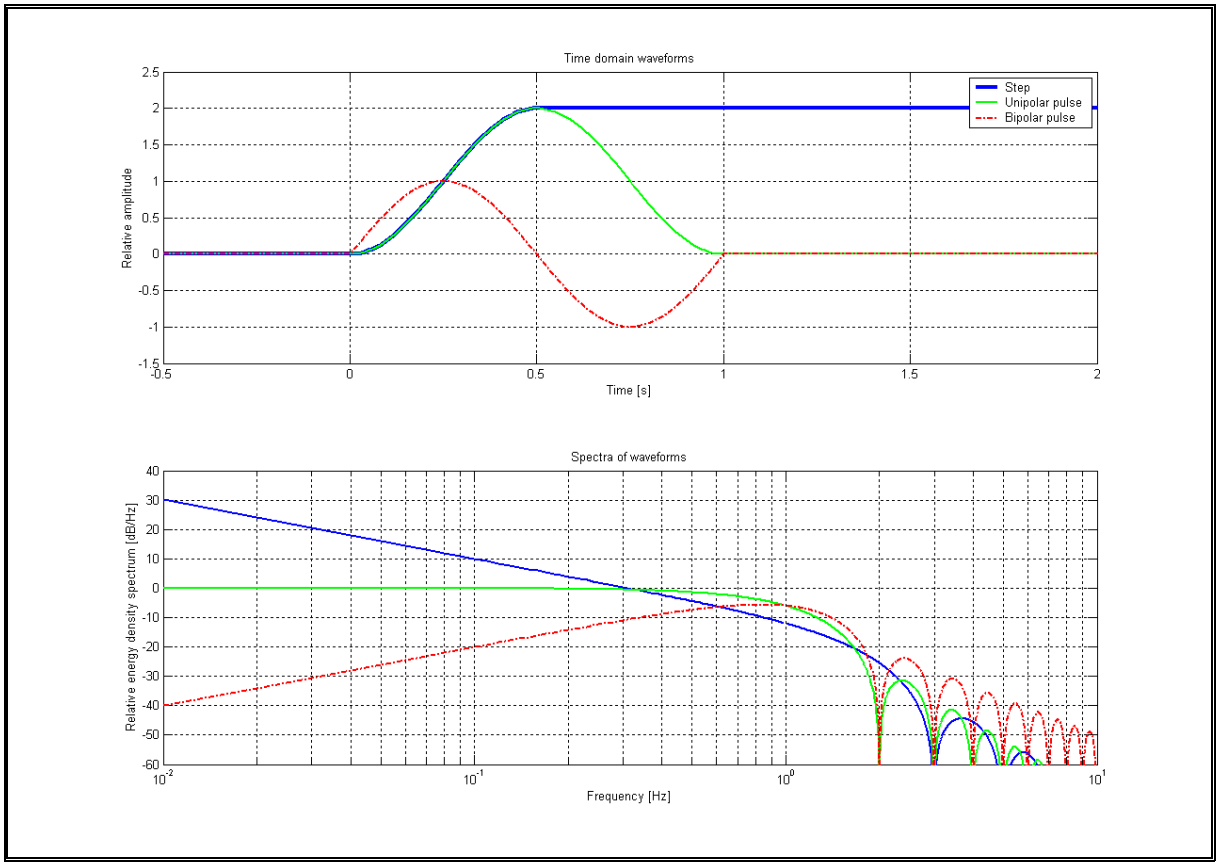

FIGURE 3-6: THEORETICAL TRANSMITTER WAVEFORMS: TIME DOMAIN AND FREQUENCY DOMAIN

Step:

The spectrum of the step function has a maximum at DC and decreases to its first zero at $3f_0$, which is equivalent to $1.5/T_{rise}$ (with T_{rise} the rise time from 0 to an amplitude of 2). More formally, the zeros are located at the following frequencies:

$$f = f_0(1+2n) \quad \ldots n \in \{1,2,3,\ldots\} \qquad \rightarrow \quad (3\text{-}12)$$

The advantage of this waveform (apart from being easy to generate) is that the first zero is at a high frequency for a given rise time. The bulk of its frequency content is however towards its lower end, where the antenna becomes inefficient and a large portion of the generated energy can consequently not be radiated.

Unipolar pulse:

The unipolar pulse has its maximum at DC, but the spectrum remains relatively flat up to its first zero at $2f_0$, equivalent to $1/T_{rise}=1/T_{fall}$ (with T_{rise} the rise time from 0 to 2 and T_{fall} the fall time from 2 to 0.) The zeros are located at:

$$f = nf_0 \quad \ldots n \in \{2,3,4,\ldots\} \qquad \rightarrow \quad (3\text{-}13)$$

If f_0 can be made significantly higher than the top end of the desired spectrum, this waveform can deliver an extremely flat spectrum across the desired band. It does however still contain significant energy towards DC, which cannot be radiated.

Bipolar pulse:

This waveform is commonly referred to as a monocycle and is extensively used in ground penetrating radar [29]. The maximum of this function's spectrum is at f_0, or $1/T_0$ (the period of the single sine cycle) and the zeros are on those of the unipolar pulse, except for an extra zero at DC:

$$f = nf_0 \quad \ldots n \in \{0,2,3,4,\ldots\} \qquad \rightarrow \quad (3\text{-}14)$$

This function has more power in the section of the spectrum surrounding f_0, compared to the other waveforms. The frequency content decreases towards zero enabling it to be matched to the radiation capabilities of the antenna used.

3.2.2.b. Conclusion

The relationship between the characteristic times associated with waveforms and their frequency spectrum has been presented and is intended as guidance during the design of the time domain waveform. Although all the waveforms have their advantages, the monocycle (a special form of the bipolar signal from the previous section) again appears to be the most suitable.

3.2.3. Tail cancellation with pole-zero networks

The output of detectors in nuclear instrumentation [30], is generally characterized by a sharp rise time of a few nanoseconds, followed by slow decay of typically a few hundred microseconds. This limits the system's ability to resolve individual events at high repetition rates. The pole-zero network of Figure 3-7 was consequently developed [31] to cancel the long "tail" and enable higher counting rates.

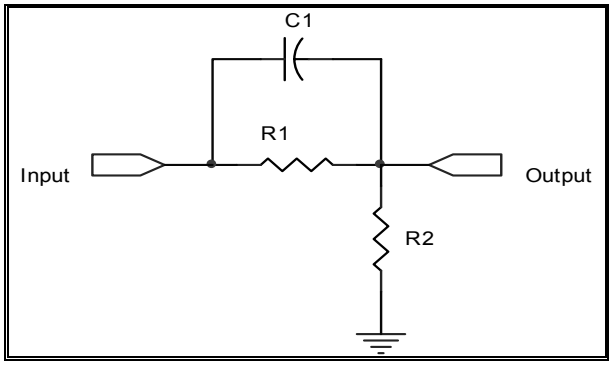

FIGURE 3-7: POLE-ZERO NETWORK PROPOSED BY BOIE [31]

3.2.3.a. Development of pole-zero network

A similar approach will now be adopted to develop a pole zero network to cancel the long tail observed in the current flowing between the antenna and transmitter through the (short circuited at that time) input of the isolation switch when the requirements highlighted in section 3.2.1.e are not met. The following generic network is proposed as the pole zero network:

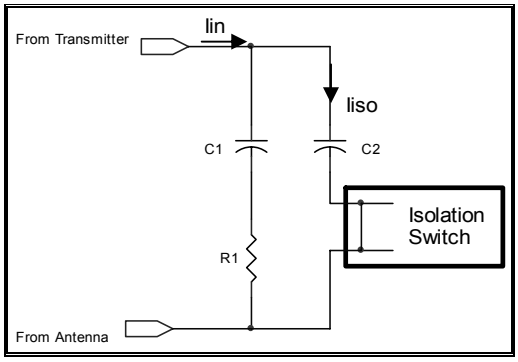

$$I_{iso}(s) = I_{in}\frac{s+\frac{1}{R_1C_1}}{s+\frac{1}{R_1C_1}+\frac{1}{R_1C_2}} \quad \rightarrow \quad (3\text{-}15)$$

FIGURE 3-8: PROPOSED POLE-ZERO NETWORK

It was found in section 3.2.1 that the general form of the input current flowing from a transmitter to a load comprising two of the sections in Figure 3-2 in parallel, is given by the following equation after the transmitter transient has completed.

$$I_{in}(s) = \frac{A}{s+\frac{1}{\tau_1}} + \frac{B}{s+\frac{1}{\tau_2}} \quad \rightarrow \quad (3\text{-}16)$$

with τ_1 a short time constant and τ_2 the undesired long time constant.

If it is assumed that the pole-zero network's effect on the current I_{in} is negligible (discussed later), the current flowing through the isolation switch is then found by substituting equation (3-16) into (3-15):

$$I_{iso}(s) = A\frac{s+\frac{1}{R_1C_1}}{\left(s+\frac{1}{R_1C_1}+\frac{1}{R_1C_2}\right)\left(s+\frac{1}{\tau_1}\right)} + B\frac{s+\frac{1}{R_1C_1}}{\left(s+\frac{1}{R_1C_1}+\frac{1}{R_1C_2}\right)\left(s+\frac{1}{\tau_2}\right)} \quad \rightarrow \quad (3\text{-}17)$$

By choosing R_1 and C_1 of the pole-zero network so that $R_1C_1 = \tau_2$, the pole at $-1/\tau_2$ is cancelled

$$I_{iso}(s) = \frac{A\left(s+\frac{1}{R_1C_1}\right)}{\left(s+\frac{1}{R_1C_1}+\frac{1}{R_1C_2}\right)\left(s+\frac{1}{\tau_1}\right)} + \frac{B}{s+\frac{1}{R_1C_1}+\frac{1}{R_1C_2}} \quad \rightarrow \quad (3\text{-}18)$$

A partial fraction expansion of this yields:

$$I_{iso}(s) = \frac{a}{s+\frac{1}{\tau_1}} + \frac{b}{s+\frac{1}{R_1C_1}+\frac{1}{R_1C_2}} + \frac{B}{s+\frac{1}{R_1C_1}+\frac{1}{R_1C_2}}$$

with

$$a = A\frac{\frac{1}{R_1C_1}-\frac{1}{\tau_1}}{\frac{1}{R_1C_1}+\frac{1}{R_1C_2}-\frac{1}{\tau_1}} \quad \rightarrow \quad (3\text{-}19)$$

$$b = A\frac{\frac{1}{R_1C_2}}{\frac{1}{R_1C_1}+\frac{1}{R_1C_2}-\frac{1}{\tau_1}}$$

The value of C_2 and the individual values of C_1 and R_1 (the R_1C_1 product has already been chosen) can then be chosen so that:

$$b = -B$$

$$A\frac{\frac{1}{R_1C_2}}{\frac{1}{R_1C_1}+\frac{1}{R_1C_2}-\frac{1}{\tau_1}} = -B \quad \Rightarrow \quad (3\text{-}20)$$

The response then simplifies to:

$$I_{iso}(s) = \frac{a}{s+\frac{1}{\tau_1}} \quad \Rightarrow \quad (3\text{-}21)$$

This translates to a time domain signal of:

$$i_{iso}(t) = a\,e^{-\frac{t}{\tau_1}} \quad \Rightarrow \quad (3\text{-}22)$$

Note that the following restrictions further exist on the elements of the pole-zero network:

- It was assumed at the start of this derivation that the pole-zero network does not have a significant effect on the total current flowing on the antenna (I_{in}). For this assumption to be valid, C_2 must be sufficiently larger than the typical capacitor values of the equivalent antenna models. This also prevents the possible degradation in transmitted power and spectrum.
- The impedance of the series combination of R_1 and C_1 must be large enough compared to the input impedance of the isolation switch when in transmission mode, as not to shunt received power away from the isolation switch and receiver.

3.2.3.b. Simulation

The operation of the pole-zero network developed in the preceding section will now be verified through simulation in Advanced Design System (ADS) from Agilent Technologies. The setup used is shown in Figure 3-9. The network is driven by two exponentially recovering current sources, one being 10 times smaller and 10 times slower than the other so that the parameters (using the notation of the discussion above) are: A=1, B=0.1, τ_1=1, τ_1=10. The values of C_1,C_2 and R_1 were chosen according to the discussion above.

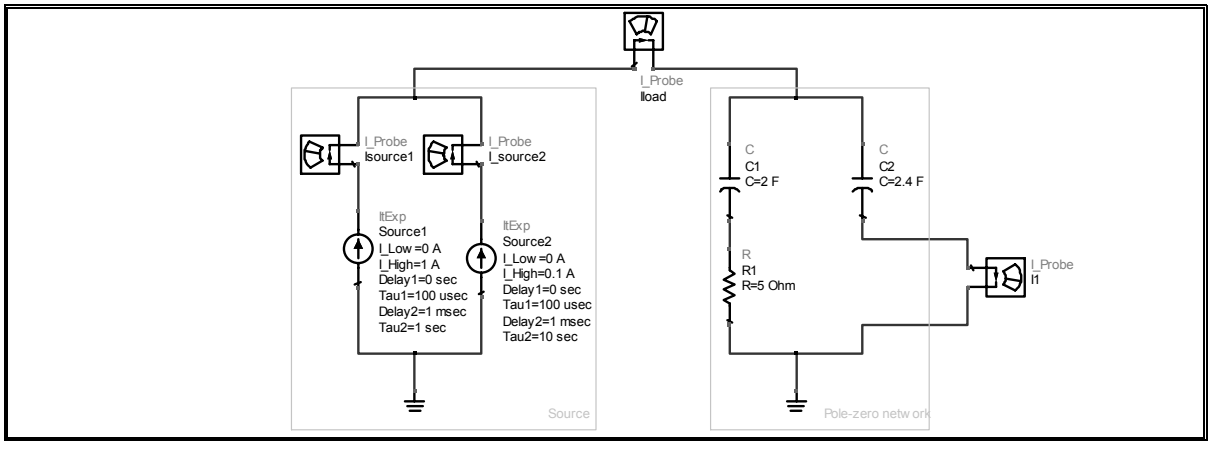

FIGURE 3-9: SETUP USED TO EVALUATE THE POLE-ZERO NETWORK THROUGH SIMULATION

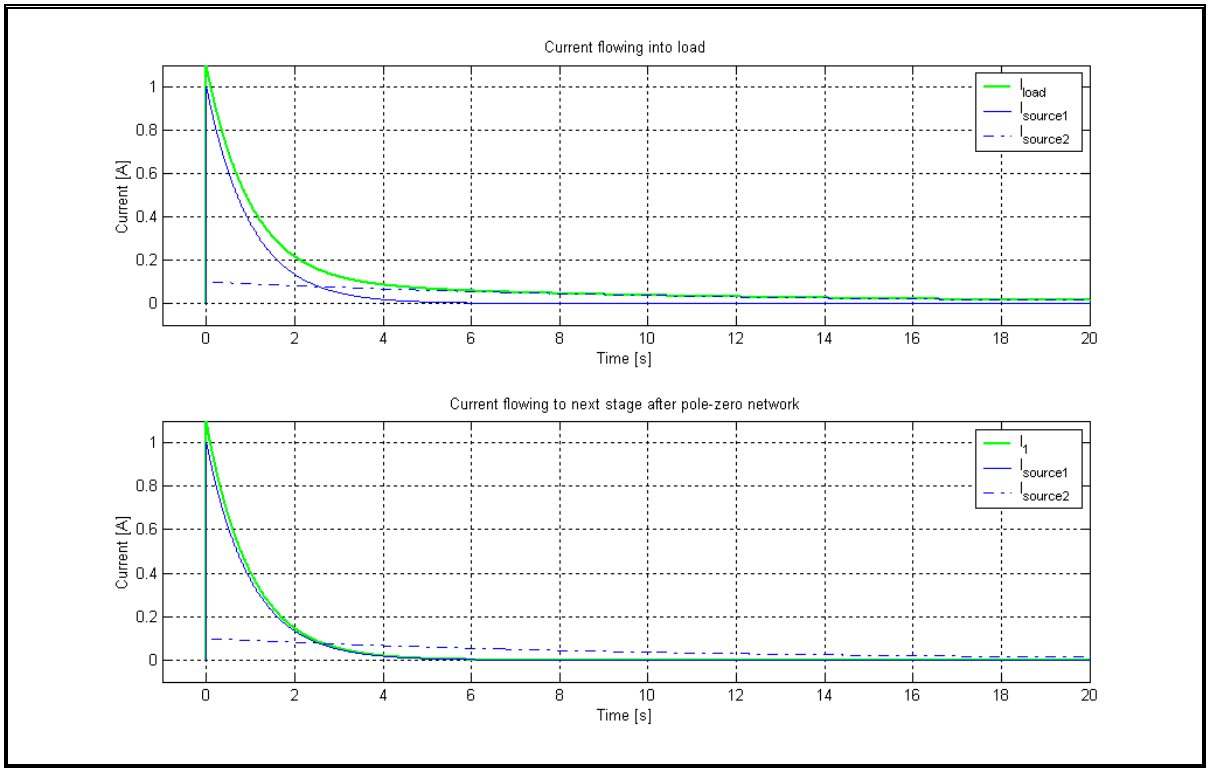

FIGURE 3-10: SIMULATED CURRENTS OF POLE-ZERO NETWORK

The total input current (Figure 3-10) is the sum of the two current sources and consequently contains a slowly recovering and quick recovering component. The output current of the pole-zero network closely follows that of the quick recovering component, with only a slight change in amplitude.

3.2.3.c. Conclusion

It is possible to cancel the pole responsible for the slow recovery of the antenna current, when driven with a non-ideal voltage waveform, with the pole-zero network proposed in this section.

This network is however still load dependent and sensitivity to variations in the load should be evaluated if this technique is to be used. This technique also assumes that the exact characteristics of the total antenna current are known, which is unfortunately not necessarily the case. It might therefore rely heavily on approximations such as the lumped element equivalent circuits developed in the previous chapter and on eventual fine tuning.

3.2.4. Differentiation of waveform

The radiated electric far field for an electrically small dipole antenna is proportional to the time delayed derivative of the current flowing on the antenna [6, p 546]. A more specific study on a Wu-King dipole's response to a Gaussian pulse [32] using a FDTD analysis yielded results that support this assumption.

The ideal currents calculated in section 3.2 have been differentiated as illustration of this concept.

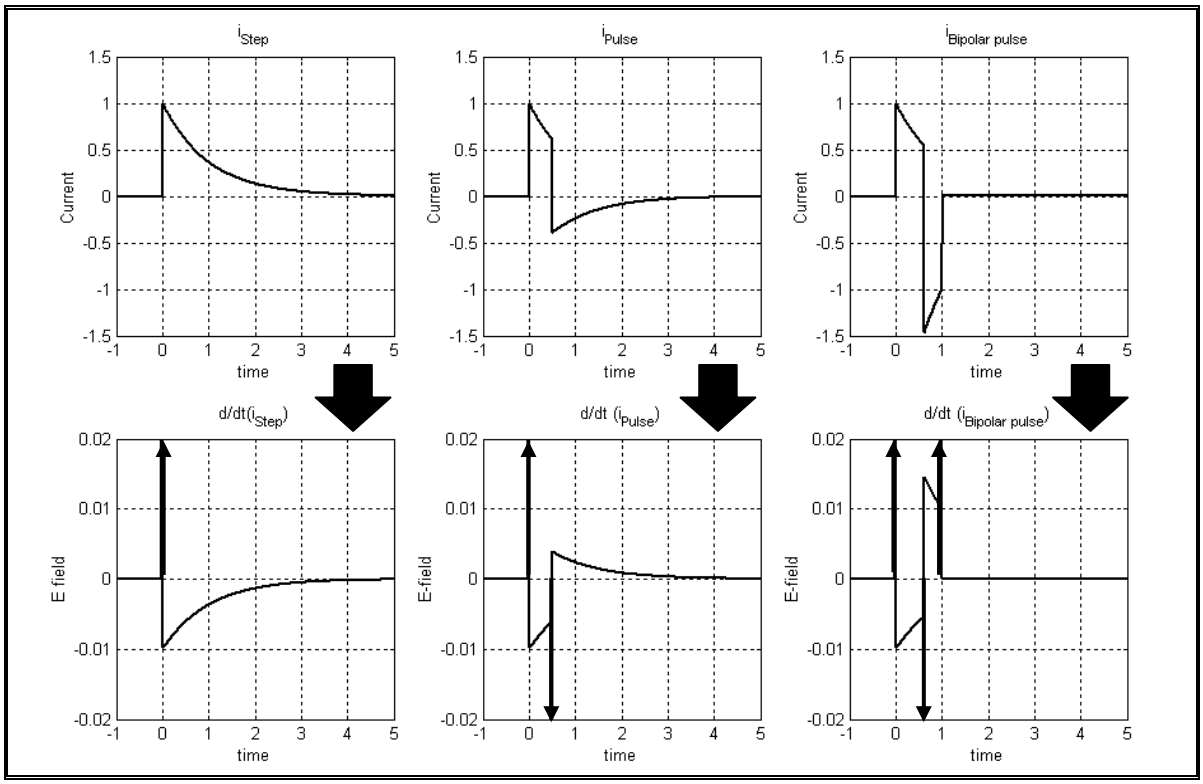

FIGURE 3-11: DIFFERENTIATION OF IDEAL CURRENT WAVEFORMS

The infinitely short transients of the ideal waveforms become impulses in the derivative. In practical circuits with finite rise times, these impulses can be expected to expand to unipolar pulses. The important thing to note is that the number of impulses (pulses in practical circuits) present in the E-field can in general be expected to increase from a step through a unipolar pulse to a bipolar pulse. This will complicate the direct interpretation of the data when multiple reflectors are present and might require additional deconvolution of the received data.

3.3. Design of step transmitter

A step waveform transmitter will now be designed that meets the requirements of a borehole radar system. The transmitter consists of two parts, a step waveform generator and a pole-zero network.

The first zero in the spectrum of a step waveform can be expected at around $1.5/T_{fall}$ (this topology creates a falling edge) according to section 3.2.2.a and its spectrum has a large low frequency component. The E-field radiated by an antenna driven by this transmitter can be expected (section 3.2.4) to be less complex than other topologies, simplifying direct interpretation of the eventual received data. There is no control over the recovery of the current flowing between load and transmitter (section 3.2.1.b), dictating the use of the pole-zero network developed in section 3.2.3.

A step waveform is generated by the simplest of switching actions for which a large number of electronic topologies are available and various techniques further exist to reduce the duration of the transient (and increase the maximum frequency [26].) The use of step recovery diodes to sharpen the pulse is well established [25], [33] and a novel topology employing a non-linear transmission line has also been proposed [34]. These pulse sharpening topologies unfortunately violate the condition that the transmitter's output impedance must approach a short circuit after transmission.

The step waveform is also the one currently employed by the bi-static borehole radar system [11], which will serve as departure point.

3.3.1. Electronic implementation

3.3.1.a. Generic circuit

The following circuit is proposed as a step waveform transmitter. The step waveform generator is topologically identical to the bi-static borehole radar system and the pole-zero network is the same as that developed in section 3.2.3.

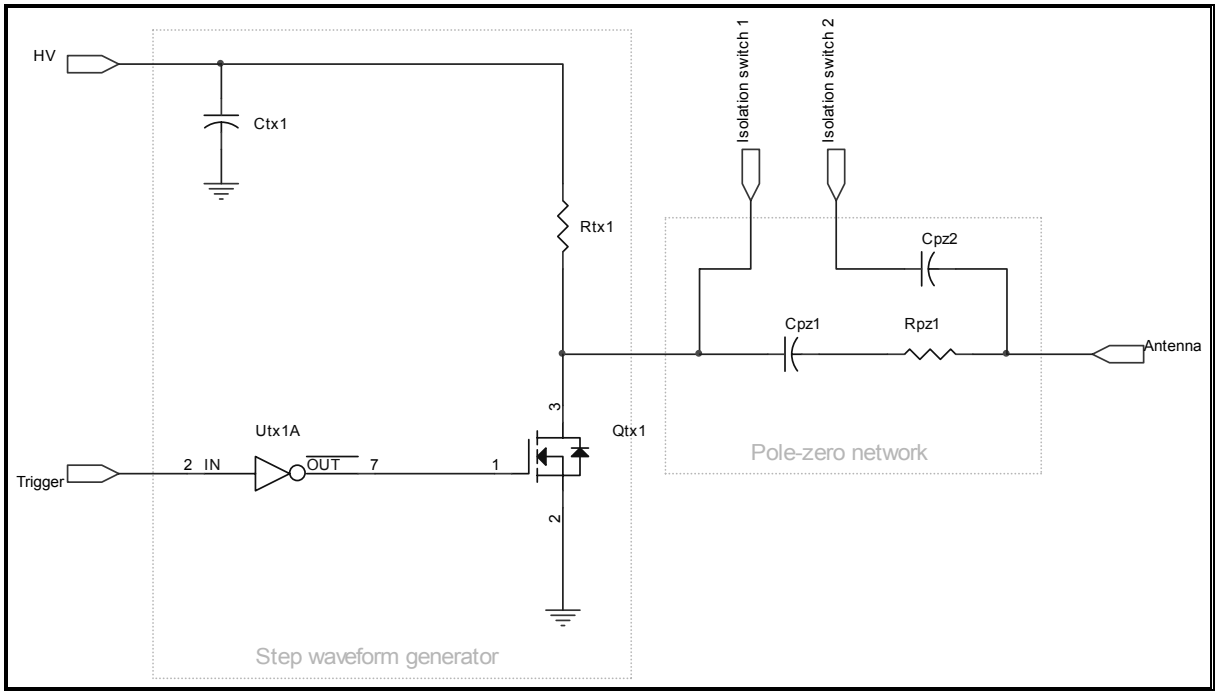

FIGURE 3-12: GENERIC CIRCUIT DIAGRAM OF STEP TRANSMITTER

3.3.1.b. Detailed considerations

The trigger signal must be at a logic low (low in this case, since the MOSFET driver U_{tx1A} is inverting) for a time longer than the acquisition time of the receiver. This causes the gate of MOSFET Q_{tx1} to be high, forcing the impedance between the MOSFET's drain and source to its minimum value ($R_{DS(on)}$ in

the datasheet.) The drain-source impedance appears in series between the antenna and receiver, and should therefore be at its minimum throughout the acquisition time of the receiver to minimize loss.

The fall time of the MOSFET's drain voltage is predominantly governed by the rate at which its gate is charged up by the MOSFET driver [35]. The current sourcing capabilities of the MOSFET driver should therefore be sufficient to facilitate the required fall time; A typical relationship between gate charge and gate voltage of a power MOSFET is shown in Figure 3-13. The x-axis is easily converted to time by dividing the units by the maximum MOSFET driver current. V_{GS} must reach its maximum voltage (typically the supply voltage of the MOSFET driver) in a time shorter than that dictated by section 3.2.2.a. The requirements for a MOSFET with a low gate charge (Q_g) and a MOSFET driver with a low output resistance and large maximum output current are clear.

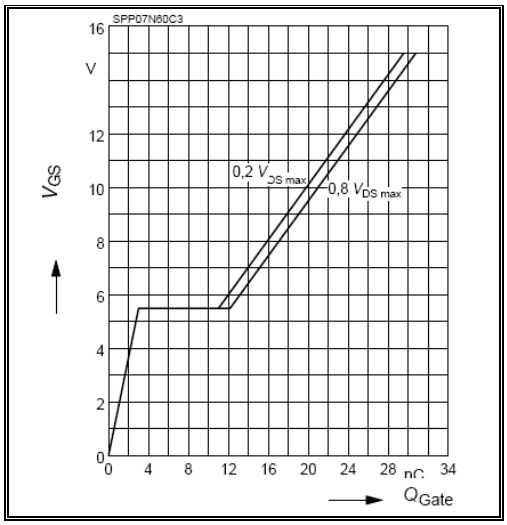

FIGURE 3-13: A TYPICAL GATE CHARGE VS GATE VOLTAGE PROFILE (EXERPT FROM INFINEON SPP07N60C3 DATASHEET)

The MOSFET driver must be powered from the highest possible supply voltage (limited by the maximum voltage allowed on the gate of the MOSFET) to ensure the MOSFET is switched on as hard as possible.

The on-state resistance ($R_{DS(on)}$) of the MOSFET must be as low as possible, since it appears in series between the antenna and receiver during receive mode. This will typically be counteracted by the requirement for low gate charge.

R_{tx1} must be chosen as large as possible to minimize unnecessary power drainage from the high voltage power supply during the receive mode, when the high voltage appears almost in its entirety across it. It will also speed up the switching action as it will cause the MOSFET to switch less current. The upper limit is however governed by the requirement that the voltage on the MOSFET's output must recover completely during the pulse repetition interval of the system. This is a typical exponential RC recovery due to the effective output capacitance ($C_{oss(eff)}$) [36] and R_{tx}.

The values of the pole-zero network must be calculated for a specific load according to the principles outlined in 3.2.3.a, for which the equivalent circuits derived in chapter 2 should be used.

3.3.2. Laboratory measurements

A version of the general step transmitter outlined above was built to meet the requirements of a borehole radar transmitter. Please refer to addendum A for a detailed circuit diagram.

The circuit is evaluated while driving a lumped element load which can be considered as a typical load presented by the antenna (from the evaluation of the antenna in chapter 2.) This lumped element load is shown in Figure 3-14. The values for the pole-zero network were calculated to operate with this specific load. The isolation switch terminals were shorted out for the purpose of these measurements.

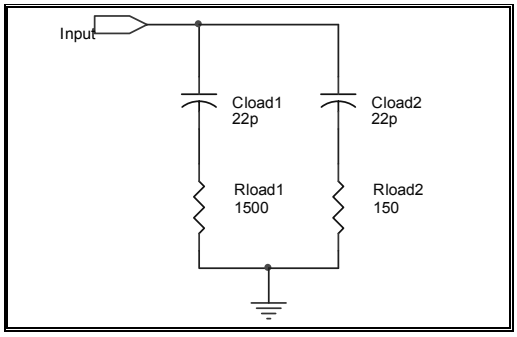

FIGURE 3-14: LUMPED ELEMENT LOAD USED TO EVALUATE STEP TRANSMITTER

3.3.2.a. Output voltage of step waveform generator

The output of the step waveform generator is defined as V_{ds} of the MOSFET, while the output of the transmitter is taken after the pole-zero-network.

The output voltage of the step waveform generator was carefully measured with a digital oscilloscope with 500 MHz analog bandwidth. A measurement was taken with 10 000 samples at a sample interval of 10 ns. This was then resampled numerically to obtain 100 000 samples in the 100 μs acquisition time. The 10 μs around the fast transient was then re-measured (with the same time reference) at a 1 ns sample interval and the corresponding section in the resampled dataset was replaced with it.

This enabled the complete waveform to be sampled with a Nyquist frequency of 500 MHz. The energy density spectrum was computed numerically with the help of a discrete Fourier transform.

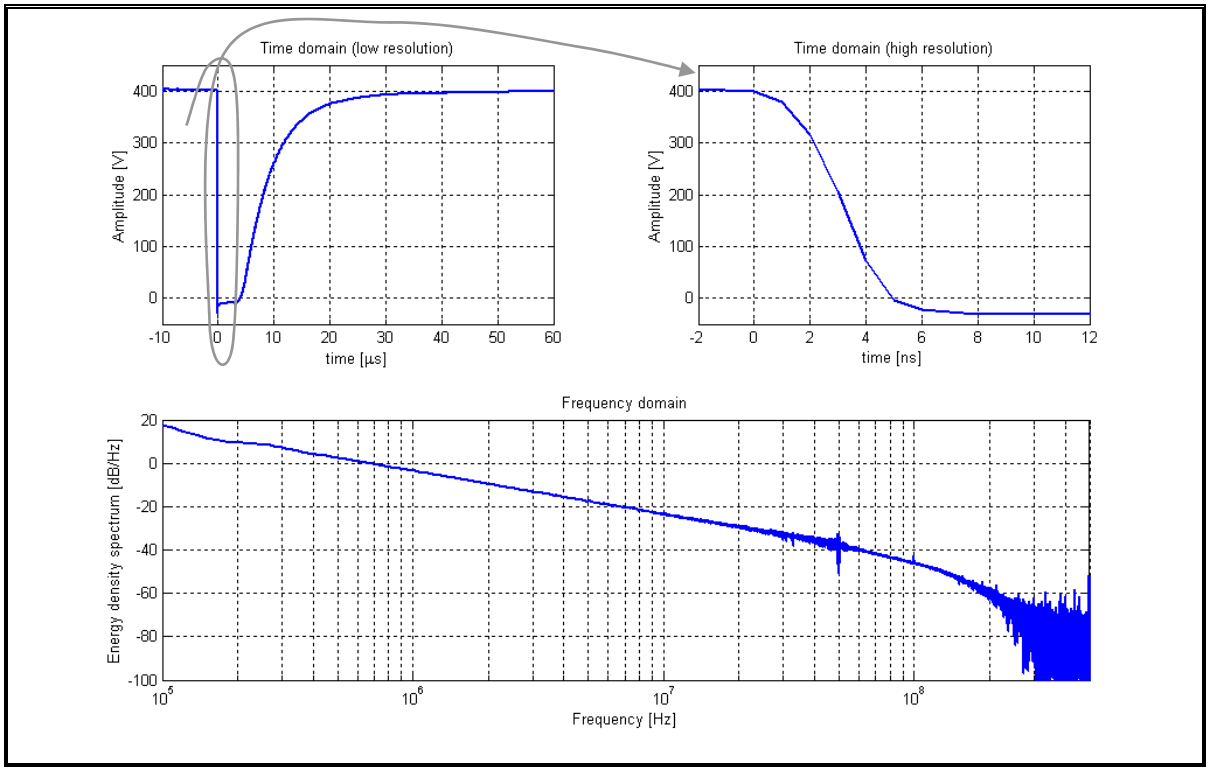

FIGURE 3-15: V_{DS} OF STEP TRANSMITTER MOSFET

The fall time of the transient is observed to be 5 ns. The spectrum can be expected to have the general shape of the step waveform in Figure 3-6 with the first zero at 300 MHz. There appears to be good correlation with the theoretical prediction, in spite of the oscilloscope being operated at the boundaries of its dynamic range,

The transmitter is in the on-state (R_{ds} = 1.8 Ω) for approximately 3 μs to match the system's acquisition time of 2 μs.

The effective output capacitance of the MOSFET is 85 pF, which combines with the 68 kΩ of R_{tx1} to create a time constant of 5.8 μs for the typical RC recovery. The system tested here would be optimal for a pulse repetition interval of around 35 μs.

3.3.2.b. Output current

The output current into the load was determined by measuring the voltages across the two resistors of the lumped element load with the 500 MHz oscilloscope and converting it to current. A digital Fourier transform was again performed on the data, but absolute power could be calculated in this instance, since the resistances through which the currents flow were known.

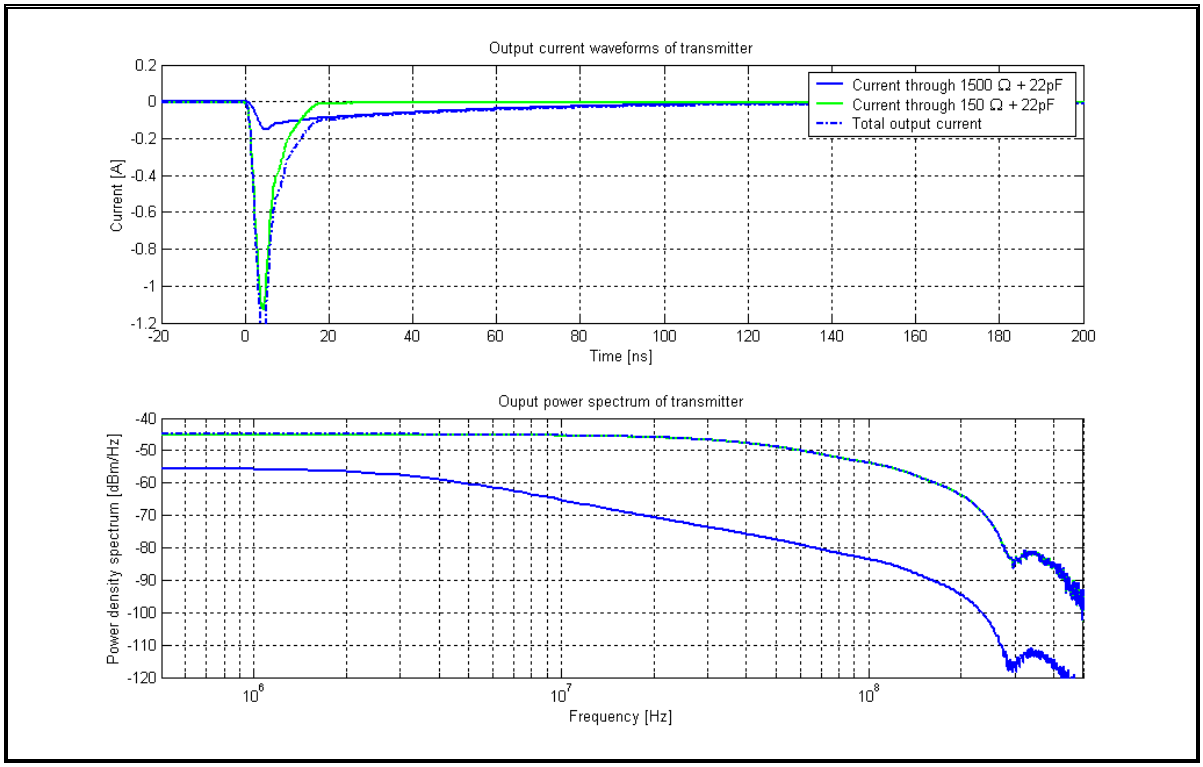

FIGURE 3-16: OUTPUT CURRENT OF STEP TRANSMITTER INTO LUMPED ELEMENT LOAD

The spectrum of the output current is dominated by the section of the current with the fast recovery, hiding the effect of the slowly recovering current later on in the time domain.

The high pass nature of the load causes the power spectrum to flatten out towards the lower frequencies (instead of following the increase of the voltage driving function's spectrum.) The zero at 300 MHz, already present in the driving function, can now clearly be seen.

3.3.2.c. Performance of the pole-zero network

The setup used for the following measurement saw the short between the isolation switch terminals replaced with a 10 Ω resistor. The current through this 10 Ω resistor was monitored to evaluate the performance of the pole zero network and represents the current that would flow into the isolation switch and ultimately the receiver when the isolation switch is in through-mode. This current is shown in Figure 3-17 with the total output current of Figure 3-16. The pole-zero network is expected to remove the recovery with the slow time constant from this current.

This current was also monitored while varying the load, according to the recommendation made in 3.2.3.c. The responses to the following loads are shown:

- 1500 Ω + 22pF || 150 Ω + 22pF (nominal load)
- **2000 Ω** + 22pF || 150 Ω + 22pF
- **1000 Ω** + 22pF || 150 Ω + 22pF

- 1500 Ω + 22pF || **220 Ω** + 22pF
- 1500 Ω + 22pF || **100 Ω** + 22pF

These represent a reasonable range of equivalent impedances for the antenna – as discussed in chapter 2.

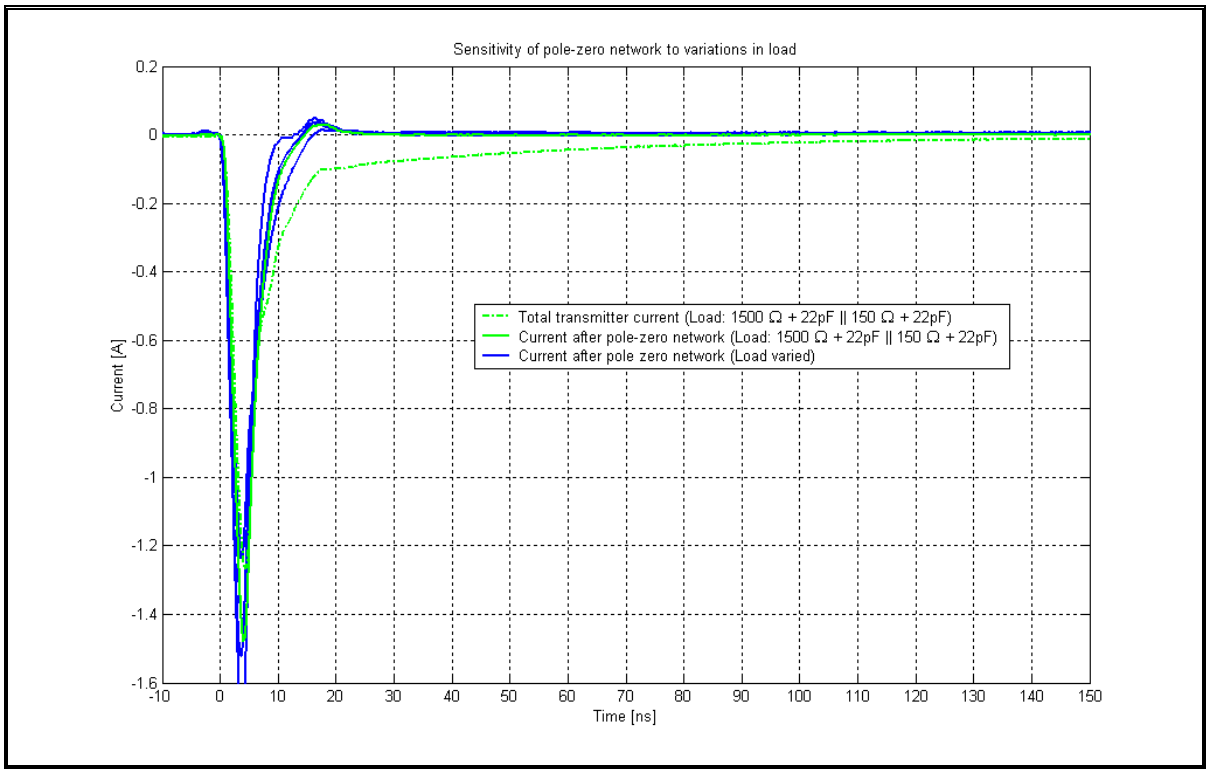

FIGURE 3-17: PERFORMANCE OF POLE-ZERO NETWORK WITH VARYING LOADS

The graph verifies the removal of the slow time constant recovery from the output current by the pole-zero network. It also indicates that the performance of the pole zero network is satisfactory with likely variations in load.

3.3.3. Conclusions

The step transmitter can be realized with simple electronics and high bandwidths can be obtained with commercially available components since only a single, sharp transient is required. The waveform does contain significant low frequency content, even without the slowly recovering section of current, which the antenna cannot effectively radiate and which is below the pass band of the receiver. The pole-zero network has been shown as a viable solution to remove the slow recovering component of the antenna current even with reasonable variations in load.

3.4. Design of bipolar pulse transmitter

In an attempt to meet all the requirements for a transmitter with a time limited response, the design process for a bipolar borehole radar transmitter will now be presented.

It was shown in section 3.2.1 that a bipolar signal is the minimum requirement for a waveform which fundamentally causes a time limited current to flow into a RC-load. A pole-zero network will consequently not be necessary. The spectrum of an ideal monocycle was shown in section 3.2.2 to peak at the fundamental frequency of the monocycle, with no frequency content at DC and a zero at double the fundamental frequency. The radiated E-field when this transmitter drives an antenna can be expected to be more complex and additional deconvolution might be required on the received data.

Various topologies have been presented to generate monocycle waveforms [37], [38], [39], which generally rely on transmission line stubs to create delayed reflections of a generated transient and form a monocycle. Adjustment of the characteristic times of the waveform (as advocated in 3.2.1.d) generally relies on the variation of the transmission line's effective lengths [40]. The low input impedance condition can again not be met with these configurations. Other options include taking the difference between two unipolar pulses(one of which is delayed) or the double differentiation of a step waveform [41]. A completely new approach is adopted here to create a bipolar signal with adjustable symmetry and low impedance after transmission.

3.4.1. Conceptual design

A bipolar waveform can be generated by taking the difference between waveforms A and B in Figure 3-18.
Waveform A is the step waveform discussed in the previous section and should be straightforward to implement. The subtraction could be done by a transformer - the main design challenge would be to generate waveform B.

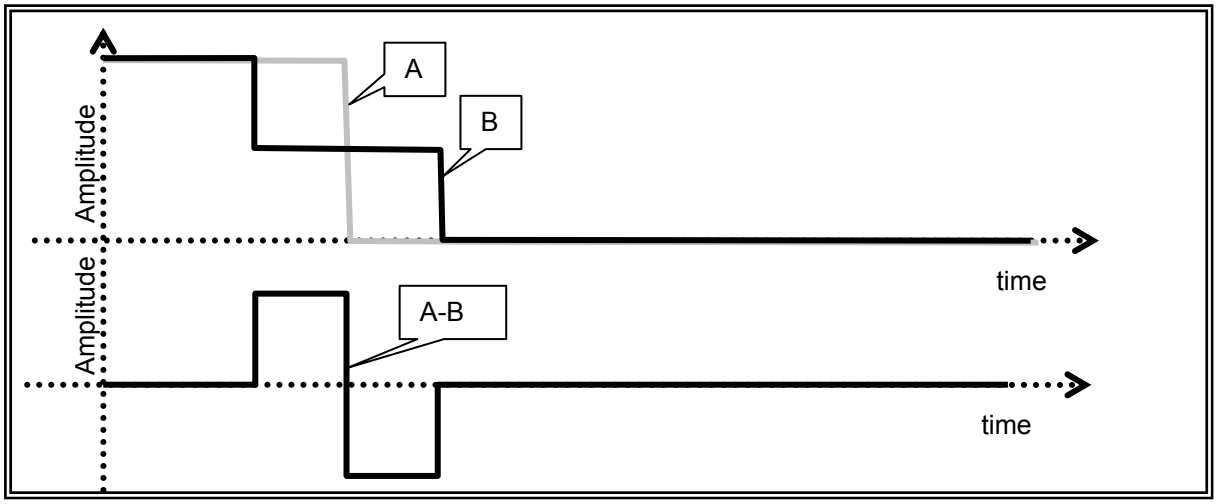

FIGURE 3-18: CONCEPTUAL DESIGN: GENERATION OF IDEAL BIPOLAR WAVEFORM

The voltage appearing over a capacitor C with Q coulomb charge stored on it is given by:

$$V = \frac{Q}{C} \quad \rightarrow \quad (3\text{-}23)$$

The halving of the signal amplitude required for waveform B can therefore possibly be achieved by having a fixed amount of charge stored on a capacitor and then suddenly doubling the capacitance. The capacitance can be doubled by switching another (discharged) capacitor of the same value in parallel with the first.

3.4.2. Electronic implementation

3.4.2.a. Generic circuit and basic operation

The following generic circuit is proposed to generate a bipolar waveform with the conceptual technique highlighted above.

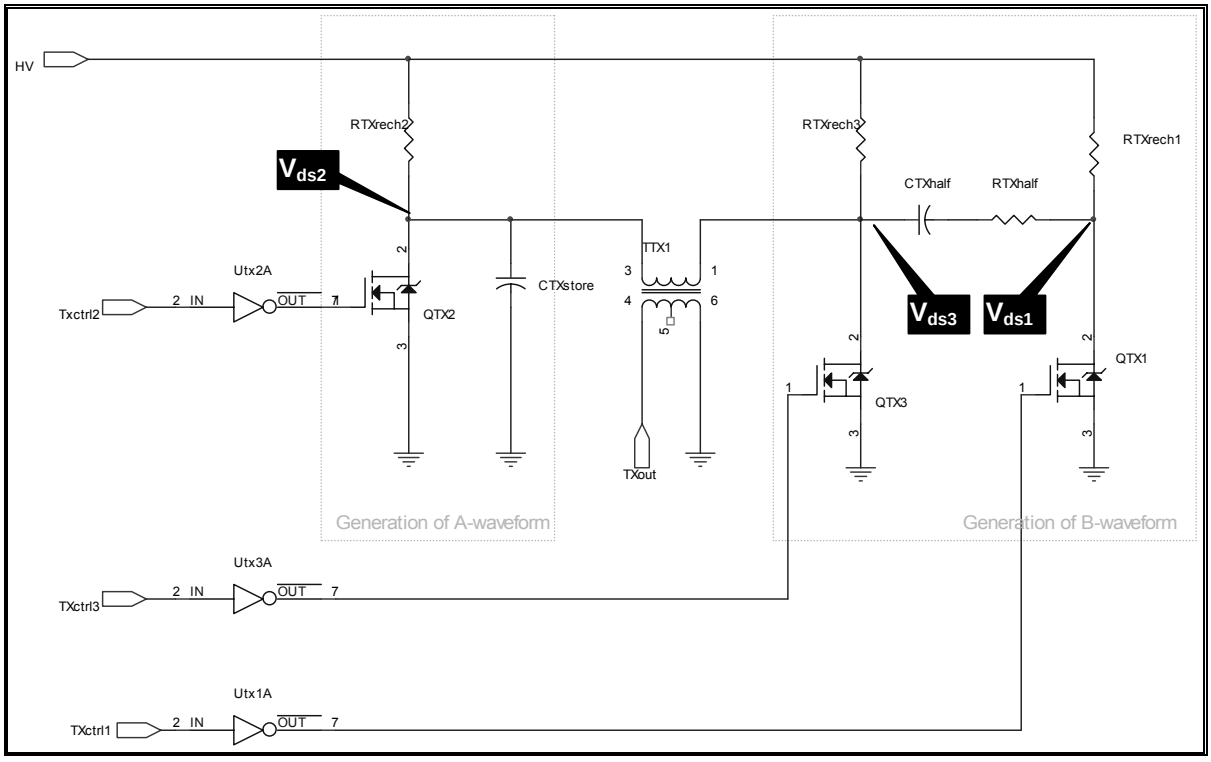

FIGURE 3-19: GENERIC CIRCUIT FOR MONOCYCLE TRANSMITTER

Note that the detailed considerations of the step transmitter discussed in section 3.3.1.b are all applicable to this circuit as well. R_{TXhalf} can be assumed a short circuit for the purpose of this discussion. The output capacitance of a MOSFET (C_{oss}) is dependent on the drain-source voltage (V_{ds}) and decreases with an increase in voltage. This effect is generally more pronounced at low voltages (compared to the maximum V_{ds}) and this capacitance will be taken as a constant to simplify the following qualitative discussion on the operation of the circuit.

Steady state:

The gate voltages of $Q_{TX1,}Q_{TX2}$ and Q_{TX3} are all zero in the steady state, so that V_{ds1}, V_{ds2} and V_{ds3} are at the DC level of the high voltage line (HV.) The transformer measures the dynamic difference between V_{ds2} and V_{ds3}, which is 0 V in the steady state. The MOSFETS can all be modelled as capacitors between their drain and sources of value C_{oss}, as specified at V_{HV} in their datasheets. The charge stored on these capacitors is given by:

$$Q_{ds} = C_{oss} V_{HV} \quad \rightarrow \quad (3\text{-}24)$$

C_{TXhalf} is completely discharged, since its two terminals appear at the same potential.

The output voltage is 0 V during steady state.

First switching action:

The gate voltage of Q_{TX1} is first raised in a way similar to that of the step transmitter system and V_{ds1} rapidly drops from the HV level to zero potential. The impedance between V_{ds1} and ground is now only

the small value of $R_{ds(on)}$, so that C_{TXhalf} effectively appears in parallel with C_{oss} of Q_{TX3}. Additional charge cannot be supplied quickly enough from the HV line through $R_{TXrech3}$, since the large value of $R_{TXrech3}$ limits the current. The only other charge source is from C_{oss} of Q_{TX2} and $C_{TXstore}$ through the transformer. Considering the case where the transmitter is driving no load, the transformer will appear as a large inductor resisting this sudden current flow and the voltage on V_{ds3} will initially drop to approximately:

$$V_{ds3} = \frac{Q_{ds}}{C_{oss} + C_{Txhalf}}$$
$$V_{ds3} = \frac{C_{oss}}{C_{oss} + C_{Txhalf}} V_{HV} \quad \rightarrow \quad (3\text{-}25)$$

The voltage appearing across the terminals of the transformer's primary winding is the difference between V_{ds2} (which is still at V_{HV}) and this V_{ds3}. It is therefore a rapidly rising voltage from 0 to

$$V_{ds2} - V_{ds3} = \left(1 - \frac{C_{oss}}{C_{oss} + C_{Txhalf}}\right) V_{HV} \quad \rightarrow \quad (3\text{-}26)$$

Current will flow through the primary winding of the transformer if a load is being driven however. The resulting current in the secondary winding is the output current. This current will have the effect of starting to drain capacitor $C_{TXstore}$ and C_{oss} of Q_{TX2} and charging the combination of C_{TXhalf} and C_{oss} of Q_{TX3} towards an equilibrium point where the charge is divided between the capacitors. The voltage appearing across the primary winding of the transformer will therefore drop as well. $C_{TXstore}$ is included to increase the capacitance of C_{oss} of Q_{TX2} and consequently reduce the voltage drop of V_{ds2} during this interval.

The first switching action will create the first rising edge to the positive peak of the bipolar signal.

Second switching action:

MOSFET Q_{TX2} is the next to have its gate voltage driven high. This will cause V_{ds2} to rapidly drop from V_{HV} (or the slightly lower value due to the draining discussed above) to zero potential. Note that the voltage transient might be slightly slower than with $V_{ds1.}$ ($Q_{TXstore}$ must be drained as well, which results in more current being switched by the MOSFET.) The difference (as measured by the transformer) between V_{ds2} and V_{ds3} will therefore drop from the value of (3-26) (or slightly lower, due to the draining) to approximately:

$$V_{ds2} - V_{ds3} = -\frac{C_{oss}}{C_{oss} + C_{Txhalf}} V_{HV} - \Delta V_{HV} \quad \rightarrow \quad (3\text{-}27)$$

ΔV_{HV} represents the effect of draining and charging in the previous interval.

There will consequently be a reversal in the output current and V_{ds3} will start dropping due the draining of C_{oss} of Q_{TX3} and C_{TXhalf} - the voltage appearing across the terminals of the transformer will also start to drop.

The second switching action will create the falling edge to the negative peak of the bipolar signal.

Third switching action:

The gate of Q_{TX3} is finally driven high, so that V_{ds3} drops to 0 potential as well and the voltage appearing across the primary winding of the transformer returns to 0.

The third switching action will create the second rising edge of the bipolar signal (from the negative peak back to zero.)

Summary:

Figure 3-20 summarizes the complete switching sequence.

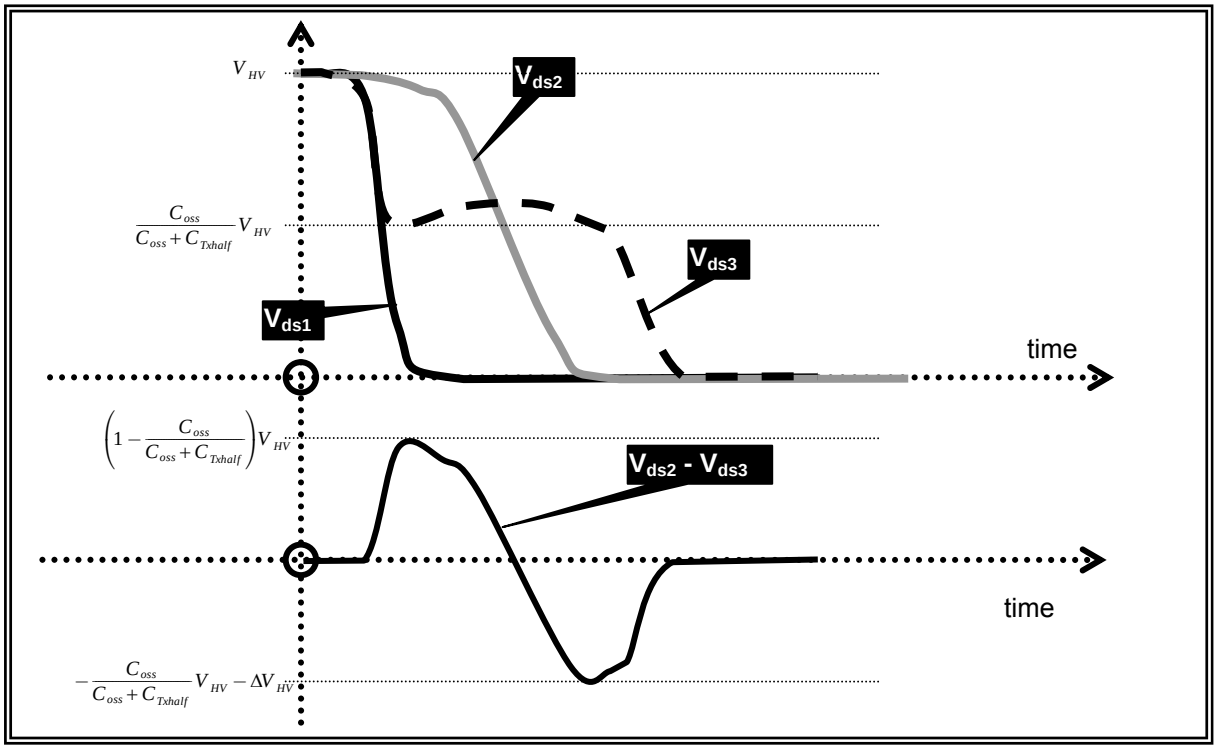

FIGURE 3-20: EXPECTED WAVEFORM SEQUENCE OF GENERIC MONOCYCLE TRANSMITTER

This waveform can be compared to the monocycle of section 3.2.2.a. The timing of the third switching action is then equivalent to $1/f_0$ for the equation in Table 3-1 and will determine the frequency of peak power and that of the first zero.

It is also an approximation for the idealized bipolar waveform of 3.2.1.d:

- The relative amplitudes of the positive and negative peak can be adjusted through variation of $C_{TXHALF.}$ This is related to variables A & B in equation (3-10)
- The relative duration of the positive and negative half cycles can also be adjusted by varying the timing of switching action two. This is related to T_1 in equation (3-10).

It now follows from equation (3-10) that the current flowing after $t>T_2$ can be made zero with the correct choice of C_{TXHALF} and the timing of the switching actions.

3.4.2.b. Detailed considerations

This discussion should be regarded as additional information to that already supplied in section 3.3.1.b for the step transmitter, since each individual switching element in this configuration is similar to the step waveform generator.

The transformer's winding ratio effectively changes the load impedance driven by the transmitter. This must be chosen to maximize output power without loading the transmitter excessively. Excessive loading will cause the shape of the output signal to be very sensitive to the load and reduce the transmitter's ability to keep the residual current close to zero as the load varies. The transformer's bandwidth must naturally exceed that of the output pulse, but it is further recommended to choose a transformer with the widest possible frequency reach. The transformer has the effect of making the load driven by the transmitter approach a short circuit outside its frequency band of operation, which will provide a heavy load to frequency content that the transmitter might generate outside the band.

$C_{TXstore}$ should be as large as possible to minimize to voltage drop in V_{ds2} between the first and second switching action, but larger values result in more current to be switched by MOSFET Q_{TX2} and decrease the switching speed. The maximum value that still allows an acceptable switching speed must be used. A MOSFET with a larger C_{oss} parameter can alternatively be used, provided the switching speed is acceptable. It must be remembered that these techniques will slow down the recovery of the MOSFET's V_{ds} between pulses - with implications to R_{rech1}, R_{rech2}, R_{rech3} and the maximum pulse repetition frequency.

C_{TXhalf} should be carefully chosen for the optimal waveform. A larger value causes a larger positive swing relative to the negative swing of the output pulse. A good initial value would be the C_{oss} value of Q_{TX3} at $½V_{HV}$, after which it can be tuned.

R_{TXHALF} has been assumed 0 Ω up to this point. A small value (significantly smaller than any load resistor) can be used to limit the current flowing to C_{TXhalf} after the first switching action if ringing is observed.

The timing of TXctrl3 must be chosen to achieve the correct occupation of the spectrum, as previously highlighted.

The timing of the control signals TXctrl2 must be left adjustable to allow for fine tuning of the output waveform to the specific load. This amounts to the practical version of zeroing the expression for the current during $t>T_2$ in equation (3-10).

3.4.3. Laboratory measurements

A bipolar pulse transmitter like the one outlined above was built, with the parameters chosen to specifically meet the requirements of a borehole radar system (see addendum A for details of the circuit.) This circuit will now be used to evaluate the feasibility and performance of the monocycle transmitter concept developed here. The load chosen for the transmitter is the same network used to evaluate the step waveform transmitter (see Figure 3-14), unless stated otherwise.

3.4.3.a. Basic operation of bipolar pulse transmitter

The ability of the electronic circuit to generate the anticipated waveforms of Figure 3-20 is investigated first. All waveforms were measured on a digital oscilloscope with 500 MHz analog bandwidth. The waveforms generated by the three MOSFETs and the resultant output waveform are shown in Figure 3-21. It shows the case for an output waveform with a nominal period of 30 ns, with the shape optimised for maximum peak amplitude and minimum residual current into the RC load of Figure 3-14.

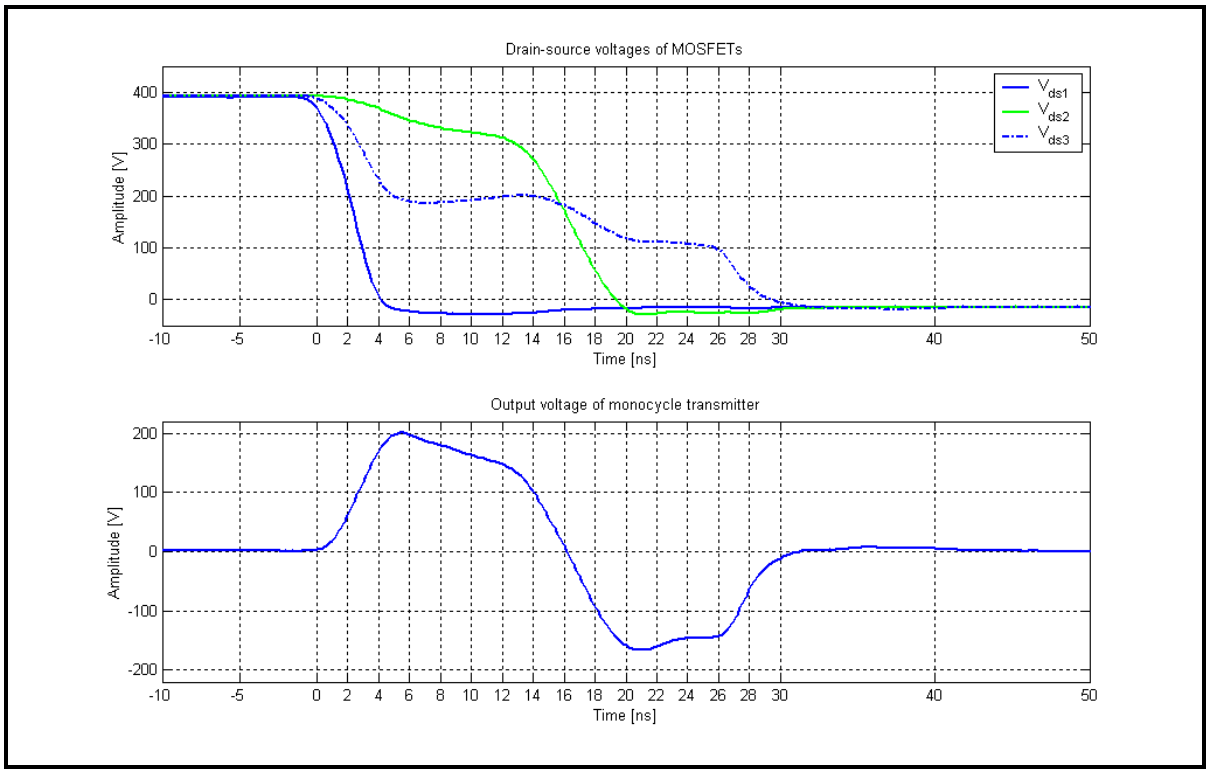

FIGURE 3-21: FUNDAMENTAL WAVEFORMS OF THE MONOCYCLE GENERATOR

The operation of this circuit is close to that of the conceptual design and this circuit is able to produce the desired bipolar waveform.

3.4.3.b. Adjustment of waveform spectrum

The frequency spectrum associated with an ideal monocycle waveform was shown in 3.2.2 and guidelines for choosing the period of the waveform was presented. The validity of that on the waveform generated by this circuit will now be investigated by evaluating the frequency content of the output pulse. The flexibility afforded by this circuit to shift its occupation of the frequency spectrum is also demonstrated.

The spectrum was shifted by adjusting the timing of signal Txctrl3 (see Figure 3-19) to change the nominal period of the signal. A corresponding correction in the timing of Txctrl2 was also required to maintain the optimal waveform shape for minimum residual current. Four waveforms are considered. The nominal periods of these waveforms, when seen as approximations of the monocycle waveform in section 3.2.2, are: 21 ns, 26 ns, 31 ns and 36 ns. The amplitude of the signal reduces rapidly for shorter periods due to the finite rise / fall times achieved by the switching elements. Conversely, the draining and charging of the capacitors (discussed in section 3.4.2.a) limits the maximum width of the pulse. This range of pulse widths is well suited to the 10 -100MHz bandwidth generally quoted for borehole radar systems (see section 1.3.)

The result is shown in Figure 3-22. Frequency domain data was again obtained with a discrete Fourier transform of the time domain data.

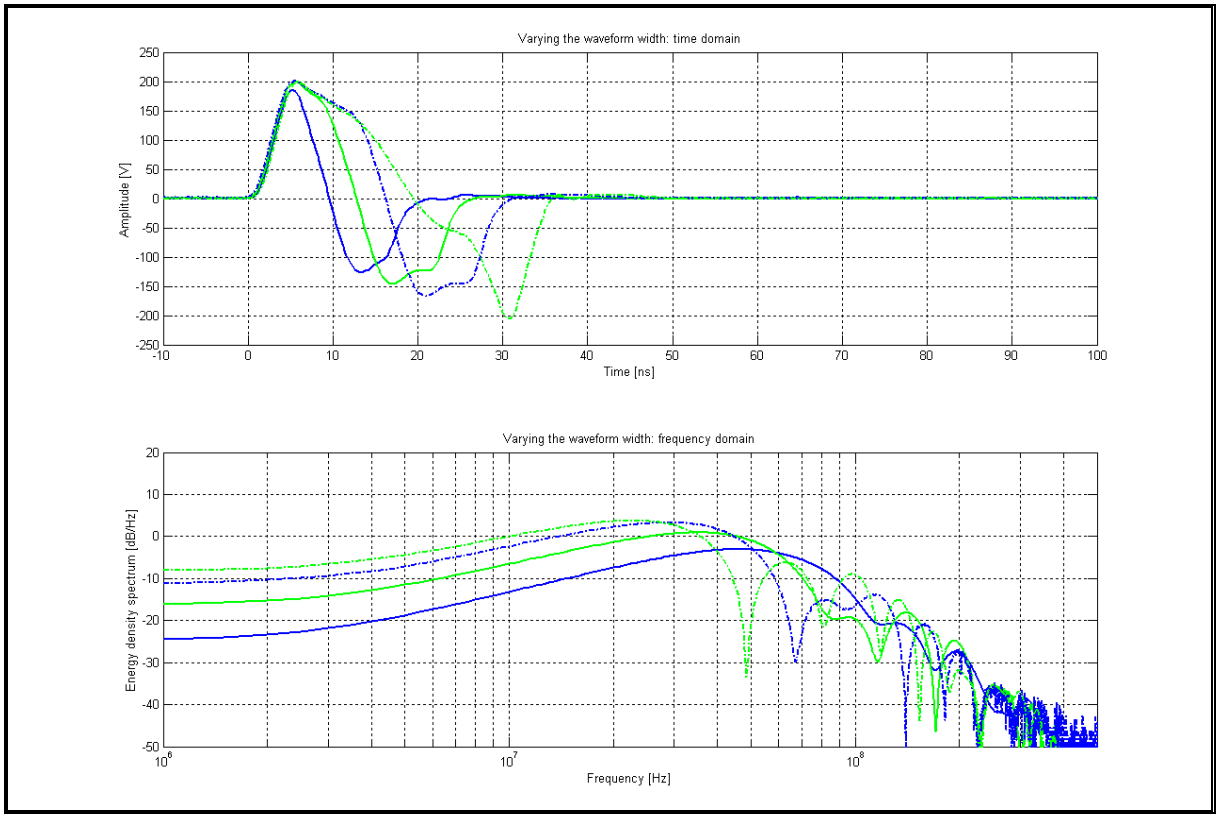

FIGURE 3-22: ADJUSTABLE SPECTRA OF MONOCYLE TRANSMITTER

The maxima predicted by section 3.2.2 and the maxima read from Figure 3-22 compare as follows:

Nominal period [ns]	Predicted frequency of maxima [MHz]	Measured frequency of maxima [MHz]
21	47.6	46
26	38.5	35.5
31	32.3	29
36	25.6	23

TABLE 3-2: PREDICTED AND MEASURED FREQUENCIES OF MAXIMA (MONOCYCLE TRANSMITTER)

The first zero appears at approximately double this frequency.

The versatility of this circuit in being able to meet various frequency domain requirements has been demonstrated. The time-frequency relationships developed for the ideal monocycle in section 3.2.2 can be used to predict the spectrum for a specific time domain waveform generated by this circuit.

3.4.3.c. Output current

The current flowing in each of the two load resistors (see Figure 3-14) was then monitored and the power spectrum calculated with the same procedure as the corresponding measurement for the step transmitter in section 3.3.2.b. The pulse width of section 3.4.3.a was used.

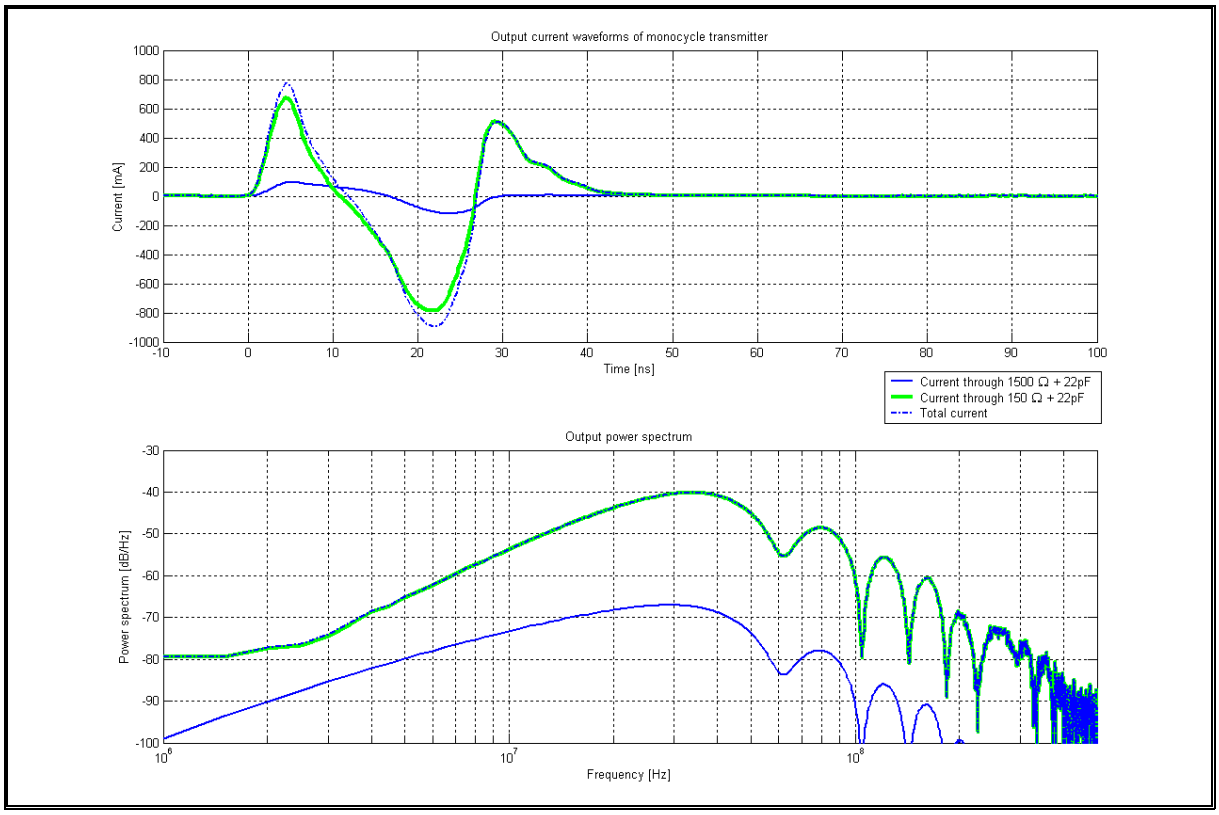

FIGURE 3-23: OUTPUT CURRENT AND POWER SPECTRUM OF MONOCYLE TRANSMITTER

3.4.3.d. Fine-tuning for minimum residual current

It was argued in section 3.2.1.d that a bipolar waveform can be adjusted so that no current is flowing after the driving voltage waveform returns to zero ($t>T_2$, where T_2 is the nominal period of the monocycle in this case.) This was achieved by the correct choice of relative amplitudes and timing. The generic design of 3.4.2.a further showed how the choice of C_{TXhalf} and the timing of the Txctrl2 signal are the practical implementation of this.

C_{Txhalf} was chosen for maximum amplitude and will stay fixed while the timing of TXctrl2 is used as the variable to adjust for zero residual current. The three settings shown in Figure 3-24 (using the notation of equation (3-10)) represent the cases where T_1 is too small, the ideal T_1 and where T_1 is too big.

Only the current flowing in the section with the slow time constant is considered. The residual current flowing in the section with the short time constant was found to not pose a problem, due to its quick recovery.

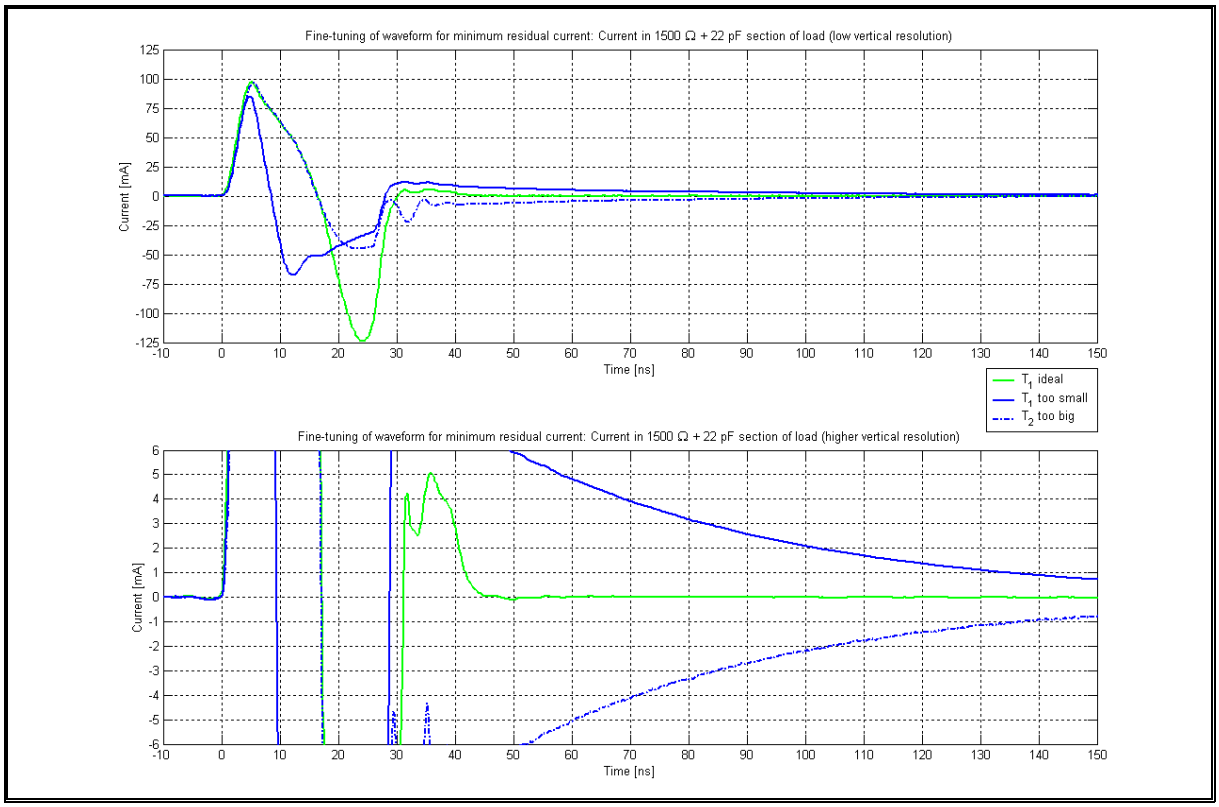

FIGURE 3-24: ZEROING THE RESIDUAL CURRENT

The characteristic overshoot and undershoot predicted by Figure 3-5 is clearly recognized in this measured waveform. The general design principles for minimizing the residual current, presented in 3.2.1.d, have been shown to be valid for the waveform generated by this monocycle transmitter.

This circuit provides the opportunity to fine-tune the waveform for zero residual current.

This fine-tuning was predicted to be load dependent - which should therefore be investigated. The waveform was adjusted for minimum residual current when driving the nominal load of Figure 3-14. The current flowing in the section with the slow time constant was then measured while the load was varied, without adjusting the waveform, across the same range as when the step transmitter's sensitivity to load variations was evaluated (3.3.2.c)

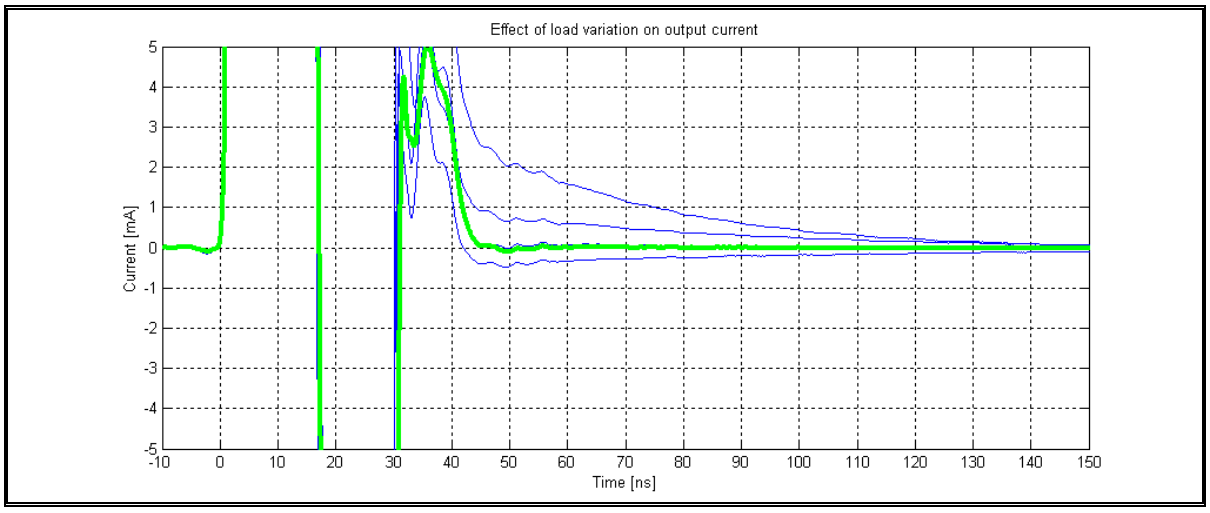

FIGURE 3-25: EFFECT OF VARIATIONS IN LOAD ON OUTPUT CURRENT

The fine-tuning of the waveform for minimum residual current is load specific. The current recovered to less than 1 mA within 50 ns after the driving monocycle waveform was complete however, over the complete range of likely output impedances.

3.4.4. Conclusion

An electronic circuit has been successfully developed to generate a bipolar signal.

The frequency response is closely approximated by that of an ideal monocycle. The frequency content of the output decreases towards the lower frequencies, with zero content at DC. The frequency at which the maximum content occurs can be chosen. A zero will occur in the spectrum at double the frequency of the maximum.

The current flowing into an RC-load can be tuned to be time limited with this circuit, with only small sensitivity to load variations.

3.5. Synopsis

The requirement for a time limited output current into an RC load was formulated and its implications to general waveforms shown. This highlighted the principle that waveform design should primarily be done in the time domain and general relationships between the time domain parameters and spectra

of common waveforms were presented to serve as guidelines when designing waveforms in the time domain.

A novel pole-zero network was presented which makes it possible to use a transmitter with a non-time limited output current (such as a step or pulse transmitter) for this transceiver.

A practical module was subsequently designed, according to the guidelines developed, to serve as a step transmitter for application in borehole radar. The system employs the pole-zero network together with an established step waveform generator. The circuit was built, measured and found to meet all the specifications of the transceiver.

A completely new bipolar pulse transmitter was also developed from conceptual design through to a built circuit. The circuit exploits all the advantages of a bipolar signal and was designed to be versatile enough to allow for tuning of the waveform to zero the residual current, while still having the desired frequency content. A specific circuit, purpose-built for a borehole radar system, was measured and found to be exceptionally suitable for the transceiver.

The performance of the two circuits is briefly compared below. The step transmitter is in general less complex to implement, generates more high frequency content for a specified switching time and the received waveform should be less complex after the differentiation effect of the antenna. The bipolar transmitter offers more versatility for fine tuning the waveform (for zero residual current) and the waveform's frequency spectrum is better matched to the antenna. Both circuits do however fulfil all the requirements and are both recommended for a monostatic borehole radar system.

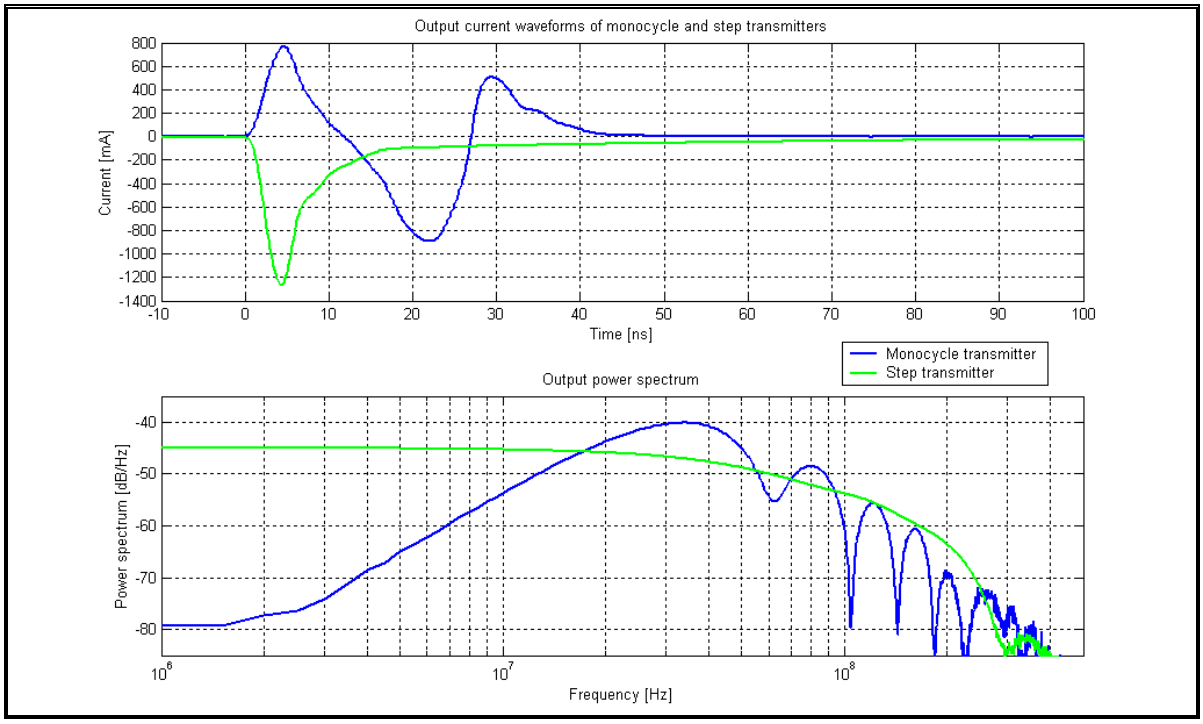

FIGURE 3-26: MEASURED OUTPUT CURRENTS AND POWER SPECTRA OF THE TWO PROPOSED TRANSMITTER CIRCUITS

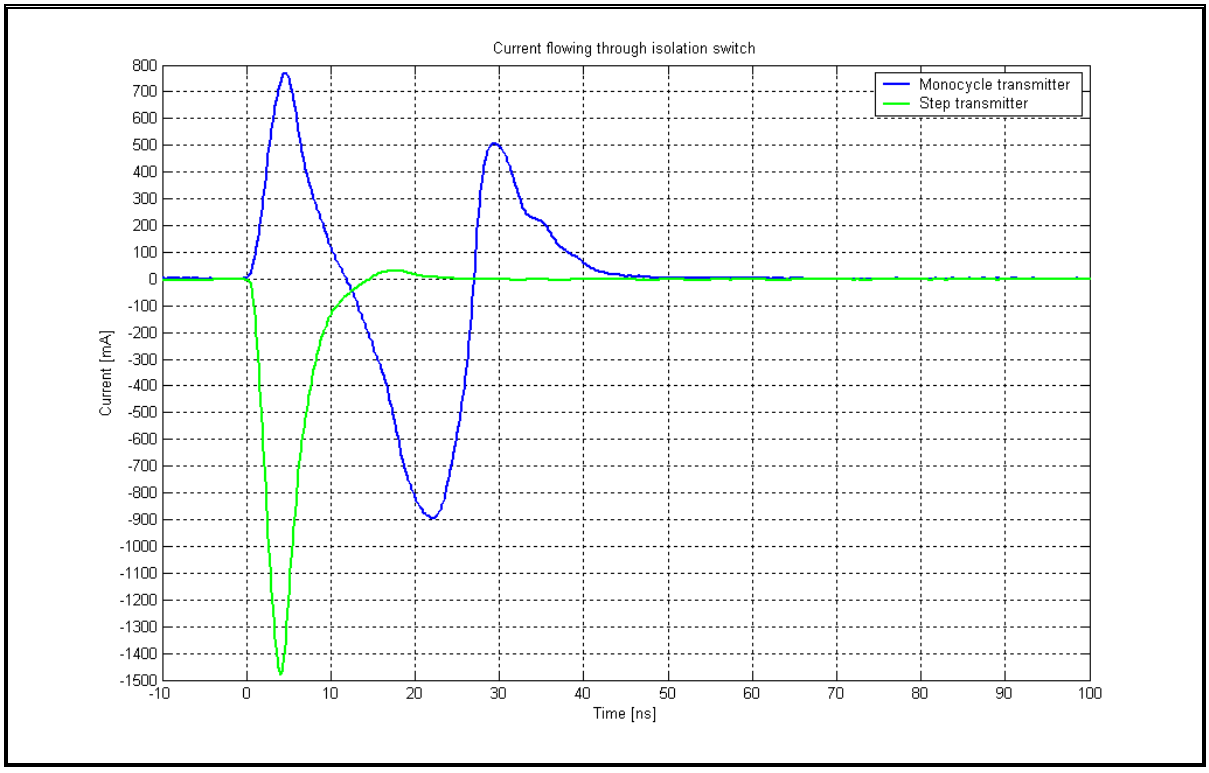

FIGURE 3-27: MEASURED CURRENT FLOWING INTO ISOLATION SWITCH FROM THE TWO PROPOSED TRANSMITTER CIRCUITS

CHAPTER 4

Isolation switch design

4.1. Background

4.1.1. Transmit/Receive switches

The use of transmit/receive switches (T/R-switches) to enable transmitters and receivers to share a common antenna (duplexing [2],) is well established in the fields of radar and communication [42], [43], [44].

A typical configuration would appear as in Figure 4-1, which can be viewed as a parallel connection between transmitter, receiver and antenna. The double throw T/R-switch connects the transmitter to the antenna while disconnecting the receiver (SW_{TX} closed, SW_{RX} open) when transmitting. It then changes over to receive by connecting the receiver to the antenna, while disconnecting the transmitter (SW_{TX} open, SW_{RX} closed)

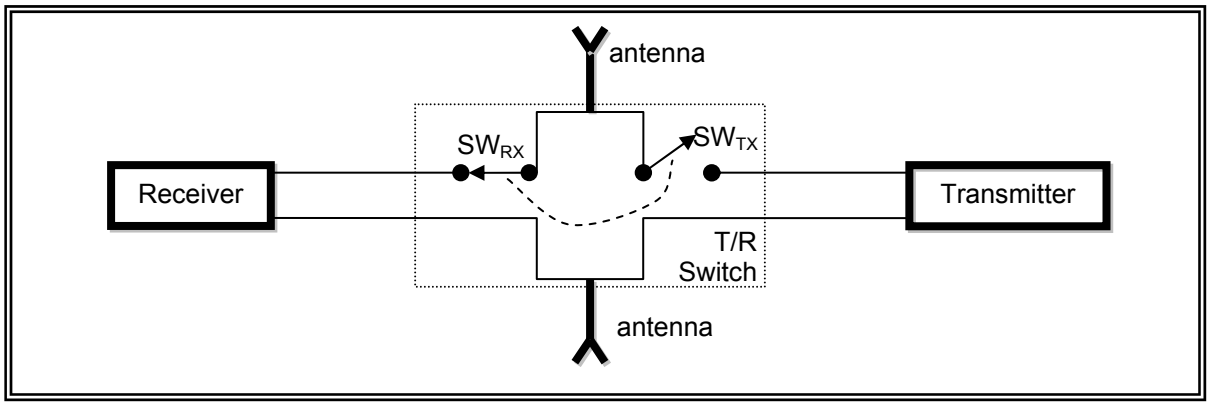

FIGURE 4-1: TYPICAL T/R-SWITCH

Note that SW_{RX} must withstand the voltage appearing on the antenna due the transmitter in transmit mode.

The duration of the T/R-switch's transition from transmit to receive mode is a crucial parameter for this transceiver design, since it is directly related to the closest target that can be observed by the receiver. This distance to the closest target can simplistically be expressed as:

$$R = \frac{\nu t}{2}$$

with

R the distance to the target

ν the speed of propagation in the medium

t the duration of the switching action

➔ *(4-1)*

4.1.2. Application: Borehole radar system

It was mentioned in chapter 1 that a typical borehole radar system utilizes separate transmitter and receiver probes (bi-static system), each with its own antenna and with sufficient spacing between them to overcome the problem of isolation between transmitter and receiver.

A properly functioning T/R-switch is therefore the fundamental requirement for the conversion to a monostatic system.

The high transmitter voltages generated by a typical borehole radar system (see section 1.3) makes it difficult to use the standard configuration highlighted in 4.1.1. It was further specified from the onset (section 1.1) that the transceiver must already detect targets at a distance comparable to the resolution of the system. From equation (4-1) it is then clear that the transition must occur immediately after the transmitter pulse, and the duration of the transition should be of the same order as that of the transmitted pulse. This will be shown in 4.2.2 to pose a significant challenge.

A completely new design is called for to address the challenges of a T/R-switch in this system.

4.1.3. Interfaces with other modules

The approach in this design will deviate from the standard approach of using a double throw T/R-switch to connect the antenna to either the receiver or the transmitter.

The transmitter, receiver and antenna are connected in series, rather than the standard parallel connection. This will in general require the receiver to be isolated from the transmitter *current* instead of the *voltage*. The transmitter was designed to isolate itself when not transmitting, by remaining in a low impedance state after transmission.

The T/R-switch then reduces to a single throw isolation switch in front of the receiver and the configuration amounts to that of Figure 4-2.

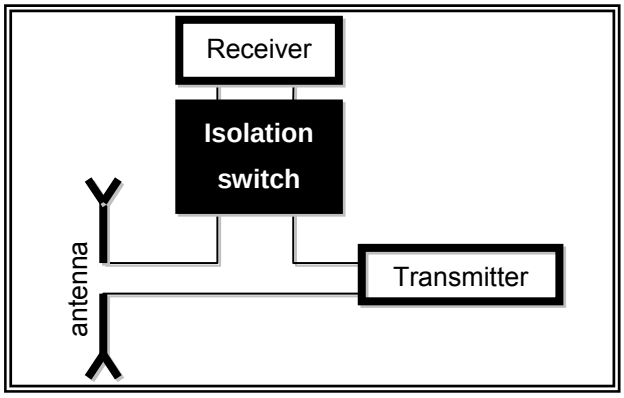

FIGURE 4-2:SYSTEMS LEVEL DIAGRAM OF TRANSCEIVER

Transmit mode:

The input of the isolation switch must ideally be a short circuit - so that the transmitter is in effect directly connected to the antenna when it fires. The receiver terminals must be completely disconnected from the antenna.

Receive mode:

The transmitter is a short circuit in receive mode and the isolation switch must effectively connect the receiver terminals to the antenna with minimum loss.

The input and the output of the isolation switch are shown as differential ports. It was already mentioned that either the transmitter or the input of the isolation switch can be single sided, provided the antenna is unbalanced. The output could also be single sided, depending on the receiver.

4.1.4. Overview of chapter

The anticipated outcome of this chapter is a novel device capable of providing sufficient isolation between the transmitter and receiver during transmit mode, while introducing minimal loss between the antenna and receiver in receive mode. The device must be able to change between these two states in a time similar to the duration of the transmit pulse, without introducing switching transients onto the RF-path.

A number of underlying concepts in the design of this isolation switch will be introduced in the next section, followed by an idealized, high level design in section 4.3. This conceptual design will be implemented with a generic electronic circuit and general guidelines for component choices and detail design issues will be presented (section 4.4.) Two practical isolation switches will then be presented to specifically meet the requirements of a borehole radar system and will be evaluated through measurement in section 4.5.

4.2. Basic concepts

4.2.1. Series and shunt switching elements

The two basic switching configurations are a series and a shunt switch [45]. The transfer function of these networks can be defined as $\left|\frac{P_o}{P_A}\right|$. P_0 is the peak power delivered to the load, given by $P_o = \frac{V_o^2}{R_L}$ if the load impedance is assumed to be real (R_L). P_A is the maximum peak power available from the source, given by $P_A = \frac{V_{in}^2}{4R_0}$ if the characteristic impedance is real (R_0)

4.2.1.a. Series switch element

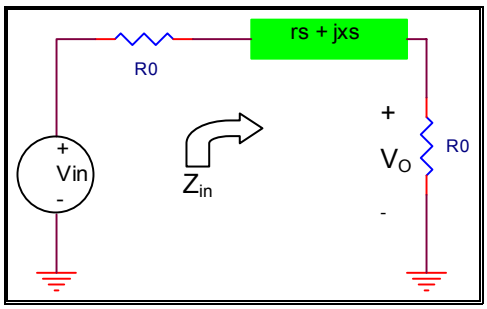

FIGURE 4-3: BASIC SERIES SWITCH ELEMENT

The transfer function of the series switching element in Figure 4-3, with load impedance equal to the characteristic impedance (R_L=R_0), is given by

$$\left|\frac{P_o}{P_A}\right| = \frac{4R_0^2}{\left(2R_0 + r_s\right)^2 + x_s^2} \quad \rightarrow \quad (4\text{-}2)$$

and the input impedance as seen from the load is given by

$$z_{in} = r_s + x_s + R_0 \quad \rightarrow \quad (4\text{-}3)$$

In through-mode, the impedance of the switch ($|r_s + jx_s|$) should be as small as possible for minimum insertion loss and so that the input impedance is matched to the source. In isolation-mode, the impedance should ideally be infinitely large for maximum isolation. The input impedance of a series switch in isolation mode approaches an open circuit.

4.2.1.b. Shunt switch element

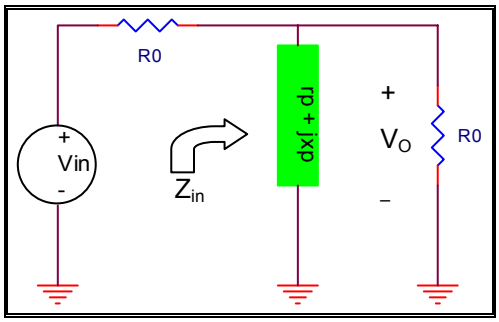

FIGURE 4-4: BASIC SHUNT SWITCH ELEMENT

The transfer function of the corresponding shunt switching element (as in Figure 4-4) is given by:

$$\left|\frac{P_o}{P_A}\right| = 4\frac{r_p^2 + x_p^2}{\left(2r_p + R_0\right)^2 + 4x_p^2} \quad \rightarrow \quad (4\text{-}4)$$

and the input impedance as seen from the load is the parallel combination

$$z_{in} = \left(r_p + jx_p\right) \| R_0 \quad \rightarrow \quad (4\text{-}5)$$

In through-mode, the switch impedance ($|r_p + jx_p|$) should be infinitely large for minimum insertion loss and so that the input impedance is matched to the source. In isolation-mode, the impedance

should ideally be zero for maximum isolation. The input impedance of a shunt switch in isolation mode approaches a short circuit.

4.2.2. Switching signal

An RF-switch can be seen as a device that modulates the incoming RF-signal with the gain function of the switch itself. In some cases, the switching action is achieved by an element switching a DC bias voltage or current. This creates an additional output due to the modulation of the DC-voltage with the gain function. (This signal will further be referred to as the switching signal.)

The characteristic times associated with the switching action are significantly longer than those of the RF-signal being switched in typical systems. This provides the opportunity to remove the switching signal from the RF-signal by means of frequency domain filtering.

It has been mentioned in section 4.1.1 that the object of this chapter is however to design an isolation switch that can switch an UWB signal where the switching time is comparable to that of the signal duration. The spectra of the switching signal and RF signal will consequently overlap and cannot be separated with basic filtering. This implies that switching elements should be used that do not modulate a DC-signal, or the switching signal must be removed in a way other than filtering.

4.2.3. Diode as switching element

Diodes are often used as switching elements, since they can exist in two distinct impedance states according to the bias applied. A forward biased diode can be approximated as a small resistance, while a reverse biased diode acts as a capacitor in general. The requirement for biasing places diodes in the category of switching devices that modulate a DC signal and it can therefore be expected that a switching signal will be generated. Two types of diodes are discussed as alternatives: the PIN diode and the Schottky diode.

4.2.3.a. PIN diode

PIN diodes are often employed as switching elements [43], [46]. White [47] recommends that the PIN diode should be viewed as a charge controlled device and develops the theory for controlling these devices. A brief summary is given for background: When forward biased, a charge equilibrium (Q_0) is reached when the bias current just replenishes the electrons and holes that recombine in the intrinsic region:

$$Q_0 = I_0 \tau \quad \rightarrow \quad (4\text{-}6)$$

where I_0 is the bias current and τ is the carrier lifetime of the diode

The on-resistance of a PIN diode is typically very small compared to other diodes and is inversely proportional to the charge - and consequently to the bias current.

This stored charge must first be removed before the diode can become reverse biased and switch to its high impedance state. The discharge of the diode to zero charge is given by

$$q = Q_0 e^{-\frac{t}{\tau}} + I_0 \tau \qquad \ldots q>0 \qquad \rightarrow \quad (4\text{-}7)$$

There is consequently a transition time associated with switching from the low impedance state to the high impedance state, but it can be sped up by applying a reverse current ($I_o < 0$ in equation (4-7).) It should be noted that a RF signal can only switch a PIN diode to its high impedance state if it moves enough charge in the reverse current direction, regardless of the applied voltage amplitude. The reverse capacitance of a PIN diode is extremely small relative to other diodes.

The transition in the opposite direction (from high impedance to low impedance) can be assumed to occur immediately when a forward bias current is applied for the purpose of this discussion.

The basic switching action of a PIN diode is illustrated with a time domain measurement on a BAT18 device from Infineon Technologies (www.infineon.com.) The diode was connected in series with a 540 Ω resistor across the terminals of a square wave generator.

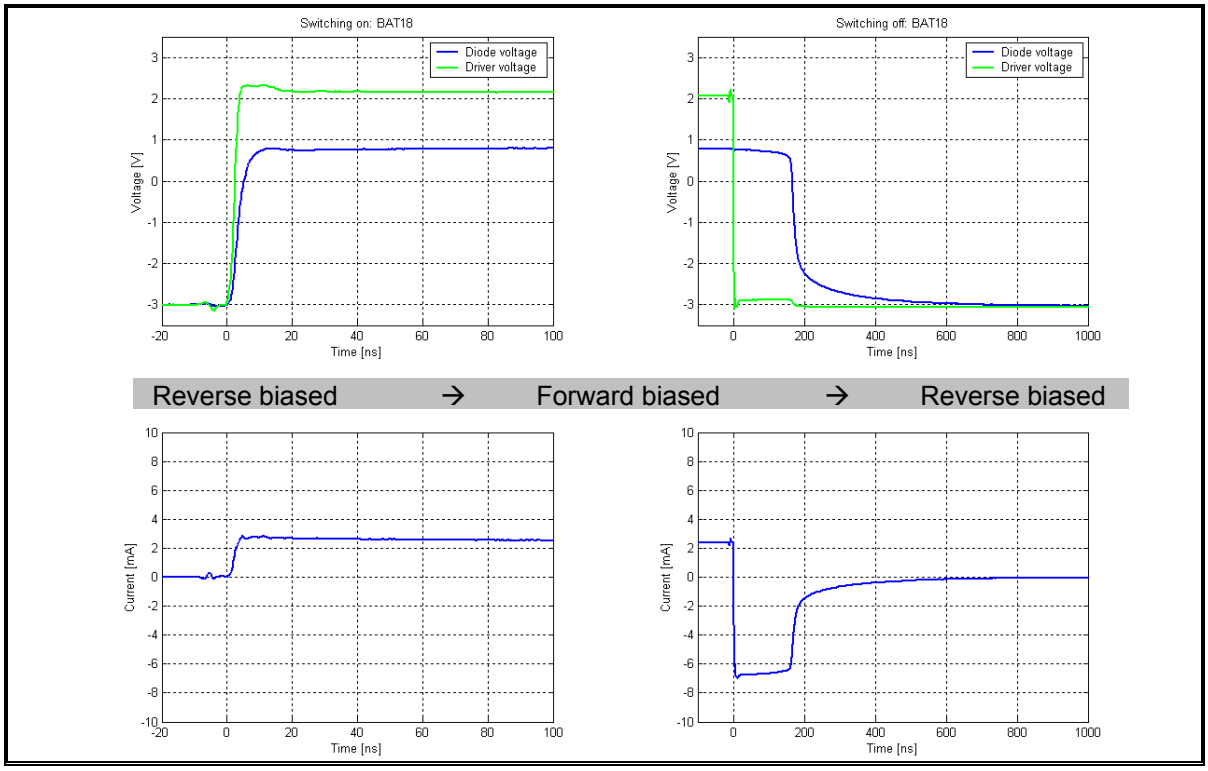

FIGURE 4-5: MEASURED SWITCHING ACTION OF A PIN DIODE (BAT18 FROM INFINEON TECHNOLOGIES USED)

4.2.3.b. Schottky diode

The low forward voltage, fast transition times and low on-resistance of Schottky barrier devices are often exploited in applications such as limiters and detectors [48].

A quick assessment of commercially available diodes' datasheets reveals that the on-resistance of Schottky diodes is typically higher than the PIN diode at the same bias current, but is still relatively low. The capacitance of a reverse biased Schottky is also higher than that of PIN diodes, but should be adequate for many applications. Higher doping concentration of the semiconductor causes the on resistance to drop, at the expense of a higher junction capacitance.

The state of a Schottky diode is simply related to the instantaneous voltage across its terminals and the switching is slightly simpler than that of a PIN diode. This also means that an RF signal bigger than the reverse bias across the diode's terminals will switch the diode into its low impedance, forward biased state. A forward biased diode can also be switched off (reverse biased) by a large RF signal, clamping the signal.

The on-resistance of a Schottky diode is inversely proportional to the bias current and the off-capacitance inversely proportional to the reverse bias voltage.

4.2.3.c. Guidelines for biasing diode switches with resistors

The bias current to a diode used as a switching element is typically supplied via inductors. This represents the filter-approach of removing the switching signal (see section 4.2.1) and relies on the fact that the inductor presents a high impedance to the RF-signal, while the low frequency bias current flows through it with minimal attenuation. The inductors can be replaced with resistors to avoid the filtering effect, with the switching signal then appearing on the output. The resistor values must be chosen big enough to present a high impedance path to the RF signal, while still being small enough to supply sufficient bias current to the diode. The relationship between the series resistance of a diode and the bias current (I_0) can be expressed by (see discussion on PIN and Schottky diodes above):

$$R_{DIO} = \frac{k_1}{I_0} \quad \rightarrow \quad (4\text{-}8)$$

Where k_1 is a constant related the physical properties of the specific device
If the voltage drop across a forward biased diode is idealized as constant, it then follows for the circuit in Figure 4-6 that:

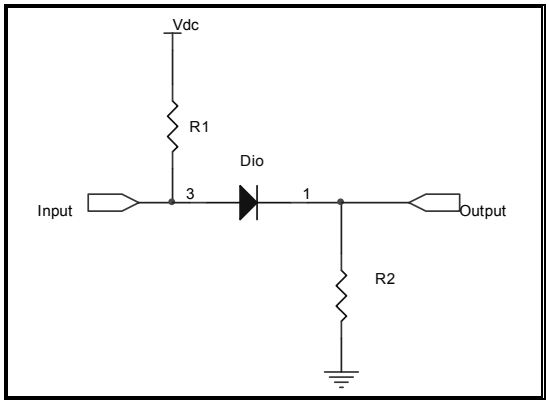

FIGURE 4-6: A SERIES DIODE SWITCH BIASED WITH RESISTORS

$$R_{DIO} = k_1 \frac{R_1 + R_2}{V_{DC} - V_{DIO}}$$

$$R_{DIO} = k_2 \left(R_1 + R_2 \right) \quad \rightarrow \quad (4\text{-}9)$$

The diode resistance is proportional to the total bias resistance when biased from a DC source.

For a series switch configuration, a bias resistor will typically appear as a shunt element in the RF-path and the diode resistance will appear in series. The RF transfer function of such a circuit can be calculated with the help of Figure 4-7. Assume R_T is the total bias resistance. The diode resistance can then, from the discussion above, be expressed as to kR_T (with k a constant.) The transfer function when driven by a source with impedance R_0 and loaded with an impedance of R_0 is given by:

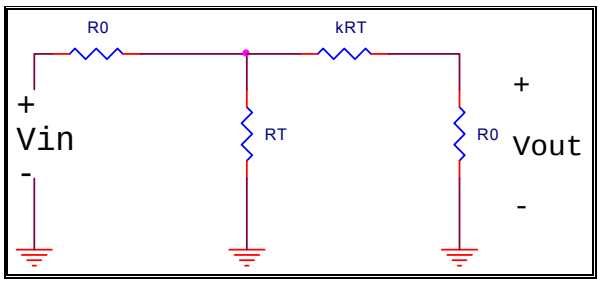

FIGURE 4-7: EQUIVALENT CIRCUIT OF SERIES DIODE SWITCH BIASED WITH RESISTORS

$$H = 4 \frac{V_{out}^2}{V_{in}^2} = 4 \left(\frac{R_T R_0}{kR_T^2 + 2R_0 R_T + kR_T R_0 + R_0^2} \right)^2 \quad \rightarrow \quad (4\text{-}10)$$

The condition for minimum attenuation can then be calculated as:

$$\frac{dH}{dR_T} = 0$$

$$R_T = \frac{R_0}{\sqrt{k}} \quad \rightarrow \quad (4\text{-}11)$$

This result can be used as a general guideline when choosing the bias resistor for a specific diode switch. Note that the switching signal will appear on the output of a diode based series switch when biasing is provided through resistors.

4.2.4. Field effect transistor as switching element

Field effect transistors (FET) are also regularly employed as a basic switching element, especially in microwave and millimetre integrated circuit (MMIC) switches [49], [50], [51]. They are typically used in their triode region, when the voltage appearing between the gate and source terminals effectively controls the resistance seen between the drain and source terminals. FET devices do not have to modulate a DC bias and the generation of switching signals can consequently be avoided (see discussion in section 4.2.2.) Further advantages of FET switches include simple driver circuits, low power consumption and fast switching speeds.

Depletion mode GaAs N-channel devices are often used [49], [51], [52] at microwave frequencies due to their low capacitance (high impedance) in the off-state and low resistance in the on-state. The depletion mode of operation complicates the driving circuitry which, in typical applications, ends up limiting the device's wideband performance [53]. MOS devices have gained on their GaAs counterparts in recent times, [53], [54], [55], offering simpler control circuitry and improved wideband performance.

A fundamental issue of FET devices that needs to be highlighted are the relationship between the on-state and off-state impedances.

4.2.4.a. Off-capacitance vs on-resistance

The on-resistance of a FET can be calculated by:

$$R_{DS(on)} = \frac{\partial V_{DS}}{\partial I_{DS}} \qquad \rightarrow \quad (4\text{-}12)$$

In the triode region, this is found [56] to be inversely proportional to the device's effective width-to-length ratio, which is a physical characteristic of the device:

$$R_{DS(on)} \propto \frac{1}{\left(\frac{W}{L}\right)_{eff}} \qquad \rightarrow \quad (4\text{-}13)$$

From a simple parallel plate argument it is then argued that the off-state capacitance will conversely be directly proportional to this ratio; or stated differently, the off-state impedance is inversely proportional to this ratio as well.

It was shown in section 4.2.1, that for both series and shunt switches, a small on-state impedance and a large off-state impedance are desirable. It is therefore clear that opposing requirements exist for the width-to-length ratio.

The off-state capacitance of the FET (C_{oss}) does however decrease as the drain-source voltage increases [57]. A typical curve obtained from the datasheet of a commercial device is shown in Figure 4-8 to validate this statement. It follows that the drain-source voltage in the off-state can be biased to reduce the capacitance and increase the eventual bandwidth of the switch. This will however cause the FET to modulate the DC voltage as well and create a large switching signal, as discussed in section 4.2.2. This is illustrated with a simulation in ADS of a simple shunt MOSFET switch of Figure 4-9.

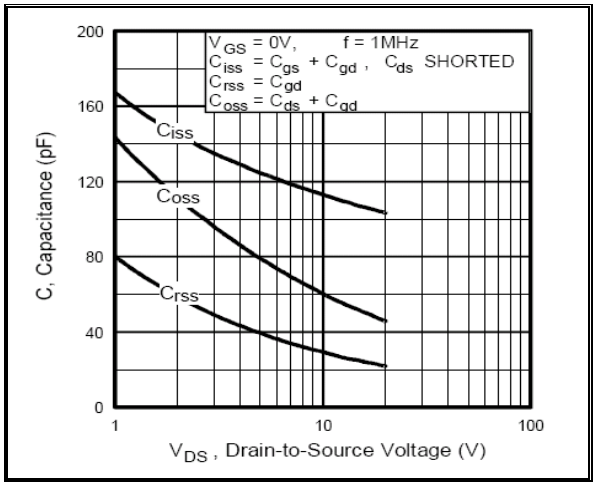

FIGURE 4-8: TYPICAL CAPACITANCES OF COMMERCIAL FET DEVICE (IRLML2402 FROM INTERNATIONAL RECTIFIER – WWW.IRF.COM)

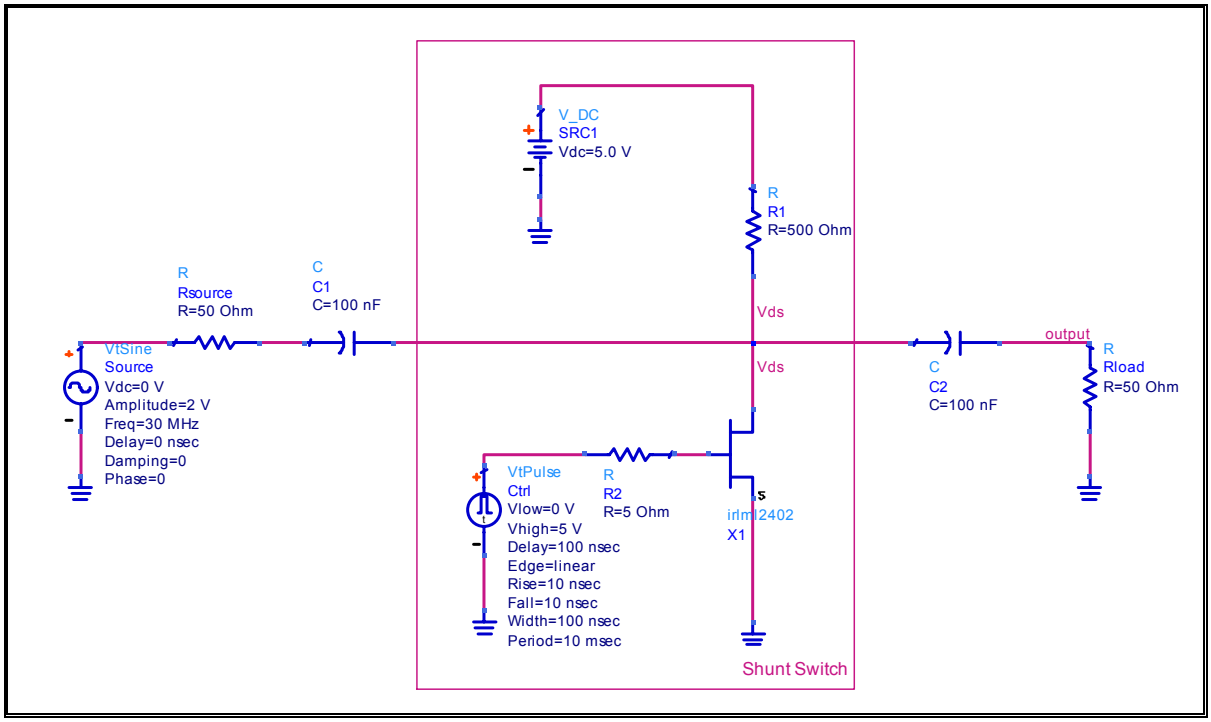

FIGURE 4-9: SHUNT MOSFET SWITCH WITH V_{DS} BIAS

The output voltage measured over R_{load} clearly shows the switched RF signal (as applied by the source) as well as the switching signal (the modulated DC bias.)

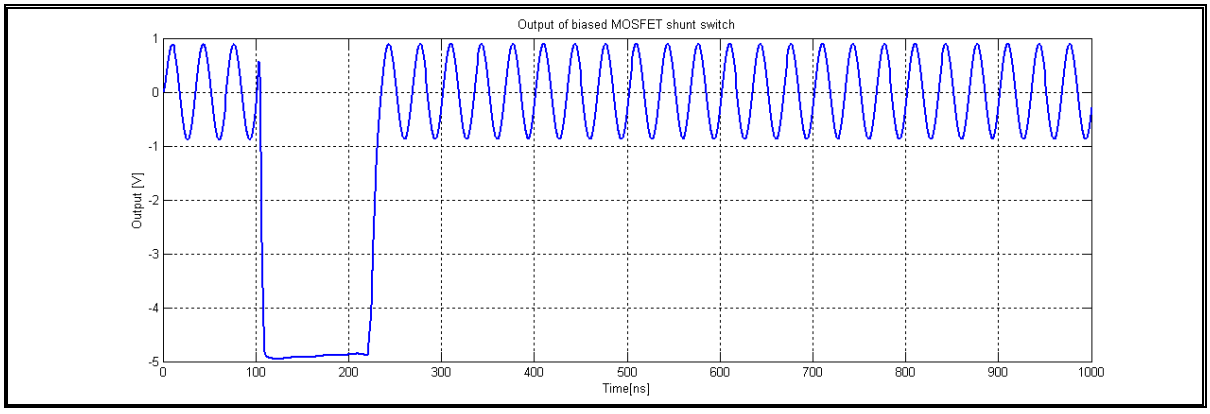

FIGURE 4-10: OUTPUT OF SHUNT MOSFET SWITCH WITH V_{DS} BIAS (SIMULATED IN ADS)

4.3. Conceptual design

A completely new configuration for the isolation switch of the transceiver must be found and the process will start with a high level conceptual design.

It was specified in section 4.1.3 that the input of the isolation switch must ideally be a short circuit in isolation mode. The switching element (or *first* switching element in the case where multiple elements are used) should therefore be a shunt element according to section 4.2.1.

It was found in section 4.2.2 that one alternative to prevent a switching signal to be introduced on the RF-output of the switch module is to use switching elements that do not use a DC bias. It was however shown in section 4.2.4.a how the effect of device parasitics (such as C_{oss} of a MOSFET) can be reduced by biasing.

The design approach will be to exploit common mode and differential mode paths to separate the switching signal (when using biased devices) from the RF signal. This was first proposed by Prof. P.W van der Walt from the University of Stellenbosch in a private communication.

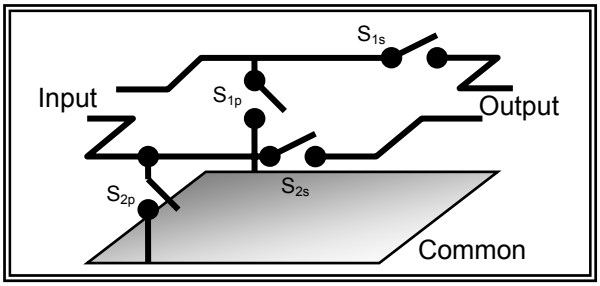

FIGURE 4-11: CONCEPTUAL DESIGN OF ISOLATION SWITCH

The general topology of Figure 4-11 is proposed to create a differential RF path, while the switching signal is generated as a common mode signal. The configuration for a set of series switches followed by a set of shunt switching elements is shown. Additional stages of these shunt and series elements can be added as required.

Shunt switches S_{1p} and S_{2p} are identical and are switched simultaneously. The switching signal will then be a common mode signal. They should be closed (low impedance) in isolation mode and open (high impedance) in through-mode. Series switches S_{1s} and S_{2s} are switched in a complementary

fashion to the shunt switches - open (high impedance) in isolation mode and closed (low impedance) in through-mode. This will also cause a purely common mode signal if the two diodes can be switched simultaneously. The signals on the two output terminals will consequently sum to double the switching signal, while the difference between the two terminals will be the applied differential RF signal only.

The single set of shunt and single set of series switch elements shown in Figure 4-11 are proposed for the transceiver's isolation switch.

MOSFETs are a natural choice for the shunt switching elements. The fixed common node eases the requirements on the driving circuitry, especially since the two devices must be driven in identical fashion. The drains can be biased, since the resulting switching signal will be a common mode signal.

Slightly more complicated driving circuitry will be required if MOSFETs were to be used as the series switching elements. The common mode switching signal generated by the shunt MOSFETs can be exploited to bias diodes for the series switch elements however. This will also eliminate the need for a second control signal.

The differential RF-path can be created by placing transformers at the input and output. This also allows for the scaling of impedance levels to optimise performance with the non-ideal series and shunt impedances of practical switches (Z_0 in equations of section 4.2.1.).

4.4. Electronic implementation

The following basic electronic circuit is proposed in response to the previous discussion. The node labelling used in this figure will be adopted throughout this section.

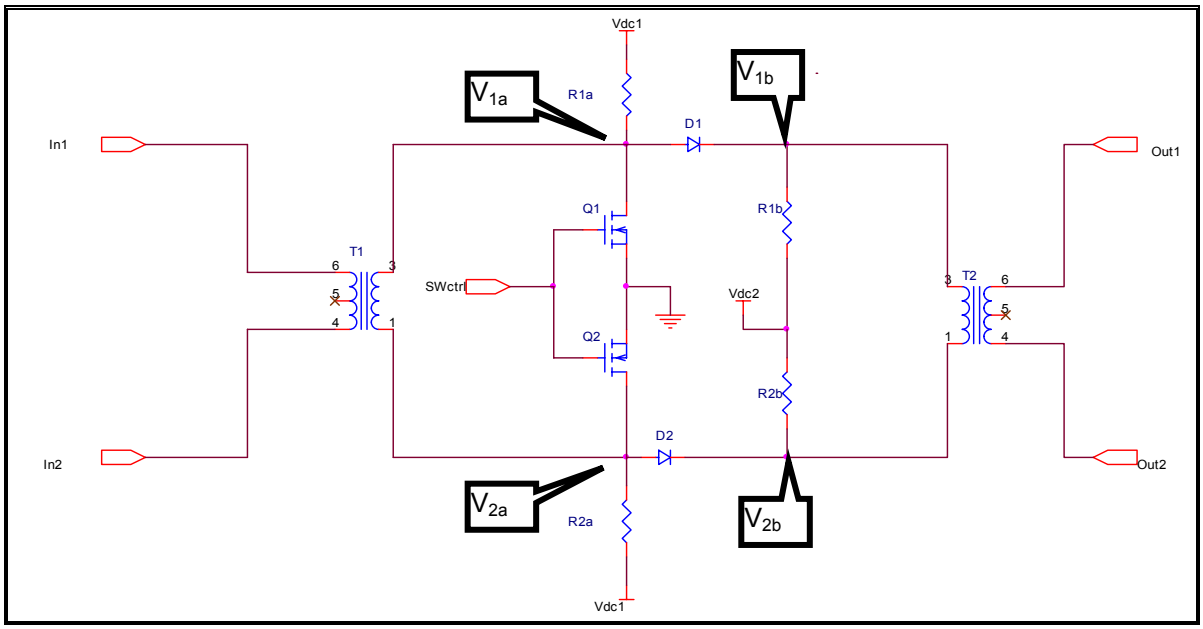

FIGURE 4-12: BASIC CIRCUIT DIAGRAM OF ISOLATION SWITCH

4.4.1. Basic operation

4.4.1.a. Isolation mode

The control signal SWctrl is high (highest permissible voltage, significantly higher than V_{GSth} of Q_1 and Q_2) during isolation mode. Identical MOSFETs Q_1 and Q_2 are consequently switched on hard and V_{1a} and V_{2a} are at a potential close to zero. These represent the shunt switches in isolation mode. Identical diodes D_1 and D_2 are now reverse biased with a voltage of approximately V_{dc2} across its terminals to realize the series switch in isolate mode.

The equivalent circuit can be represented by the following circuit. The bias resistors are assumed to be significantly larger than the other impedances and are ignored. The MOSFETs are represented by their drain-source resistances $R_{ds(on)}$ and the reverse biased diodes as capacitors.

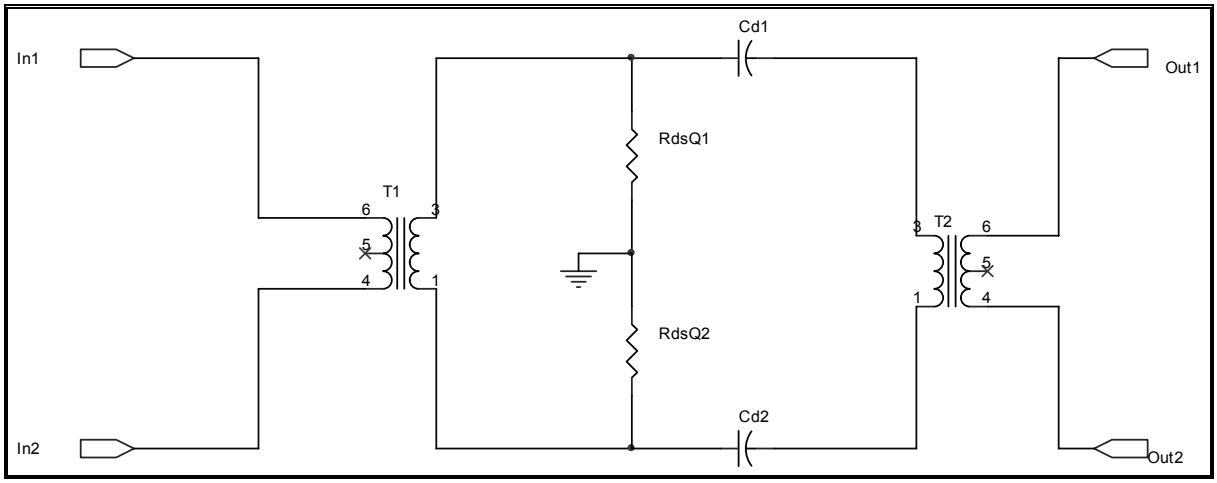

FIGURE 4-13: EQUIVALENT CIRCUIT OF ISOLATION SWITCH IN ISOLATION MODE

Note that $R_{dsQ1} = R_{dsQ2}$ since the two MOSFETS are identical and $C_{d1} = C_{d2}$, since the two diodes are identical. If ideal 1:1 transformers are assumed and the output is loaded with $Z_{0,}$ the input impedance of this network is given by:

$$Z_{in} = 2R_{dsQ1}\frac{\left(Z_0 C_{d1}\right)j\omega + 2}{\left(2R_{dsQ1}C_{d1} + Z_0 C_{d1}\right)j\omega + 2} \qquad \rightarrow \quad (4\text{-}14)$$

If $R_{ds} << Z_0$, as can be expected from proper shunt switches:

$$Z_{in} \approx 2R_{dsQ1} \qquad \rightarrow \quad (4\text{-}15)$$

Applying this approximation, the transfer function (as defined in section 4.2.1) becomes:

$$\frac{P_D}{P_A} \approx 16\left(\frac{R_{dsQ1}}{Z_0}\right)^2\left(\frac{j\omega}{j\omega + \frac{2}{Z_0 C_{d1}}}\right)^2 \qquad \rightarrow \quad (4\text{-}16)$$

The requirements for the isolation switch in isolation mode are minimum input impedance and maximum isolation. It clearly follows from these equations that the on resistance of the MOSFETs and the reverse capacitance of the diodes should both be as small as possible, which is in line with the general requirements for series and shunt switches highlighted in 4.2.1. Note that lower frequencies can in general be expected to be isolated better than the high frequency content.

4.4.1.b. Transition from isolation to through-mode

The isolation switch's transition from isolation mode to through-mode is initiated by a falling edge in the control signal SWctrl. As the gates of Q_1 and Q_2 discharge, the drain current of the MOSFETs decreases, so that the voltages on node V_{1a} and V_{2a} start to rise simultaneously. This voltage rise is dominated by the effect of charging the MOSFET drain-source capacitances through R_{1a} and R_{1b} respectively – with time constant $R_{1a}C_{oss(eff)Q1}$.

At some stage the voltages of V_{1a} and V_{2a} will have risen sufficiently above V_{dc2} to forward bias diodes D_1 and D_2. If the voltage at which the diode becomes forward biased is idealized and assumed to be exactly V_{FD1}, the time required to reach this point can be approximated by:

$$V_{dc2} + V_{FD1} \approx V_{dc1}\left(1 - e^{-\frac{t}{R_{bias1}C_{oss(eff)Q1}}}\right)$$
$$t = -R_{bias1}C_{oss(eff)Q1}\ln\left(1 - \frac{\left(V_{FD1} + V_{dc2}\right)}{V_{dc1}}\right) \quad \rightarrow \quad (4\text{-}17)$$

This point can be considered as the moment the isolation switch changes over to through-mode since the MOSFETs are now in a high impedance state and the diodes switches to a low impedance state. The voltages of V_{1a} and V_{2a} will continue to rise, but with a different time constant due to the current directed away from the MOSFETs' outputs through the conducting diodes. The currents flowing through the diodes increase as these voltages rise, so that their resistances drop further. V_{1a} and V_{2a} appear directly across the drain-source terminals of the MOSFETs. The rise in these voltages will reduce the output capacitances (C_{oss}) of the MOSFETs (see section 4.2.4.a) and consequently increase the impedances at higher frequencies. The insertion loss of the isolation switch can therefore be expected to decrease marginally during this interval after the primary transition from isolation mode to through-mode and the upper frequency of operation can also be expected to increase.

The final value of V_1 and V_2 can be expected at:

$$V_{1(\max)} \approx \frac{R_{1a}\left(V_{FD1} + V_{dc2}\right) + R_{1b}\left(V_{dc1}\right)}{R_{1a} + R_{1b}} \quad \rightarrow \quad (4\text{-}18)$$

This signals the beginning of the absolute through-mode.

4.4.1.c. Through-mode

The voltages of V_{1a} and V_{2a} during through-mode is given by equation (4-18). The MOSFETs can be assumed to be completely off and approximated by their output capacitances (C_{oss}) at this voltage. The diodes can be represented by their on resistance at the bias current flowing through them, given by:

$$I_{dio} \approx \frac{V_{dc1} - V_{FD1} - V_{dc2}}{R_{1a} + R_{1b}} \quad \rightarrow \quad (4\text{-}19)$$

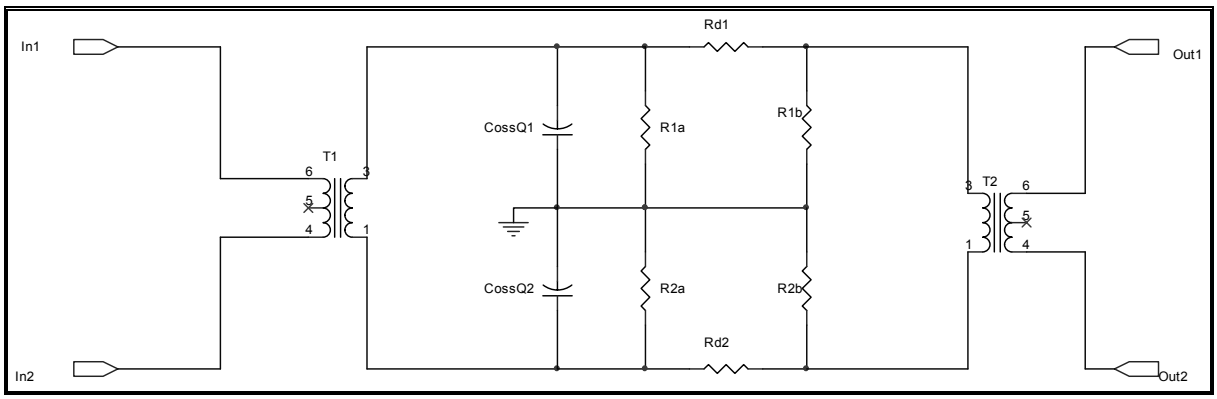

FIGURE 4-14: EQUIVALENT CIRCUIT OF ISOLATION SWITCH IN THROUGH-MODE

A general guideline for choosing the optimal bias resistors (R_{1a}, R_{1b} , R_{2a} and R_{2b}) for given diode resistances (R_{d1} and R_{d2}) and the resultant transfer function has been discussed in section 4.2.3.c. It can in general be expected that R_{1a} and R_{1b} will be significantly larger than the characteristic impedance Z_0 and that R_{d1} and R_{d2} will in turn be much smaller than Z_0. The input impedance of this circuit when loaded with Z_0 can then be approximated as:

$$Z_{in} \approx \frac{\frac{2}{C_{ossQ1}}}{j\omega + \frac{2}{Z_0 C_{ossQ}\,1}} \quad \rightarrow \quad (4\text{-}20)$$

The reflection coefficient of the switch is then given by:

$$S_{11} = \frac{Z_{in} - Z_0}{Z_{in} + Z_0}$$

$$S_{11} \approx \frac{-j\omega}{j\omega + \frac{4}{Z_0 C_{ossQ1}}} \quad \rightarrow \quad (4\text{-}21)$$

The reflection coefficient with Z_0 real approaches unity at higher frequencies, so less energy is passed through - the response is similar to a first order low pass filter. Note that the input impedance approaches a short circuit as the frequency increases. The isolation switch's principle of operation for high frequencies in through-mode is therefore similar to the general principle in isolation mode.

4.4.2. Improvements to frequency response

It was seen in the previous section that the isolation switch acts as a first order, shunt element low pass filter in through-mode. Transmitter topologies such as the step transmitter of section 3.3 have significant low frequency content that does not contribute to the radar information, since it cannot be efficiently radiated by the antenna. It would therefore be advisable for the isolation switch's transfer function to be extended to a bandpass response to reflect frequencies below the pass band.

A shunt inductor between terminals V_{1a} and V_{2a} (of Figure 4-12) is the preferred option to achieve this. A low input impedance (due to the shunt inductor) will ensure the isolation switch in through-mode provides isolation to low frequency content on the same principle as when in isolation mode. This option also forces the low frequency voltages of V_{1a} and V_{2a} to be equal (no differential voltage on the RF signal path) in steady state. The size of the inductor is discussed below.

The order of the filter can further be increased by adding reactive elements between V_{1b}, V_{2b} and the output transformer. The parasitic elements of the MOSFETs, transformers and the added shunt inductor should be integrated into this filter design.

4.4.2.a. Higher order reflective filter

This approach converts the entire isolation switch (in through-mode) to a typical ladder type bandpass filter network. The circuit appears as in Figure 4-15.

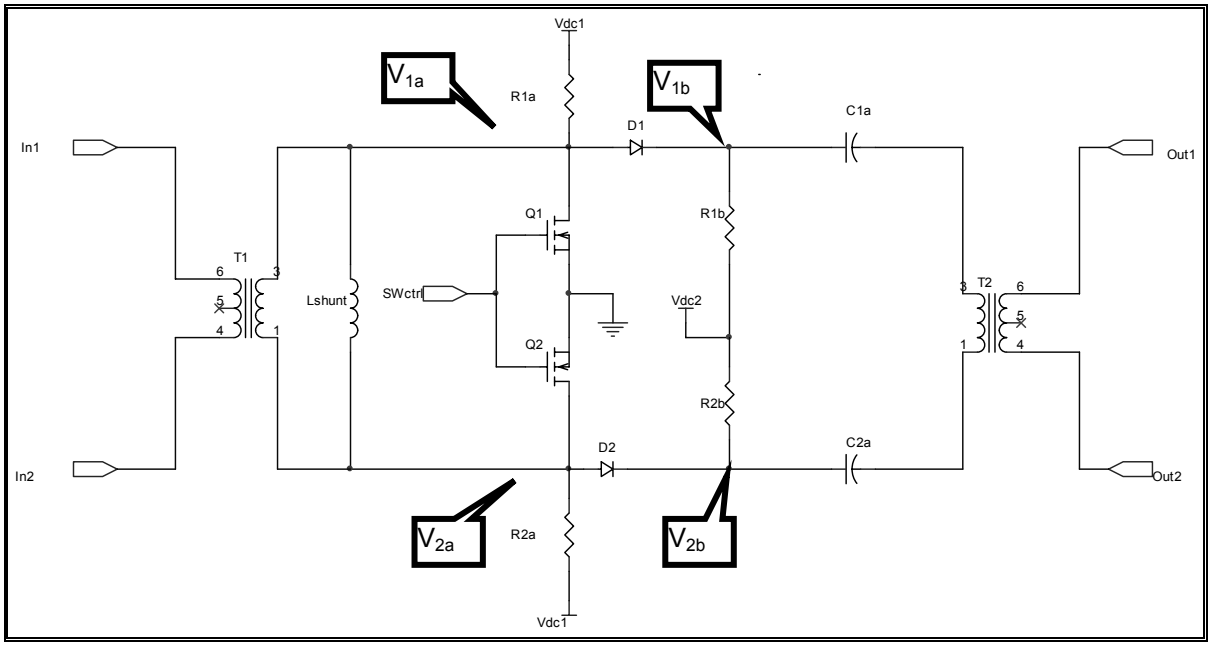

FIGURE 4-15: BASIC CIRCUIT DIAGRAM OF ISOLATION SWITCH EMPLOYING A SECOND ORDER BANDPASS FILTER

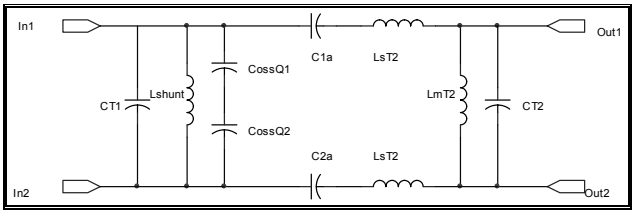

FIGURE 4-16: EQUIVALENT CIRCUIT OF ISOLATION SWITCH IN FIGURE 4-15.

The ladder network is clearly seen in the equivalent RF circuit of Figure 4-16, where the following approximations were made:

- The inductances associated with the input transformer are dominated by the effect of the added L_{shunt} and are consequently omitted. Only the interwinding capacitance (C_{T1}) of the transformer is taken into account, which will just add to the MOSFETs' output capacitances.
- The bias resistors and on resistance of the diode are not taken into account as their effect can be assumed to be negligible.
- The output transformer is represented by its mutual inductance (L_{mT2}), stray inductance (L_{sT2}) and inter-winding capacitance ($C_{T2.}$)
- The value of C_{ossQ1} and C_{ossQ2} should be taken as the value specified at $V_{1a(max)}$ of equation (4-18).

Standard design techniques can now be used to create a bandpass response according to a certain polynomial approximation with a good pulse response [58]. The upper and lower corner frequencies of UWB systems are typically spaced so far apart that the low pass section and high pass section can be designed independently. The following should be taken into account:

- C_{ossQ1} and C_{ossQ2} are limited by the specifications of the MOSFETS and can be slightly varied by choosing V_{dc1}, but too high values of V_{dc1} should be avoided as it is good practice to minimize the amplitude of the common mode switching signal. The value of the capacitor can be increased with additional capacitors in parallel, but not decreased.
- L_{mT2}, L_{sT2} and C_{T2} are characteristics of the transformer. L_{mT2} can be decreased with an additional parallel inductor, L_{sT2} can be increased with another series inductor and C_{T2} can be increased with a parallel capacitor. The transformer can alternatively be chosen with a sufficiently wide bandwidth to not influence the primary filter response.
- The input transformer's inter-winding capacitance (C_{T1}) simply adds to the MOSFETs' output capacitances. A transformer with sufficiently high upper frequency limit will again cause only a minimal increase.
- The characteristic impedance of the system can be chosen, courtesy of the input and output transformers, but its effect on isolation and insertion loss in the presence of non-ideal the switching elements (see section 4.2.1) should be taken into account.

4.4.2.b. Additional dissipative filter

The advantages of dissipative filtering will be discussed in detail during the design of the receiver module (Chapter 5). Suffice to mention that this filter dissipates energy outside the passband rather than reflecting it back.

The requirement for a reflective high pass filter at the input of the isolation switch was discussed earlier and led to the inclusion of $L_{shunt.}$ It can be argued that this should then be followed by a dissipative filter. The proposed circuit is shown in Figure 4-17.

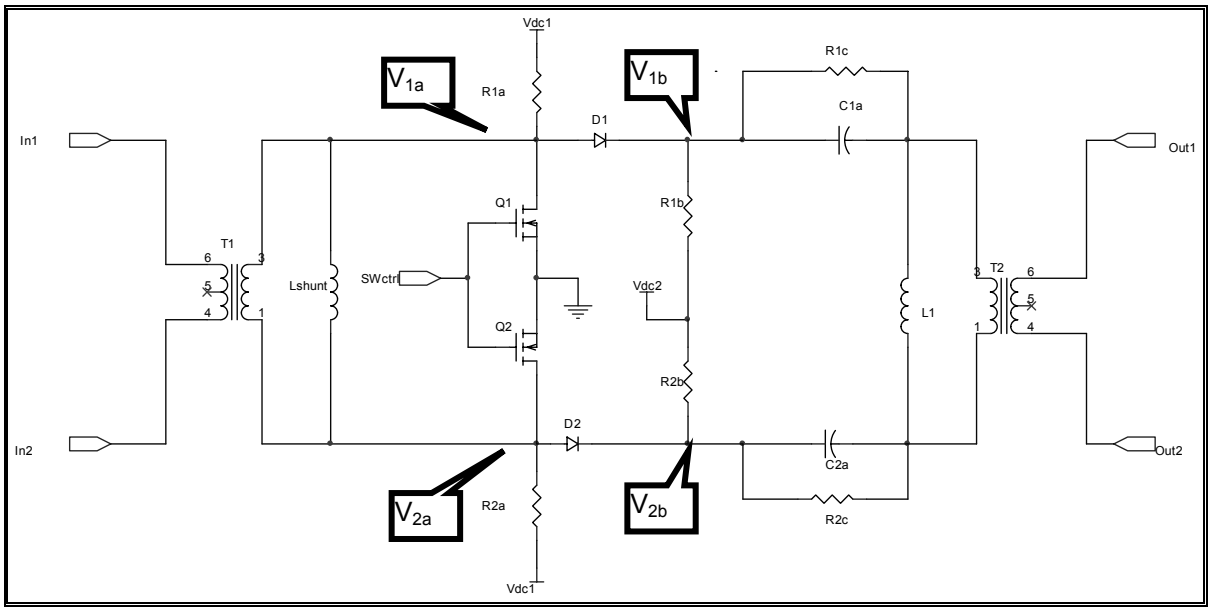

FIGURE 4-17: BASIC CIRCUIT DIAGRAM OF ISOLATION SWITCH EMPLOYING DISSIPATIVE FILTERING

Resistors R_{1c} and R_{2c} combine with capacitors C_{1a} and $C_{2a,}$ inductor L_1 and the load resistance to form the required dissipative filter. The design can be evaluated by using the equivalent circuit of Figure 4-18, with some approximations and assumptions similar to those made in the previous section:

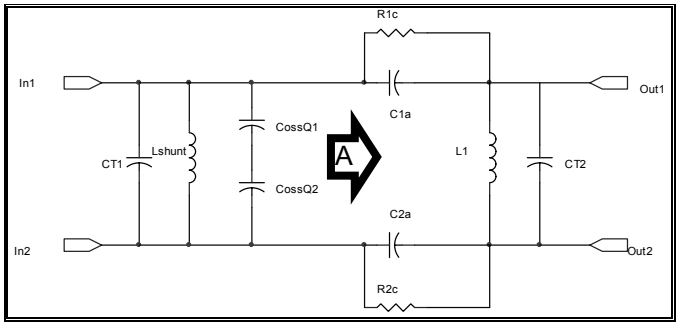

FIGURE 4-18: EQUIVALENT CIRCUIT OF FIGURE 4-17.

- The input transformer is ignored as before, due to the effect of L_{shunt}.
- L_1 similarly now dominates the inductances of the output transformer.
- The bias resistors and on resistances of the diodes are again ignored.
- It will be assumed that the output transformer have sufficient bandwidth for C_{T2} to be negligible.
- The value of C_{ossQ1} and C_{ossQ2} should again be determined at $V_{1a(max)}$ of equation (4-18).

The input impedance looking into A can be taken as Z_0, the characteristic impedance of the network (this attribute of a dissipative filter is discussed in 5.2.1.) L_{shunt} and the capacitance of $\left(C_{T1}+\frac{C_{ossQ1}}{2}\right)$ can therefore be seen as a first order band pass filter and should be designed as such. Z_0 can again be chosen with the correct choice in transformers, as outlined in the previous topology.

The dissipative filter is the differential diplexer of section 5.2.1.d – where the details of its design can be found as well. The transfer function of the isolation switch will now be a bandpass system comprising a second order high pass and a first order low pass roll off.

4.4.3. Detailed considerations

In order to realize the preceding generic circuits in practice, some details concerning component specifications need to be considered.

4.4.3.a. Transformers

The transformers must in general be as wideband as possible, except if their parasitic reactances are incorporated into the filter design (as discussed in section 4.4.2.) The transformer ratio is chosen to match the isolation switch to the rest of the system, while creating the desired impedance level for the isolation switch internally. The isolation switch's characteristic impedance is a trade-off between a number of parameter. Series switches generally provide better isolation with low impedances and shunt switches with high impedances (section 4.2.1.) The requirements for minimum insertion loss are exactly opposite by the same argument. The upper frequency limit of the isolation switch in through-mode will typically limited by C_{oss} of the MOSFETs, which can be countered by a low impedance.

4.4.3.b. MOSFETs

The $R_{ds(on)}$ parameter of the MOSFETs must provide sufficient isolation and introduce minimum loss between transmitter and antenna (see section 4.4.1.a.) The opposing parameter of output capacitance C_{oss} must be small enough to achieve the required bandwidth at the chosen impedance level in through-mode, as discussed in 4.4.1 and 4.4.2. A small output capacitance will also ensure a fast transition between modes according to equation (4-17) and will require a lower supply voltage. The gate charge and gate driving circuitry should be evaluated in a similar fashion as with the design of the transmitter in section 3.3.1.b. A dual-packaged device would be ideal to ensure the two MOSFETs are identical.

4.4.3.c. Diodes

The diodes should be chosen to have the smallest possible on-resistance at the lowest possible bias current, defined by the parameter k_1 in section 4.2.3.c. This provides the opportunity to use bigger bias resistors, which reduces the insertion loss in through-mode. The diode should further have the lowest possible capacitance in reverse bias, as it will increase the isolation in isolate mode and increase the bandwidth over which the isolation is provided. Should PIN diodes be used, the timing of the SWctrl signal must be such that sufficient time is given for the diodes to switch from low impedance to reverse biased - after the acquisition time of the receiver, before the next pulse. PIN diodes allow for bigger bias resistors to be used, and the possibility of the PIN diodes becoming

conductive during isolation mode is extremely remote. A Schottky diode's on-resistance and reverse capacitance are inferior to that of the PIN diode and smaller bias resistors or a higher supply voltage might be required. V_{dc2} must also be chosen high enough to prevent the diode from becoming conductive in isolation mode. The transitions between states of these devices can be taken as instantaneous in most cases however.

4.4.3.d. Other components

R_{1a} and R_{2a} should be identical, as should R_{1b} and R_{2b} – the use of low tolerance components is recommended. The design approach would be to start off with the same value for all these bias resistors, according to guideline for the *total* bias resistance of equation (4-11):

$$R_{1a} = R_{1b} = R_{2a} = R_{2a} = \frac{R_0}{2\sqrt{k}} \quad \rightarrow \quad (4\text{-}22)$$

It can then be fine tuned if the transition time (see equation (4-17)) is not as required.

The capacitors and inductors should be low tolerance components when possible to ensure symmetry.

V_{dc2} can be supplied by a zener diode and smoothing capacitor fed from V_{dc1} through a resistor.

4.5. Laboratory measurements

Two configurations of the basic isolation switch discussed above were built to evaluate this module specifically for application in a borehole radar system.
The main differences between the two configurations are summarized in the table below:

	Configuration 1	Configuration 2
Basic circuit diagram	Figure 4-17	Figure 4-15
Filtering principle	Dissipative filtering	2nd order bandpass filter (Butterworth)
MOSFETs	Dual package Low on-resistance Very low off-capacitance	2 separate devices Very low on-resistance Low off-capacitance
Diodes	PIN diode	Schottky diode
Power supply	5 V	14 V

TABLE 4-1: DIFFERENCES BETWEEN CONFIGURATION 1 AND CONFIGURATION 2

Detailed circuit diagrams of the two prototypes are included in addendum A.

The power supply voltage had to be increased for configuration 2 to lower the MOSFET off-capacitance sufficiently to achieve the desired frequency response and to increase the current through the Schottky diodes. The timing of the control signal was such that the PIN diode had

adequate time to recover from the conducting to reverse bias state. The systems both have a 50 Ω characteristic impedance.

4.5.1. Time domain

4.5.1.a. Switching action

The internal node voltages of the isolation switch give a clear illustration of its basic operation (as discussed in section 4.4.1.) The input and output were terminated with 50 Ω resistors and the measurement was performed on an oscilloscope with 500 MHz analog bandwidth. The node labelling adopted in Figure 4-17 (for configuration 1) and Figure 4-15 (for configuration 2) is again used. Only one trace is shown for common mode voltages. The control signal to the switch (SWctrl) is used as reference for t=0.

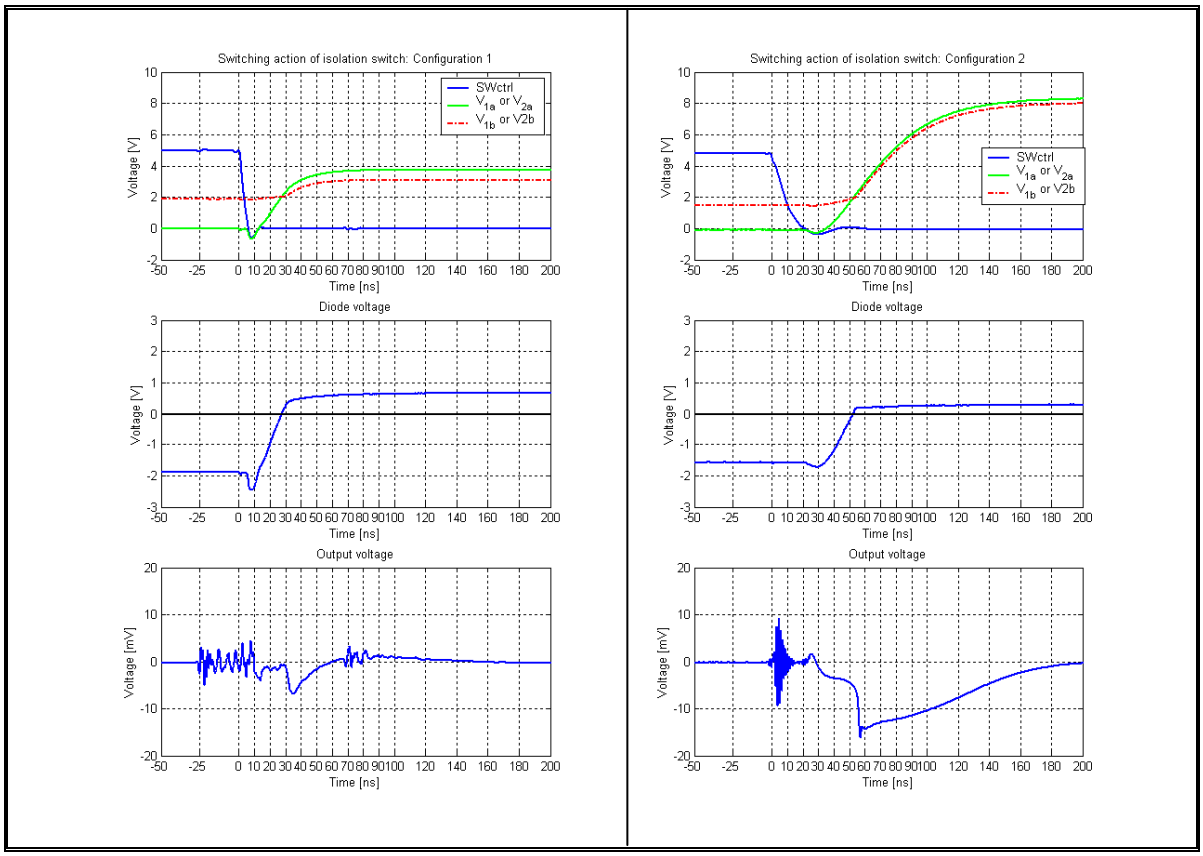

FIGURE 4-19: BASIC OPERATION OF ISOLATION SWITCH (MEASURED)

The common mode switching signals are as expected; note the difference in time constants between the two configurations due to the difference in output capacitances of the MOSFETs used. This causes the diode of configuration 1 to become forward biased 20 ns earlier than for configuration 2 (as predicted by substituting the component's datasheet parameters into equation (4-17).)

The output voltage represents the leakage of the switching signal onto the differential RF signal path. A 7 mV peak is observed in configuration 1 and a 16 mV peak is observed in configuration 2. This switching signal rejection ratio therefore amounts to 54 dB in both cases - if the switching signal is assumed to be the output of the MOSFET (V_{1a} and V_{2a}). The lower supply voltage (and consequently lower absolute switching signal leakage) and quicker response time of configuration 1 makes it the preferred choice from this discussion, but both systems perform satisfactorily.

4.5.1.b. Transfer function

The 50 Ω input termination of the previous measurement was then replaced with a 50 Ω pulse source. The pulse source generates a monocycle (it was in fact a low voltage replica of the bipolar transmitter developed in section 3.4) with variable delay. The output voltage of the isolation switch was then monitored while this delay was adjusted to sweep the pulse through the transition interval from isolation mode to through-mode. The output of this pulse source when driving a 50 Ω load has been included for comparison. The control signal is again used as a zero time reference, and the instant when the diodes become forward biased is indicated, so that the waveforms measured in the previous section can be referred to for an indication of the time when the isolation switch switches over between states.

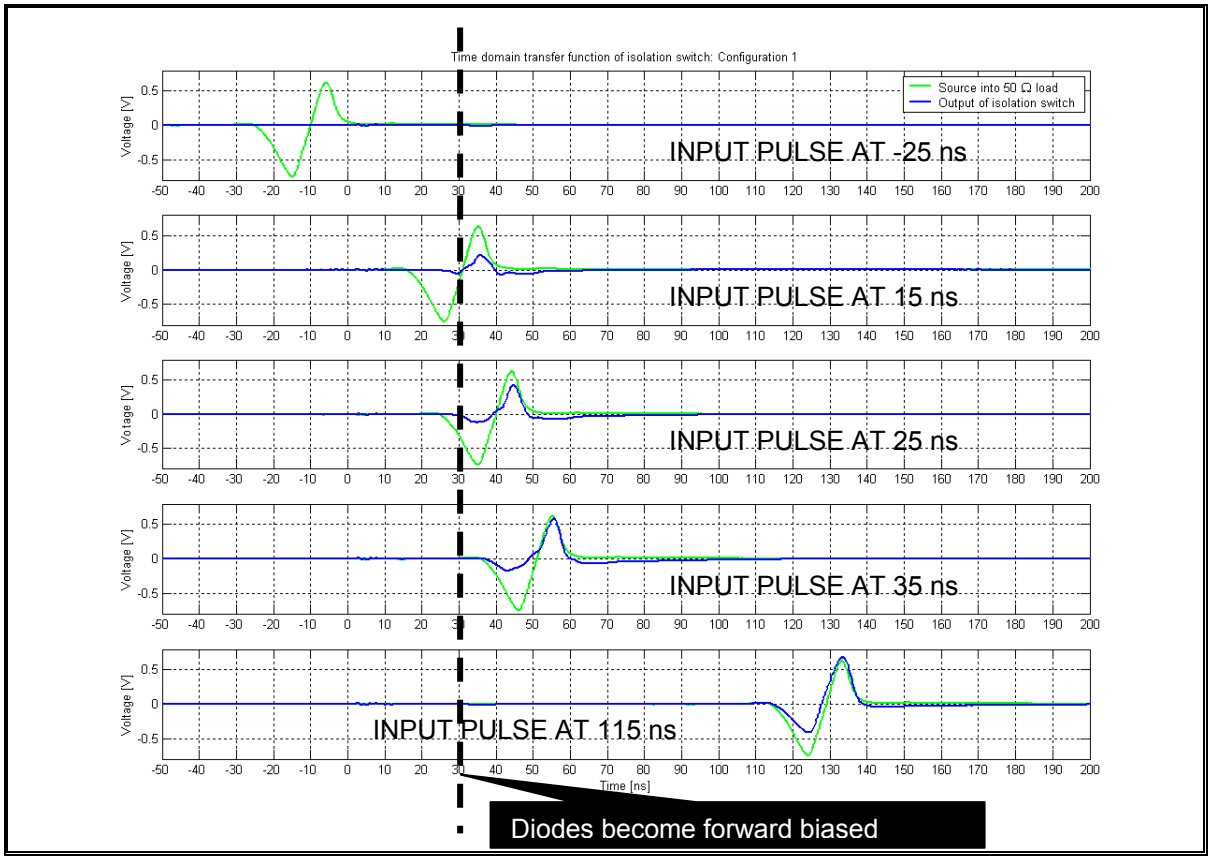

FIGURE 4-20: TIME DOMAIN TRANSFER FUNCTION OF ISOLATION SWITCH - CONFIGURATION 1 (MEASURED)

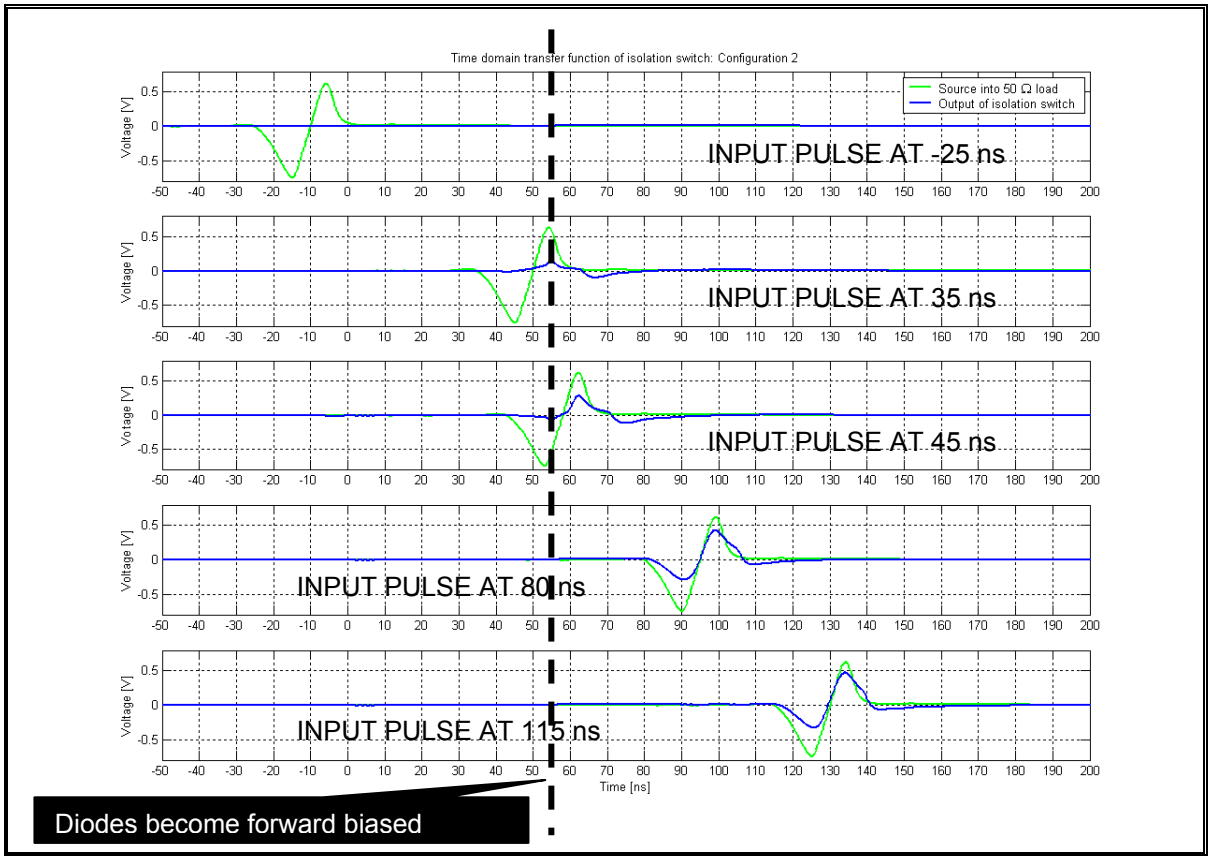

FIGURE 4-21: TIME DOMAIN TRANSFER FUNCTION OF ISOLATION SWITCH - CONFIGURATION 2 (MEASURED)

The difference between isolate and through-mode is clear, the isolation is good and the insertion loss does not appear to be excessive. This will be quantified in the frequency domain later. The expected correlation between the diodes becoming forward biased and the change-over to through-mode (see section 4.4.1.b) is confirmed and occurs at 30 ns and 54 ns for configuration 1 and 2 respectively. This corresponds to the time given by equation (4-17) and the difference can be attributed to the smaller effective output capacitance of configuration 1's MOSFETs, as well as its slightly smaller bias resistors. The switches take around 20 ns to change over completely.

4.5.2. Frequency domain

The transmission coefficient and matching is best evaluated in the frequency domain and were measured on a calibrated network analyser between 500 kHz and 500 MHz. Each configuration was measured twice, with a DC voltage of 5V applied to SWctrl (isolate mode) and a DC voltage of 0 V applied to SWctrl (through-mode).

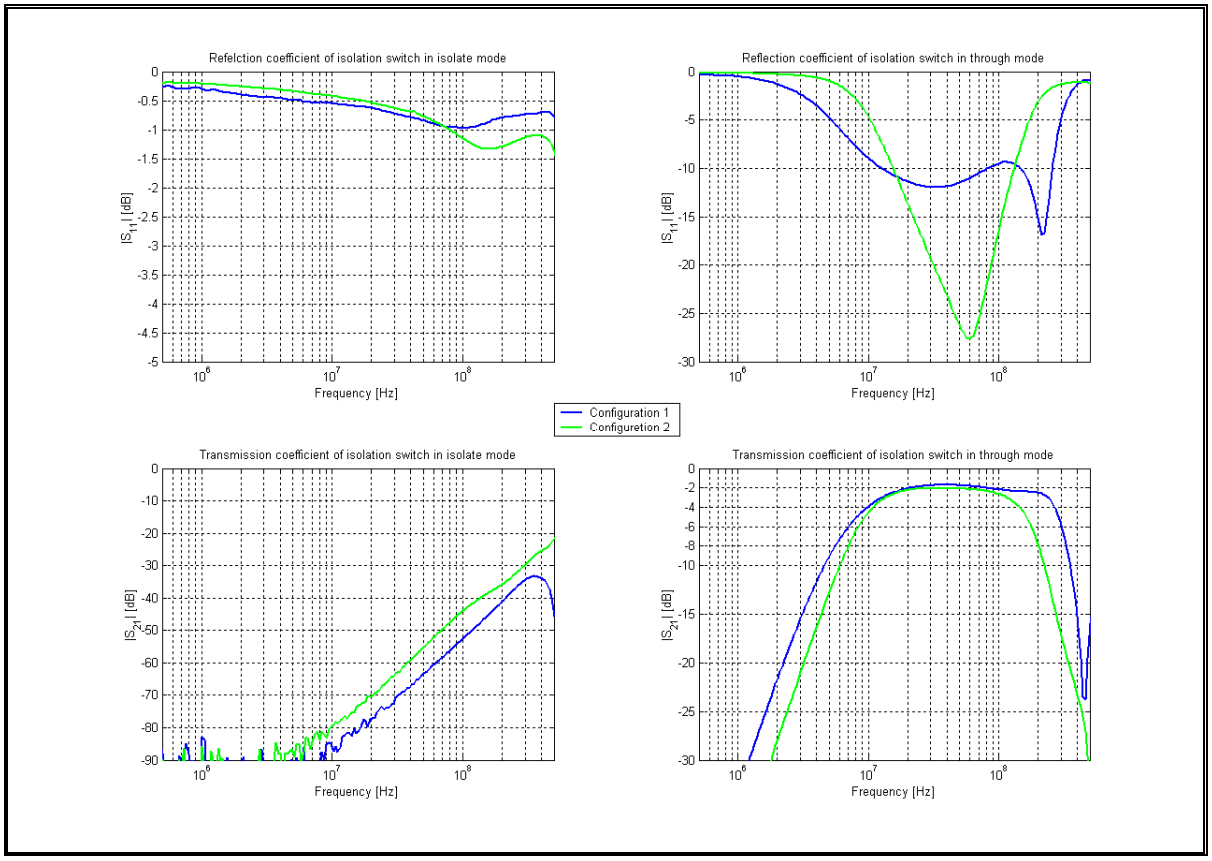

FIGURE 4-22: SCATTERING PARAMETERS OF ISOLATION SWITCH (MEASURED)

The input impedance is close to the required short circuit in isolate mode for both configurations. The isolation is between 44 dB and 80 dB in the 10 – 100 MHz interval for configuration 2 and between 53 dB and 87 dB for configuration 1. The decrease in isolation towards the higher frequencies can be attributed to the capacitance of the diodes.

The input in through-mode is sufficiently well matched to 50 Ω in the operating frequency band. The insertion loss in through-mode is 2 dB across the frequency band with the second order response clear at the low frequency side. The lower MOSFET capacitance of configuration 2 increases its high frequency cut off, until it is eventually limited by the transformer. The nominal insertion loss can be attributed mainly to the transformers. This loss, occurring between the antenna and receiver, combined with the noise generated by the additional components can be expected to degrade the noise performance of the system.

4.6. Synopsis

The design of a completely new configuration was presented to enable a high energy pulse transmitter and sensitive UWB receiver to use the same antenna for the radar detection of targets at a distance comparable to the resolution of the system. Features of this design are:

- A series connection of the transceiver's modules was proposed to enable a system where isolation can be provided from the transmitter *current* as opposed to the more conventional approach of isolating from the *voltage*.
- The use of a transmitter that stays in a low impedance state after transmission enabled the use of a single throw isolation switch instead of the conventional double throw T/R-switch.
- A novel technique was developed to separate a RF signal from a switching signal with similar frequency content by exploiting common mode and differential mode signal paths. This enabled the system to rapidly switch from transmit to receive mode and detect close-in targets.
- The intelligent employment of FETs and diodes enabled the use of a single control signal, while minimizing the effect of parasitic reactances associated with these devices.

A number of guidelines were developed to design a practical switch and prototypes of two configurations were built and tested for specific application in a borehole radar system. The performance of the two configurations seems to be well matched, with only subtle differences. Configuration 1 operates with a lower supply voltage and consequently introduces smaller switching artefacts into the signal path. The response time is also quicker and the only complication is the additional time required to reverse bias the PIN diodes after the acquisition time – which should not pose a problem with typical PRF's. Both configurations will nonetheless be evaluated in the field.

The design discussed in this chapter has been patented [14].

CHAPTER 5

Receiver design

5.1. Background

The term *receiver* in radar systems refers to the device that converts the electromagnetic signal received on the antenna to a form that conveys relevant information to the operator. The relevant information has however started to entail an increasing amount of intelligence and automation of functions previously left to the operator [42]. With the advance in analog to digital converter (ADC) technology, processes traditionally associated with analog electronics are also increasingly being shifted to after the ADC and performed digitally.

The term receiver will, for the purpose of this dissertation, be defined as the analog electronics responsible for conditioning the signal received on the antenna so that the full dynamic range of the ADC is utilized.

The transceiver designed here is specified as a baseband system and no demodulation, correlation or interpretation of the signal is required in the receiver. The receiver must simply amplify the detected signal to a convenient level for the ADC with high fidelity and minimum addition of noise.

The fidelity of a system will, for the purpose of this dissertation, be defined as the ability to accurately realize its theoretically expected transfer function.

The receiver discussed here will find a wide range of applications beyond baseband radar; it has, for instance, the same basic structure as some ultra sound receivers [59], [60] and shares a number of fundamental principles with nuclear instrumentation amplifiers [30], [61].

5.1.1. Application: Borehole radar

The design specifications for a receiver employed specifically in a bi-static borehole radar system [11], [62] will typically include bandwidth, gain and the maximum voltage swing that should be passed on to the ADC. In keeping with the approach of using the performance of the current GeoMole bi-static radar as the design specification for the monostatic system, the systems level parameters can be summarized as follows:

- The bandwidth is typically stated to be approximately 10 -100 MHz. Any signal below 10 MHz can be assumed to be undesired artefacts generated by the radar system (such as late time

antenna discharge signals, transmitter leakage, switching signals, etc), since the antenna cannot efficiently receive frequency content below 10 MHz. The low frequency rejection is typically achieved by interstage filtering, while the limitations of the amplifiers usually determine the upper frequency of operation.

- The receiver of the GeoMole bi-static radar (from internal documentation) is in effect just an amplifier with around 60 dB gain. Some work has been done on the use of automatic gain control [12] (AGC) in borehole radar receivers, but the current system employed by GeoMole makes use of sensitivity time control (STC) to increase the gain gradually over the acquisition interval.
- The maximum input range of the particular ADC, which will also be used for the monostatic system designed here, is 1 V_{pp}. It is an 8 bit device, so that the smallest quantifiable signal amplitude is 4 mV_{pp}.
- Current receiver chains operate with typical noise figures of between 3 and 4 dB.

5.1.2. Interfaces with other modules

The input of the receiver connects to the isolation switch and the output with the ADC. The isolation switch was shown to have a transformer at its output, enabling it to interface to either a differential or single sided receiver. The turns ratio of the transformer also affords for some flexibility in receiver impedance. The receiver should consequently be designed closely with the isolation switch.

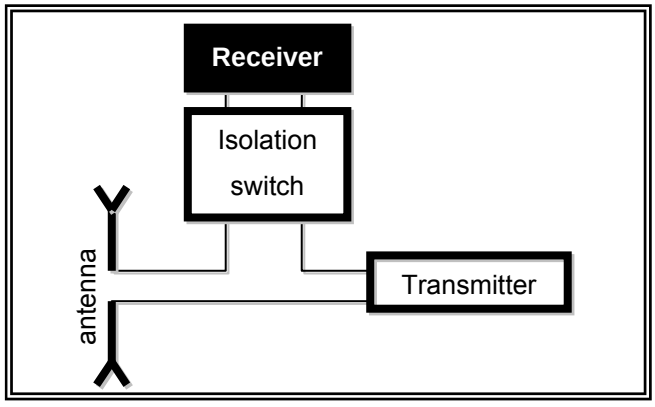

FIGURE 5-1:SYSTEMS LEVEL DIAGRAM OF TRANSCEIVER

The ADC will typically require a differential signal at a certain bias point. The gain of the receiver should also be chosen to make optimal use of the dynamic range of the ADC. This implies sufficient gain to enable digitisation right down to the noise level, without letting the signal amplitude exceed the maximum input voltage swing of the ADC.

5.1.3. Overview of chapter

The anticipated outcome of this chapter is a general design guide for an analog receiver chain that can amplify a baseband input signal with high fidelity to enable sensible digitisation of its output by the ADC. The signal will consist of the signal received on the antenna, as well as leakage from the

transmitter and artefacts from the isolation switch's switching action. A further outcome of this chapter is a monostatic borehole radar receiver as illustration of how these guidelines should be applied.

A number of basic concepts will be discussed in section 5.2, which is in effect a formalization of standard receiver design principles, as applicable to this design specifically. The exception is the discussion on dissipative filtering, which is not an established technique in the design of receiver modules and will eventually form the fundamental concept that sets this design apart from standard configurations.

These principles will then be used to design two receiver prototypes to meet the requirements of a borehole radar system (section 5.3.) It was deemed necessary, for a sensible discussion, to deviate from the more generic approach adopted in previous chapters and discuss the design process with reference to specific commercial components.

These receiver configurations are then evaluated through laboratory measurement in section 5.4.

5.2. Basic concepts

5.2.1. Dissipative filtering

5.2.1.a. Background

Consider the following diagram of a typical receiver chain section. An amplifier (characterized by its scattering parameters) is preceded and followed by filter elements, which could be a simple DC blocking capacitor or a complex high order filter. The corresponding signal flow graph is shown for the case where the source and load is perfectly matched to the system, and where the elements can be represented by lumped elements.

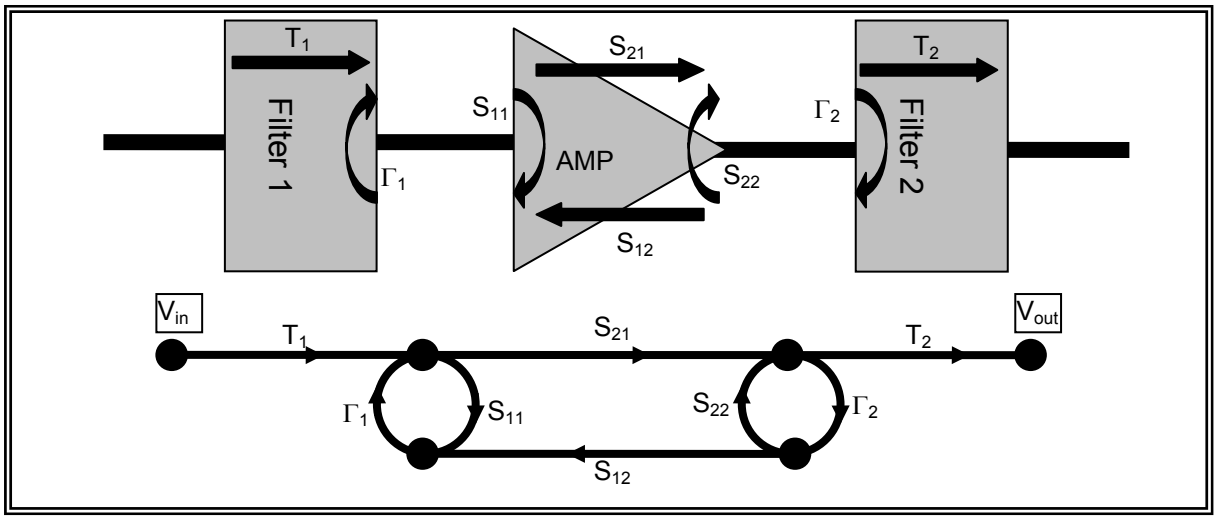

FIGURE 5-2: SECTION FROM A TYPICAL RECEIVER CHAIN WITH CORRESPONDING SIGNAL FLOW GRAPH

Signal flow graph reduction [63], [64] of this system yields the following result:

$$V_{out} = \frac{S_{21} T_1 T_2 V_{in}}{1 - \Gamma_2 S_{22} - \Gamma_1 S_{11} + \Gamma_1 \Gamma_2 S_{11} S_{22} - S_{21} \Gamma_2 S_{12} \Gamma_1} \quad \rightarrow \quad (5\text{-}1)$$

The amplifier is assumed to be ideal ($S_{11}\approx 0$, $S_{22}\approx 0$, $S_{12}\approx 0$) for most applications, resulting in the more generally used form of the transfer function.

$$V_{out} \approx S_{21} T_1 T_2 V_{in} \quad \rightarrow \quad (5\text{-}2)$$

It is emphasized that the full form of the equation should receive consideration in high fidelity (as defined in section 5.1) systems:

- While transmission through the filters (T_1 and T_2) decreases outside the pass band, the magnitude of their reflection coefficients (Γ_1 and Γ_2) approach unity.
- The reflection coefficients of amplifiers (S_{11} and S_{22}) are often large outside the pass band.
- A cursory glance at commercial amplifier datasheets reveals that the product $S_{21}S_{12}$ (as seen in the last term of equation (5-1)'s denominator) usually approaches unity.

It is clear that these conditions could lead to unexpected degradation in signal fidelity when large signals out of the pass band enter the system and effectively circulate within the system without being dissipated.

5.2.1.b. Reflective filter elements

Traditional LC filters have reflection coefficients whose magnitudes approach unity outside the pass band, in order to reflect the energy not passed to the load. A simple decoupling capacitor ($C_{decoupl}$) in a matched system with characteristic impedance of R_0, for example, forms a doubly terminated high pass filter with the following S-parameters:

$$T_{decoupl} = \frac{j\omega}{j\omega + \frac{1}{2R_0 C_{decoupl}}} \quad \rightarrow \quad (5\text{-}3)$$

$$\Gamma_{decoupl} = \frac{\frac{1}{2R_0 C_{decoupl}}}{j\omega + \frac{1}{2R_0 C_{decoupl}}} \quad \rightarrow \quad (5\text{-}4)$$

The high pass corner frequency is at $\omega_c = 1 / (2R_0C_{decoupl})$ rad.s^{-1} and the reflection coefficient approaches +1 at low frequencies, which might cause the transfer function to deviate from the simplified form of equation (5-2).

5.2.1.c. Constant impedance equaliser

Inspection of equation (5-1) reveals that the ideal transfer function of (5-2) can be achieved with a non-ideal amplifier, as long as the reflection coefficients of the filters, Γ_1 and Γ_2, are identically zero. This amounts to a filter that passes in-band frequency content, while dissipating out of band energy instead of reflecting it. Alternatively, it can be viewed as a filter with a constant, real input impedance equal to the characteristic impedance of the system at all frequencies.

The bridged-T configuration in Figure 5-3 has been presented [65] as a constant impedance equaliser circuit under the following conditions:

$$R_1 = R_2 = Z_0$$
$$Z_1 Z_2 = Z_0^2 \quad \rightarrow \quad (5\text{-}5)$$

where Z_0 is the characteristic impedance of the system. By choosing Z_1=Z_2, the network becomes symmetric and the input impedance of either a port (when the other port is terminated by Z_0) is constant:

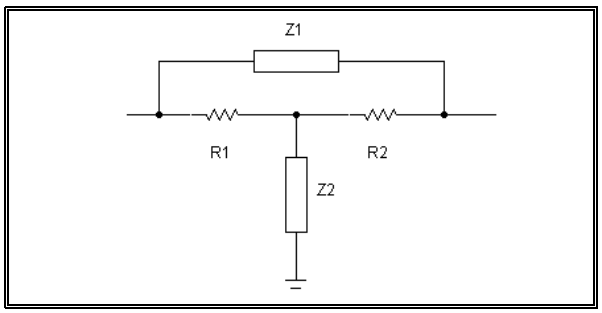

FIGURE 5-3: GENERIC BRIDGED-T CONSTANT IMPEDANCE EQUALIZER

$$Z_{in} = Z_0 \quad \rightarrow \quad (5\text{-}6)$$

The S-parameter transmission coefficient (T, as used in equation (5-1)) of the network can then be found as:

$$T_{equ} = \frac{1}{1 + \frac{Z_1}{Z_0}} \quad \rightarrow \quad (5\text{-}7)$$

This can be used to achieve a filter response in a system with a real characteristic impedance (Z_0=R_0) by using reactive components for Z_1 and Z_2. A first order high pass response can for example be achieved by substituting a capacitor C_1 for Z_1 and an inductor L_1 for Z_2. The transmission coefficient is then given by:

$$T_{equ} = \frac{j\omega}{j\omega + \frac{1}{R_0 C_1}} \quad \rightarrow \quad (5\text{-}8)$$

Z_2 then follows from (5-5) as:

$$Z_2 = \frac{R_0^2}{Z_1}$$
$$Z_2 = j\omega R_0^2 C_1 \quad \rightarrow \quad (5\text{-}9)$$

This is can be achieved with an inductor L_1 of the following value:

$$L_1 = R_0^2 C_1 \quad \rightarrow \quad (5\text{-}10)$$

The transmission coefficient is clearly similar to that obtained with a decoupling capacitor of size $C_{decoupl}$ = ½ C_1, but the reflection coefficients at both ports are identically zero.

The resultant network for a 1 rad/s corner frequency in a 50 Ω characteristic impedance is shown in Figure 5-4 and the simulated characteristics are included in Figure 5-5. The network has a reflection coefficient of zero at all frequencies on both ports, while still exhibiting a first order high pass response between the two ports. This network fulfils all the requirements for the filtering element outlined above.

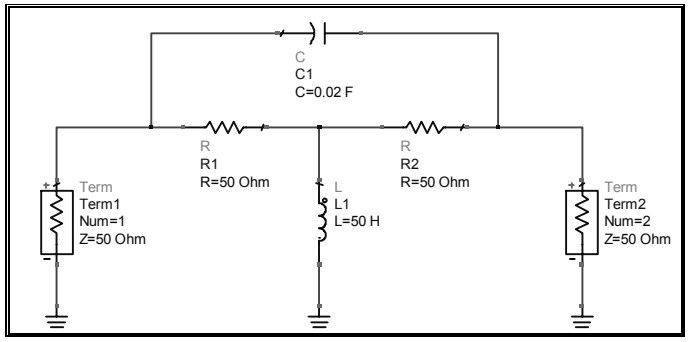

FIGURE 5-4: CONSTANT IMPEDANCE EQUALISER WITH 1 RAD/S HIGH PASS RESPONSE IN 50 Ω SYSTEM

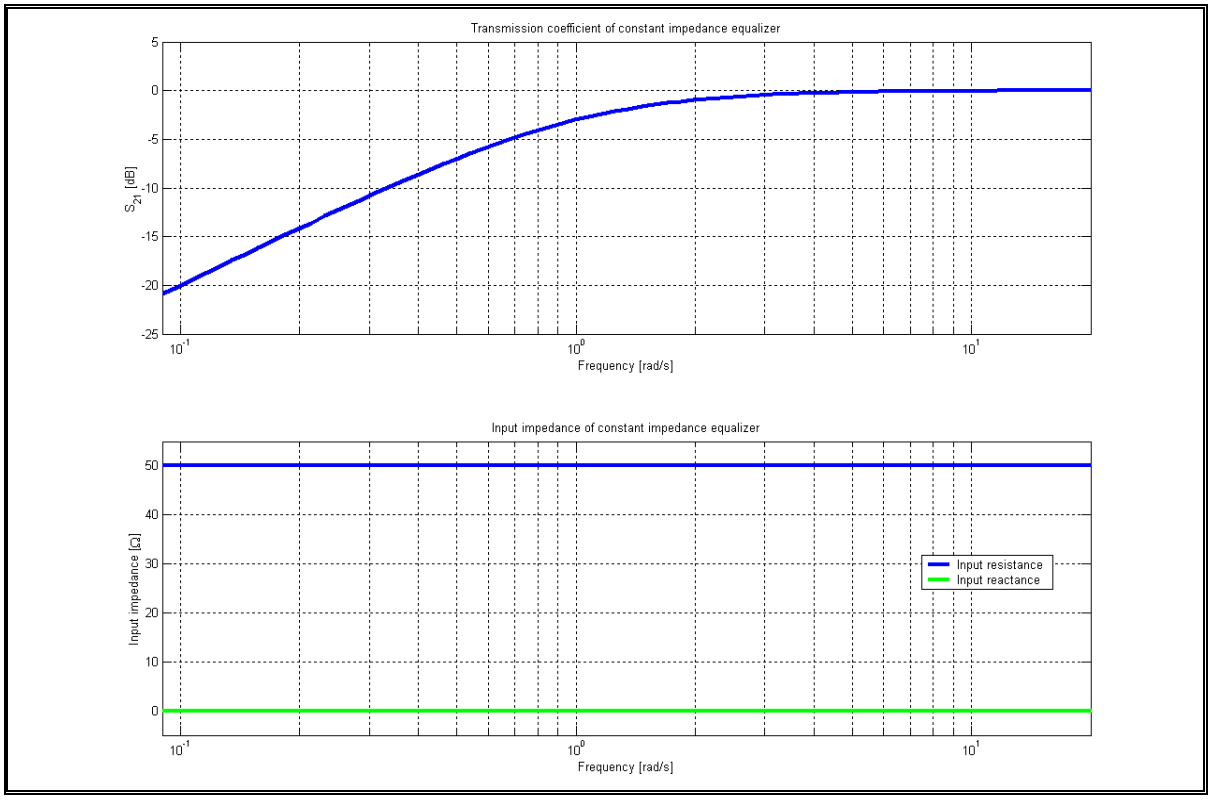

FIGURE 5-5: CHARACTERISTICS OF A CONSTANT IMPEDANCE EQUALISER WITH 1 RAD/S HIGH PASS TRANSFER FUNCTION (SIMULATED)

5.2.1.d. Diplexer

It has also been pointed out [65] that no current is flowing in R_2 of Figure 5-3 when a matched load is connected to the right hand port and R_2 can consequently be replaced by either a short circuit or an open circuit. The circuit then reduces to either of the following:

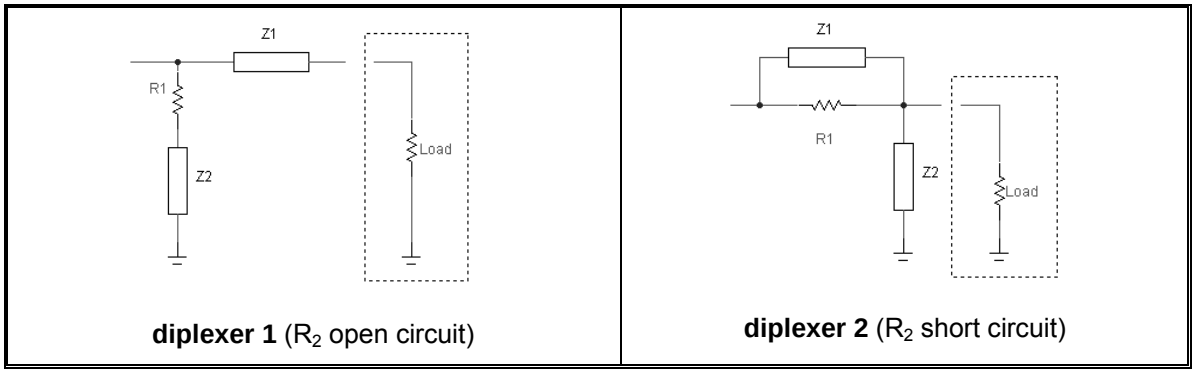

diplexer 1 (R_2 open circuit) **diplexer 2** (R_2 short circuit)

FIGURE 5-6: GENERIC DIPLEXER NETWORKS

When substituting Z_1 with a capacitor C_1 and Z_2 with an inductor L_1 as discussed in the preceding section, these networks (combined with the load resistance) are recognized as diplexer circuits [66].
In **diplexer 1**, R_1 and Z_2 (L_1) form a first order low pass section and Z_1 (C_1) with the load resistor form a first order high pass section. These two sections' input *admittance*s are complementary and when connected in parallel like this, the input admittance will remain real and constant.
In **diplexer 2**, R_1 and Z_1 (C_1) form the first order low pass section and Z_2 (L_1) with the load resistor form the first order high pass section. The two sections' input *impedances* are now complementary and connected in series to realize a real, constant input impedance.

The characteristics of the two circuits are identical. Both have a reflection coefficient of zero at all frequencies on the left hand port, while still exhibiting a first order high pass response from left to right. The reflection coefficient looking into the right hand port is not zero, and should only be used in systems where no energy enters the network from the right hand side, i.e. driving a matched load.

The calculation of the actual component values is similar to that for a singly terminated filter [66].

5.2.1.e. Measurement

The impact of reflective and absorptive filtering is illustrated through the measurement of the step response of an amplifier section similar to that shown in Figure 5-2. A commercial 50 Ω amplifier (MAR1-SM from Mini-Circuits, www.minicircuits.com) was characterized on an oscilloscope by connecting a matched step waveform generator to its input and measuring its output when driving a 50 Ω load. DC decoupling capacitors were required at the input and output, so 220 nF capacitors were used. That places the high pass corner frequency at 7 kHz, significantly below the filter frequencies used for the rest of the experiment. Their effect is assumed to be negligible and with the matched input and output ports, the measured output (expressed in the frequency domain) is simply:

$$V_{out} = S_{21} V_{in} \quad \rightarrow \quad (5\text{-}11)$$

with V_{in} the generator output voltage when driving a matched load

Decoupling capacitors are often chosen to create a corner frequency just below the spectrum of the RF signal, in order to filter out undesired artefacts and reduce noise. The capacitor values of the

decoupling capacitors were subsequently reduced to 150 pF to shift the corner frequency to 10.6 MHz and the measurement was repeated. If the simplified form of the transfer function (equation (5-2)) is applied (i.e. the amplifier is assumed as ideal), the output will be expected to be the time domain equivalent of the following frequency domain expression:

$$V_{out}(j\omega) = \left(\frac{j\omega}{j\omega + \frac{1}{2(50)\left(150 \times 10^{-12}\right)}} \right)^2 V_{out\,(amp)}(j\omega) \qquad \rightarrow \quad (5\text{-}12)$$

with $V_{out(amp)}$ the output of the amplifier with large decoupling capacitors

The reflective filters were then replaced with dissipative filtering elements for a comparative measurement. The decoupling capacitors were retained, since the diplexer and equaliser present constant 50 Ω impedances to the amplifier at DC, which interferes with the biasing of the amplifier, but the large 220 nF values were again used. A constant impedance equaliser was placed at the input port and a diplexer placed at the output port (see Figure 5-7.) The output port drives a matched load and no energy is consequently expected to enter the output port, prompting the use of a diplexer instead of an equaliser there. It can be verified that the transfer function of this circuit is also given by equation (5-12). It is in fact also the complete transfer function (5-1) of this system, on account of the reflection coefficients of the filter elements being zero.

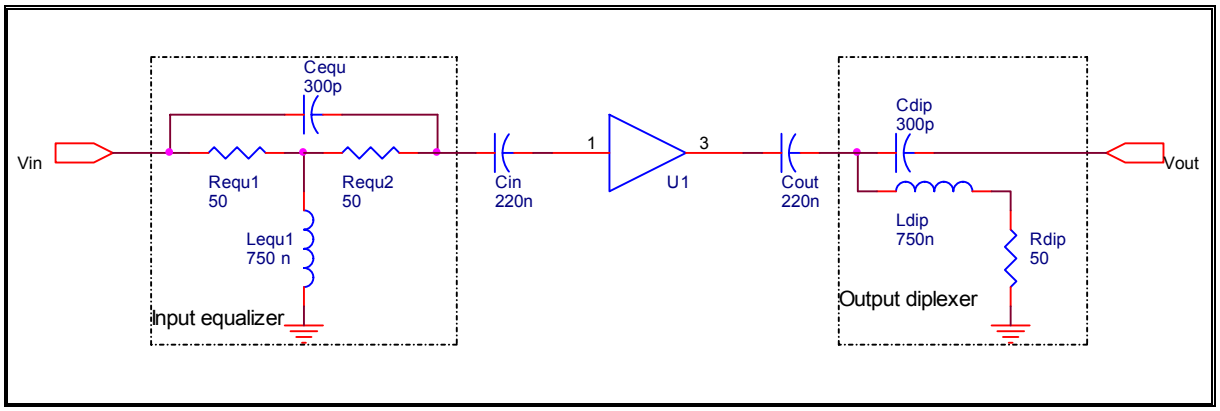

FIGURE 5-7: AMPLIFIER WITH ABSOPTIVE FILTERING (EQUALISER AT INPUT AND DIPLEXER AT OUTPUT)

The expected time domain output was found by numerical evaluation of this shared transfer function, using the measured data for $V_{out(amp)}$. This was then compared to the output measured with the system incorporating reflective filtering and with the output of the system employing dissipative filtering, to establish how well these outputs correlate with that predicted by the simplified transfer function it is supposed to implement.

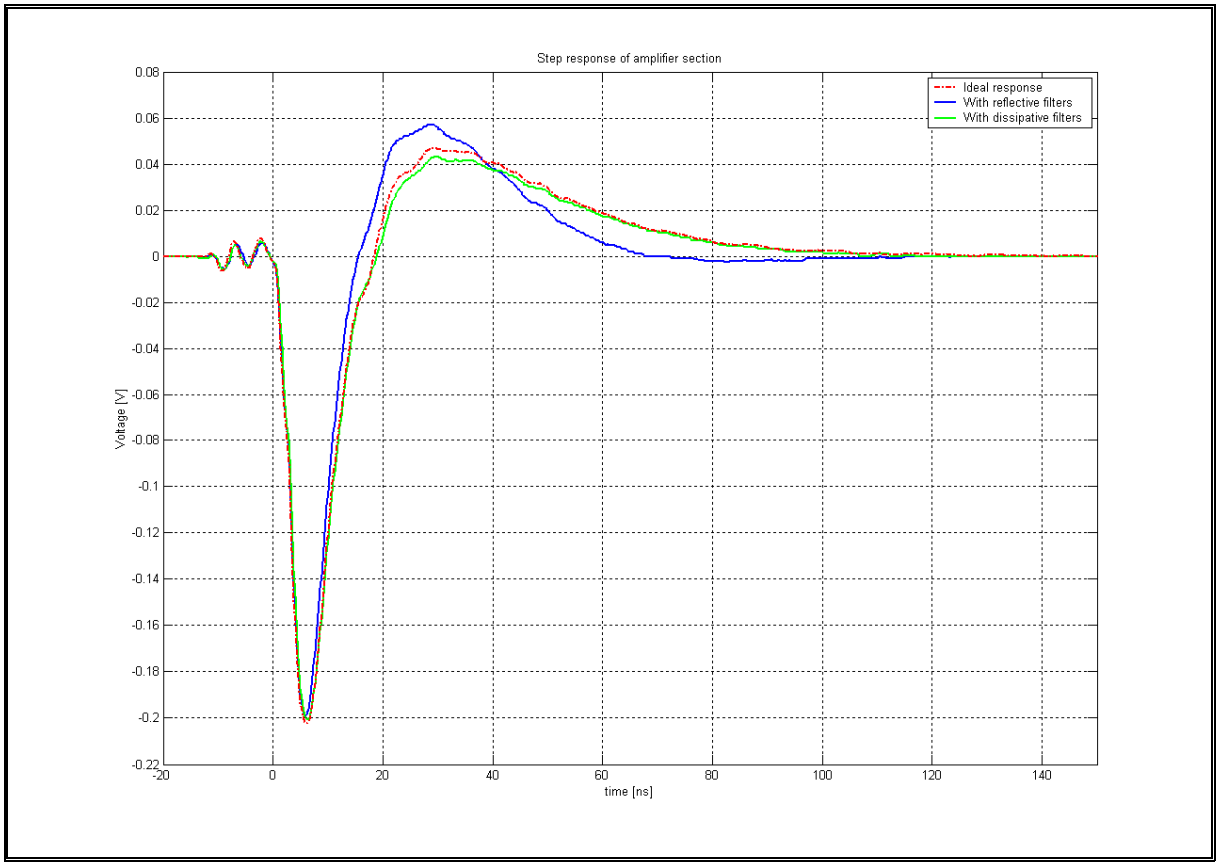

FIGURE 5-8: STEP RESPONSE OF AMPLIFIER SECTION (MEASURED), COMAPARING DISSIPATIVE FILTERING AND REFLECTIVE FILTERING WITH IDEAL FILTER FUNCTION

It is clear from Figure 5-8 that the output of the system employing dissipative filtering is closer to the expected output and will yield a more predictable and accurate response. The system with reflective filters shows a response which is visibly of a higher order than anticipated and could result in unexpected distortion, especially with complex input waveforms.

5.2.1.f. Conclusion

It has been shown that the use of absorptive filters can significantly improve the fidelity (as defined in 5.1) of a receiver and the effect can be expected to become increasingly pronounced for higher order systems. It is therefore recommended that absorptive filters are used as the basic filter element for this transceiver (and indeed in all high fidelity systems) and that the general principle of dissipating out of band energy, instead of reflecting it, should be applied whenever possible.

The diplexer and constant impedance equaliser networks both rely on their termination to be matched for proper operation. It should therefore ideally be used on systems that are reasonable well matched.

It is important to note that the input and output ports of the amplifier will be presented with a 50 Ω load at DC when used with absorptive filtering modules. This must be kept in mind when the amplifier's ports require a DC bias.

5.2.2. Op-amp vs standard gain block

5.2.2.a. Advantages of operational amplifiers

Recent advances in operational amplifiers [67], [68] have seen these devices employed in applications traditionally reserved for gain blocks such as MMIC and single transistor amplifiers. The following characteristics of a modern operational amplifier make them particularly attractive for pulse applications:

- It can handle large voltage swings, typically close to the supply voltage.
- Power consumption is typically less than their standard gain block counterparts.
- The slew rate and overdrive characteristics (which play an important role in pulse applications) are typically well defined and specified.
- The device has no inherent high pass response and can even be DC-coupled.
- The gain function can be varied by changing the external components.
- The input impedance of the operational amplifier itself is normally very high and the output impedance approaches 0. Input and output impedances of the amplifier configuration can be set to any value by the external components of the specific configuration.

Noise performance is another aspect of operational amplifiers which has seen major advances and operational amplifiers have been employed as low noise amplifiers in ultrasound systems [69]. In order to compare the noise performance of operational amplifiers to standard gain blocks, some discussion is required.

5.2.2.b. Noise in operational amplifiers

Noise in operational amplifiers is typically expressed as a noise voltage source and noise current source at the input. This is similar to the formulation used for transmission (ABCD) matrices [70] and can be represented as follows:

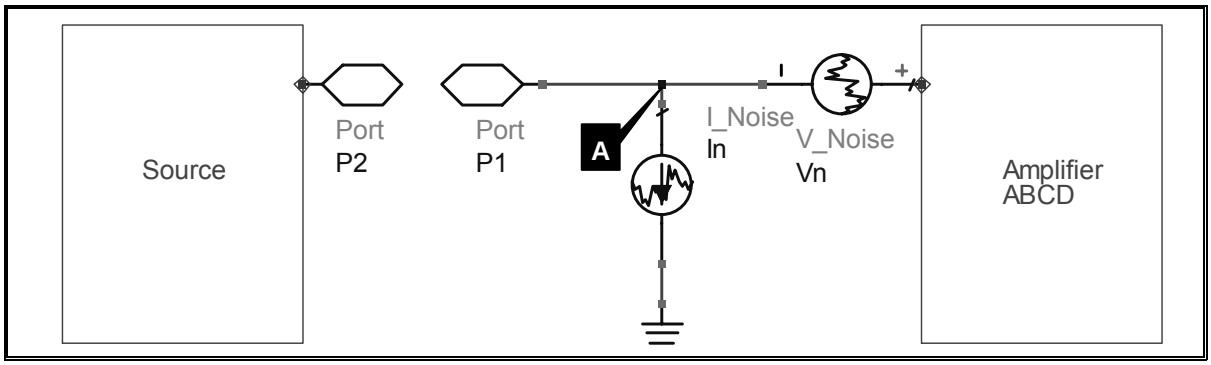

FIGURE 5-9: SPECIFICATION OF NOISE IN OPERATIONAL AMPLIFIERS

The input voltage and current noise parameters can then be used to accurately determine the noise figure of various op-amp configurations [71]. When such a system is driven by a source with impedance R_s, the noise figure can however be calculated in a general sense. Uncorrelated noise is

assumed and noise is expressed in terms of their square voltages throughout, since they add [72]. The input and output signal (S_i and S_o) are both measured at terminal A of Figure 5-9 and are assumed equal. The input noise (N_i) is assumed to be the thermal noise contributed by the source resistance and the output noise (N_o) is this noise plus the contribution of the noise sources I_n and V_n.

$$S_i = S_o = V_s^2$$
$$N_i = 4kTBR_s$$
$$N_o = 4kTBR_s + I_n^2 BR_s^2 + V_n^2 B \quad \rightarrow \quad (5\text{-}13)$$

With k Boltzmann's constant, T the ambient temperature and B the bandwidth of the system

The noise factor is then calculated as:

$$F = \frac{\frac{S_i}{N_i}}{\frac{S_o}{N_o}} = 1 + \frac{I_n^2 R_s}{4kT} + \frac{V_n^2}{4kTR_s} \quad \rightarrow \quad (5\text{-}14)$$

The source impedance for optimum noise performance can be found as:

$$\frac{dF}{dR_s} = 0$$
$$\Rightarrow R_s = \frac{V_n}{I_n} \quad \rightarrow \quad (5\text{-}15)$$

Note that this is not the input impedance of the operational amplifier (which is usually a high impedance) and is therefore not impedance matched to the source impedance of R_s. The importance of matching the amplifier to the source has however been highlighted in section 5.2.1.

5.2.2.c. Interfacing with operational amplifiers

The large input impedance of operational amplifiers then raises the question of how a device with a large input impedance should be connected to a source with much lower source resistance for optimal noise performance while still presenting a matched impedance to the source, as required by section 5.2.1.

It was noted that a physical, external resistor typically determines the input impedance of an operational amplifier. The exact placement of this resistor varies with op-amp configurations (e.g. inverting / non-inverting), but in all cases the resistor will generate thermal noise that will appear on the input of the operational amplifier. The value of this resistor can be expected to be very close to that of the source resistance in order for the operational amplifier to be impedance matched to the source. If the value of this resistor is assumed to be exactly R_S (the source resistance) and assumed to appear in parallel with the input impedance, the noise factor is given by:

$$S_i = S_o = \frac{V_s^2}{4}$$
$$N_i = kTBR_s$$
$$N_o = kTBR_s + kTBR_s + I_n^2 B\frac{R_s^2}{4} + V_n^2 B \quad \rightarrow \quad (5\text{-}16)$$
$$F = \frac{\frac{S_i}{N_i}}{\frac{S_o}{N_o}} = 2 + \frac{I_n^2 R_s}{16kT} + \frac{V_n^2}{4kTR_s}$$

Even when using an idealized noiseless operational amplifier, the noise figure cannot be less than 3 dB when using an external resistor to achieve an impedance match.

A transformer can alternatively be used to match the source impedance to the high input impedance device, provided the impedance ratio can be practically achieved. If the turn ratio is taken as n, so that $n^2R_s = R_{in(op\text{-}amp)}$, the noise figure is given by:

$$S_i = S_o = n^2 V_s^2$$
$$N_i = 4n^2 kTBR_s$$
$$N_o = 4n^2 kTBR_s + n^4 I_n^2 BR_s^2 + V_n^2 B \quad \rightarrow \quad (5\text{-}17)$$
$$F = \frac{\frac{S_i}{N_i}}{\frac{S_o}{N_o}} = 1 + \frac{I_n^2 n^2 R_s}{4kT} + \frac{V_n^2}{4kTn^2 R_s}$$

The thermal noise added by the shunt resistor clearly causes deterioration of the noise figure in the first configuration, but an amplifier with an impractically high input impedance or an optimal noise resistance (see equation (5-15)) closer to the source resistance than to the amplifier's input resistance might still perform better with this configuration.

5.2.3. Gain requirements

5.2.3.a. Minimum and maximum gain

It was pointed out in section 5.1.2 that the receiver output will eventually be fed to an ADC and stored digitally.

The switching signal generated by the isolation switch and the leakage from the transmitter through the isolation switch can be expected to be quite large compared to the incoming signal from the antenna. The incoming signal will be superimposed on these signals when it arrives at the input of the receiver, with the switching and leakage signals not containing any useful radar information. It is therefore vitally important that the gain of the receiver does not cause these non-information signals to drive the receiver into saturation or to exceed the maximum discretisized voltage swing of the ADC, since the superimposed data will then be lost.

At the other end of the scale, the radar equation [42] dictates that the amplitudes of reflected signals reduce rapidly as the distance to the reflector increases, even more so in lossy media. The limit in detectable amplitude is reached when the signals drop below the noise floor. To ensure that the noise floor is in fact the limiting factor and not the discretisation of the data by the ADC, the gain should be sufficient to let the noise toggle the 2 least significant bits of the stored trace. Each data trace eventually stored by the digital control circuitry is typically the average of a number of traces obtained by the ADC over a certain interval. Provided the noise is random, the noise level is then reduced by the square root of the number of traces [72]. Although this reduced noise level must be used when designing the maximum gain, care should be taken to ensure the initial noise does not drive the receiver chain or ADC into its non-linear mode of operation. It should be noted at this stage that the resistive loading of the antenna will generate thermal noise [73], [74]. This will appear at the input of the system and could potentially be responsible for a significant contribution to the noise figure of the system - especially for heavily loaded antennas, such as those discussed in section 2.2. An accurate model for the loss and radiation resistance of the antenna is however required to quantify this noise and falls beyond the scope of this dissertation.

5.2.3.b. Variable gain amplifiers

It should be noted that the requirement for low gain to prevent saturation and associated data loss is generally applicable early in the acquisition cycle (when the transmitter fires and the isolation switch switches), while high gain is required later, when small signals need to be discretisized. Variable gain amplifiers provide the opportunity to increase the gain over the acquisition interval and meet both requirements. These devices can broadly be divided into two categories according to the method of gain control: digital or analog [75].

Digital gain control

These devices typically consist of an attenuator and amplifier. The amplifier provides a fixed gain, while sections of the attenuator can be digitally switched in or out of the circuit to control the total gain of the amplifier. These devices are not well suited to applications with a smooth gain transition during the acquisition period, due to the discrete steps in gain [75], [12].

Analog gain control

The core of devices featuring continuous (analog) gain control is generally an analog multiplier based on a differential amplifier configuration modulated by its current source [76]. The control signal can be designed to be linear [75] and Gilbert multipliers [77] are often employed to facilitate this, while linear-in-dB gain control approximations are also popular [76]. These configurations allow for the bandwidth of the gain control signal to be close to that of the amplifier itself, which makes these devices particularly well suited for systems requiring a continuous gain ramp. The presence of a differential amplifier at the core of the device results in most of the general principles of operational amplifiers highlighted in section 5.2.2 to be applicable to these devices.

The primary purpose of variable gain amplifiers in this design is to accommodate input signals with a large dynamic range without driving the receiver chain into saturation *at any point*. The initial gain before the variable gain function is applied is therefore crucial; reduction in gain is worthless once data has been lost due to the preceding amplifier entering its non-linear regime. This is also applicable to the variable gain amplifier internally, where the signal must be kept as small as possible before it enters the multiplier cell to prevent non-linear effects. The inclusion of amplification before the variable gain amplifier is however motivated by noise considerations, since purpose built low noise amplifiers generally have better noise figures than the variable gain amplifiers. The inclusion of a low noise amplifier before the variable gain amplifier can therefore improve the overall noise figure of the system.

5.3. Proposed configurations

Two receiver configurations will be built according to the guidelines developed above. The application in a borehole radar system is again used as framework for the designs.

Some generality will be sacrificed by referring to specific commercial devices, but these devices often differ too much to formulate a general approach. These two designs should however provide informative examples of the issues that will be encountered and how the guidelines highlighted above should be applied.

5.3.1. Configuration 1

This system employs a low noise amplifier followed by a variable gain amplifier and is closely related to that currently employed by the bistatic GeoMole receiver. The circuit diagram is shown in Figure 5-10, followed by a discussion on some of the important considerations.

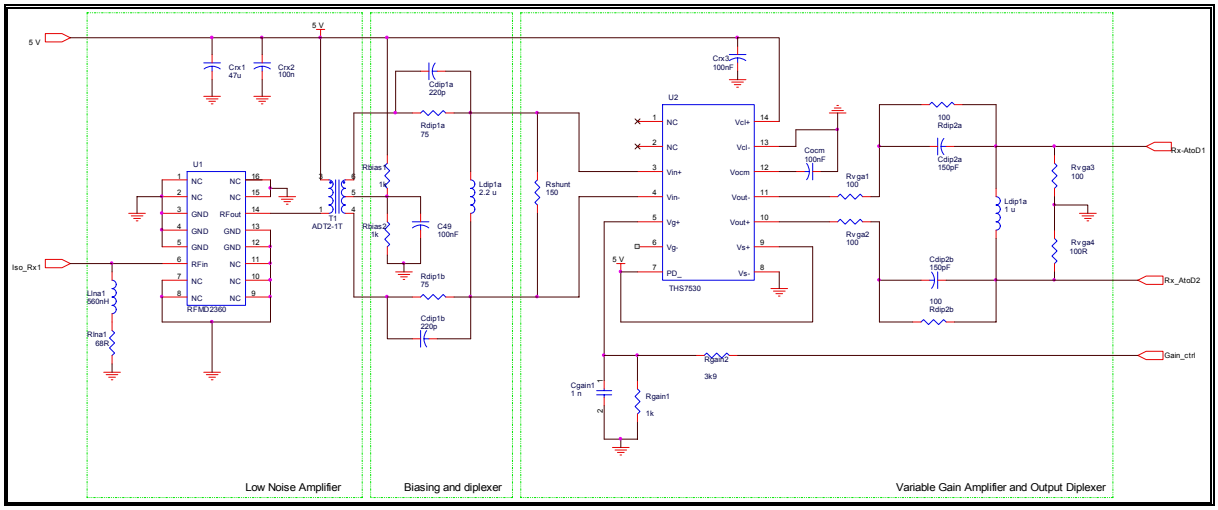

FIGURE 5-10: CIRCUIT DIAGRAM OF RECEIVER CONFIGURATION 1

5.3.1.a. Low noise amplifier

The RF2360 from RF Micro Devices (www.rfmd.com) is used as a low noise amplifier. Commercial low noise amplifiers are optimised for noise performance, so that the impedance match of its ports are often not good – which was highlighted as an important requirement for this transceiver. The input impedance of a standard RF2360 amplifier was measured on a network analyser and found to be closely approximated by a series combination of a 75 Ω resistor and 100 pF capacitor.

From the diplexer theory of section 5.2.1.d (see "Diplexer 1"), it follows that a complimentary admittance can be added in parallel to this port to create a purely resistive impedance. R_{lna1} and L_{lna1} seen in Figure 5-10 were consequently added. The improvement is clear from the measured input impedance shown in Figure 5-11 .

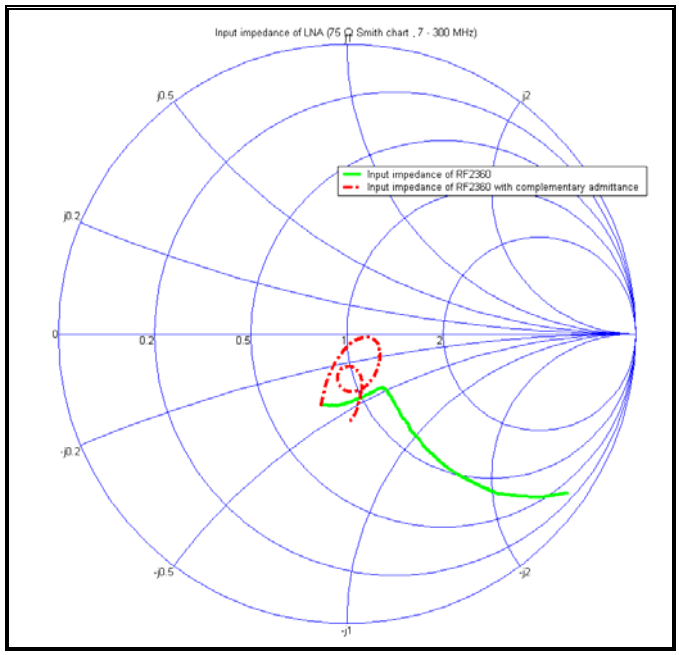

FIGURE 5-11: INPUT IMPEDANCE OF RF2360 WITH AND WITHOUT THE COMPLEMENTARY ADMITTANCE (MEASURED)

This is a single ended 75 Ω device. The output transformer of the preceding isolation switch should be chosen to match this amplifier to the impedance of the isolation switch and one output terminal of the transformer will have to be connected to ground.

The output of the low noise amplifier must be biased through an inductor. This violates the specification of a purely resistive load for the amplifier. No equaliser or diplexer configuration can unfortunately be used without affecting the DC bias current and the largest possible inductor should be used to at least minimize the effect. Commercially available transformers typically have large magnetizing inductances and also provide the opportunity to transform the single sided output to a balanced output and to match the output impedance to the next stage. T_1 is a transformer with a 2:1 impedance ratio.

This amplifier provides 20 dB gain, with a noise figure of 1.2 dB (noise factor of 1.32.) It has also been found that this amplifier has an inherent first order high pass response with a corner frequency of 8.9 MHz.

5.3.1.b. Variable gain amplifier

The THS7530 from Texas Instruments (www.ti.com) is chosen as the variable gain amplifier. It employs a modulated differential amplifier and features analog, linear-in-dB gain control. The input and output ports are both differential. The input impedance of the device is quoted as 8.5 kΩ. It would be impractical to match this impedance to the 75 Ω output impedance of the low noise amplifier by means of transformer T_1. The optimal noise resistance of the variable gain amplifier is in addition found to be small. Following the discussion in section 5.2.2.c, R_{shunt} is rather placed across the input terminals. The input ports must further be biased at mid-supply, which is easily done by biasing the centre tap of transformer T_1.

The amplifier operates as a sensitivity time control (STC) system and the control signal (Gain_ctrl) for this will typically by supplied from the digital control circuitry. This signal is attenuated from the logic level (TTL in this case) to the 1 V required by the gain control pin of the amplifier. A basic RC network is also incorporated into this attenuator to create a simple voltage ramp over the acquisition interval.

The output attenuator is included to match the maximum voltage swing of the amplifier to that of the ADC. V_{ocm} can further be driven by the ADC bias voltage to match the bias points of the ADC and the output of the amplifier.

The datasheet specifies the noise figure as 9 dB when driven with a 50 Ω input termination, and the input voltage noise is given as 1.1 nV/√Hz. From equation (5-15) it must then be assumed that the input noise current is 75 pA/√Hz. The noise figure can now be re-calculated with equation (5-15) , but using the shunt resistor value of 150 Ω.

The gain of this amplifier can be swept from 11.6 dB to 46.5 dB with a calculated noise figure of 12 dB at maximum gain.

5.3.1.c. Filtering

Further filtering is required to remove undesired low frequency content at the interface of the two amplifiers. It must be noted that a DC path should remain between the transformer's centre tap and the amplifier's input pins for the bias current. A balanced equaliser circuit would be the natural choice for this application, but another consideration exists. Any offset in the DC bias of the amplifier's inputs will be modulated with the gain signal so that a replica of the gain function appears at the output of the amplifier. L_{dip1a} is placed between the two terminals to force the DC bias points to the same value. A complementary impedance is then added with R_{dip1a}, $R_{dip1b,}$ C_{dip1a} and C_{dip1b} to form a balanced diplexer. No power will be reflected back from the perfectly matched R_{shunt} resistor and the diplexer should therefore be sufficient, provided the power leaving the amplifier's input ports is negligible. This is accomplished by including a diplexer at the output, which will filter out any low frequency artefacts

from the amplifier without reflecting any power back that might end up at the input ports of the amplifier. This argument can be verified by equation (5-1) and noting that S_{11}=0 due to R_{shunt} and Γ_2=0 due to the output diplexer.

5.3.1.d. Specifications

A number of expected parameters can now be theoretically calculated for this configuration.

The noise figure of the cascade system [45] at maximum gain can be calculated as:

$$F = F_{LNA} + \frac{1}{G_{LNA}}\left(F_{VGA} - 1\right) \quad \rightarrow \quad (5\text{-}18)$$
$$F = 2.48$$
$$NF = 3.94\,\text{dB}$$

The effect of the output termination was ignored, as its contribution is negligible. This can alternatively be expressed as 27.2 μV noise at the input of the LNA (75 Ω input resistance, 100 MHz bandwidth.)

The use of diplexers results in each individual section being presented a purely resistive load by the next section, so that the theoretical transfer function of the receiver can be expressed in the Laplace domain simply as the product of the sections' transfer functions:

$$\frac{V_{out}}{V_{in}}(s)\Big|_{\max} = H_{\text{LNA}} \cdot H_{\text{tranformer}} \cdot H_{\text{diplexer1}} \cdot H_{\text{VGA}} \cdot G_{\text{termination}} \cdot H_{\text{diplexer2}}$$

$$\frac{V_{out}}{V_{in}}(s)\Big| = \left(\frac{10s}{s + \frac{1}{18\times10^{-9}}}\right) \cdot \sqrt{2} \cdot \left(\frac{s}{s + \frac{1}{17\times10^{-9}}}\right) \cdot Gain_{\text{VGA}} \cdot \frac{1}{2} \cdot \left(\frac{s}{s + \frac{1}{15\times10^{-9}}}\right) \quad \rightarrow \quad (5\text{-}19)$$

The high frequency roll-offs were ignored for simplicity, the transformer was taken as ideal and the amplifiers were assumed to remain in their linear mode of operation. The minimum voltage gain of the cascade occurs when the variable gain amplifier has 11.6 dB gain. The gain for a signal in the pass band is then given as:

$$\frac{V_{out}}{V_{in}}\Big|_{\min} = 26.9$$
$$\frac{V_{out}}{V_{in}}\Big|_{\min} = 28.6\,\text{dB} \quad \rightarrow \quad (5\text{-}20)$$

The output of the variable gain amplifier itself is slightly bigger, due to the 6 dB attenuation of the output termination. The biggest signal (at the input of the LNA) that can be accommodated by this system without saturation is therefore 27 times smaller than the maximum swing of the ADC ($1V_{pp}$/27 = 37 V_{pp}), or 54 times smaller than the maximum swing of the variable gain amplifier – whichever comes first. The maximum gain can be calculated similarly, using 46.5 dB gain for the variable gain amplifier:

$$\left.\frac{V_{out}}{V_{in}}\right|_{\min} = 1496$$
$$\left.\frac{V_{out}}{V_{in}}\right|_{\min} = 63.5\ \text{dB} \quad \Rightarrow \quad (5\text{-}21)$$

Following the noise calculation of equation (5-18), the noise voltage appearing at the output of the receiver will consequently be 40.7 mV.

5.3.2. Configuration 2

This configuration is much simpler and consists of just a variable gain amplifier. The variable gain amplifier employed here has an input impedance which can realistically be matched to the impedance of the isolation switch with a transformer. Since the isolation switch already has the transformer at its output, this configuration should be designed closely with the isolation switch. For the purpose of this discussion, the isolation switch presented as configuration 1 in section 4.5 will be used. A circuit diagram is shown in Figure 5-12. Note that the circuitry preceding the amplifier is similar (although single sided instead of balanced) to that seen at the output of the isolation switch. The elements of the isolation switch will naturally replace these components when these systems are eventually integrated.

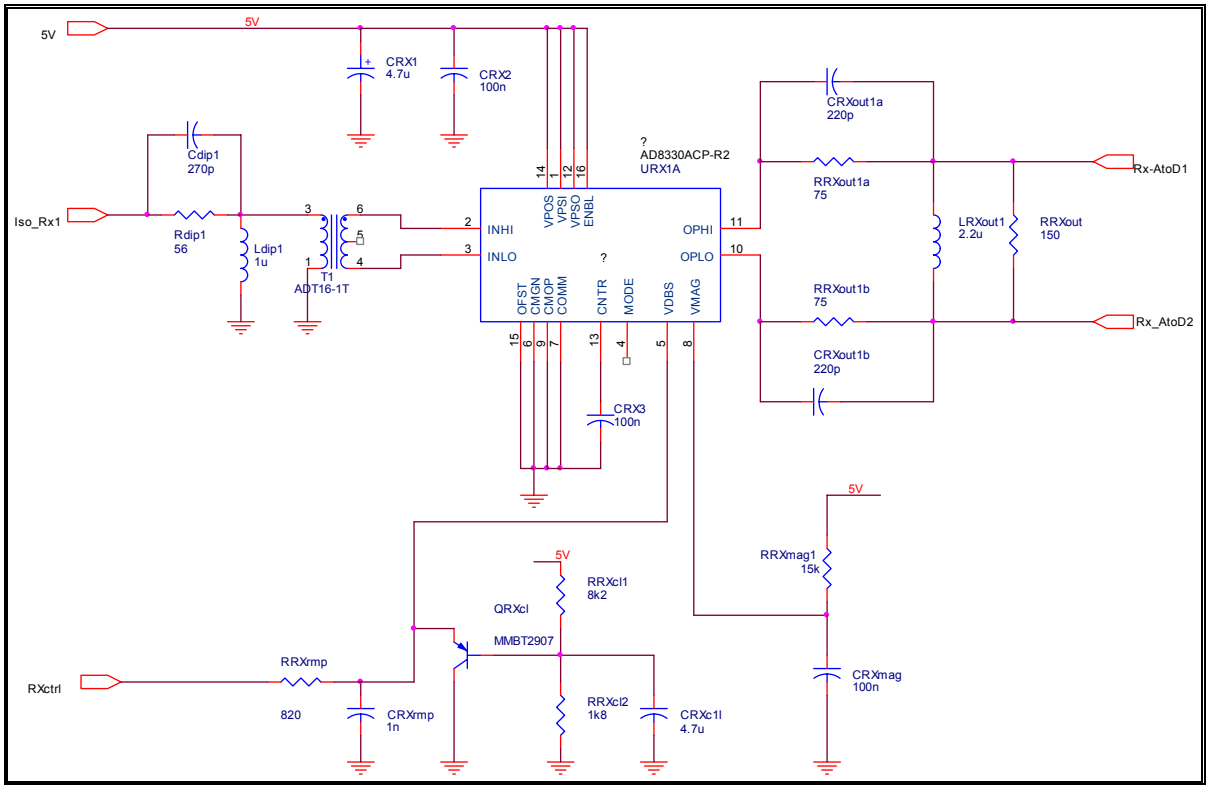

FIGURE 5-12: CIRCUIT DIAGRAM OF RECEIVER CONFIGURATION 2

5.3.2.a. Variable gain amplifier

The AD8330 amplifier from Analog Devices (www.analog.com) is used and consists of two multiplier cells based on differential amplifiers. The input feeds a multiplier with a linear-in-dB control and this cell's output is then passed to a linear multiplier. It was highlighted in section 5.2.3.b that the variable gain should be applied as early as possible in the amplifier chain to prevent saturation and the input multiplier is consequently used to sweep the gain, with the output multiplier just providing additional fixed gain of 3 V/V. An STC system is again created and the digital gain control signal given a voltage ramp with a basic RC network. A clamping circuit is used instead of an attenuator in this case, so that only the first 1.5 V of the ramp is used (the maximum input of the amplifier gain control input is 1.5 V.) This will create a very linear gain control signal, sweeping the total gain of the amplifier itself from 10 dB to 60 dB.

The differential output impedance of the amplifier is 160 Ω. This is connected to a balanced diplexer to filter out low frequency amplifier artefacts without reflecting power back to the amplifier. The CNTR-pin can be used to bias the output at the bias point of the ADC.

5.3.2.b. Interface with isolation switch

The differential input impedance of the AD8330 is 1000 Ω. Transformers with a 4:1 turns ratio are readily available in the desired frequency band and can be placed in front of the amplifier. The input impedance of the amplifier, as seen through such a transformer will therefore be 62.5 Ω and the transformer will ensure that no DC voltage appears across the input pins of the amplifier. This 62.5 Ω is a realistic impedance level for the isolation switch. The diplexer in front of the transformer can then be designed for a 60 Ω system and the input of this complete circuit (including the diplexer) will be extremely close to a purely resistive 60 Ω, even below the operating frequency band of the transformer. It should further be noted that the transformer will cause the signal voltage to increase 4 fold, even though the power remains constant.

The noise voltage and current of this amplifier is 4.1 nV/√Hz and 3 pA/√Hz respectively. The optimal noise resistance of this amplifier is therefore 1367 Ω, according to equation (5-15). The amplifier will consequently be operating close to the optimal noise impedance as well.

5.3.2.c. Specifications

The parameters highlighted for configuration 1 is again calculated.

The noise figure of the system at maximum gain is just the noise figure of the variable gain amplifier when driven with a matched load (see equation (5-17).) The output termination was again ignored.

$$F = 2.61$$
$$NF = 4.2 \text{ dB}$$

➔ *(5-22)*

This is equivalent to a 25.6 μV noise voltage over a 60 Ω resistor in a system with 100 MHz bandwidth.

The transfer function of this receiver can by the same argument and with the same assumptions as in 5.3.1.d be calculated for this configuration. The voltage gain will be defined with reference to the voltage observed before the transformer.

$$\frac{V_{out}}{V_{in}}(s)\Big|_{max} = H_{\text{diplexer1}} \cdot H_{\text{transformer}} \cdot H_{\text{VGA (in)}} \cdot H_{\text{VGA (out)}} \cdot G_{\text{termination}} \cdot H_{\text{diplexer2}}$$

$$\frac{V_{out}}{V_{in}}(s)\Big| = \left(\frac{s}{s+\frac{1}{15x10^{-9}}}\right) \cdot 4 \cdot Gain_{\text{VGA}} \cdot 3 \cdot \frac{1}{2} \cdot \left(\frac{s}{s+\frac{1}{16x10^{-9}}}\right) \quad \rightarrow \quad (5\text{-}23)$$

Note that the input and output modulation of the amplifier was defined separately. The minimum gain of the variable gain amplifier is 0 dB, so that - in the pass band - the following applies:

$$\frac{V_{out}}{V_{in}}\Big|_{\min} = 6.0$$

$$\frac{V_{out}}{V_{in}}\Big|_{\min} = 15.6\,\text{dB} \quad \rightarrow \quad (5\text{-}24)$$

This system consequently allows for much bigger input signals before the receiver or ADC saturates. The maximum input signal amplitude is 6 times smaller than the maximum swing of the amplifier or 6 times smaller than the maximum voltage swing of the A2D ($1V_{pp}/6 = 166mV_{pp}$), whichever comes first. The maximum gain of the variable gain amplifier is 50 dB, so that the maximum gain of the receiver is given by:

$$\frac{V_{out}}{V_{in}}\Big|_{\min} = 1897$$

$$\frac{V_{out}}{V_{in}}\Big|_{\min} = 65.5\,\text{dB} \quad \rightarrow \quad (5\text{-}25)$$

The noise voltage appearing at the output of the receiver at maximum gain will consequently be 48.6 mV.

5.4. Laboratory measurements

The two configurations developed in the preceding sections were built and evaluated through laboratory experiments. The circuit diagrams are included in addendum A for completeness.

5.4.1. Frequency domain response (fixed gain)

The scattering parameters of the two receiver configurations, as measured on a vector network analyser, are used to evaluate their frequency domain responses.

The nominal input impedances of configuration 1 and configuration 2 are 75 Ω and 60 Ω respectively and will be slightly mismatched to the 50 Ω of the network analyser. The resultant degradation in the transmission coefficient is negligible and will be ignored. The input impedance will however be converted for representation on 75 Ω and 60 Ω Smith charts.

The output ports of both configurations are differential and terminated with resistors equal to their characteristic impedances of 150 Ω and 200 Ω in Figure 5-10 and Figure 5-12. The load resistors were removed and a transformer with a 2:1 turns ratio (-3 dB bandwidth of 0.2 – 350 MHz) was used to convert it to a single sided output and match it to the 50 Ω of the network analyser. The output of configuration 1 is now 50 Ω and that of configuration 2 is now 37.5 Ω (-17 dB match to 50 Ω.) The transmission coefficient measured by the network analyser represents the power gain of the eventual 50 Ω system. The measured transmission coefficient had to be doubled in order to obtain the voltage gain of the system without the output transformer. These converted transmission coefficients are shown in Figure 5-13.

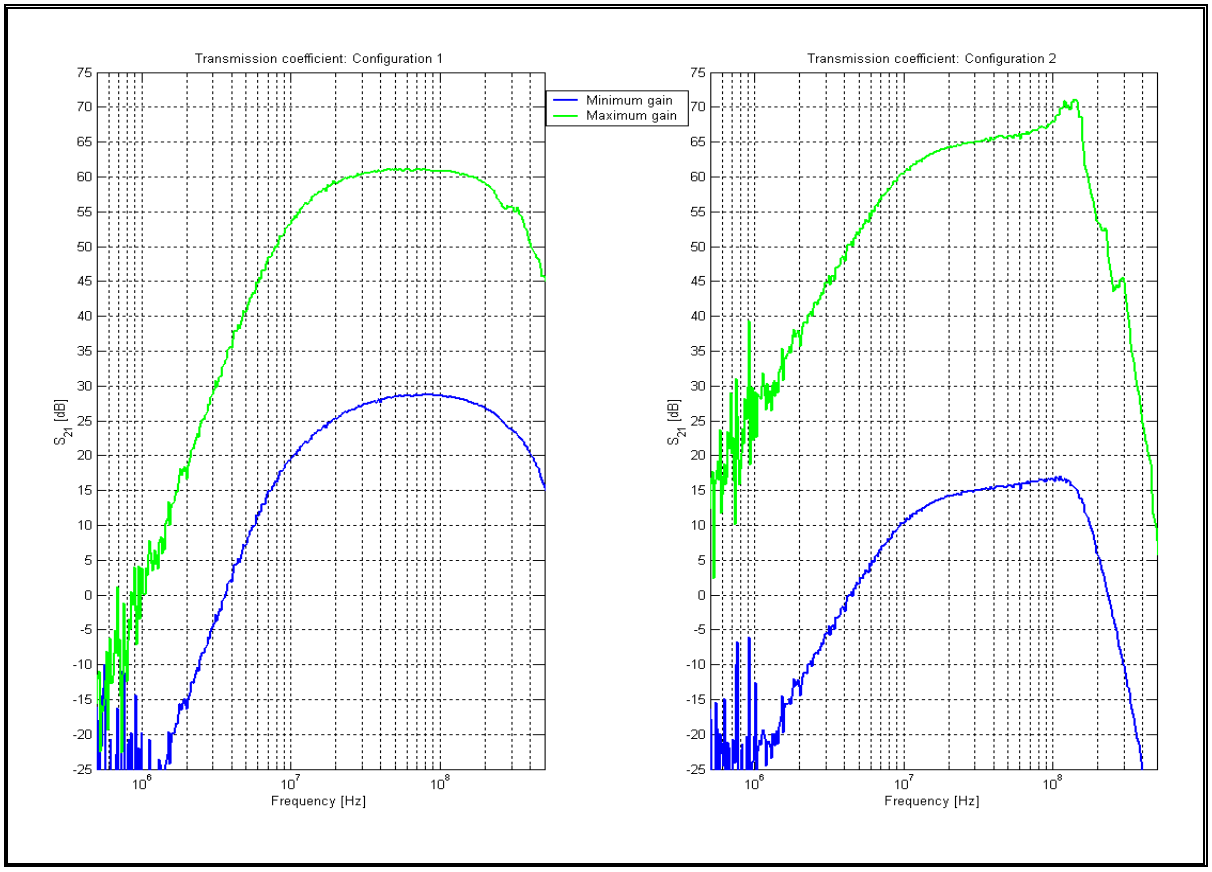

FIGURE 5-13: TRANSMISSION COEFFICIENTS OF AMPLIFIER CONFIGURATIONS (MEASURED)

The gain of configurations 1 and 2 correlate well with the expected gains calculated in sections 5.3.1.d and 5.3.2.c. The low frequency cut-off due to the filtering is clear and the high frequency limits are set by the bandwidth of the transformers and amplifiers. Both receivers perform well in the required 10 – 100 MHz band, although slight peaking is observed for configuration 2 above 100 MHz.

The measured input impedances are shown in Figure 5-14. Configuration 1 is extremely well matched to 75 Ω up to 100 MHz, indicating that the input diplexer is performing well. The input impedance of configuration 2 also remains close to 60 Ω at lower frequencies, thanks to the input diplexer. The inter-winding capacitance of the transformer T_1 and shunt input capacitance of the amplifier itself causes degradation at higher frequencies however– the reflection coefficient is -5 dB at 100 MHz.

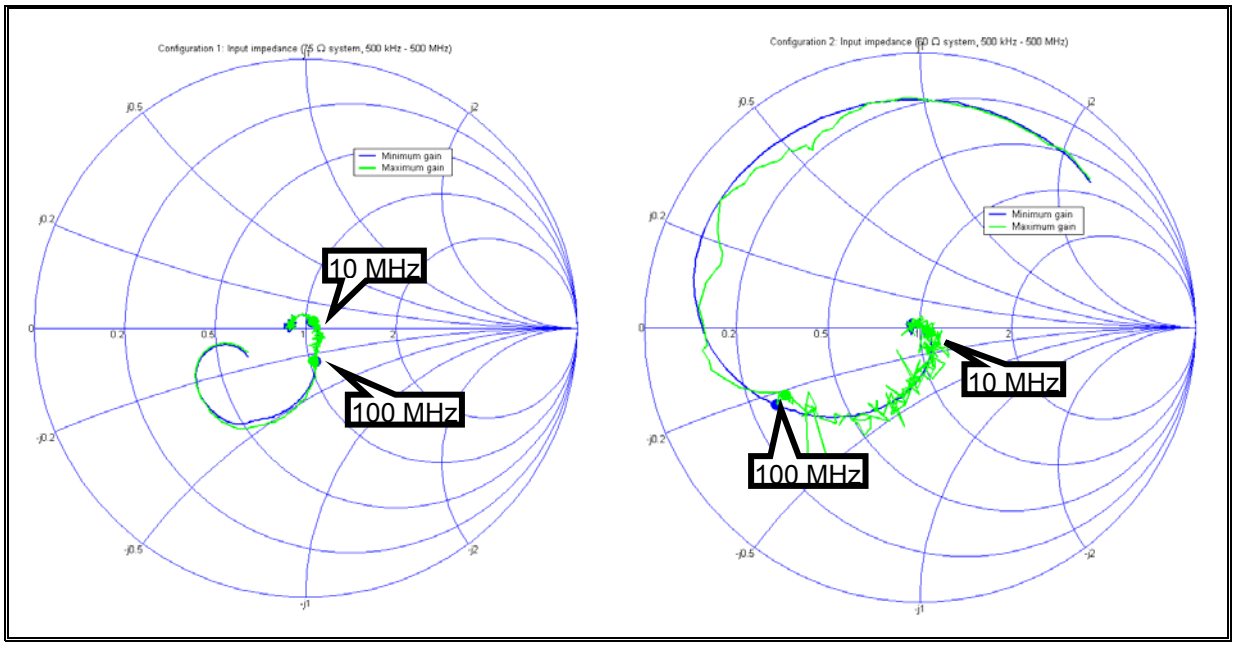

FIGURE 5-14: INPUT IMPEDANCES OF AMPLFIER CONFIGURATIONS WITH ARROWS INDICATING THE 10 – 100 MHZ BAND (MEASURED)

5.4.2. Time domain response (fixed gain)

The time domain transfer functions of the two receiver configurations were evaluated in terms of their step response. This was done by connecting a matched step waveform generator to the receivers, which in turn were set up with fixed gains. The gain levels were chosen to facilitate accurate measurement of both the input and output on an oscilloscope without the receiver saturating.

An expected output is required for the evaluation of the systems' fidelity (see section 5.1.) This is determined through the numerical convolution of the input waveform (measured into a matched load beforehand) and the theoretical transfer functions calculated in section 5.3.1.d and 5.3.2.c.

5.4.2.a. Configuration 1

This configuration was set up for a nominal gain of 21 dB and showed exceptional agreement with its theoretical transfer function, with no spurious responses. The voltage was monitored at each stage in the configuration (not shown here) and was exactly as expected. Both the diplexers exhibited the anticipated first order high pass response and the gain of the amplifiers was as specified. The slight

reduction in the peak voltage can be attributed to the limit in the maximum bandwidth of system – which was not taken into account with the theoretical transfer function.

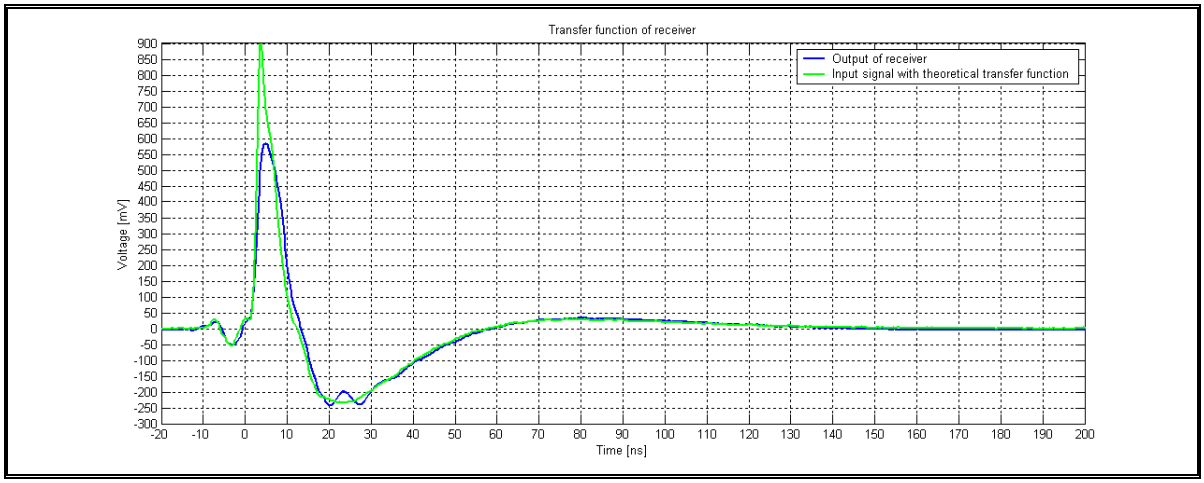

FIGURE 5-15: STEP RESPONSE OF RECEIVER CONFIGURATION 1 (MEASURED)

5.4.2.b. Configuration 2

The second configuration was set up for a gain of 24 dB and also followed the calculated transfer function closely with no significant spurious responses.

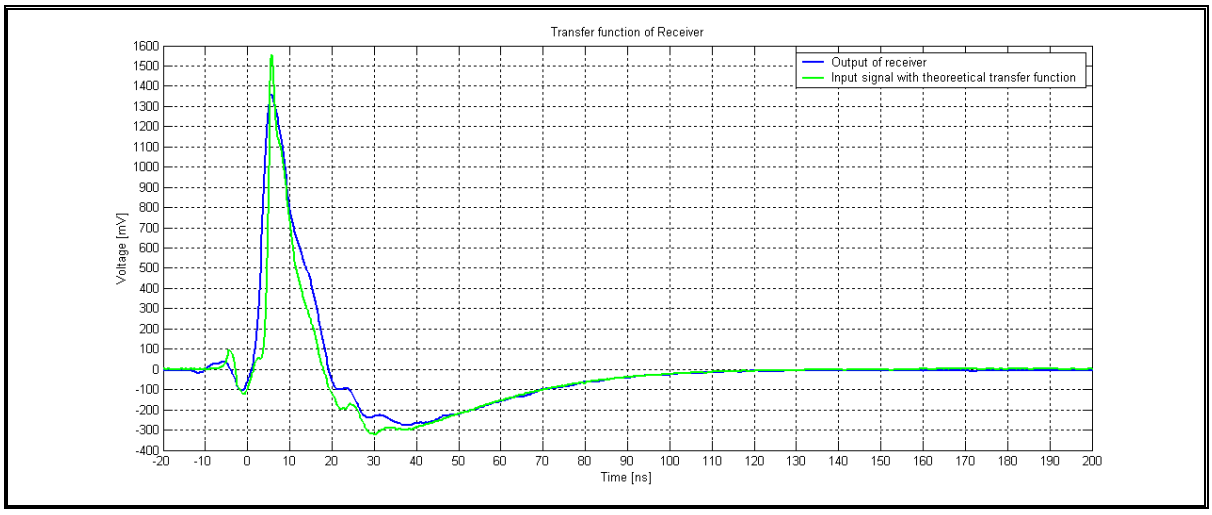

FIGURE 5-16: STEP REPONSE OF RECEIVER CONFIGURATION 2 (MEASURED)

5.4.3. Dynamic gain control

It was mentioned earlier that both configurations will be operated in an STC mode and this dynamic variation in gain is investigated next.

5.4.3.a. Configuration 1

It was expected that the 1dB output compression point of the THS7530 amplifier will be independent of the gain setting. This would result in the input compression point to increase as the gain is lowered,

so that saturation can be prevented by just lowering the gain for large signals. This was tested by monitoring the amplifier's output while the amplitude of a matched 70 MHz signal generator connected to the input was varied. It was found that the output compression point was dependent on gain and the details are shown on a linear voltage scale in Figure 5-17*. The 1dB compression drops from an output voltage of 1240 mV for maximum gain to 460 mV for minimum gain. This corresponds to an input signal of 17 mV for minimum gain instead of 46 mV, had the output compression point stayed constant at 1240 mV. This might be due to non-linear effects of the transistors making up the device's input and reducing the dynamic range of the system, but the 460 mV compression point does match well to the 1 V_{pp} digitised range of the ADC. The emphasis for this system is the prevention of data loss and it should be noted that a slight amount of distortion can be tolerated, but the plateaus seen in Figure 5-17 should be avoided. A maximum input amplitude of around 20 mV should therefore be acceptable at minimum gain.

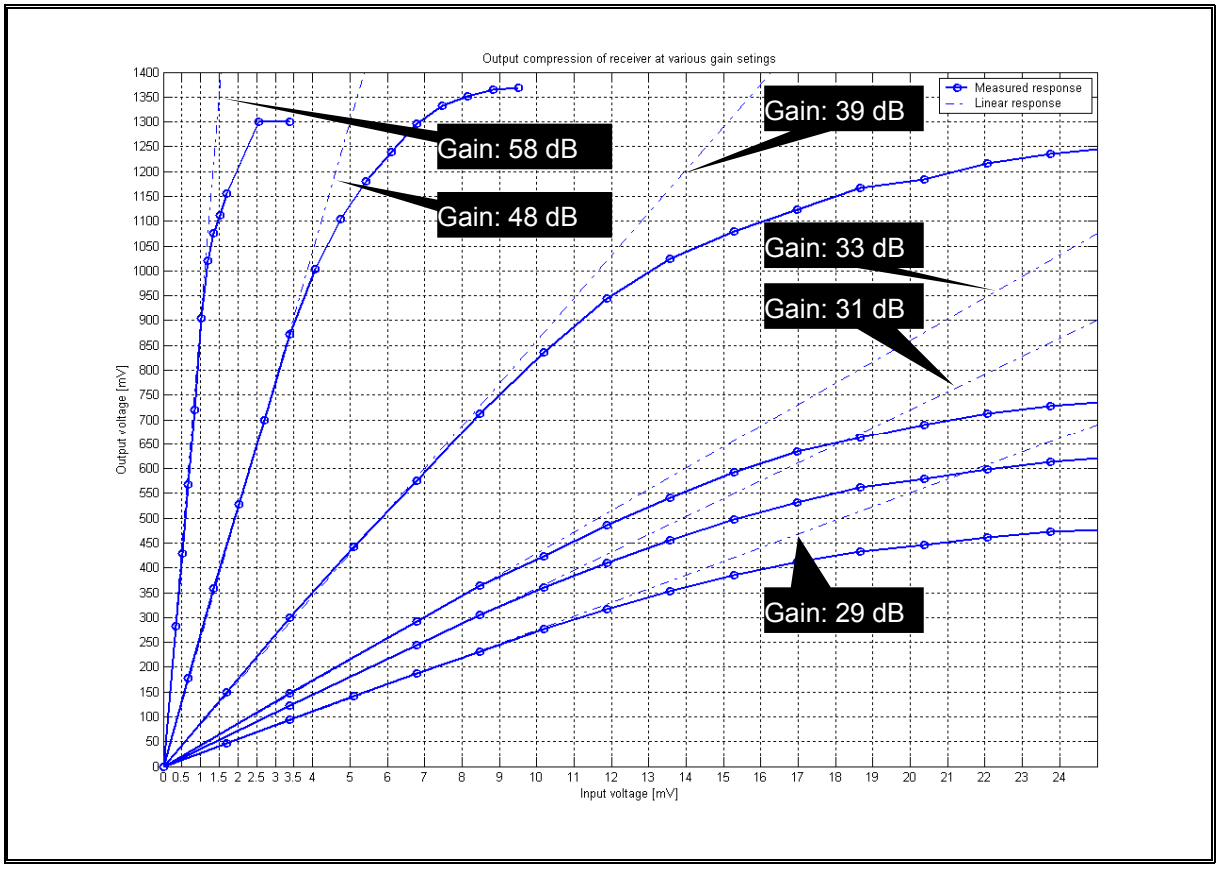

FIGURE 5-17: COMPRESSION OF CONFIGURATION 1 (MEASURED)

The gain control signal of this configuration is created by attenuating the digital gain control signal and passing it through a simple RC network to create a ramp function. The resultant voltage appearing on the gain control pin of the variable gain amplifier is shown in Figure 5-18. The output was monitored

* Note that, on these scales, the 1dB compression point coincides with the point where the output amplitude has dropped to 0.89 times the expected linear output.

while the gain was swept in this fashion without any input signal applied (the input port was terminated), to establish the leakage of the gain function onto the RF-channel.

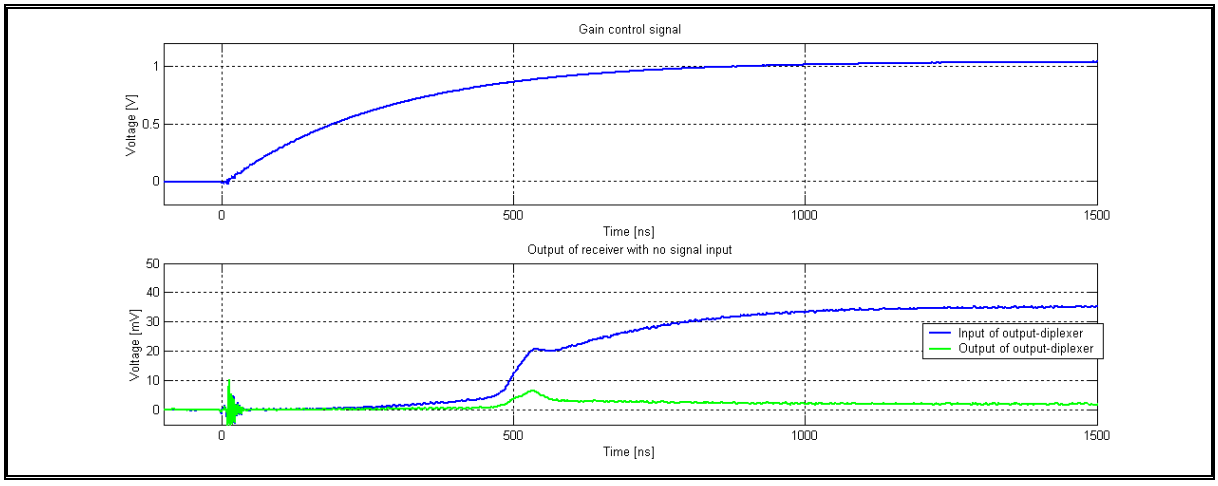

FIGURE 5-18: LEAKAGE OF GAIN CONTROL ONTO RF-SIGNAL PATH FOR CONFIGURATION 1 (MEASURED)

A peak voltage of about 35 mV associated with the gain control is observed at the load of the variable gain amplifier when no input signal is applied. Due to the slow time constant relative to the expected RF signal, the filter response of the diplexer reduces it to a peak voltage of 7mV. This should not have a significant effect on data quality.

A simple illustration of the STC mode of operation is finally provided in Figure 5-19. A 500 μV, 30 MHz sine wave was applied to the input by a matched signal generator while the gain was swept as in Figure 5-18. The gain function was determined by converting the measured gain control signal with the help of the datasheet parameters.

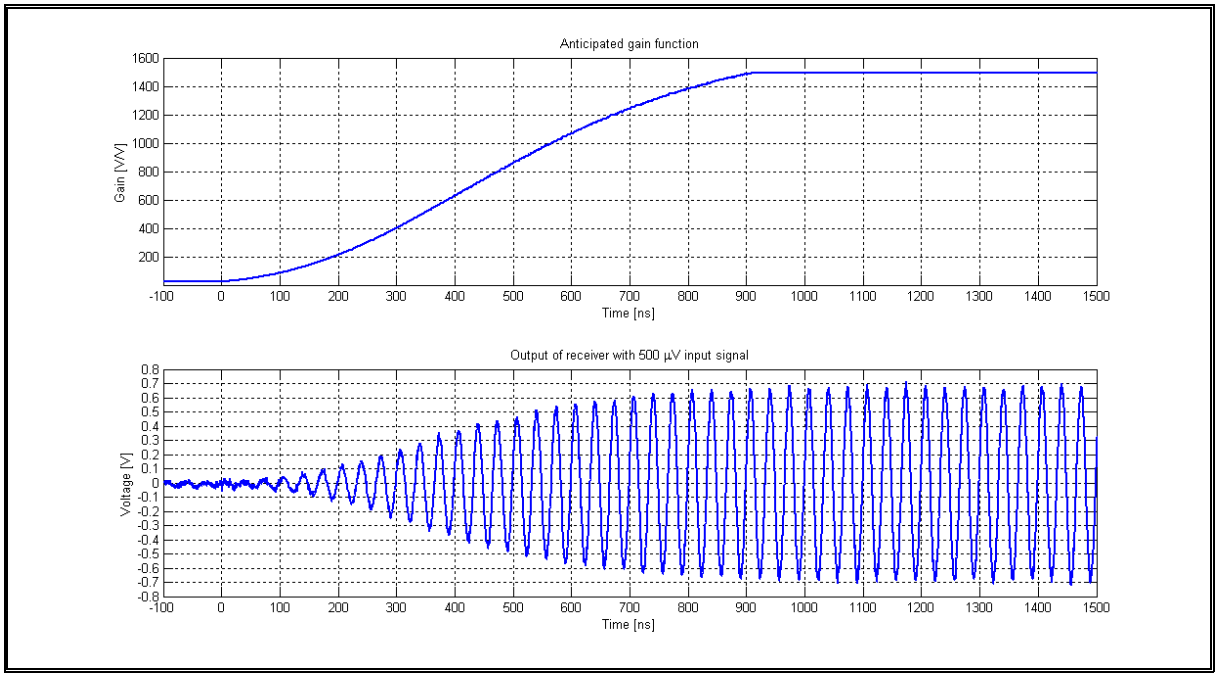

FIGURE 5-19: STC MODE OF OPERATION FOR CONFIGURATION 1 (MEASURED)

5.4.3.b. Configuration 2

The output compression of this configuration was measured with a similar setup as for configuration 1 and found to be significantly less dependent on the gain. Even though distortion starts to occur at lower amplitudes, the output amplitude plateaus between 2 V and 2.4 V for all gain settings. The 1dB compression point with minimum gain occurs at 370 mV input voltage, but reasonable performance can still be expected up to around 500 mV.

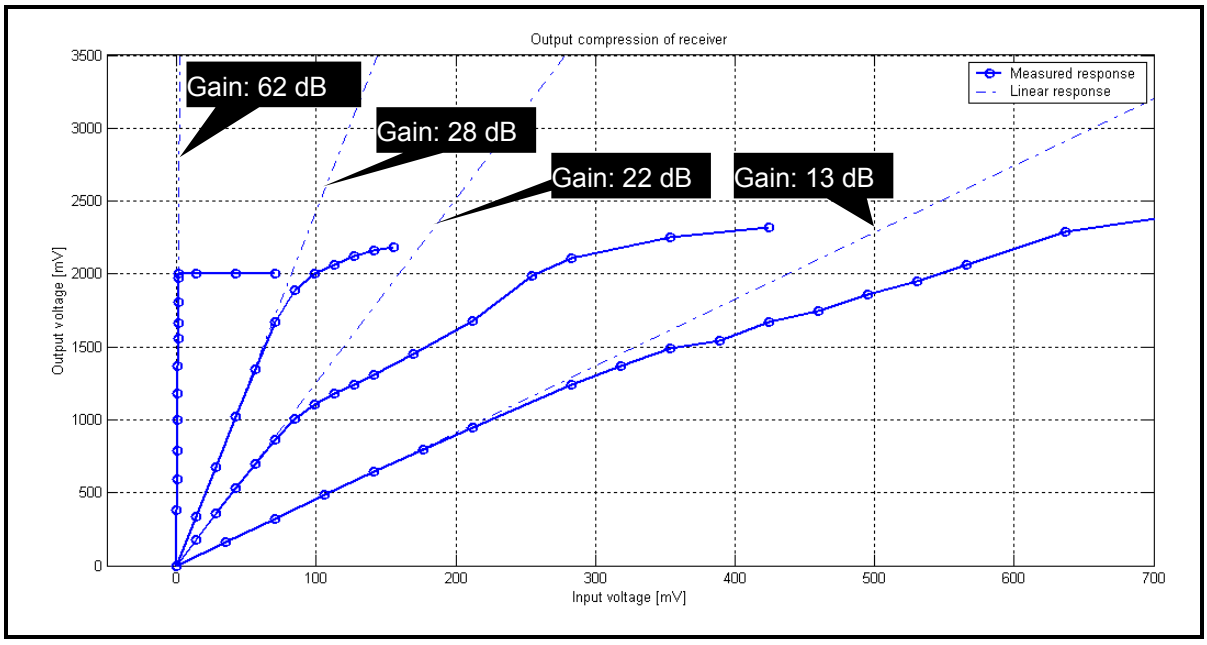

FIGURE 5-20: COMPRESSION OF CONFIGURATION 2 (MEASURED)

A clamper circuit was employed in this configuration to use only the first - almost linear - 1.5 V of the 5 V ramp created by an RC network off the digital control signal. This ramp is shown in Figure 5-21 together with the leakage of the gain control signal onto the RF-path when no input signal is applied, similar to the measurement done with configuration 1.

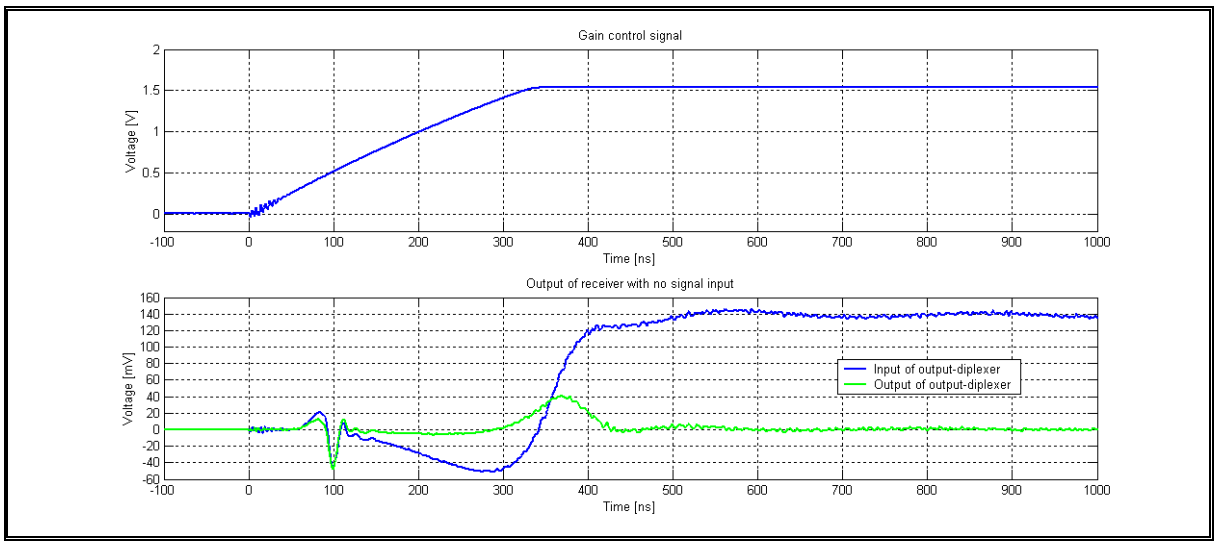

FIGURE 5-21: LEAKAGE OF GAIN CONTROL ONTO RF SIGNAL PATH FOR CONFIGURATION 2 (MEASURED)

The leakage in this configuration is significantly larger than in configuration 1, with a signal approaching 150 mV_{pp} appearing on the RF-path. The output diplexer is again able to reduce it to a more respectable 40 mV.

The STC mode of operation is again illustrated by applying the 500 μV, 30 MHz input signal and converting the measured gain control signal to the gain function with the help of the datasheet parameters.

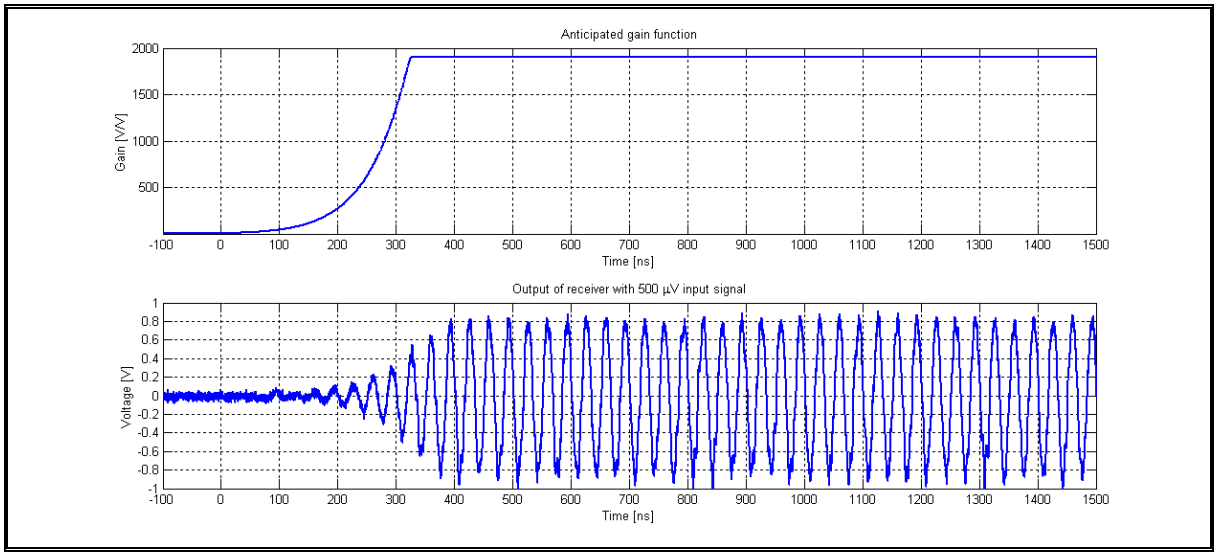

FIGURE 5-22: STC MODE OF OPERATION: CONFIGURATION 2 (MEASURED)

5.5. Synopsis

It has been shown theoretically that the non-ideal characteristics of an amplifier can combine with the reflective filter elements (however simple) bordering it to result in degradation of signal fidelity. The use of absorptive filters was proposed from a theoretical argument to improve the preservation of signal fidelity. Basic absorptive filter networks were then presented and shown theoretically to meet the set requirements. Measurements were conducted that clearly showed the improvement in signal fidelity when these absorptive filters are used instead of reflective filters.

A number of basic principles regarding gain and noise when using and interfacing operational amplifiers, variable gain amplifiers and standard gain blocks were further formalized for reference during the rest of the design.

Two receiver configurations were designed for application in a borehole radar system. The designs were carried right through to component level to illustrate practical application of these design principles, especially the use of dissipative filtering. Their operation was then confirmed through laboratory testing.

The performance of the two configurations is very similar and the only major difference exists at low gain. Configuration 2 starts off at 15.5 dB gain compared to the 28.6 dB gain of configuration 1. The output compression point of configuration 2 is further significantly less dependent on gain, so that the maximum amplitude which can practically be handled by configuration 1 is only 20 mV, compared to the 500mV of configuration 2. The deciding factor between the two configurations is consequently expected to be related to the handling of the large signals during the initial section of the acquisition time.

CHAPTER 6

A monostatic borehole radar system

6.1. Background

Borehole radar has been referred to throughout this dissertation as an application for this transceiver and configurations for each individual module were presented as alternatives for a monostatic borehole radar transceiver. This chapter will endeavour to evaluate the performance of the designed transceiver when used in such a system.

It will be shown in section 6.2 how a complete borehole radar system can be implemented by using a single configuration of each of the modules presented in the preceding chapters. The general functioning of this integrated system will be evaluated by laboratory measurements in section 6.3. This system serves as an example of the possibilities afforded by the design principles developed here.

Although the integration of only one complete system is discussed here, a number of the possible module combinations were in fact built and tested in the field. A quick overview of these measurements is provided in section 6.4 and represents the first known monostatic borehole radar measurements performed in the field. This will further be used to compare the various configurations developed in this dissertation and to formulate a recommendation on the preferred configuration.

This chapter is in many ways the culmination of all the preceding work and should be viewed as an evaluation of the developed transceiver's overall performance.

6.2. A complete monostatic borehole radar system

Table 6-1 provides a summary of the individual modules that were chosen to assemble a complete borehole radar for evaluation in the laboratory. It will be shown during the discussion of field measurements to be the recommended configuration. Addendum A can be referred to for details of these circuits.

Module	Configuration
Antenna	Asymmetric resistively loaded antenna
Transmitter	Bipolar pulse transmitter
Isolation switch	Configuration 1 (PIN diode, dissipative filtering etc.)
Receiver	Configuration 2 (Transformer and VGA)
Timing control circuitry	Purpose-built circuit based on logic hex inverter
Central control **Digitization** **On-board data storage** **Communication**	Circuitry used in GeoMole bi-static receiving probe
Mechanical structure	Structure used in GeoMole bi-static receiving probe

TABLE 6-1: SUMMARY OF MODULES USED IN BOREHOLE RADAR TRANCEIVER EVALUATED IN LABORATORY

6.2.1. Integration of modules

A block diagram of the electronics of the monostatic borehole radar system is shown in Figure 6-1; the power supply has been omitted for simplicity.

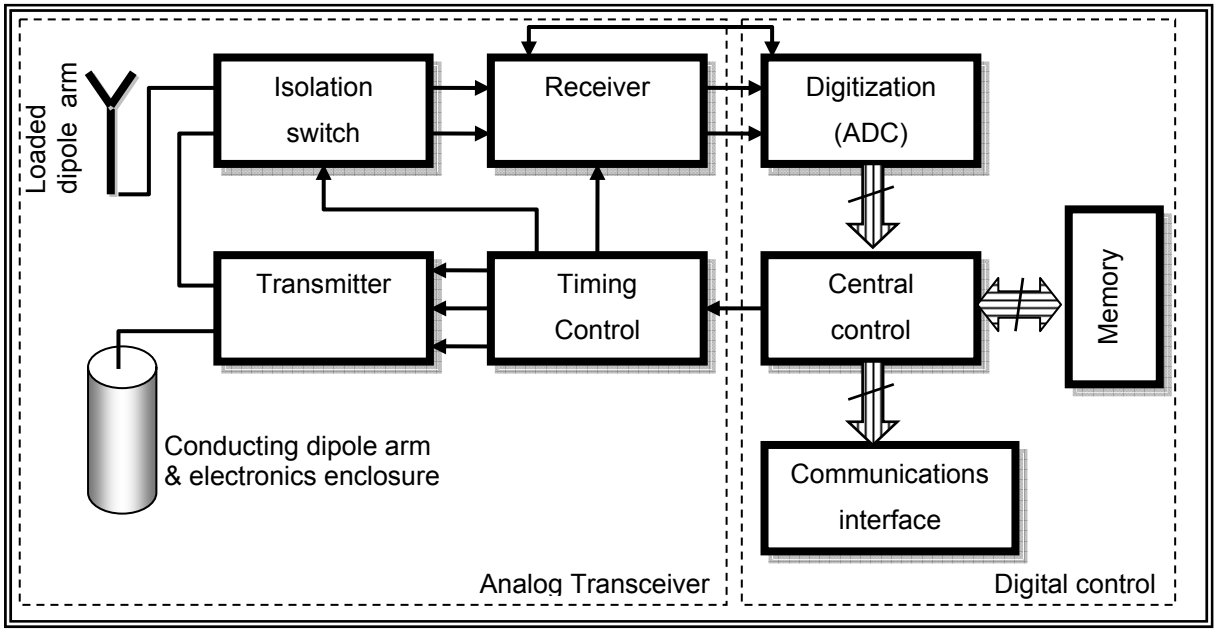

FIGURE 6-1: BLOCK DIAGRAM OF COMPLETE MONOSTATIC BOREHOLE RADAR

6.2.1.a. Central control – timing control interface

The digital control subsection itself will not be discussed here, as it is part of the commercial GeoMole borehole radar system, but will just be characterized by its interfaces with the analog transceiver. One such interface is the trigger signal sent to the timing control unit. It provides a trigger signal to the timing control module with the following specifications:

Frequency	10 kHz
Duty cycle	50 %
Amplitude	3.3 V logic level
Trigger event	Rising edge

TABLE 6-2: DETAILS OF TRIGGER SIGNAL

6.2.1.b. Timing control signals

A subcircuit had to be developed to facilitate the timing and distribution of trigger signals to the transmitter (to drive the three MOSFET drivers), receiver (the gain control signal) and isolation switch (to switch between isolate and through-mode.) The circuit diagram is included as Figure 6-12.

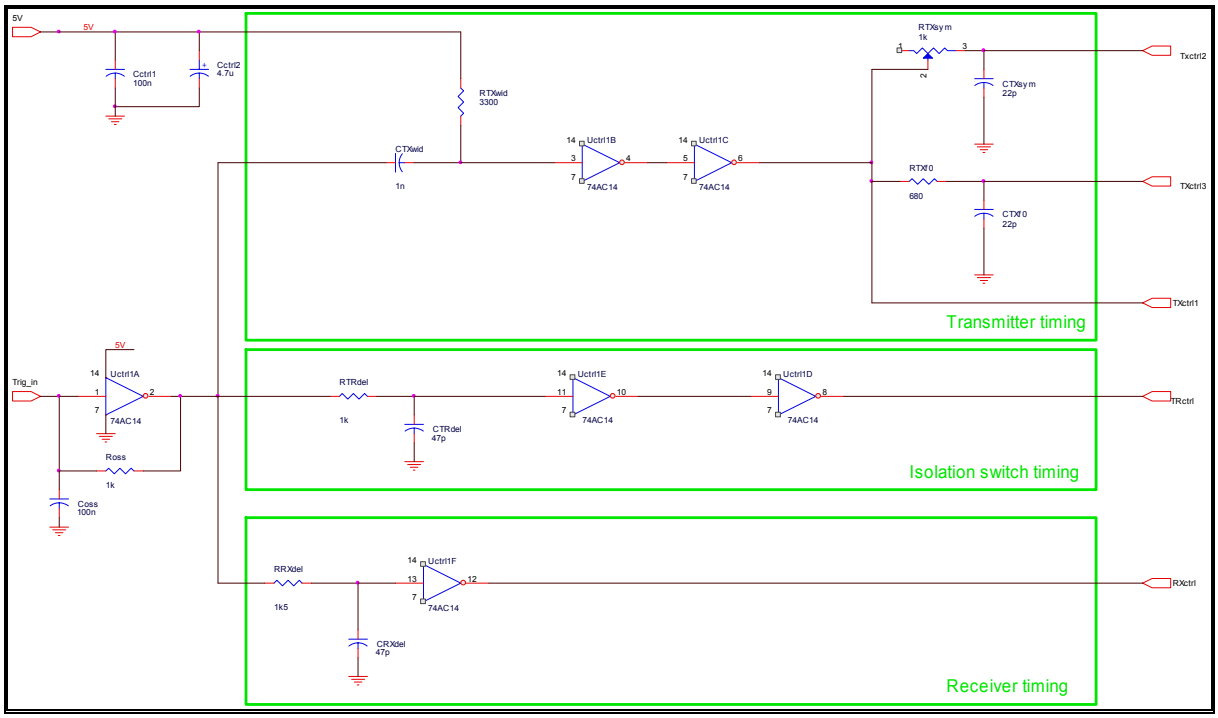

FIGURE 6-2: TIMING CONTROL SUBCIRCUIT

A 5 V logic hex inverter is used but is still toggled by the 3.3 V level of the central control module. Pulse widths and delays are set by resistive-capacitive networks in conjunction with the Schmitt trigger inverter.

- C_{TXwid} and R_{TXwid} are responsible for keeping the transmitter in the low impedance state for approximately 3 μs (slightly more than the acquisition time of the radar) only.
- R_{TXsym} was included as a trim pot to allow for fine tuning of the transmitter pulse's symmetry to zero the residual current.
- R_{TFXf0} and C_{TXf0} set the nominal transmitter pulse width to 35 ns.
- Negative logic is used for the transmitter control signals, since an inverting MOSFET driver is used in the transmitter.
- R_{TRdel} and C_{TRdel} determine the time when the isolation switch changes from isolate to through-mode – these values were empirically found during laboratory testing.

- R_{RXdel} and C_{Rxdel} cause the gain to increase as soon as the isolation switch has finished switching. This signal will eventually be converted to a ramp and clipped at 1.5 V by the receiver electronics.

6.2.1.c. Transmitter –isolation switch – antenna interface

This crucial interface has been extensively discussed during the design of the transceiver. The output of the transmitter and the input of the isolation switch both consist of transformers, while the antenna consists of a loaded dipole arm and a conducting tube which houses the electronics. The loaded arm of the antenna is closely spaced to the conducting arm (to form the feed point of the antenna) and a coaxial arrangement is used to connect the loaded antenna arm to one terminal of the isolation switch-transformer, housed inside the conducting arm. The other terminal of the isolation switch-transformer is then connected to a terminal of the transmitter-transformer. The other terminal of the transmitter-transformer is grounded. The conducting tube is connected to the ground of the circuit. The balun effect of this arrangement has been discussed in literature [13].

6.2.1.d. Isolation switch – receiver interface

It was pointed out that this receiver configuration (configuration 2) must be designed in conjunction with the isolation switch, as was done in section 5.3.2. The balanced diplexer at the output stage of the isolation switch (configuration 1) replaces the unbalanced input diplexer of the receiver discussed in section 5.3.2. A transformer with a 4:1 turns ratio is used (this is indicated as T_{Rx1} on the circuit diagram of the receiver in addendum A) and replaces the output transformer of the isolation switch (indicated at T_{iso2} in addendum A) so that the isolation switch can operate with a 60 Ω characteristic impedance internally.

6.2.1.e. Receiver-ADC interface

The receiver has a balanced output and is connected directly to the balanced input of the ADC. The common mode output voltage of the ADC is available on one of its pins and is used to force the receiver amplifier's bias point to the same value through the V_{ocm} pin.

6.2.2. Board layout

The top and bottom layers of the printed circuit board layout used for the analog transceiver section of this system are shown in Figure 6-3. It is a four layer board, with the two inside layers being solid ground planes. The dimensions of the board are 80 x 25 mm. This interfaces with the established borehole radar digital control and power supply printed circuit board.

Top layer

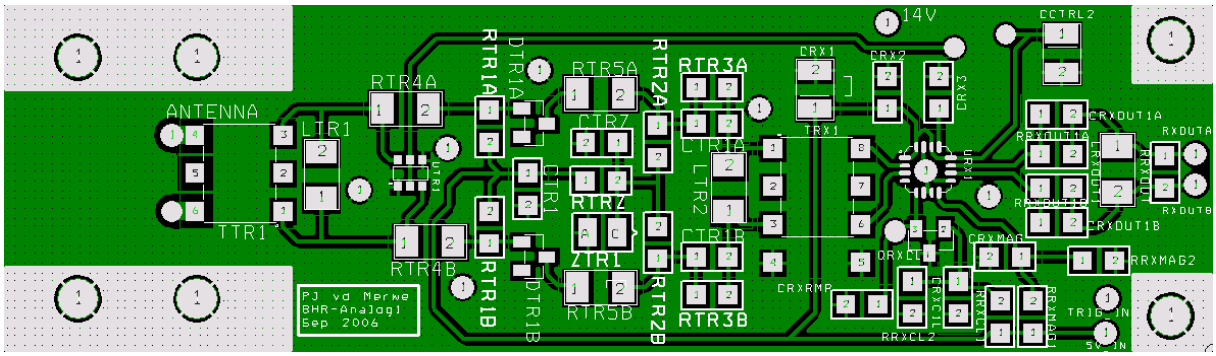

Bottom layer (as seen *through* top layer)

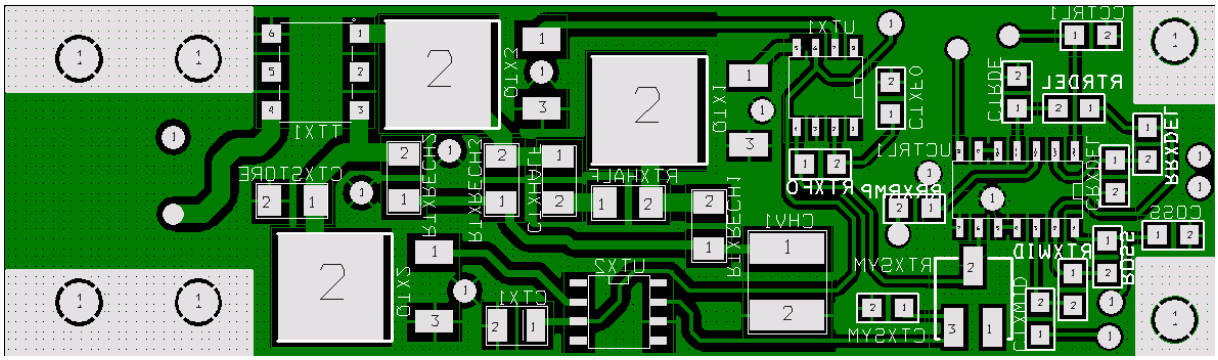

FIGURE 6-3: PRINTED CIRCUIT BOARD LAYOUT FOR BOREHOLE RADAR ANALOG TRANSCEIVER

The layout will not be discussed in detail, but a number of special considerations should be highlighted.

- The large signal electronics are separated from the sensitive electronics by a solid ground plane with the transmitter on one side of the board and the isolation switch and receiver on the other side. The ground plane combined with the conducting pipe in which it is housed then results in each being contained in its own, shielded half cylinder. It will be noted that only surface mount components are used to further isolate the two sections.
- An effort was made to maintain symmetry as far as possible in the layout of the isolation switch, since symmetry is crucial to its performance. R_{TR4A} and R_{TR4B} are 0 Ω resistors that act as bridges to allow the control signal and power supply lines to enter the isolation switch. The tracks carrying these signals were kept perpendicular to the signal tracks of the isolation switch in an attempt to reduce coupling.
- The clearance around the tracks carrying high voltage was enlarged to prevent sparking due to some imperfections.
- The tracks between the MOSFET drivers (U_{TX1} and U_{TX2}) and the transmitter MOSFETs (Q_{TX1}, Q_{TX2}, Q_{TX3}) carry large peak currents and should be as short as possible with the return path (ground plane) as close as possible to the track to reduce magnetic coupling to the rest of the circuit. The same applies to the tracks at the transmitter-antenna-isolation switch interface.

- The high voltage line (from C_{HV1}) is conversely prone to electric coupling and must have a ground plane in close proximity to terminate the electric field before coupling to other devices.
- Ground vias were added whenever possible to force the various ground planes to the same potential throughout.

6.2.3. Probe

The mechanical structure of the monostatic radar probe is as discussed in the antenna section 2.2. The printed circuit boards of the analog transceiver (presented above), digital control circuitry and power supply are housed inside the 1 m, 28 mm diameter conducting tube, together with the battery stack. A brass control head is added to one end as user interface, but care is taken to prevent ohmic contact between the conducting tube and the control head – which is in contact with the environment during measurements. A coaxial feed arrangement is implemented at the other end of the conducting tube to feed the loaded antenna arm, which is housed in a dielectric tube. The whole system is enclosed in a watertight, 32 mm diameter PVC tube, with just the control head protruding. The total length of the probe is 1.8 m.

6.3. Signal path through system

The complete system will now be tested on the laboratory bench to verify its operation. This is in effect a repeat of the laboratory measurements conducted on the individual modules earlier, but referenced to a single trigger signal, to highlight the relative timing and general interaction between the signals of the various modules in an integrated system. The loaded antenna arm was replaced by the lumped element equivalent network for a 48 mm water filled borehole (as found in section 2.4.2) for the purpose of the laboratory measurements.

6.3.1.a. Transmitter

The waveforms associated with the transmitter module are shown in Figure 6-4. The control signals to the transmitter stay low for 3 μs, which is not shown in the figure. The voltage level for a logic “low” of the MOSFET drivers is specified as 0.8 V. The exponential recovery of the control signals consequently result in the required delays at the outputs of the MOSFET drivers. The relative timing of the three MOSFETs shown here is the result of fine tuning for zero antenna current after the transmitter transient.

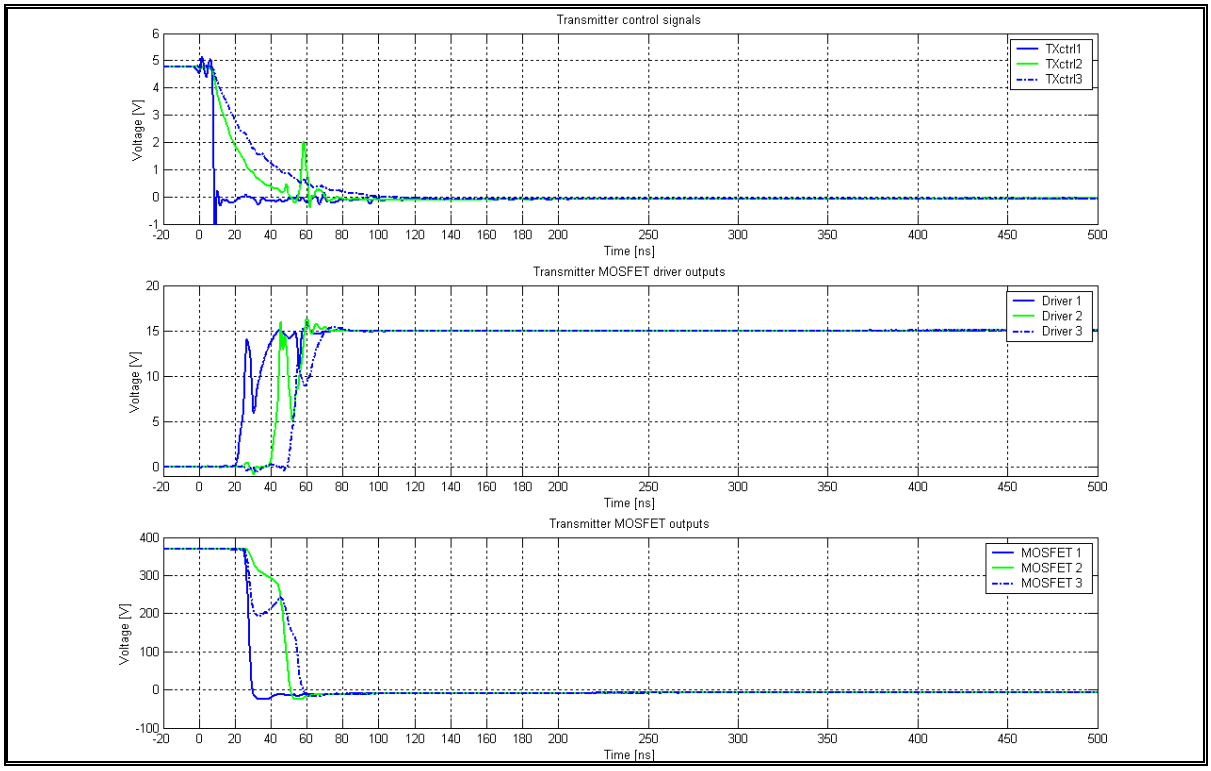

FIGURE 6-4: TRANSMITTER WAVEFORMS OF MONOSTATIC BOREHOLE RADAR (MEASURED IN LABORATORY)

6.3.1.b. Antenna

The voltage appearing on the terminal normally connected to the loaded antenna arm is shown below, Figure 6-5. The peak to peak amplitude exceeds 400 V. This represents the waveform which results in minimum current flow into the lumped element equivalent antenna circuit after the transmitter transient has been completed. The voltage and current waveform appearing on the antenna is then time limited to between 25 ns and 74 ns (the primary pulse width is 35 ns with a small tail of 14 ns.)

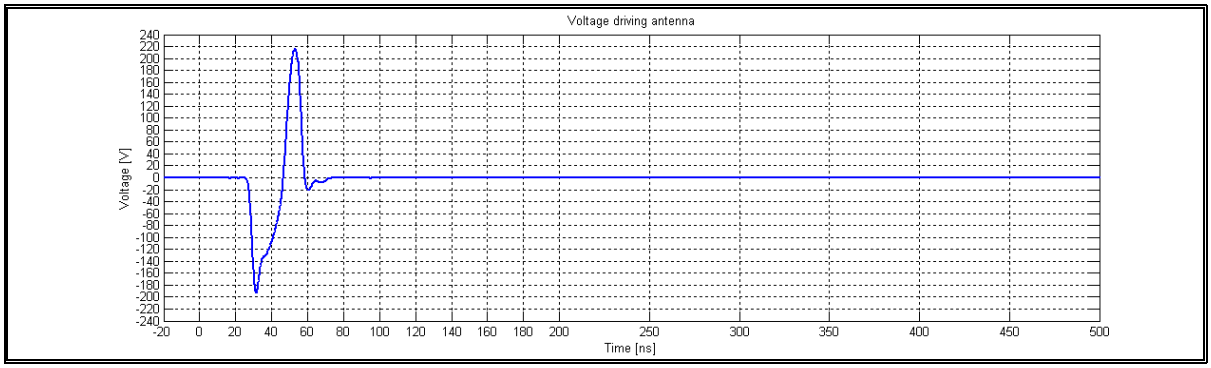

FIGURE 6-5: ANTENNA OUTPUT OF MONOSTATIC BOREHOLE RADAR (MEASURED IN LABORATORY)

6.3.1.c. Isolation switch

The control signal to the isolation switch was delayed by 60 ns relative to the first control signal of the transmitter (TXctrl1). It was found that a further reduction of this delay results in large signals coupling through at the instant when the isolation switch switches over to through-mode. This is to be

expected, since the recommended delay causes the FETs of the isolation switch to start switching at 74 ns – exactly the time when the transmitter transient stops. It has been pointed out earlier that the isolation switch can be considered as in its through-mode when the diodes start conducting. This occurs at 106 ns, 81 ns after the transmitter transient began. The signals on both the differential arms are shown at two points in the isolation switch: after the shunt switches (output of FETs) and after the series switches (output of diodes.) The two signals at each point can be seen as the switching signals, which occur in common mode. The signal path is represented by the difference between the two signals at each point. The two differential arms follow each other closely, except at the output of the FETs when the transmitter fires. This represents the leakage from the transmitter through the shunt switches, but the difference is significantly reduced by the series diode switches' isolation. Good isolation from the transmitter and good suppression of the switching signal can therefore be expected.

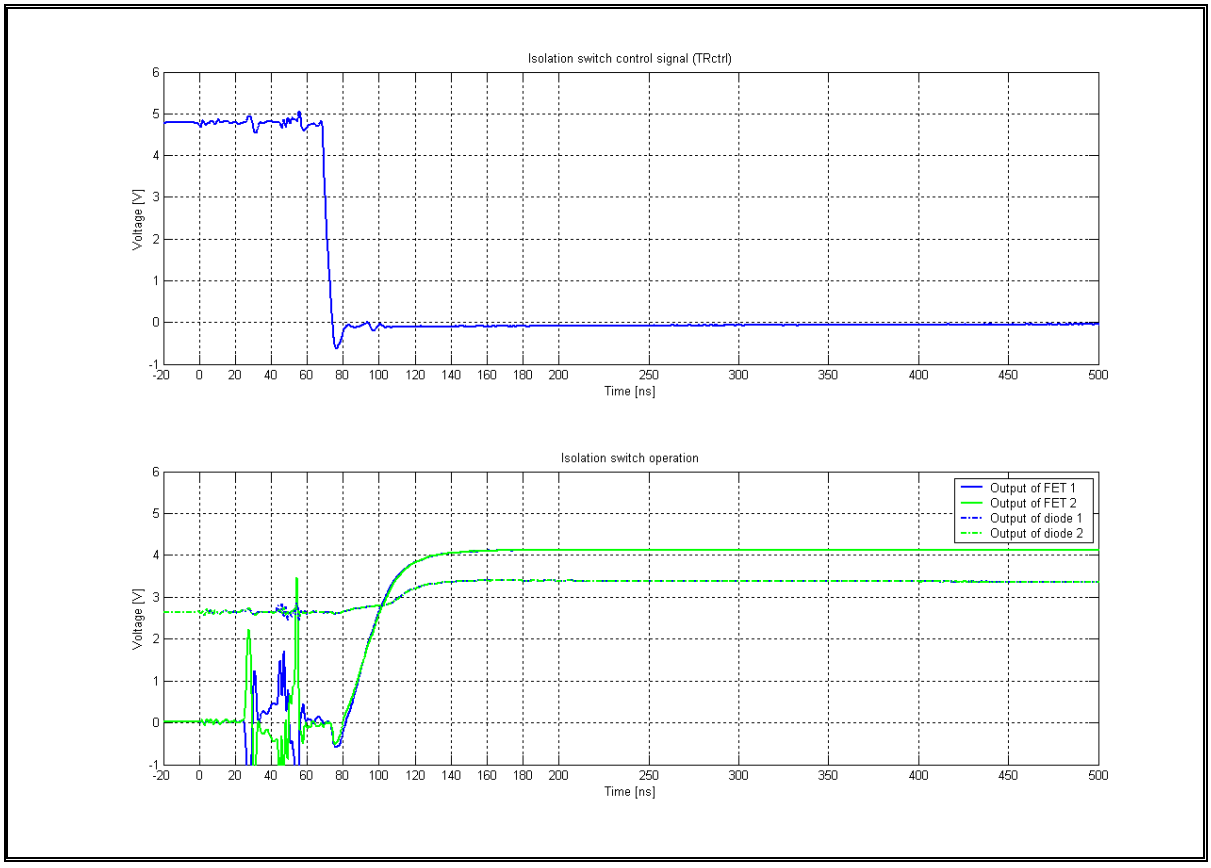

FIGURE 6-6: ISOLATION SWITCH WAVEFORMS OF MONOSTATIC BOREHOLE RADAR (MEASURED IN LABORATORY)

6.3.1.d. Receiver

The gain ramp commences at 94 ns, 20 ns after the FETs of the isolation switch start switching and the ramp reaches 1.5 V at 420 ns. The artefacts of the amplifier are similar to that measured earlier, with small effects seen between 170 ns and 200 ns (a predominantly common mode signal is seen at

the 2 input terminals, but some of it leaks through to the differential signal path), as well as the characteristic roll between 400 ns and 550 ns.

The signal coupling through the (isolating) isolation switch between 25 ns and 74 ns, when the transmitter transient occurs, is less than 0.3 V_p and is markedly of higher frequency content.

The signal coming through the isolation switch when it switches to through-mode at 106 ns is barely seen, indicating exceptional suppression of the switching signal in the data, as well as near-zero residual current flowing.

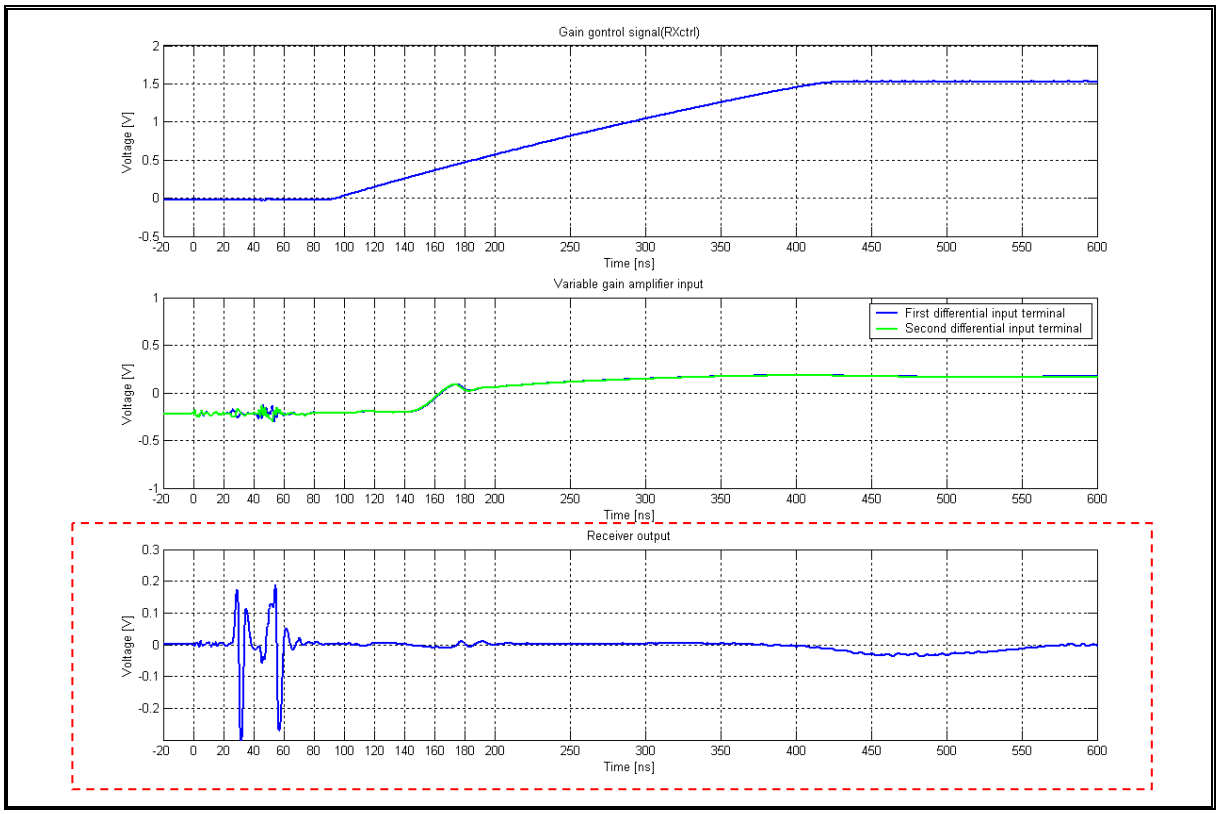

FIGURE 6-7: RECEIVER WAVEFORMS OF MONOSTATIC BOREHOLE RADAR (MEASURED IN LABORATORY)

6.3.1.e. Conclusion

Laboratory testing of the monostatic borehole radar system yielded remarkable results. A 400 V bipolar waveform of 35 ns duration can be transmitted with coupling of less than 0.5 V_{PP} to the eventual ADC. This is followed by a near-to-ideal transition to receive mode 81 ns after the transmitter transient started and receiver gain is swept to its maximum in excess of 60 dB within 400 ns.

6.4. Field measurements

FIGURE 6-8: A MONOSTATIC BOREHOLE RADAR MEASUREMENT IN PROGRESS IN A HORIZONTAL UNDERGROUND BOREHOLE.

A large number of field measurements were performed during the design process. Various combinations of the modules developed here were incorporated into complete borehole radar probes for deployment in boreholes [78]. All measurements used in this chapter were performed in diamond drilled boreholes in South African gold, platinum and diamond mines. A table of the borehole gauges referred to in this section can be found in [23]. Measurements could not necessarily be performed in a systematic manner by changing one parameter at a time due to the logistics of the mining environment and any opportunity presenting itself had to be exploited.

Only a few datasets will be presented here; those that revealed important information during the design process and which are considered landmark results. The complete radar images from the field measurements are presented along with individual traces extracted from these datasets.

The individual trace is simply the RF signal as digitised by the ADC. It is, where necessary, compared to that of a control experiment performed with another configuration of the transceiver, in order to highlight a specific aspect.

The radar images were obtained using GeoMole's SeisWin© software package and incorporates the following basic processing: removal of the mean trace, 10 MHz high pass filtering and automatic gain control. Further notes on the processing and interpretation of these radar images can be found in [10] and [79]. It was noted earlier that the design specification is simply to deliver similar results than the GeoMole bistatic system. For that purpose, the radar image from a control measurement performed in the same borehole with the Geomole system is usually also included to evaluate the absolute performance of the transceiver configuration employed in the monostatic radar.

Details of the tested transceiver are provided in each section with reference to the configurations developed in the preceding chapters. This is shown alongside details of the probes used as control measurements for the single trace and complete radar image. The actual subsystems used may differ slightly from the configurations in the chapters, but the general principle of operation stays the same.

6.4.1. Residual current

The concept of a time limited impulse response for the current flowing between antenna and transmitter was a fundamental design principle for the transmitter. It was noted that any residual current flowing when the isolation switch changes over to through-mode will be passed to the receiver and might saturate it. This is clearly illustrated in this measurement conducted with a probe incorporating a step transmitter without the pole-zero network. This measurement did not yield a usable radar image and only the individual trace is presented.

Module	**Configuration:** **Test measurement**	**Configuration:** **Single trace** **Control measurement**
Antenna	Resistive loading	Resistive loading
Transmitter	Step (without pole zero network)	Step (without pole zero network)
Isolation switch	Configuration 2	Configuration 2
Receiver	Configuration 1 (without output diplexer)	Configuration 1 (without output diplexer)
Environment		
Borehole diameter	75 mm (NQ gauge)	Free air
Borehole state	Water filled	
Geological environment	Dolomite host with Kimberlite pipe intrusion	

TABLE 6-3: DETAILS OF FIELD MEASUREMENT: EFFECT OF RESIDUAL CURRENT

Note that the roll in the data was later found to be related to a resonance in the power supply's smoothing capacitors.

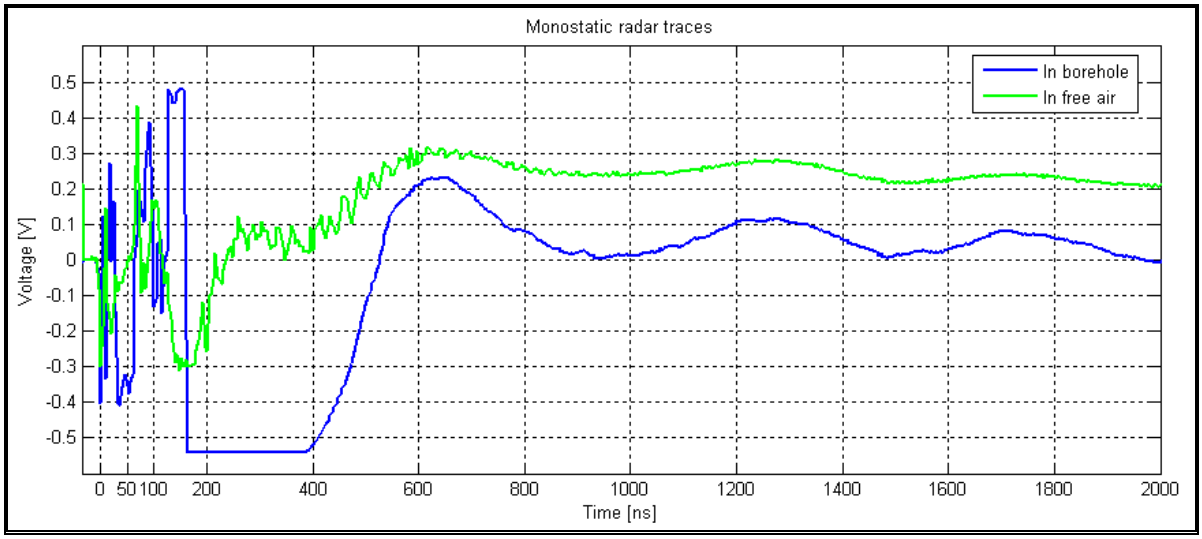

FIGURE 6-9: SINGLE TRACE FROM FIELD MEASUREMENT: EFFECT OF RESIDUAL CURRENT

The borehole environment caused an increase in the relaxation time of the transmit-current so that the residual current flowing when the isolation switch opened up at 90 ns was sufficient to generate an output amplitude bigger than the maximum swing (0.5 V_p) of the ADC and resulted in data loss up to 400 ns. The absence of the output diplexer enables the easy identification of this.

6.4.2. Pole-Zero network (wet borehole)

A pole-zero network was presented in section 3.2.3 as a way to cancel out the slowly recovering section of the transmit current, when used as part of the step waveform transmitter. The following measurement sees a similar radar deployed in the same borehole as above, but with the complete step waveform transmitter as proposed in section 3.3 – with the pole-zero network. Note that the output diplexer was also included and the resonance in the power supply removed. The details of the radar probes used for this measurement are given below:

Module	Configuration: Test measurement	Configuration: Single trace Control measurement	Configuration: Radar image Control measurement
Antenna	Resistive	Resistive	GeoMole Bi-static system
Transmitter	Step	Step (Without pole-zero network)	
Isolation switch	Configuration 2	Configuration 2	
Receiver	Configuration 1 (with output diplexer	Configuration 1 (without output diplexer)	
Environment			
Borehole diameter	75 mm (NQ gauge)	75 mm (NQ gauge)	75 mm (NQ gauge)
Borehole state	Water filled	Water filled	Water filled
Geological environment	Dolomite host with Kimberlite pipe intrusion	Dolomite host with Kimberlite pipe intrusion	Dolomite host with Kimberlite pipe intrusion

TABLE 6-4: DETAILS OF FIELD MEASUREMENT: POLE-ZERO NETWORK IN WET BOREHOLE

6.4.2.a. Single trace evaluation

Two traces are shown in Figure 6-10 - the one is the trace obtained in section 6.4.1 without the pole-zero network and the other is with a pole zero network.

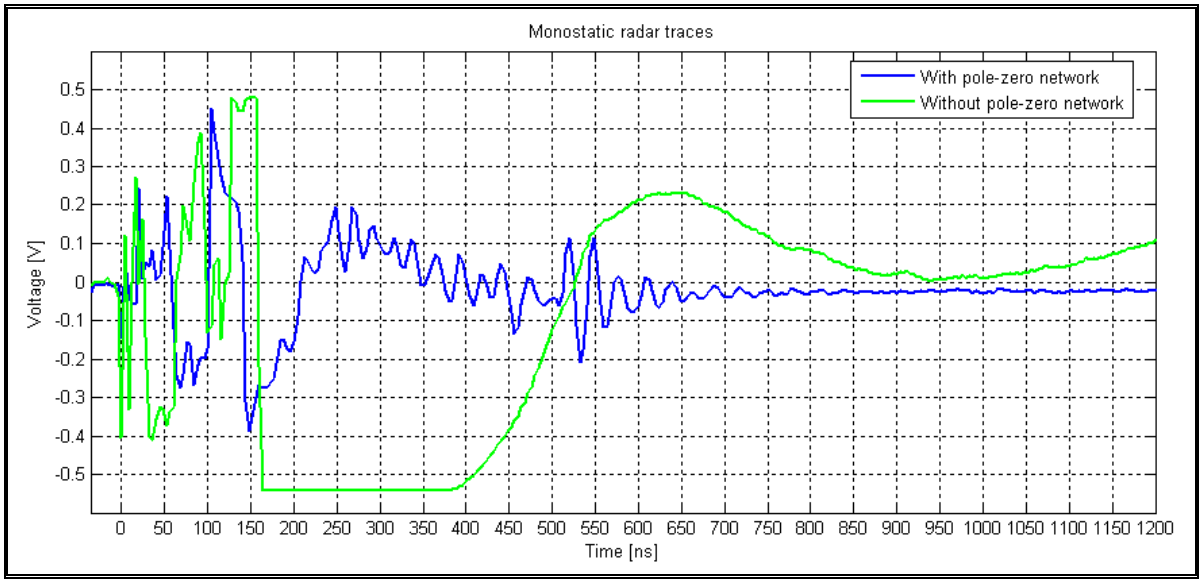

FIGURE 6-10: SINGLE TRACE FROM FIELD MEASUREMENT: EFFECT OF POLE-ZERO NETWORK

The pole-zero network clearly has a dramatic effect and enabled the monostatic borehole radar to acquire data in the field. A large reflector can already be discerned at 500 ns in this particular trace. It is slightly obscured by the filtering, but the receiver remains saturated up to 150 ns at a voltage lower than the maximum swing of the ADC. This can be attributed to saturation of the variable gain amplifier of receiver configuration 1, which enters its non-linear mode at a lower voltage for lower gain settings (as pointed out during its design.).

6.4.2.b. Radar image evaluation

The actual radar data obtained by the monostatic system with the pole-zero network is compared to the commercial bi-static dataset gathered in the same borehole on the next page. The maximum range of the two systems compares well and the visual appearance of the data is very similar. The monostatic radar is however blind for the first 150 ns, as anticipated from the single trace evaluation. At a propagation velocity of 106 m/μs [8], this amounts to the radar being unable to discern targets closer than 8 m from the borehole.

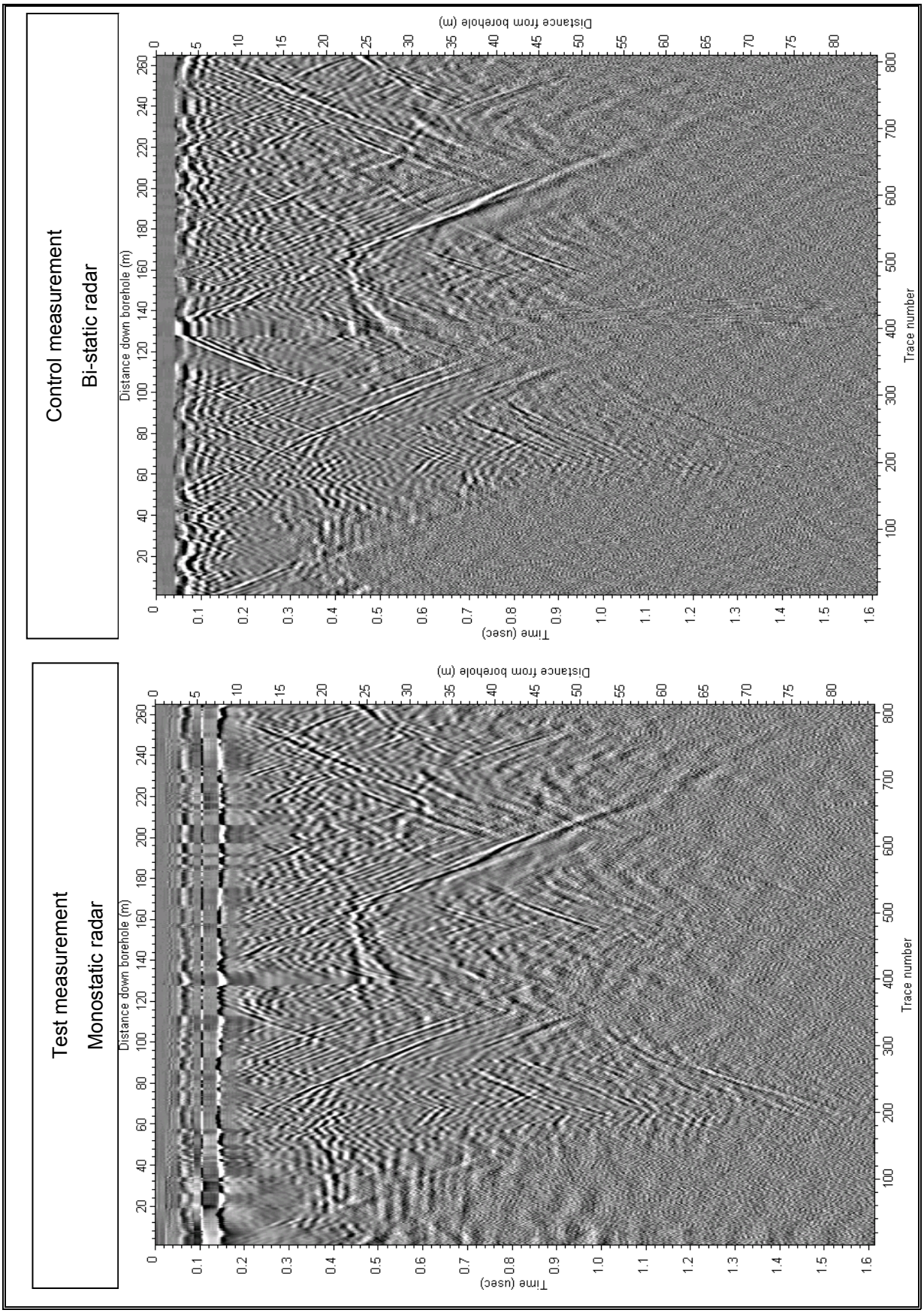

FIGURE 6-11: RADAR IMAGE FROM FIELD MEASUREMENT: EFFECT OF POLE-ZERO NETWORK IN WET BOREHOLE

6.4.3. Pole-zero network (dry borehole)

The opportunity also arose to deploy the radar of section 6.4.2 in a dry, 48 mm diameter borehole and this result is also included. Only the radar image will be considered (not individual traces) and the control experiment is again the commercial bi-static system, deployed in the same borehole.

Module	Configuration: Test measurement	Configuration: Radar image Control measurement
Antenna	Resistive	GeoMole Bi-static system
Transmitter	Step	
Isolation switch	Configuration 2	
Receiver	Configuration 1	
Environment		
Borehole diameter	48 mm (AQ gauge)	48 mm (AQ gauge)
Borehole state	Dry	Dry
Geological environment	Bushveld Igneous Complex	Bushveld Igneous Complex

TABLE 6-5: DETAILS OF FIELD MEASUREMENT: POLE-ZERO NETWORK IN DRY BOREHOLE

The results are similar to that obtained in the wet borehole and are displayed on the next page (Figure 6-12). An additional observation can be made from this radar image however: the monostatic radar is able to detect a strong reflector while the isolation switch is still in isolate mode (up to around 80 ns.) Note that the propagation velocity used for this measurement is 112.5 m/μs [9].

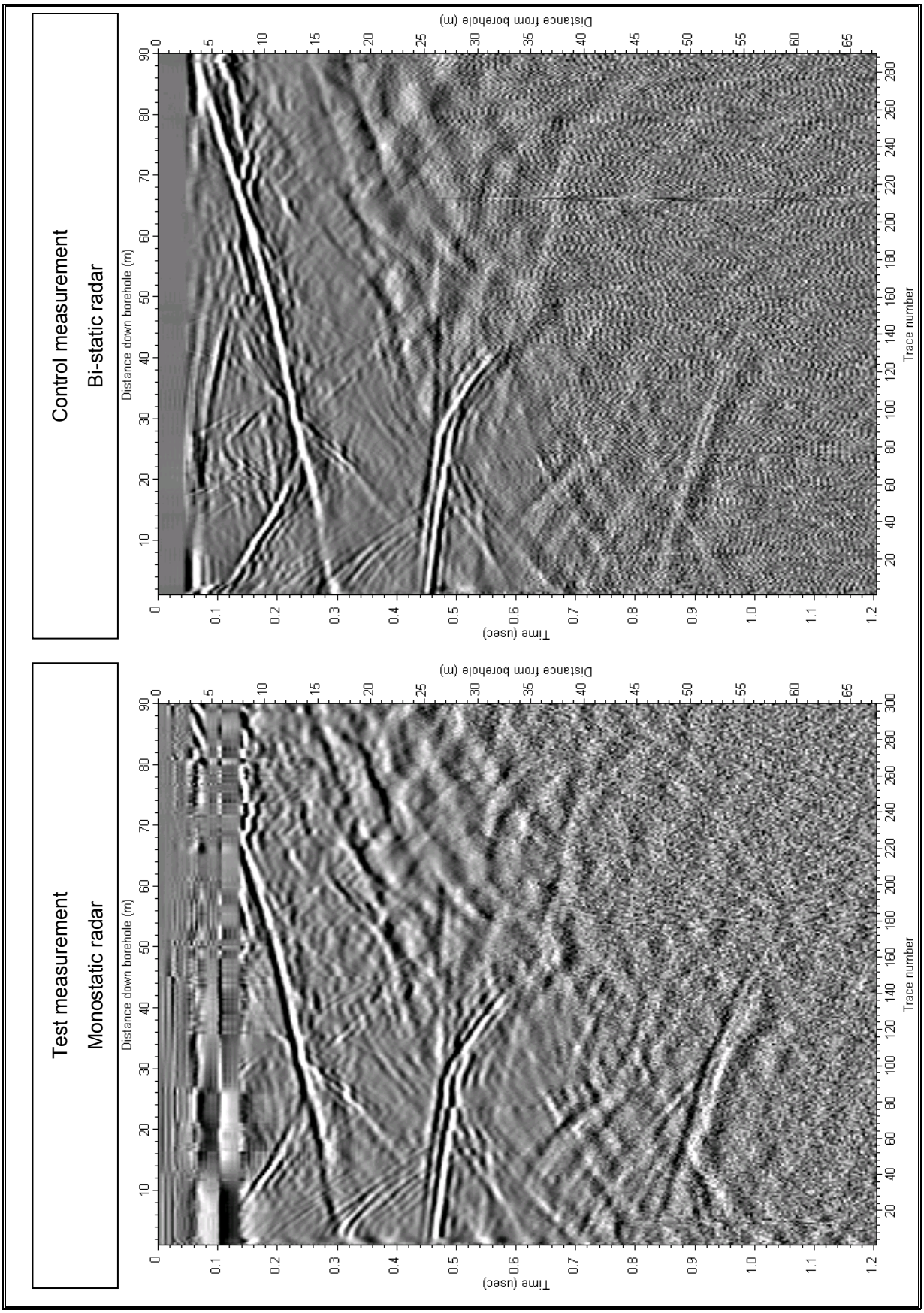

FIGURE 6-12: RADAR IMAGE OF FIELD MEASUREMENT: EFFECT OF POLE-ZERO NETWORK IN DRY BOREHOLE

6.4.4. Resistive-capacitively loaded antenna (RC-antenna)

The addition of capacitors to the loading profile of the antenna was proposed by Gouws to reduce the recovery time of the antenna current. The following measurement (found in his thesis [22]) was conducted in the same borehole as in section 6.4.1 and 6.4.2 and with a similar probe (the output diplexer was included and the resonance removed however) as in section 6.4.1. This provides an opportunity to evaluate the RC antenna as another possible solution to reducing the residual current after the transmitter transient has completed.

Module	Configuration: Test measurement	Configuration: Single trace Control measurement	Configuration: Radar image Control measurement
Antenna	Resistive-capacitive	Resistive loading	GeoMole Bi-static system
Transmitter	Step (without pole-zero network)	Step (without pole-zero network)	
Isolation switch	Configuration 2	Configuration 2	
Receiver	Configuration 1 (with output diplexer)	Configuration 1 (without output diplexer)	
Environment			
Borehole diameter	75 mm (NQ gauge)	75 mm (NQ gauge)	75 mm (NQ gauge)
Borehole state	Water filled	Water filled	Water filled
Geological environment	Dolomite host with Kimberlite pipe intrusion	Dolomite host with Kimberlite pipe intrusion	Dolomite host with Kimberlite pipe intrusion

TABLE 6-6: DETAILS OF FIELD MEASUREMENT: RC ANTENNA

6.4.4.a. Single trace evaluation

The single trace obtained with a step waveform but without the pole-zero network, depicted in Figure 6-9, is compared to a single radar trace of this radar with the RC loaded dipole arm instead of the purely resistive arm. Note that this particular trace corresponds to the trace obtained with the pole-zero network system in Figure 6-10, with the large reflector at around 500 ns.

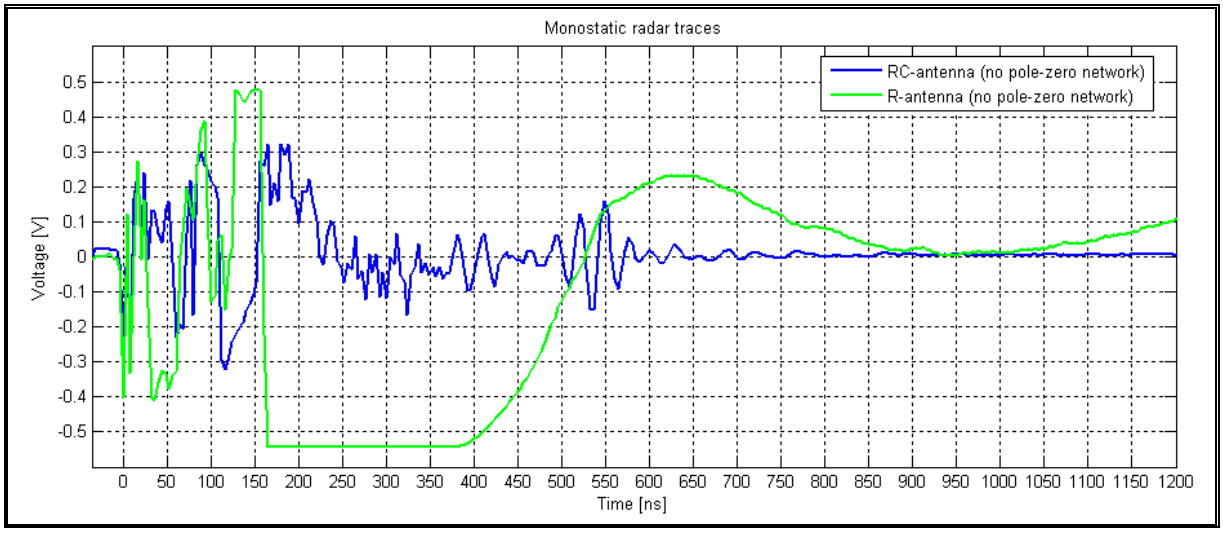

FIGURE 6-13: SINGLE TRACE FROM FIELD MEASUREMENT: EFFECT OF RC ANTENNA

The RC-antenna also enables this monostatic radar to obtain data and the performance appears to be very similar to the system with the pole-zero network, with saturation up to 150 ns.

6.4.4.b. Radar image evaluation

The effect of this saturation is again apparent in the complete radar image shown on the following page (Figure 6-14), next to that obtained with the commercial bi-static system. Maximum range of the two systems again appear similar but the data obtained with the RC-antenna, as a subjective comment, seems to lack the low frequency content of the bi-static system, which makes the data visually more difficult to interpret.

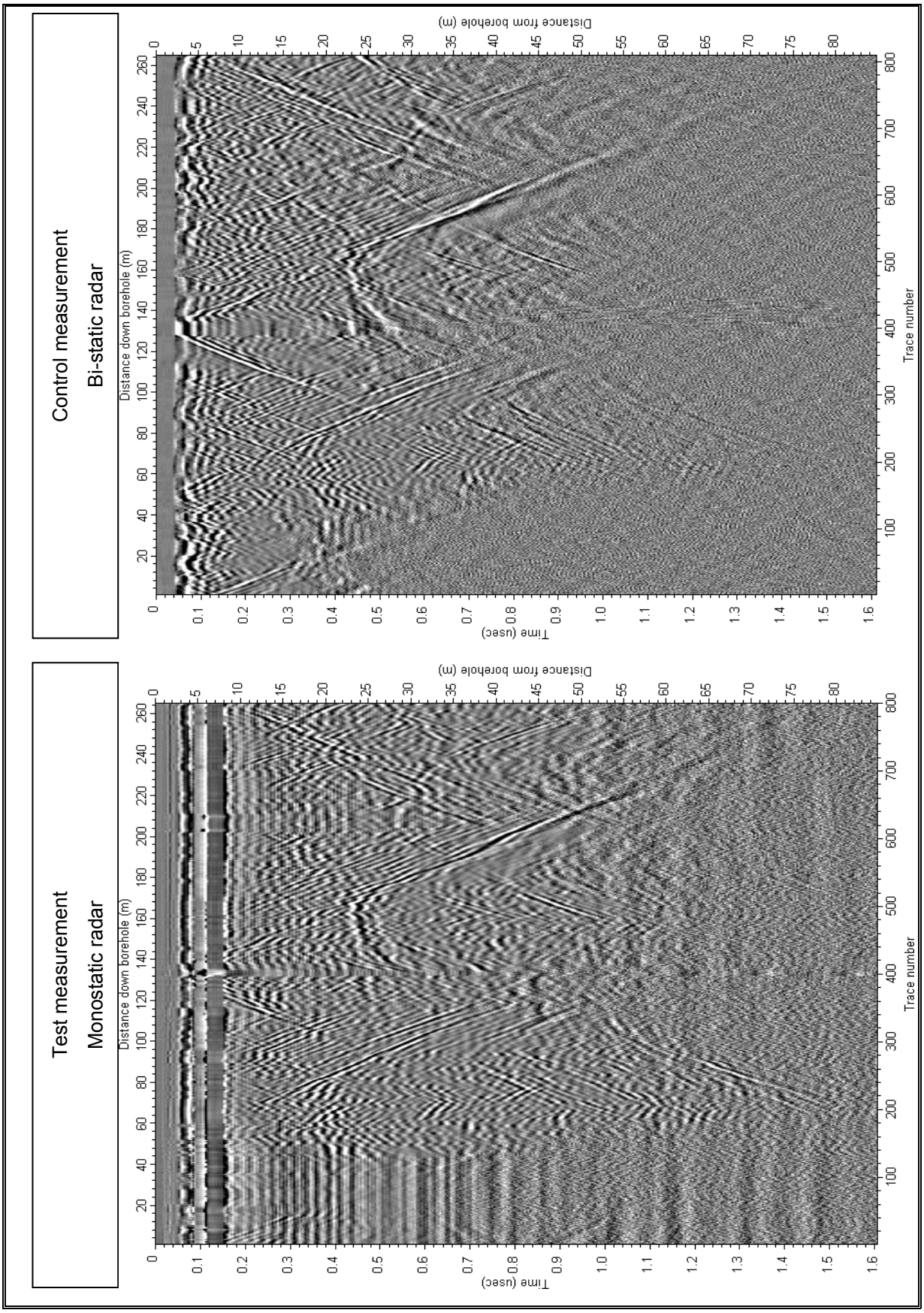

FIGURE 6-14: RADAR IMAGE OF FIELD MEASUREMENT: EFFECT OF RC ANTENNA

6.4.5. Bipolar transmitter

The bipolar transmitter was proposed as yet another way to limit the duration of the antenna current flow in section 3.4. Two radar probes were deployed in the same borehole, with the only difference being the transmitter, to investigate the effect of the bipolar transmitter.

Module	Configuration: Test measurement	Configuration: Single trace & radar image Control measurement
Antenna	Resistive	Resistive
Transmitter	Bipolar (20 ns pulse width)	Step
Isolation switch	Configuration 2	Configuration 2
Receiver	Configuration 1	Configuration 1
Environment		
Borehole diameter	48 mm (AQ gauge)	48 mm (AQ gauge)
Borehole state	Water filled	Water filled
Geological environment	Hanging wall lava above Ventersdorp Contact Reef	Hanging wall lava above Ventersdorp Contact Reef

TABLE 6-7: DETAILS OF FIELD MEASUREMENT: BIPOLAR TRANSMITTER

6.4.5.a. Single trace evaluation

The individual traces shown below (Figure 6-15) serve as a good comparison between the bipolar and step waveform transmitter, as all other variables are the same.

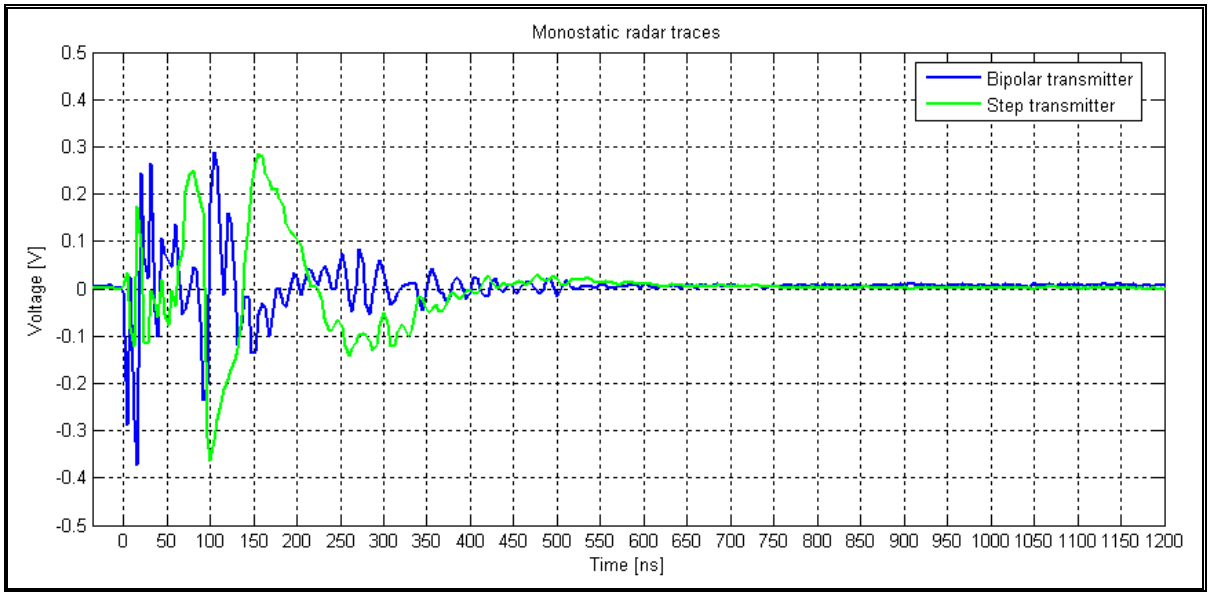

FIGURE 6-15: SINGLE TRACE FROM FIELD MEASUREMENT: BIPOLAR VS STEP WAVEFORM TRANSMITTER

It is clear that the system with the bipolar transmitter recovers much quicker after the isolation switch switches to through-mode at 90 ns. The receiver of the system with the bipolar transmitter also does

not appear to enter its non-linear region, which in turn translates to minimum data loss. This is an extremely encouraging result and if this measurement is used as criterion, the bipolar transmitter should be the transmitter configuration of choice.

6.4.5.b. Radar image evaluation

The two complete radar images from which the individual traces were taken are shown on the next page (Figure 6-16). The environment was unfortunately such that no clear reflectors were close to the borehole to compare the radars' close-in performances, but the maximum range of the step and bipolar transmitters seem to be similar. It was mentioned (in a private communication on 6 May 2006 with Prof. I.M. Mason from the School of Geosciences at the University of Sydney) that the data obtained with the step transmitter was easier to interpret. The pulse width of the bipolar system was set to 20 ns for this measurement, in order to create a spectral peak at 50 MHz. It was then empirically established that data with a high spectral content around 30 MHz generally provides visually the best borehole radar image for interpretation, although a higher frequency peak provides better resolution. This is in agreement with the general rule that penetration should enjoy preference to resolution, as stated in [80]. The versatility of the bipolar transmitter fortunately allows for easy adjustment of the pulse width.

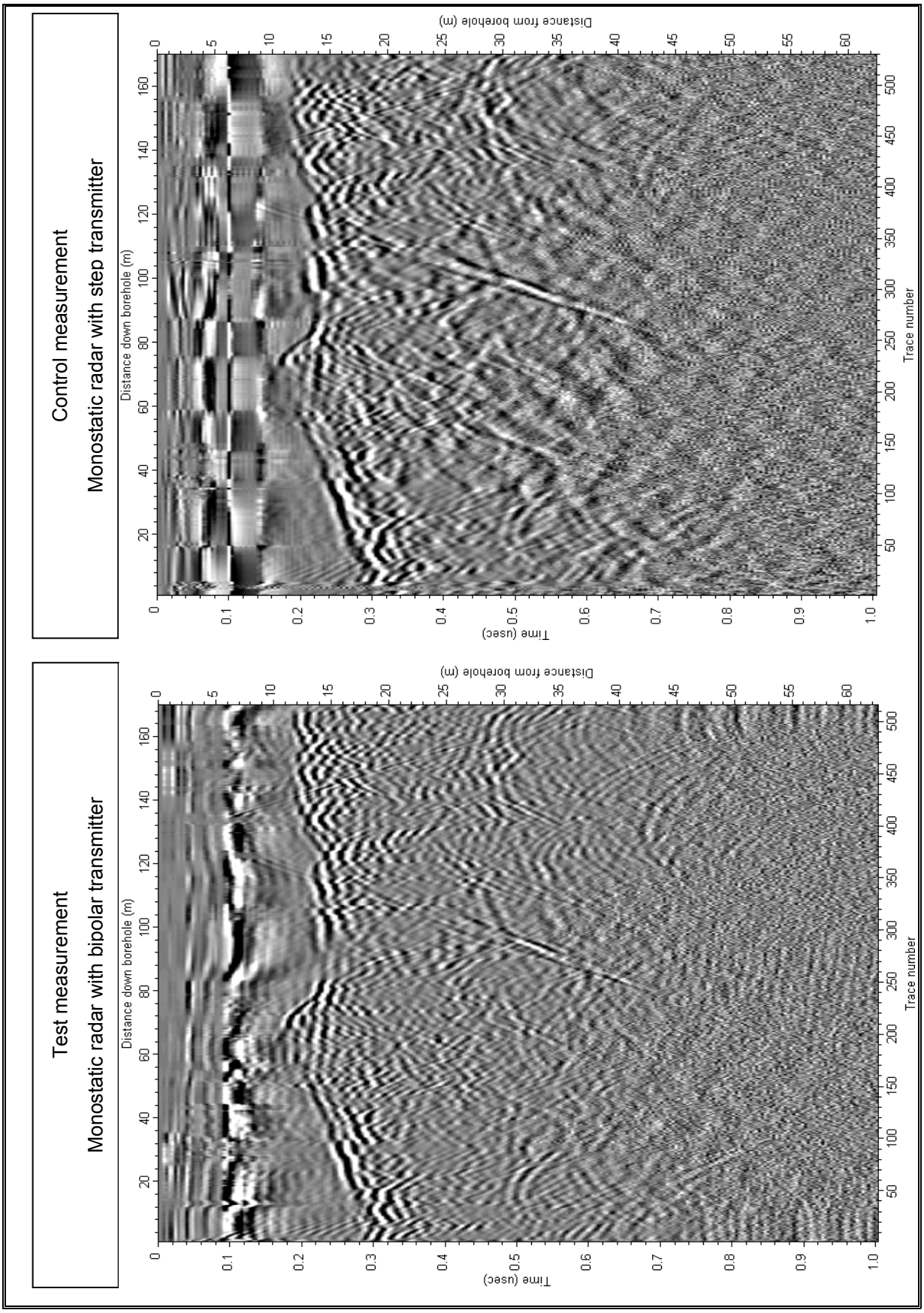

FIGURE 6-16: RADAR IMAGE OF FIELD MEASUREMENT: EVALUATION OF BIPOLAR TRANSMITTER

6.4.6. Recommended borehole radar system

It was found in section 6.4.4 that the radar image obtained with a resistively loaded antenna is visually easier to interpret than with a resistive-capacitively loaded antenna. It was further seen on numerous occasions that the reduced maximum swing of receiver configuration 1 limits the performance of the system. The results of section 6.4.5 indicated that the bipolar transmitter should be used for better close-in performance, but with a nominal pulse width of around 33 ns, to facilitate a spectral peak at 30 MHz. These recommendations were consequently incorporated into a probe, the details are as follows.

Module	Configuration: Test measurement	Configuration: Single trace Control measurement	Configuration: Radar image Control measurement
Antenna	Resistive	Resistive	GeoMole Bi-static system
Transmitter	Bipolar	Bipolar	
Isolation switch	Configuration 1	Configuration 1	
Receiver	Configuration 2	Configuration 2	
Environment			
Borehole diameter	48 mm (AQ gauge)	60 mm (BQ gauge)	48 mm (AQ gauge)
Borehole state	Dry	Dry	Dry
Geological system	Bushveld Igneous Complex	Bushveld Igneous Complex	Bushveld Igneous Complex

TABLE 6-8: DETAILS OF FIELD MEASUREMENT: RECOMMENDED CONFIGURATION

6.4.6.a. Single trace evaluation

The single traces shown below (Figure 6-17) are included to evaluate to ability of this recommended system to perform in varying environments; exactly the same probe was deployed in two different diameter boreholes.

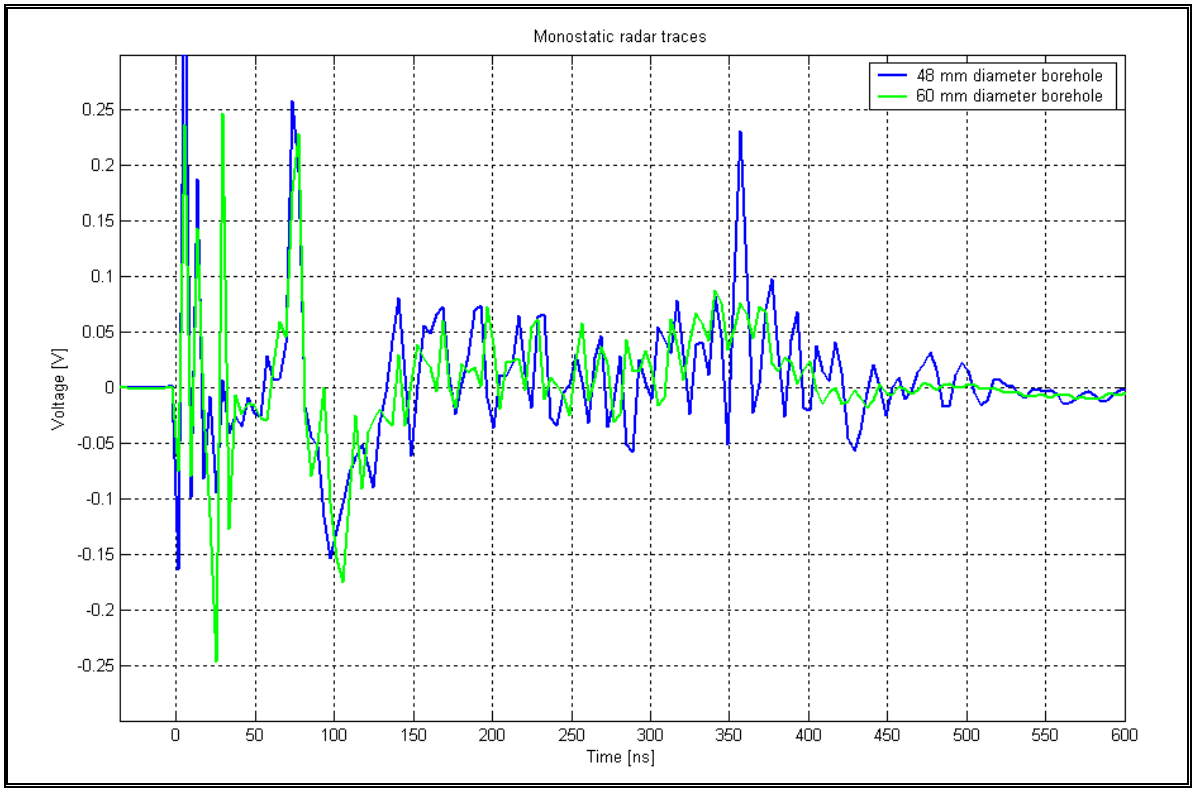

FIGURE 6-17: SINGLE TRACE FROM FIELD MEASUREMENT: RECOMMENDED SYSTEM IN VARIABLE DIAMETER BOREHOLES

The environment shows minimal effect on the general performance of the system. The use of receiver configuration 2 results in the maximum allowable voltage swing of the system to be limited by the $1V_{pp}$ of the ADC instead of the amplifier. It is clear that this system is well clear of the non-linear region of operation and minimal data loss can be expected. The characteristic roll (seen here between 300 ns and 400 ns, the gain sweep was slightly faster than that used for laboratory measurements) of receiver configuration 2 is clear, with a clear reflector superimposed on the 48 mm diameter data. Useful data can therefore be expected from the moment the isolation switch switches to through-mode at around 74 ns - or even earlier, if the results of section 6.4.3 are any indication.

6.4.6.b. Radar image evaluation

The performance of this monostatic radar is exceptionally close to that of the commercial bi-static system, as seen in Figure 6-18. The radar image from the monostatic system can in general be interpreted from 80 ns, with some strong reflectors that can be followed even closer. The velocity of propagation in this medium is 112.5 m/μs [9], so that a two-way propagation time of 80 ns translates to a distance of 4.5 m from borehole. The reduced gain of this receiver configuration initially prevents the radar from seeing through the isolation switch while it is in isolate mode as before. The data is in general visually at least on par with that obtained by the commercial system, confirming that the larger pulse width increases the general interpretability of the data.

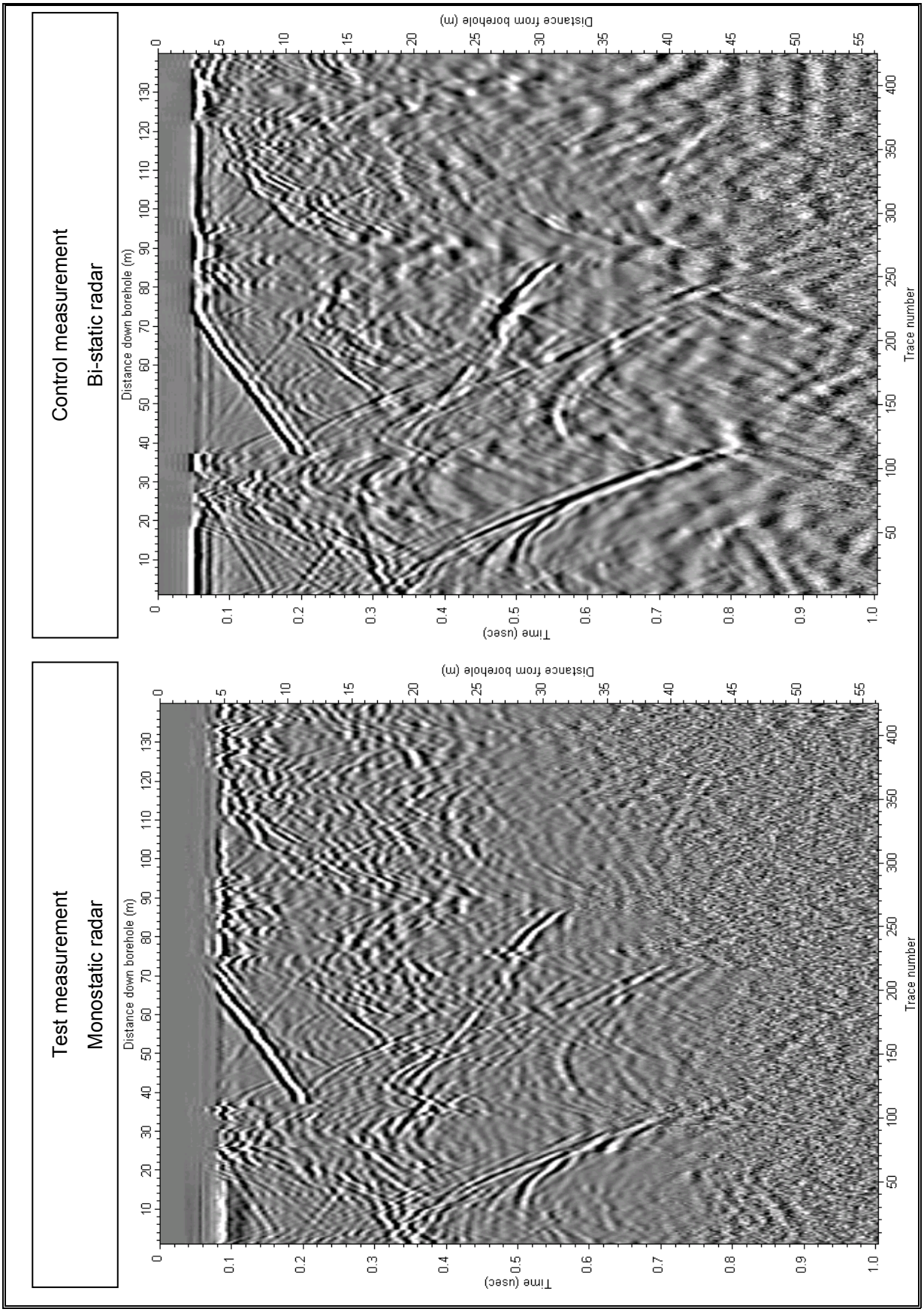

FIGURE 6-18: RADAR IMAGE OF FIELD MEASUREMENT: EVALUATION OF RECOMMENDED MONOSTATIC BOREHOLE RADAR SYSTEM

6.4.7. Additional example from recommended system

Another radar image obtained with the recommended monostatic radar system used above is included as Figure 6-19. It shows data from a 48 mm diameter dry borehole in the Bushveld Igneous Complex with very clear reflectors and serves as a good indication of the capabilities of this system.

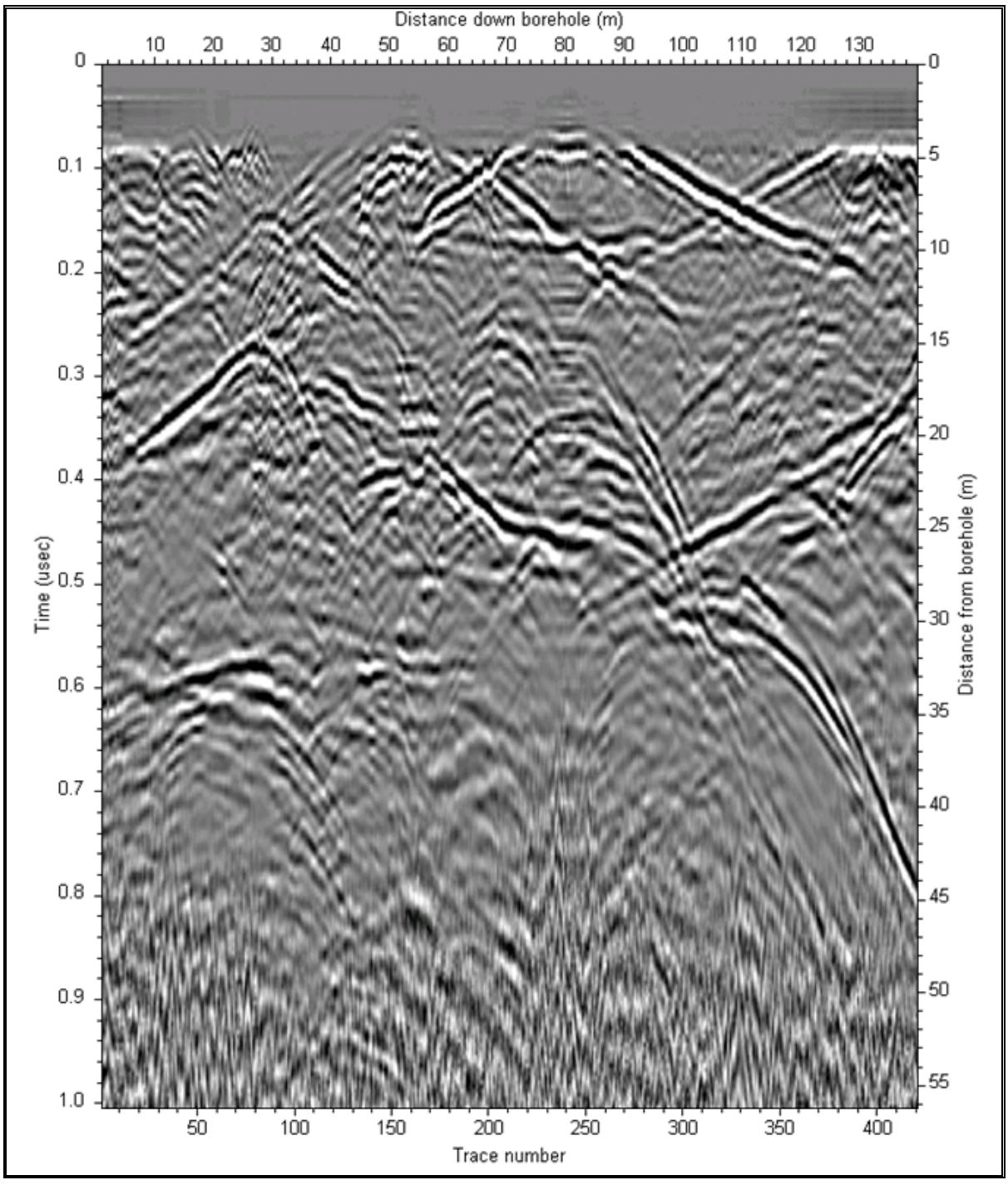

FIGURE 6-19: RADAR IMAGE OBTAINED WITH MONOSTATIC BOREHOLE RADAR SYSTEM

6.5. Synopsis

The construction of a complete monostatic borehole radar transceiver was presented as an example on how to integrate the modules and apply the principles developed in the preceding chapters. The successful functioning of this system was then verified through laboratory measurements - leading to the remarkable result of Figure 6-7.

A number of configurations were tested in the field, of which a few were presented here; yielding the industry's first known monostatic borehole radar data images.

The extensive field evaluation of borehole radar systems led to a recommendation as to the preferred configuration for the application of borehole radar. The radar image in Figure 6-19 proves that a monostatic system has been developed which competes with the bi-static systems currently available.

CHAPTER 7

Conclusion

7.1. Overview

The analog section of a monostatic, baseband radar system able to detect close-in targets in varying media was developed and implemented as a monostatic borehole radar system. A series interconnection of a transmitter, antenna, isolation switch and receiver was proposed for this and the modules were individually developed to operate in this configuration.

Asymmetric borehole radar antennas, consisting of one conducting arm and one resistively or resistive-capacitively loaded arm, were investigated as possible antennas for the transceiver and used as an example. It was pointed out that the exponential decay of the current after the transmitted transient, which is typical of such antennas, would have a deleterious effect on the operation of the transceiver. An approach was adopted whereby this antenna characteristic is assumed as a given, with the onus of curbing the effect shifted to the transmitter design. This emphasized the need to accurately quantify this tail in the antenna current. A measurement technique was devised to practically perform this measurement *in-situ*, taking advantage of a logarithmic representation for effective digitisation of the exponential decay.

The constraints for a transmitter waveform that inhibits the exponential decay in the eventual antenna current were formalized and a transmitter was designed to meet these requirements. The result was a novel transmitter configuration generating a bipolar signal where the symmetry is adjustable. This effectively tunes out the tail in the current. Another approach was also presented whereby the exponential tail in the antenna current is removed with a pole-zero network. A transmitter generating a step waveform and using a pole-zero network to remove the tail was then designed as another alternative for the transmitter module of the transceiver.

No known configuration could be found for an isolation switch which meets the requirements for this transceiver. A completely new configuration was consequently designed from first principles and taken right through to a practical electronic circuit. The proposed isolation switch exploits the use of differential and common modes to separate the switching signal from the RF-signal, thereby enabling switching transitions of similar durations to that of the RF pulse signal. The configuration makes effective use of both FETs and diodes as switching stages with a single control signal and incorporates their parasitics into the design.

It was argued extensively, both theoretically and through measurement, that dissipative filtering is essential in the design of high-fidelity systems. The application of this principle was illustrated by the design of two receiver configurations. Special attention was also given to the use of operational amplifiers and variable gain amplifiers in such circuits, especially in terms of their noise performance.

Borehole radar antennas were characterized while deployed in boreholes with a probe employing the measurement technique developed for characterizing antenna current. These measurements were performed in various boreholes and the results were used during the design of modules for a transceiver earmarked specifically for application in a monostatic borehole radar system. Step and bipolar transmitter prototypes were built for a monostatic borehole radar system, using the general designs of this dissertation with the specifications of the established bi-static borehole radar transmitter. Two isolation switch and receiver prototypes were similarly built to operate with these borehole radar transmitters and antennas. Each module was tested individually in the laboratory and yielded promising results. The integration of these modules was illustrated by the building of a complete borehole radar transceiver, which successfully underwent further laboratory testing. Various other combinations of the developed modules were also incorporated into complete monostatic radar borehole radar probes and deployed in the field. Remarkable radar data were acquired with these probes and a preferred configuration was found through evaluation of their performance in the field. The radar data obtained with this probe compares well with radar data obtained with a bi-static borehole radar system.

7.2. Future work

7.2.1. Antenna

The opportunities to deploy the antenna current measurement probe of section 2.3 were limited and equivalent models for the antennas could consequently only be found for a small range of boreholes, as seen from the results in section 2.4.2. These parameters have proven themselves to be invaluable during the design of the other modules and further measurements should be done with the goal of compiling an extensive database of equivalent models for the antenna in all standard [23] boreholes. Another objective of this investigation should be to find possible reasons for the discrepancy between the models found by Gouws [22] through simulation and those found through measurement in this disseratation.

The measurement probe of section 2.3 only provides information on the section of the antenna current governed by the slow time constant and allows for the extraction of R_2 and C_2 in the equivalent circuit of the antenna presented in Figure 2-5. The complete equivalent circuit will however provide valuable additional information regarding the loading on the transmitter and the peak transmitter current. A measurement system performing some form of peak-hold function should be

considered to determine these parameters and will contribute significantly to predicting and understanding the antenna response.

It was mentioned in section 5.2.3.a that the resistive loading of the antenna will contribute to the total noise of the system [73], [74]. This needs to be studied in detail to determine whether this noise does not dominate the noise generated by the receiver, in which case more freedom exists in the design of the receiver.

The resistive-capacitive antenna proposed by Gouws [22] has been shown to reduce the rate of the exponential decay in antenna current after the transmit transient has been applied to the antenna and promised to be the antenna of choice. It was however found in section 6.4.4 that the radar image obtained with this antenna is not visually as easy to interpret as that obtained with the resistively loaded antenna. This decidedly subjective remark clearly warrants further study.

7.2.2. Transmitter

Field measurements (sections 6.4.5 and 6.4.6) confirmed that shorter pulse widths provide better resolution, but it was noted (albeit subjectively) that a larger pulse width might be required to ease interpretation of the eventual radar image. This contradiction, combined with the ease of adjusting the bipolar transmitter's pulse width (as seen in section 3.4.3.b) raises the question if the virtues of both longer and shorter pulses cannot be accessed through a well-defined adjustment of the pulse width during the measurement. This will require the digital control circuitry to control the timing of all three transmitter trigger signals and a certain protocol for adjusting the pulse width.

Theory indicates that the residual current flowing after a bipolar transient is still a function of the antenna impedance (section 3.2.1.d), although the measurements in section 3.4.3.d suggested that the effect is insignificant in a system such as borehole radar. The option could however be considered to create a feedback loop to zero the residual automatically as the antenna impedance changes, by varying the symmetry of the bipolar pulse in response to feedback of the residual current amplitude.

7.2.3. Isolation switch

It is recommended that measurements are performed to establish the optimal impedance level for the borehole radar antenna when deployed in a borehole. This impedance level should then be created by choosing the appropriate input transformer for the isolation switch to transform the isolation switch's internal impedance to the required value. The borehole radar systems developed in this dissertation operated with input impedances between 100 Ω and 200 Ω, in accordance with the levels used by the bi-static radar receivers.

7.2.4. Receiver

The step transmitter of section 3.3 benefited from the pole-zero network borrowed from the field of nuclear instrumentation, where signals very similar to that of baseband radar systems are encountered. These instrumentation amplifiers employ various signal shaping techniques, of which the pole zero network form an integral part [30], [31], [61], [81] and an investigation into the rigorous application of these techniques to the receiver of this transceiver can be justified.

7.3. This monostatic borehole radar's impact on industry

The use of a single probe and the absence of an optical fibre spacer in a monostatic borehole radar result in a system which is generally more robust and easier to handle and operate than its bi-static counterpart. To this end, the monostatic borehole radar probe developed in this dissertation has already had a significant impact on the use of borehole radar systems in industry.

Elimination of the need to handle optical fibre and the making of sensitive, watertight connections between the probes and spacer during a borehole radar survey reduce the involvement of the operator and the possibility of failure. Apart from the obvious advantages in ease of operation and reliability, it has opened the door for technicians with only a basic knowledge of the actual operation of the system to perform the surveys independently.

The availability of a system consisting of a single probe with no ridges has allowed for surveys to be conducted in boreholes which could not be entered with the bi-static system, due to questionable ground conditions in the borehole. The flexible optical fibre spacer and the connectors connecting it to the probes make the bi-static system more prone to snagging, damage or tool loss.

This monostatic radar also facilitated the development of a new geophysical technique to accurately detect geological structures, such as bedding planes, which intersect the borehole [82]. This is achieved by deploying the monostatic radar in a water filled borehole with a conducting wire. The radar excites and detects pulses propagating and reflecting in a mode along the wire. Echoes are observed from any discontinuities in the electromagnetic properties of the borehole such as changes in the geological host of the borehole.

Surveys have been performed where this monostatic radar was deployed by a drill rig instead of by a winch with a dielectric string (see Figure 7-1). The shorter length and absence of a spacer again made the monostatic radar the only practical option.

FIGURE 7-1: THE MONOSTATIC BOREHOLE RADAR BEING DEPLOYED WITH A DRILL RIG

The radar is screwed onto the front of the drill string, where the first 3m is dielectric, followed by the standard metal drill rods. This technique is extremely attractive, given that there is no need for the borehole to be rigged or a winch to be on site. Extracting a clear radargram from the data obtained with the irregular movement of the drill rig does however require extensive processing. Data have been captured and the technique warrants further attention, especially if a form of motion sensing can be incorporated into the hardware.

A requirement exists for borehole radar surveys to be performed in near vertical, water filled boreholes exceeding 1 km in length. The extreme water pressure associated with these holes prompt the use of hardened radar and spacer housings. The weight of the probes consequently increases and the spacer of the bi-static system is typically a rigid structure. This leads to an awkwardly long and heavy bi-static system (see Figure 7-2) which requires special deployment techniques and equipment. This is often impractical in the confined spaces of an underground mine. The single probe of the monostatic radar does not suffer from these drawbacks; although heavier than a standard pressure monostatic, the weight compares well with a standard pressure bi-static. Surveys previously considered to be unfeasible can consequently be performed with minimal additional effort.

FIGURE 7-2: THE BI-STATIC BOREHOLE RADAR IN ITS HARDENED HOUSING BEING DEPLOYED IN A DEEP, VERTICAL, WATER FILLED BOREHOLE

It is clear that the advantages of a monostatic borehole radar over a bi-static system goes beyond just convenience and has already found important industrial applications which could previously not be considered.

References

1 Caspers, J.W., “Bi-static and multistatic radar.” in *Radar Handbook* , Sklonik, M.I. Ed., New York: McGraw-Hill, 1970, chapter 36.

2 Barton, D.K., Leonov, S.A. Ed., *Radar Technology Encyclopedia,* Massachusetts*:* Artech House Inc., 1997.

3 Bennet, C.L. and Ross, G.F., “Time-domain electromagnetics and its applications,” *Proceedings of the IEEE*, vol. 66, nr. 3, pp 299-318, 1978.

4 Taylor, J.D. “Ultra-wideband radar overview” in *Introduction to Ultra-Wideband Radar Systems*, Taylor J.D. Ed., Florida: CRC press, 1995.

5 Daniels, D.J. Ed., *Ground Penetrating Radar,* 2nd edition, IEE Radar, Sonar and Navigation Series 15, pp 1-36, 131-181.

6 Haus, H.A., Melcher, J.R., *Electromagnetic Fields and Energy,* New Jersey: Prentice Hall Inc., 1989.

7 Mason, I.M., Cloete, J.H., “VHF band slimline borehole radar experiences in the South African mining industry,” in *Ground Penetrating Radar,* IEE Radar, Sonar and Navigation Series 15, Daniels, D.J. Ed., 2004, pp 489-493.

8 Wolmarans, A.V., Cloete, J.H., Ekkerd, J., Mason, I.M., Simmat, C.M., “Borehole radar application to kimberlite delineation at Finsch diamond mine”, *Exploration Geophysics*, vol. 36, no. 3, September 2005, pp. 310-317.

9 Herselman, P.leR., “Detecting geological defects in the Bushveld Igneous Complex,” PhD dissertation, University of Stellenbosch, December 2003.

10 Simmat, C.M., “Mine scale three-dimensional borehole radar imaging”, PhD dissertation*,* University of Sydney, June 2005.

11 Hargreaves, J.H., “Multichannel borehole radar for three dimensional imaging,” PhD dissertation, Oxford University, 1995.

12 Woods, B.K., “The development of an active pulsed radar receiver for a monostatic borehole radar,“ MSc thesis, University of Stellenbosch, March 2003.

13 Van der Merwe, P.J., “The design of a monostatic, ultra wide band, VHF, pulse radar for detection of close-in targets,” MSc thesis, University of Stellenbosch, March 2003.

14 Van der Walt, P.W, Van der Merwe P.J., Cloete J.H., Mason I.M., "Method and device for transceiver isolation," 503428: International Application PCT/AU2005/001201, Chilean application 2027-2005(pending).

15 Franceschetti, G., Papas, C.H., “Pulsed antennas,” *IEEE Transactions on Antennas and Propagation,* vol. AP-22, nr. 5, September 1974, pp 651-661.

16 Foster, P.R., “Ultra-wideband antenna technology,” in *Introduction to Ultra-Wideband Radar Systems*, Taylor, J.D. Ed., Florida: CRC press, 1995.

17 De Jongh, R.V., Yarovoy, A.G., Ligthart, L.P., Kaploun, I.V., Schukin, A.D., “Design and analysis of new GPR antenna concepts,” *Proceedings of 7th International Conference on Ground Penetrating Radar*, Lawrence, Kansas, May 1998, vol. 1, pp 81-86.

18 Claassen, D.M., “Electromagnetic characterization of a wideband borehole radar imaging system”, PhD dissertation, Oxford University, 1995.

19 Wu, T.T., King, R.W.P., “The cylindrical antenna with non-reflecting resistive loading*,” IEEE Transactions on Antennas and Propagation*, vol. 13, May 1965, pp 369-373.

20 Keller, S., “Design of impedance loaded antennas for borehole radar applications,” MSc thesis, University of Stellenbosch, July 2000.

21 Van Wyk, M., “An active receiving antenna for borehole pulsed radar applications," MSc thesis, University of Stellenbosch, December 2002.

22 Gouws, M., “Modeling of a monostatic borehole radar antenna,” MSc thesis, University of Stellenbosch, April 2006.

23 Heinz, W.F., *Diamond drilling handbook*, 3rd edition, Halfway House: Sigma press, 1994, pp 120-136.

24 Chatterjee, A., Mallik, K., Oak, S.M., “The principle of operation of the avalanche transistor-based Marx bank circuit: a new perspective,” *Review of Scientific Instruments,* vol. 69, nr. 5, May 1998, pp 2166-2170.

25 Moll, J.L., Hamilton, S.A., “Physical modeling of the step recovery diode for pulse and harmonic generation circuits,” *Proceedings of the IEEE,* vol. 57, nr. 7, July 1969, pp1250-1259.

26 Barret, T.W., “History of ultra wideband (UWB) radar & communications: pioneers and Innovators”, *Progress in Electromagnetics Symposium*, Cambridge, July 2000.

27 Kardo-Sysoev, A.F., "New power semiconductor devices for generation of nano- and subnanosecond pulses" in *Ultra-Wideband Radar Technology*, Taylor, J.D. Ed., Florida: CRC press, 2001, pp 205 – 290.

28 Engler, H.F., “Technical issues in ultra wideband radar systems” in *Introduction to Ultra-Wideband Radar Systems,* Taylor, J.D. Ed., Florida: CRC press, 1995, pp 11-50.

29 Schukin, A.D., Kaploun, I., Yarovoy, A.G., Ligthart, L.P., “Evolution of GPR antennas, pulse generators and sample recorders,” presented at *Millennium Conference on Antennas & Propagation,* Davos, Switzerland, April 2000.

30 Canberra, “Basic counting systems,” www.canberra.com/literature.

31 Boie, R.A., Hrisoho, A.T., Rehak, P., “Signal shaping and tail cancellation for gas proportional detectors at high counting rates,” *IEEE Transactions on Nuclear Science, v*ol. NS-28, nr. 1, February 1981, pp 603-609.

32 Maloney, J.G., Smith, G.S., “A study of transient radiation from the Wu-King resistive monopole – FDTD analysis and experimental measurements,” *IEEE Transactions on Antennas and Propagation,* vol. 41, nr. 5, May 1993, pp 668-676.

33 Johannessen, P., “High power step recovery diodes and saturable inductors in radar pulse modulators,” *IEEE Transactions on Magnetics,* vol. 3, nr. 3, September 1967, pp 256-260.

34 Baker, R.J., Hodder, D.J., Johnson, B.P., Subedi, P.C., Williams, D.C., “Generation of kilovolt-subanosecond pulses using a nonlinear transmission line,” *Measurement, Science and Technology*, vol. 4, 1993, pp 893-895.

35 Frey, R., “Capabilities of low cost high voltage RF-power MOSFETs at HF and VHF,” *Microwave symposium digest, IEEE MTT-S international*, vol. 2, June 1998, pp 1117-1120.

36 International Rectifier, Application Note AN1001, pp 1-3.

37 Han, J., Nguyen, C., “A new ultra-wideband, ultra-short monocycle, pulse generator with reduced ringing”, *IEEE Microwave and Wireless Components letters*, vol. 12, nr. 6, June 2002, pp 206-208.

38 Kim, H., Park, D., Joo, Y., “Design of a CMOS Scholtz’s monocycle pulse generator”, *IEEE Conference on Ultra Wideband systems and technologies*, November 2003, pp 81-85.

39 Lee, J.S., Nguyen, C., Scullion, T., “New uniplanar subnanosecond monocycle pulse generator and transformer for time-domain microwave applications,” *IEEE Transactions on Microwave Theory and Techniques*, vol. 49, nr. 6, June 2001, pp 1126-1129.

40 Han, J., Nguyen, C., “On the development of a compact sub-nanosecond tunable monocycle pulse transmitter for UWB applications”, *IEEE Transactions on Microwave Theory and techniques*, vol. 54, nr. 1, January 2006, pp 285-293.

41 Tiuraniemi, S. , Opperman, I.,”Integrated circuit topologies” in *UWB Theory and Applications,* Opperman, I, Hämäläinin, M, Iinatti, J Ed., West Sussex: Johan Wiley & Sons inc, 2004, pp 87-126.

42 Skolnik, M.I., *Introduction to Radar Systems*, 3rd ed, Boston: McGraw Hill, 2001.

43 White,J.F., ”Origins of high power diode switching,” *IEEE Transactions on Microwave Theory and Techniques, v*ol. 32, nr. 9, September 1984, pp 1105-1117.

44 Zhang, Y.P., Li, Q., Fan, W., Ang, C.H., Li, H.,”A differential CMOS T/R switch for multistandard applications,” *IEEE Transactions on Circuits and Systems – II: Express briefs, v*ol. 53, nr. 8, August 2006.

45 Pozar,D.M., *Microwave Engineering,* 2nd edition, USA: John Wiley & Sons inc.,1998.

46 Microsemi Corporation, *PIN diode circuit designers' handbook*, 1998.

47 White, J.F., *Microwave semiconductor engineering,* New York: Van Nostrand Reinhold, 1982, pp 39-89.

48 Infineon, Application note 065, 2001.

49 Shindler, J., Morris, A.,"DC-40 GHz and 20 -40 GHz MMIC SPDT switches," *IEEE Transactions on Microwave Theory and Techniques,* vol. MTT-35, nr. 12, December 1987, pp 1486-1493.

50 Imai, N., Minawaka, A., Okazaki, H., "Novel high-isolation FET switches," *IEEE Transactions on Microwave Theory and Techniques,* vol. 44, nr. 5, May 1996, pp 685 – 691.

51 Joshi, J.S., "Switches and attenuators," in *RFIC and MMIC Design and Technology, IEE Circuits, Devices and Systems Series 13,* Robertson, I.D. and Lucyszyn, S. Ed., 2001, pp 347-380.

52 Hittite corporation, Product selection guide, www.hittite.com.

53 Corrigan, T., Goggin, R., "CMOS switches offer high performance in low power, wideband application," *High Frequency Electronics,* Summit Technical Media, 2004.

54 Novak, R, "RF CMOS switches address multiband requirements of next generation handsets," *RF Design*, 1 Jul 2006, www.rfdesign.com.

55 Kelly, D.; Brindle, C.; Kemerling, C.; Stuber, M., "The state-of-the-art of silicon-on-sapphire CMOS RF switches," *IEEE Compound Semiconductor Integrated Circuit Symposium,* Nov. 2005.

56 Botchek, C.M., *Basic MOS engineering,* Vol. 1, Chicago: Pacific Technical Group inc., 1983, pp 127-153.

57 Richman, P., *MOS field-effect transistors and integrated circuits,* New York: John Wiley & sons, 1973, pp 47-73.

58 Zverev, A.I., *Handbook of Filter Synthesis*, New York: John Wiley & sons, 1967, pp 380-414.

59 Havlice, J.F.; Taenzer, J.C., "Medical ultrasonic imaging: An overview of principles and instrumentation," *Proceedings of the IEEE*, vol. 67,nr. 4, April 1979, pp 620-641.

60 Brunner, E., "How ultrasound system considerations influence front-end component choice," *Analog Dialogue*, vol. 36, no.3, May 2002.

61 ORTEC technical staff, *Model 572 Spectroscopy Amplifier and Pile-Up Rejector Operating and Service Manual,* Ortec, 1984.

62 Vogt, D., "Borehole radar," in *Ground Penetrating Radar,* 2nd ed, IEE Radar, Sonar and Navigation series 15, Daniels, D.J. ed., 2004, pp 475-483.

63 Mason, S.J., "Feedback theory – some properties of signal flow graphs, " *Proceedings of the IEEE,* vol. 41, September 1953, pp. 1144-1156.

64 Kuhn, N., “Simplified signal flow graph analysis”, *Microwave Journal,* vol. 6, November 1963, pp 59-66.

65 Bode, H.W., *Network Analysis and Feedback Amplifier Design,* New York: D. Van Nostrand Company, 1945, pp 270-275.

66 Matthaei, G.L., Cristal, E.G., “Theory and design of diplexers and multiplexers,” *Advances in Microwaves,* Vol. 2, Young, L. Ed., New York: Academic Press, 1967, pp 237-324.

67 Allen, R. “Monolithic IC op amps keep pace with design needs,” *Electronic Design,* Online ID #6853, Penton Media, November 2003, www.elecdesign.com.

68 Dobkin, R. “Op amps: as good as they will get?,” *Electronic Design,* Online ID #7049, Penton Media, January 2004, www.elecdesign.com.

69 Turo, A., et al., “Ultra-low noise front-end electronics for air coupled ultrasonic non-destructive evaluation,” *NDT& E International*, vol 36, 2003, pp 93-100.

70 Hillbrand, H., Russer, P., “An efficient method for computer aided noise analysis of linear amplifier networks,” *IEEE transactions on Circuits and Systems,* vol. CAS-23, nr. 4, April 1976, pp 235-238.

71 Karki, J., “Calculating noise figure in op amps,” *Analog Applications Journal*, Texas Instruments, 4th Quarter 2003, pp 31-37, www.ti.com/sc/analogapps.

72 Peebles, P.Z., *Probability, Random Variables, and Random Signal Principles*, 3rd Edition, New York: McGraw-Hill Inc., 1993, pp 235-318.

73 Maclean, T.S.M., “Signal/noise ratio of traveling-wave dipole,” *The Radio and Electronic Engineer,* vol. 43, nr.9, September 1973, pp 534-436.

74 Ramsdale, P.A., “Signal/noise-ratio performance of loaded wire antennas,” *Proceedings of the IEE, v*ol. 124, nr. 10, October 1977.

75 Duong, Q-H., Le, Q., Kim, C-W., Lee, S-G., “A 95-dB linear low-power variable gain amplifier,” *IEEE Transactions on Circuits and Systems,* vol. 53, nr. 8, August 2006, pp 1648-1657.

76 Otaka, S., Takemura, G., Tanimoto, H., “A Low-power low-noise accurate linear-in-dB variable-gain amplifier with 500 MHz bandwidth,” *IEEE Journal of Solid-State Circuits, v*ol. 35, nr. 12, December 2000, pp 1942-1948.

77 Gilbert, B., “A precise four quadrant multiplier with subnanosecond response,” *IEEE journal of Solid-State circuits,* vol. SC-3, nr.4, December 1968, pp 365-373.

78 Van der Merwe, P.J., “Manual: Operating the GeoMole IQ radar,” GeoMole, May 2006.

79 Li, M., “Seismic application of interactive computational methods”, MSc thesis, University of Sydney, 2000.

80 Annan, A.P. “Ground penetrating workshop notes," Sensors and Software, September 2001.

81 Kandasamy, A., O'Brien, E., O'Connor, P., Von Achen, W., "A monolithic pre-amplifier-shaper for measurement of energy loss and transition radiation," *IEEE Transactions on Nuclear Science,* vol. 46, nr. 3, June 1999, pp 150-155.

82 Mason, I.M., Cloete, J.H., Van Brakel, W., Hargreaves, J.H., "Electromagnetic reverberation at VHF on wires in uncased water-filled boreholes," *Electronics letters,* vol 42, nr.5, March 2006, pp 306-307.

Addendum A

Circuit diagrams

A.1. Antenna current measurement probe

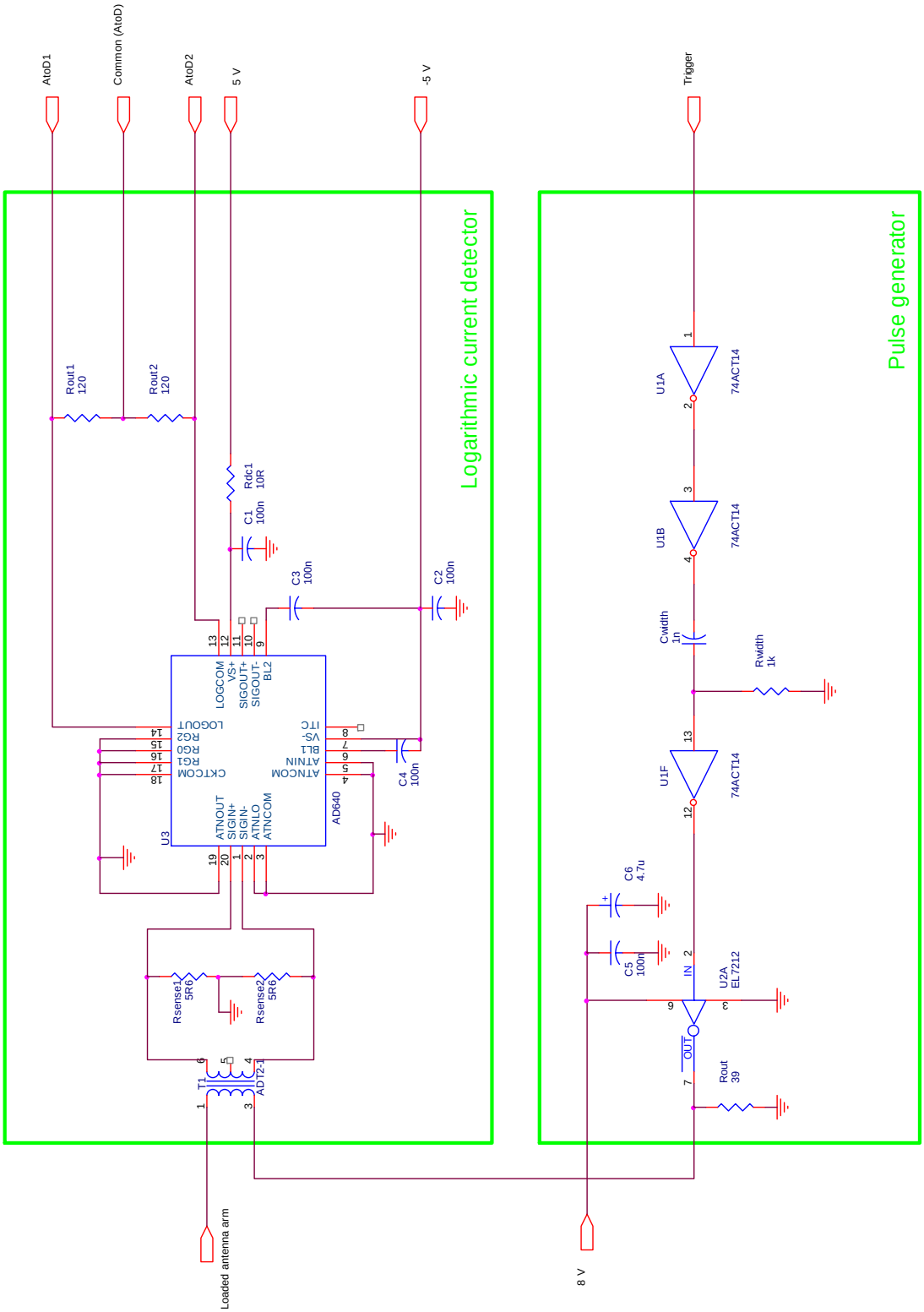

A.2. Step waveform transmitter

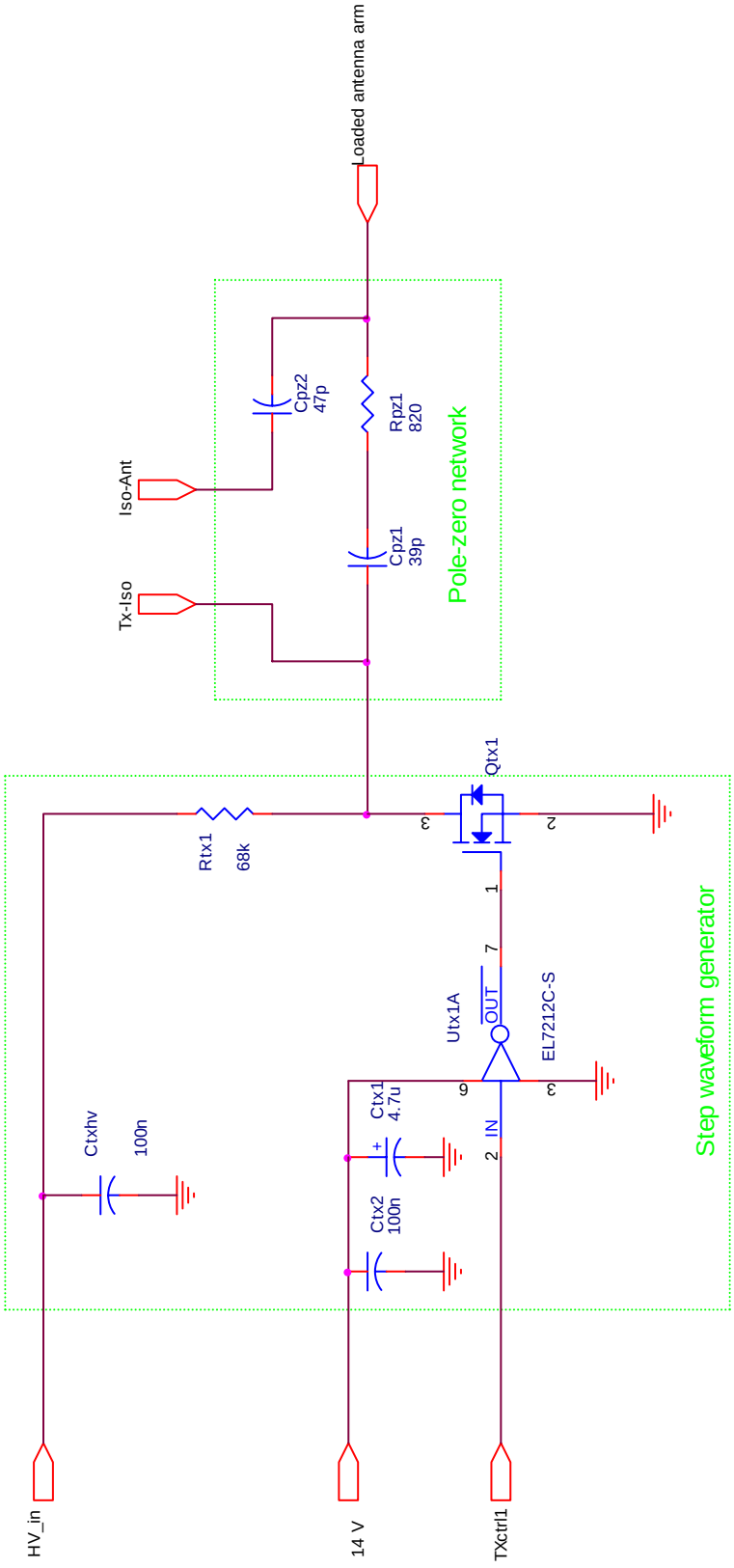

A.3. Bipolar waveform transmitter

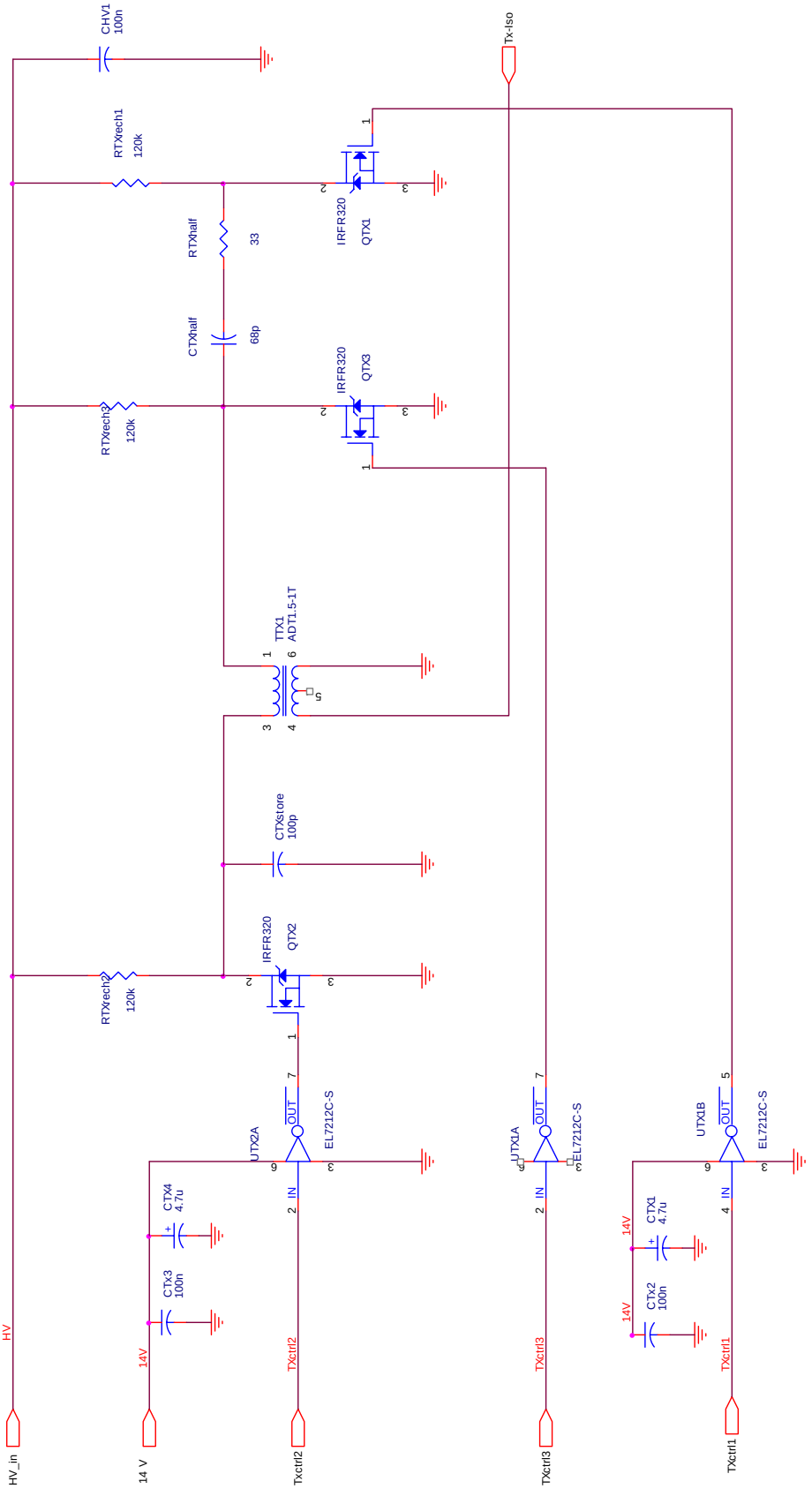

A.4. Isolation switch: Configuration 1

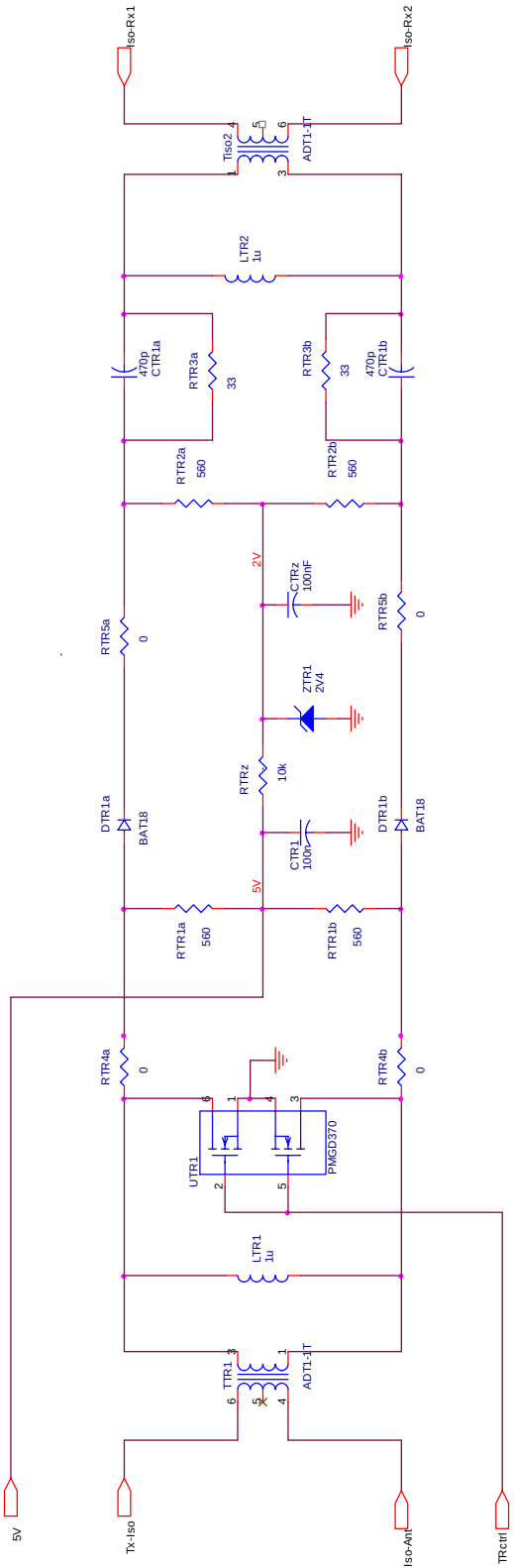

A.5. Isolation switch: Configuration 2

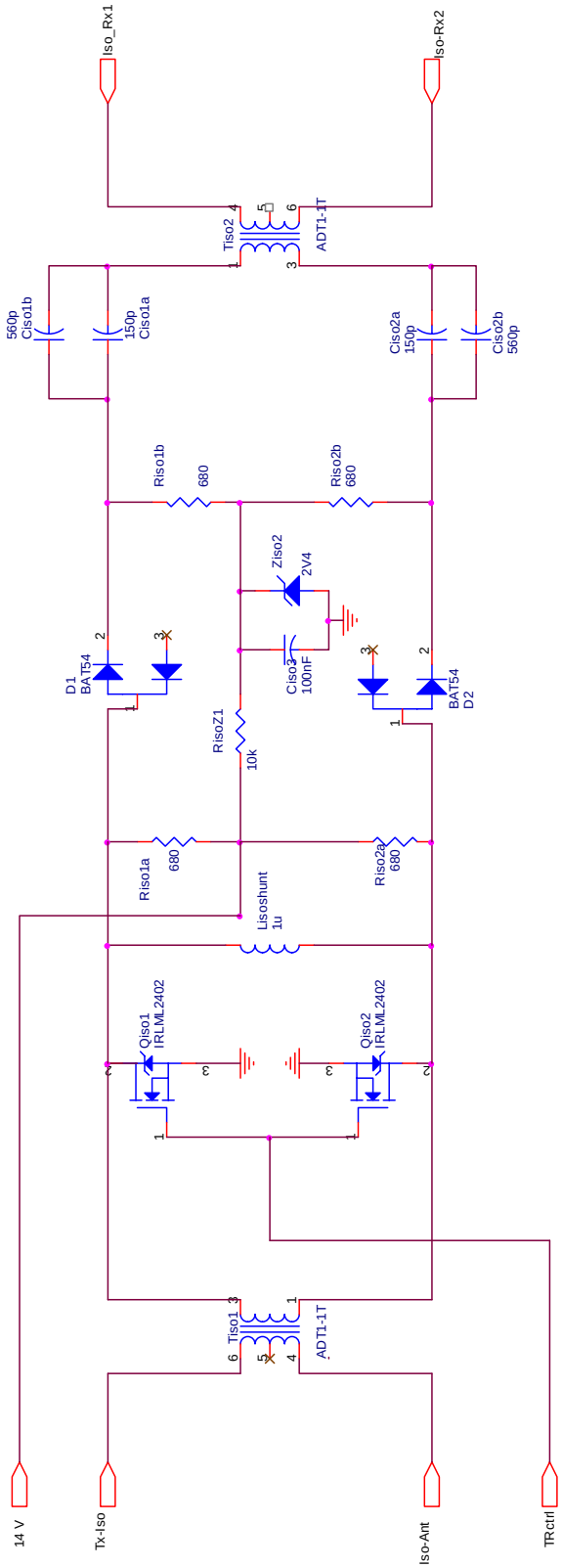

A.6. Receiver: Configuration 1

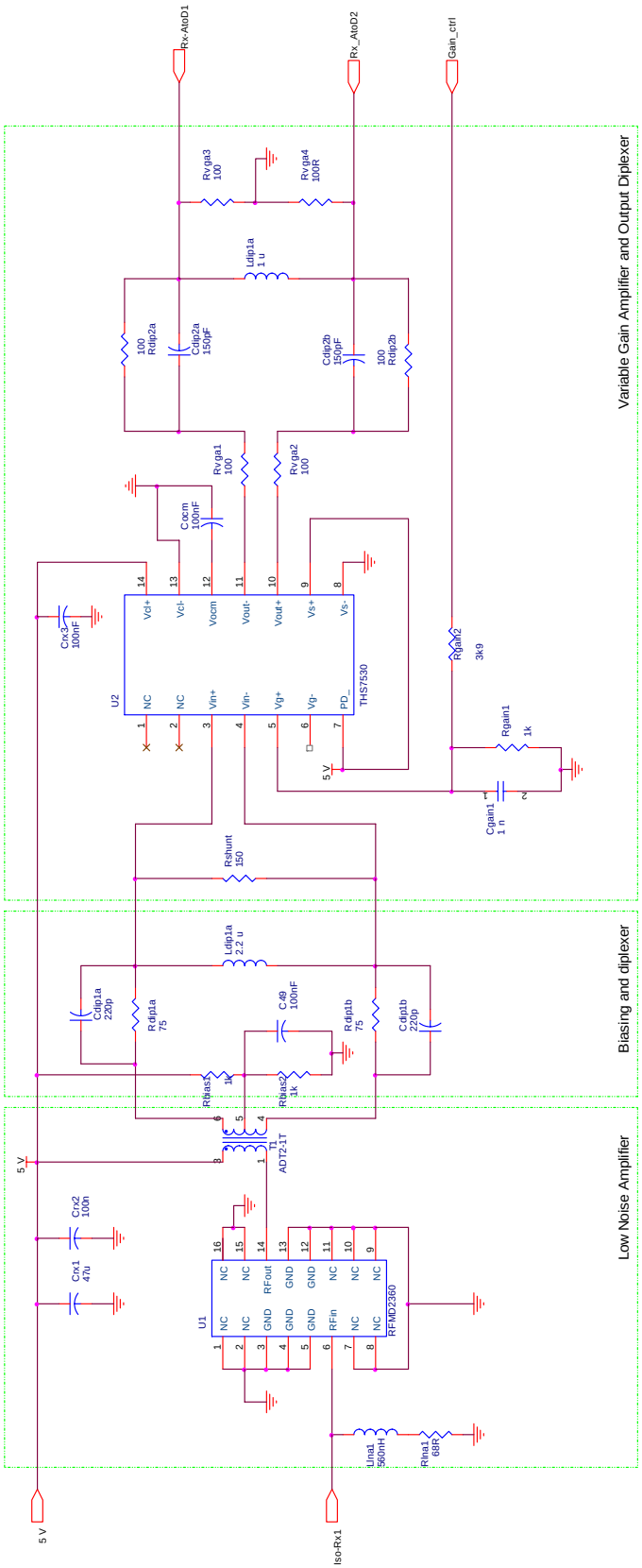

A.7. Receiver: Configuration 2